# Facile hydrothermal fabrication of nano-oxides hollow spheres using monosaccharide as sacrificial templates

Dissertation

zur

Erlangung des Doktorgrades

der Naturwissenschaften

(Dr. rer. nat.)

dem

Fachbereich Chemie

der Philipps-Universität Marburg

vorgelegt von

**Haitham Mohammad Abdelaal Abdelaal**

aus Sharkia, Ägypten

Marburg/Lahn 2013

This work was carried out from October 2009 to October 2012 at the Department of Chemistry, Philipps University, Marburg under the supervision of Prof. Dr. B. Harbrecht.

Vom Fachbereich Chemie
der Philipps-Universität Marburg als Dissertation am 15.02.2013 angenommen.
Erstgutachter Prof. Dr. B. Harbrecht
Zweitgutachter Prof. Dr. B. Roling

Tag der mündlichen Prüfung am 20.02.2013

***To my beloved mother***

***To my dear sister***

***To my lovely wife (Sherihan) and my dear son (Jibreel)***

## Guidance Lights

- **Galileo Galilei, 1564 – 1642**

"All truths are easy to understand once they are discovered; the point is to discover them."

- **Isaac Newton, 1643 – 1727**

"To myself I am only a child playing on the beach, while vast oceans of truth lie undiscovered before me."

- **Max Planck, 1858 – 1947**

"We have no right to assume that any physical laws exist, or if they have existed up to now, that they will continue to exist in a similar manner in the future."

- **Marie Curie, 1867 – 1934**

"One never notices what has been done; one can only see what remains to be done."

- **Albert Einstein, 1879 – 1955**

"A man should look for what is, and not for what he thinks should be."

## Table of Contents

## List of Figures

### *Chapter 1: General introduction*



### *Chapter2: Experimental Section*

***Chapter 3: Hydrothermal synthesis of carbonaceous spheres from aqueous glucose and fructose solutions in closed system***

### *Chapter 4: Facile one-pot fabrication of hollow porous silica nano-particles*

***Chapter 5: Use of fructose derived-carbonaceous spheres as templates for the fabrication of metal oxide hollow spheres***

## *Chapter 6: Use of glucose derived-carbonaceous spheres as templates for the fabrication of metal oxide hollow spheres*

## *Chapter7: Glucose and fructose as sacrificial templates: similarities and differences*

## List of Tables

## Abbreviations

| | |
|---|---|
| µm | micrometer |
| $^0$C | Celsius temperature |
| A | surface area |
| Å | Angstrom |
| AcOH | Acetic acid |
| BET | Brunauer Emmett Teller theory |
| bnb | Ball in ball |
| CCD | charge-coupled device |
| CS-PAA | chitosan-polyacrylic acid |
| CSs | carbonaceous spheres |
| CTAB | cetyl trimethylammonium bromide |
| DMF | dimethylformamide |
| Fr | fructose |
| FT-IR | Fourier Transform Infrared spectroscopy |
| FWHM | full width at half maximum |
| G | glucose |
| HR-TEM | high resolution transmission electron microscopy |
| HSMS | hollow spheres with mesoporous shells |
| HSNPs | hollow silica nanoparticles |
| HSSs | hollow silica spheres |
| ICTA | International Confederation of Thermal Analysis |
| IR | Infrared Spectroscopy |
| IUPAC | International Union of Pure and Applied Chemistry |
| LbL | layer-by-layer |
| mg | milligram |
| ml | milliliter |
| nm | nanometer |
| NPs | Nanoparticles |

| | |
|---|---|
| O/W | oil-in-water |
| OCT | optical coherence tomography |
| PDADMAC | poly (diallyldimethylammonium chloride) |
| PHS | pours hollow silica |
| PHSNPs | porous hollow silica nanoparticles |
| PMMA | polymethylmetacrylate |
| PS | polystyrene |
| PSA | polystyrene acrylic acid |
| PSD | particle size distribution |
| SCMS | solid core and mesoporous shell |
| SDBS | dodecylbenzenesulfonate |
| SEM | scanning electron microscope |
| T | temperature |
| t | time |
| TALH | titanium (IV) bis(ammonium lactate) dihydroxide |
| TBT | tetra-n-butyl titanate |
| TEM | transmission electron microscopy |
| TEOS | tetraethyl orthosilicate |
| TG | thermogravimetry |
| TIPP | titanium(IV) isopropoxide |
| W/O | water-in-oil |
| XRD | X-Ray Diffraction |

# Chapter 1

## General introduction

### 1.1. Nanotechnology

Nano-, a prefix refers to a factor of $10^{-9}$ has its origin in the Greek nanos, meaning dwarf. In its broadest terms, nanoscience and nanotechnology includes visions of making, imaging, manipulating and utilizing things really small.
In general, nanotechnology is a collective definition referring to every technology and science which operates on a nanoscale and refers to the scientific principles and new properties that can be found and mastered when operating in this range. In addition, nanotechnology is considered by some to be the next industrial revolution and is believed to cause enormous impacts on the society, economy and life in general in the future.[1-3]

When we bring materials down to the nanoscale, physical, chemical, and biological properties of the particles change significantly, and nanoparticles (NPs) have other optical, magnetic or electrical properties than larger particles. Some materials used for electrical insulations can become conductive and other materials can become transparent or soluble.[3] For example gold NPs have a different colour, melting point and chemical properties, due to the nature of the interactions among the atoms that make up the gold, as compared to a nugget of gold. Nano gold does not look like bulk gold, the nanoscale particles can be orange, purple, red or greenish depending on the size of the particle.[2] These properties are and will be utilized in a wide range of areas as in medical applications, information technologies, energy production and storage, materials, manufacturing, instrumentation, environmental applications and security.[4,5]

Also with a decrease in the size from macro- to nanosize, the surface area per unit volume increases, which enhances the properties due to the available surface area.[6,7]

These nano-scale particles (NPs) can be spherical, nanotubes, irregularly shaped, and may also exist in aggregated formations.[8] NPs are not new to science and are plenty in nature. NPs are by-product of fires, volcanic eruptions, and other natural processes. NPs are nature components of all living things such as many proteins, enzymes and RNA/DNA actually fit the criteria for NPs.[9 -11] In addition to these naturally formed NPs, there are a number of engineered NPs already in use in many industrial applications. the engineered NPs was defined by *Meili et al.* as the intentional manufactured solid particles with at least two dimensions between 1 and 100 nm.[12]

The interest in NPs stems from the fact that their properties are a function of their size. The impact of size is already known for decades. The pioneer research studies were done by the great *Faraday* who, in 1856, was the first to try to study the size dependence of the physical properties of material. He used gold, which he started with very small pieces of gold (nanocrystalline gold) in solution and, by pressing them together, made bigger pieces of gold. *Faraday* distinguished that the color of a metal can become size dependent below a certain critical size. What this critical size was, and why it was different for the different metals that he investigated, was something that *Faraday* did not understand, and could not have understood at that time.[13]

In 1959, physicist and future Nobel prize winner *Richard Feynman* gave a lecture to the American physical Society called" there 's plenty of room at the bottom", his speech focused on how he believed man would create smaller, powerful devices. This lecture came to history as the first throwing light on the importance of nanotechnology. He presented a technological vision of extreme miniaturization several years before the word "chip" became part of the lexicon..

He talked about the problem of manipulating and controlling things on a small scale. Extrapolating from known physical laws, *Feynman* envisioned a technology using the ultimate toolbox of nature, building nano-objects atom by atom or molecule by molecule.[14] The first published material that used the term nanotechnology was in 1986, by *Eric Drexler* who published a book entitled "Engines of creation" the coming era of nanotechnology. This book was the first thorough description of nanotechnology. In this book, Drexler considers the implications of this technology.[15]

There are two principal ways of manufacturing nanoscale materials; the top-down nanofabrication starts with a large structure and proceeds to make it smaller through successive cuttings ,while the bottom-up nanofabrication starts with individual atoms and builds them up to a nanostructure.[2,3,5]

## 1.2. Inorganic hollow materials

The attention to the hollow materials was paid since the pioneering works on the fabrication of hollow spheres were performed by *Kowalski et al*.[16] In last decade materials with a hollow interior, as a special class of materials in comparison to other solid counterparts, has gained increasing attention, owing to their unique properties that are substantially different from those of particles in general such as low density, large specific surface area, stability, surface permeability, and hollow structure thus making them attractive from both scientific and technological point of view.[17]

The hollow particles represent a distinct class of materials which are of great interest in the fields of medicine, pharmacy, materials science, water treatment, and the paint industry. They find potential widespread applications such as chromatography, protection of sensitive components (as enzymes and proteins), catalysis, hollow inorganic shells with meso- and macroporosity might find uses in encapsulation of chemicals (for the controlled-release of drugs,

cosmetics, inks and dyes), coatings, composite materials, artificial cells and as inorganic fillers. Additionally, some hollow oxide particles can be used to fabricate highly porous structures with applications in light-weight materials, adsorption, insulation and filters. Moreover, other interesting application can be also suggested depending on the chemical composition of the hollow shell, size, and morphology of the hollow objects.[18-29]

A variety of chemical and physicochemical methods, including self-assembly techniques, sol-gel process, emulsion/interfacial polymerization strategies, spray-drying methods, surface polymerization processes, surfactant-assisted solvothermal decomposition, colloidal templating methods and template free approaches have been used for the fabrication of micro- and nano hollow materials. Among these methods, sacrificial templating approach is considered to be the most often and efficient way of fabricating hollow structured micro- and nano particles which are based on the synthesis of core-shell composite particles and subsequently removal of the core by dissolution in a solvent or heating (calcination).[30-39]

In general, manipulation of hollow materials is implemented by template directed synthesis. The size and the shape of the hollow materials are solely determined by the shape and dimensions of the template. There are two types of templates, (i) hard, and (ii) soft templates that are usually used to fabricate hollow spheres with homogeneous, dense layers. In the hard-template assisted synthesis inorganic or organic solid particles such as polymer,[40] carbon,[41] and silica spheres [42] are commonly used as colloidal templates. These templates are advantageous for several reasons including their narrow size distribution, ready availability in relatively large amounts, availability in a wide range of sizes from commercial sources, and simplicity of their synthesis using well-known formulations. Other colloidal systems, such as carbon nanospheres and nanoparticles of metals and metal oxides, have also been used as templates for preparation of hollow structures. The template particles were subsequently

etched or removed by selective dissolution in an appropriate solvent or calcination at elevated temperature in air to generate hollow structures. In the soft-template assisted synthesis, the templates used mainly include liquid crystals, surfactant vesicles, polymer micelles, microemulsion droplets and even gas bubbles have been used.[43-45]

## 1.3. Fabrication methods of the inorganic hollow materials

Up to now, several excellent articles have reviewed the progress of micro- and nano hollow inorganic materials with respect to architectural design and synthesis. Before 1998, most hollow particles were of spherical shape and were synthesized using methods suitable for controlling structure on the macro- and nano-scale, such as spray-drying and gas-blowing.[46] *Matijevic´* and coworkers as early as the 1980s, presented core/shell type colloids, primarily in the context of surface functionalization.[47] These efforts demonstrated the use of the simple sol–gel-based approaches for coating Au and Ag nanoparticles with silica[48,49] and in 1998 *Caruso et al.*[50] presented the colloidal templating synthesis of hollow spheres for the first time. This heralded a new, more versatile, synthesis strategy for hollow structures based on hard-templating methods. Because these methods can be used to fabricate hollow structures from templates of essentially any size, shape, and chemistry, they have dramatically expanded the range of hollow particles available for applications. In fact, starting around 2001, there has been a large increase in research activity focused on synthesis of hollow micro-/nanostructures based on templates, hard and soft, utilizing shells of a wide range of chemistries.[51- 52] These advances have in turn catalyzed applications and fundamental research on nanostructured materials in a wide range of fields, such as biomedical engineering, chemical catalysis, energy storage, and photonics.

Generally, hollow systems fabrication usually involves the preparation of core@shell composite particles, followed by the removal of the cores. Such hybrid particles can often be fabricated by controlled precipitation of inorganic precursors of the desired hollow materials onto the core particles. In another approach, small particles of the coating material are deposited on the cores. this is performed, for instance, in the layer-by-layer self-assemmbly route, in which case successive layers of anioinic particles were deposited, alternated by layers of cationic polymer.[46,47] Several templating agents have been used in synthesis of inorganic hollow materials such as silica,[42] gold,[53] AgCl,[54] calcium carbonate,[55] Ag nanoparticles,[56] hematite,[57] polystyrene (PS) latex,[40] polymethylmetacrylate (PMMA),[58] chitosan-polyacrylic acid (CS-PAA),[59] and n-propyle amine.[60] The template can be removed by soaking the core in appropriate solvent (in case of inorganic templates), or calcination in case of organic templates. Due to the limitations related to their polydispersity or difficulties concerning the coating procedures, a considerably smaller number of methods have used liquid cores as templates for the coating. These were either emulsion droplets, or vesicles.[43,44] based on the kind of desired coating, the resulting hollow shells have been made of diverse materials.

The sacrificial templating methods for the fabrication of the inorganic hollow materials based on the sacrificial cores and core@shell composite preparation can be classified into categories based on the origin of the core such as (i) organic templating method which is designed to use organic materials such as PS and PMMA and the organic cores are removed by calcinations or exposing to solvent,[40] (ii) inorganic templating method which is based on the use of nano-sized inorganic material (e.g. silica) as the sacrificial core to prepare hollow sphere particles followed be removal of the inorganic core by acid solution,[42] (iii) emulsion templating method which is designed to produce hollow structure by inheriting the emulsion template.[45]

In this section we present a comprehensive overview of the various common techniques used for the fabrication of the micro- and nano hollow inorganic materials, with particular emphasis on the sacrificial templating methods.

### 1.3.1 Layer by layer assembly strategy

The layer by layer (LbL) templating technique is of particular interest as a simple, highly versatile approach that has been widely used to fabricate hollow nanostructured materials with tailored properties due to the benefits of allowing multiple layers of different functional materials to be coated onto a sacrificial template particle. The process involves the sequential deposition of species, such as polymers, nanoparticles, lipids, proteins, and dye molecules, onto various templates. Subsequent template removal results in free-standing hollow structures. Although fine control of the material properties (e.g., size, composition, thickness, permeability, function) is afforded by the type of species LbL assembled, the morphology and composition of the templates also play a crucial role in determining the properties, and hence potential applications, of the materials generated.

Layer-by-layer method developed by *Decher* [61] in early 1990s has been applied to three-dimensional templates and since the pioneering work done by *Caruso et al.*[62] the layer-by-layer (LbL) assembly technique has rapidly expanded to become a premier method for the preparation of nanoscale films with tailored properties and extensively used to obtain hollow shells of inorganic materials.[63] This method permits unprecedented control over capsule properties such as size, composition, thickness, permeability, function through the choice of the sacrificial colloids and the coating components.

Typically, as shown in Fig.1.1 the LbL process starts with the adsorption of a charged species onto a substrate of opposite charge, thereby reversing the

substrate surface charge. Further layers are then deposited by the alternate adsorption of oppositely charged species onto the substrate, until the desired film thickness is achieved.

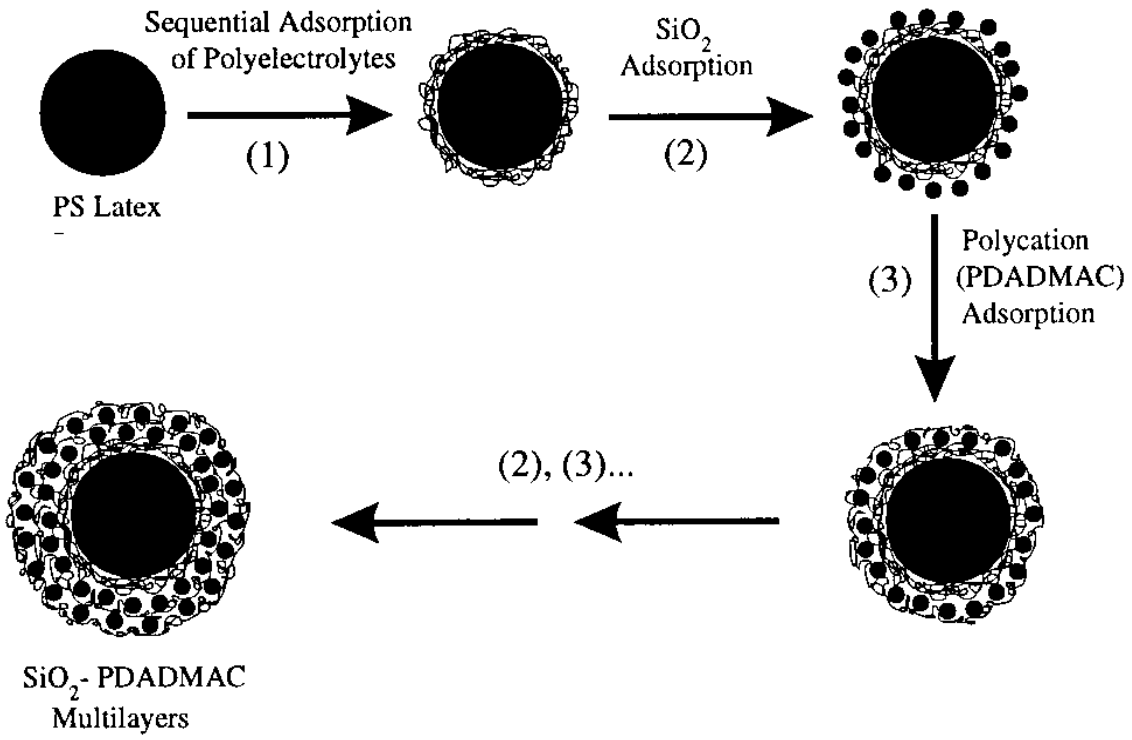


**Fig.1.1** *Schematic illustration of the assembly of composite multilayers on PS beads as presented by Curoso et al. in 1998 , The first stages involves the sequential adsorption of oppositely charged polyelectrolytes (PDADMAC [poly( diallyldimethylammonium chloride)] / PSl / PDADMAC) in order to produce a smooth surface and facilitate the adsorption of negatively charged $SiO_2$. Subsequent alternate adsorption of SiO2 (step2) and PDADMAC (step3) result in $SiO_2$- PDADMAC multilayers being formed on the PS latices [from ref. 62]*

The versatility of the LbL approach has allowed a broad range of materials (e.g., polymers, nanoparticles, lipids, proteins, dye molecules) to be

assembled on various substrates, on the basis of not only electrostatic interactions but also hydrogen bonding, hydrophobic interactions, covalent bonding, and complementary base pairing.[61,65] The properties of LbL films, such as composition, thickness, and function, can be readily tuned by simply varying the type of species adsorbed, the number of layers deposited, and the conditions employed during the assembly process.[61,65-66] Removal of the templating substrate following LbL film formation can give rise to free-standing nanostructured materials with different morphologies and functions. This approach known as the LbL templating technique.[66]

*Caruso and coworkers* [64] have presented their pioneer result on the synthesis of hollow silica and silica- polymer spheres by LbL self assembly approach. Their first step involved the deposition of three layers poly (diallyldimethylammonium chloride) (PDADMAC) film onto the negatively charged polystyrene (PS) latex particle. This film provides a positively charged surface to aid subsequent adsorption of $SiO_2$. The $SiO_2$- PDADMAC multilayer films wre then formed by alternate adsorption of $SiO_2$ and PDADMAC. The PS core was subsequently removed by thermal treatment at about 500 $^oC$. *S. Sadasivan,et al.* have used the layer-by-layer approach to deposit preformed mesoporous silica nanoparticles onto polystyrene beads to form silica macrospheres. After that they have obtained silica hollow sphere after etching the core by calcination.[67] *Zhang et al.* have fabricated $SnO_2$ hollow spheres by LbL approach, using silica spheres as a template. The as-synthesized $SnO_2$ hollow spheres have been applied in lithium-ion battery and show improved performance compared with $SnO_2$ nanoparticles.[68] The approach has been extended to fabricate other metal oxide and sulfide hollow spheres as $In_2O_3$ and ZnS. Several inorganic molecular precursors have been used for the fabrication of inorganic capsules via LBL colloid templating technique. For instant, $TiO_2$ capsules were obtained by coating PS particles with alternate layers of the water-stable titanium precursor, titanium (IV) bis(ammonium lactate) dihydroxide (TALH), after which the template and the polycation were decomposed by calcinations.[69]

### 1.3.2 Sol-Gel method

Sol-gel technique has been widely used for the coating of colloidal templates and then forming hollow structures by removing templates. This is because of the simplicity, versatility and ease of control over particle size and shell thickness that can be performed through the sol-gel approach. *Sols* are dispersions of colloidal particles in a liquid. *Colloids* are solid particles with diameters of 1-1000 nm. A *gel* is an interconnected, rigid network with pores of submicrometer dimensions and polymeric chains whose average length is greater than a micrometer.[70]

$SiO_2$ and $TiO_2$ hollow capsules are considered among the most reported hollow materials in the literature that formed by the sol-gel reaction. Hollow titania spheres were obtained by coating PS beads by templating the sol-gel precursor solution against crystalline PS beads. The PS template was removed by soaking the composite in toluene to obtain mesoscale titania hollow spheres.[71] *Li et al.* have reported the synthesis of $TiO_2$ hollow particles utilizing sulfate-stabilized PS particles as a template in conjunction with the sol-gel methods.[72] *Bourgeat-Lami et al.* fabricated composite particles with PS as the core and silica as the shell via an ammonia- catalyzed sol-gel process. In a subsequent step, the PS cores were removed and hollow $SiO_2$ spheres were formed by thermal treatment at 600 $^{o}$C.[73] *Kim et al.* used these surface-modified PS spheres as sacrificial template to fabricate silica-coated PS and titania- coated PS composites by co-condensation between hydroxyl groups with tetraethyl orthosilicate (TEOS) and titanium(IV) isopropoxide (TIPP) in a sol-gel process, respectively. The hollow silica and titania can be generated by the subsequent removal of the PS core using tetrahydrofuran. *Li et al*.[74] reported a novel method for preparing hollow silica nano-spheres with a porous shell structure via the sol–gel route and using inorganic $CaCO_3$ nanoparticles as templates, and the produced PHSN were applied as a carrier to study the controlled release behaviors of Brilliant Blue F (BB), which was used as a model drug.

Recently, *Wu et al.*[75] reported the fabrication of hollow titania spheres via a one-step process. In that method, aqueous ammoniacal alcohol was used as the catalyst and medium. Monodisperse positively charged PS particles were prepared by dispersion polymerization using the cationic monomer 2-(methacryloyl)ethyltrimethylammonium chloride as the comonomer, which ensured that the generation of titania sol from the hydrolysis and the condensation of tetra-n-butyl titanate (TBT) could be rapidly captured by PS particles via electrostatic interaction in aqueous ammoniacal alcohol medium at 50 $^{o}$C. Under these conditions, PS particles were “dissolved” subsequently and even synchronously to directly form titania hollow spheres, as shown in Fig.1.2 the formation of the inorganic shells and the dissolution of core template spheres occurred in the same media; neither additional dissolution nor calcination process was used to remove the PS cores. Ammonia was not only used as the catalyst in the sol-gel reaction of TBT, but also served as a key parameter to “dissolve” the PS template particles.

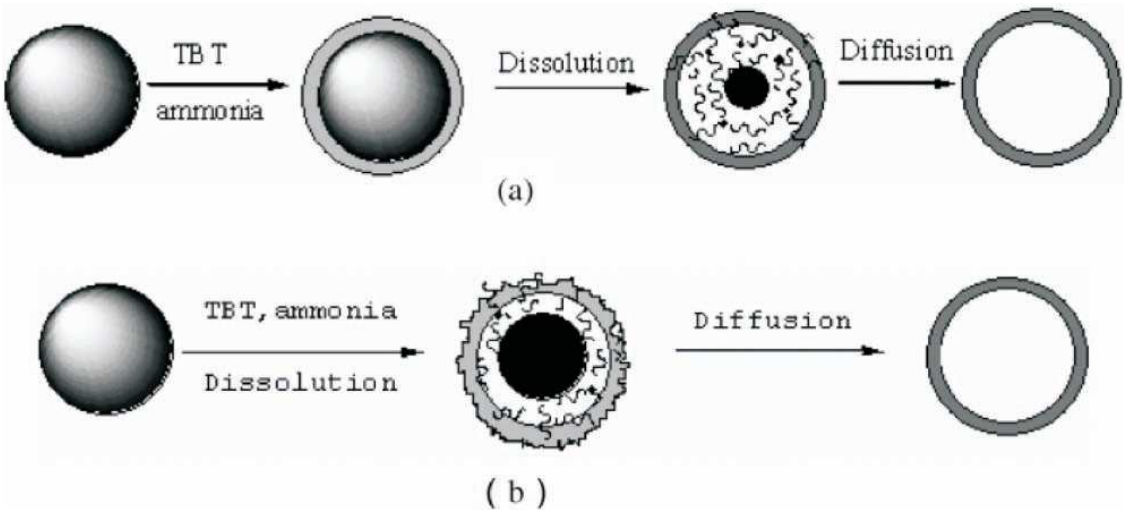


**Fig.1.2** *Schematic illustration of the formation mechanism for hollow titania spheres: (a) titania-formed and PS-dissolved subsequently, and (b) PS-dissolved and titania formed synchronously [from ref. 75]*

### 1.3.3 Hydrothermal method

Crystalline metal oxides hollow spheres were fabricated through hydrothermal approach in simple one-pot synthesis. The metal salts and the carbohydrate solutions jointly added into water, followed by a hydrothermal treatment and then calcination, hollow spheres of various metal oxides, such as $Ni_2O_3$, $CeO_2$, MgO, and CuO, were obtained.[76] The method involves the initial absorption of metal ions from the solution into the functional surface layer of carbonaceous saccharide microspheres; these are then densified and cross linked in a subsequent thermal treatment and oxidation step to produce metal oxide hollow spheres. The hollow spheres exhibit diameters from one to several micrometers and consist of nanocrystals of the respective metal oxides.

*Y. Dia et al.*[77] reported the fabrication of $Fe_2O_3$ hollow spheres with novel cage-like architectures by a controlled hydrothermal precipitation reaction of $FeCl_3$ in the presence of urea, ethanol, and carbon spheres, and then calcined at 500 $^oC$. The obtained $Fe_2O_3$ hollow spheres showed a good visible-light photocatalytic activity for the photocatalytic decolorization of RhB aqueous solution under the visible-light illumination in the presence of $H_2O_2$. Due to the unique cage-like hollow structures, the prepared $Fe_2O_3$ hollow spheres are also of great interest in sensor, lithium secondary batteries, solar cell, catalysis, separation technology, biomedical engineering.

*Yadong Li* and coworkers used polysaccharides as template for the fabrication of metal oxides hollow spheres through hydrothermal method. Series of oxides hollow spheres have been fabricated in micro scale (e.g. $ZrO_2$, SnO, $TiO_2$, $Ga_2O_3$, CoO and $Y_2O_3$). The sacrificial cores have been removed and the hollow oxides were obtained after the calcinations of the as-prepared composite materials at 500 $^oC$.[28]

### 1.3.4 Nanocasting from mesoporous shells

Hollow spheres with mesoporous shells (HSMS) can be prepared using spherical templates with solid core and mesoporous shell (SCMS) structure. Fig.1.3 illustrates the general approach. This method requires that the shell materials (usually precursors) efficiently impregnate into the mesoporous shells. SCMS silica templates are most commonly used, which can be facilely prepared by incorporating a suitable porogen agent (e.g., n octadecyltrimethoxysilane)[78] during the conventional synthesis of silica particles by the *Stöber's* method.[79] Carbon HSMS have been prepared by infiltrating and carbonizing different polymers such as phenol resin and poly(divinylbenzene) inside the mesopores of SCMS silica template.[80]


**Fig.1.3** *Schematic illustration of a nanocasting process for the hollow spheres fabrication with mesoporous shells [from ref. 80]*

### 1.3.5 Precipitation method

Precipitation method involves the precipitation of the precursors of the desired materials into the sacrificial template particles via various chemical or physical interactions with the template. Generally, the precursor metal cations are first precipitated on the template surface in the form of hydroxide or other intermediate phases through controlled hydrolysis under basic conditions. The

precipitation process is typically followed by thermal treatment to remove the cores and obtain hollow structures with compacted metal oxide or metallic shells.

The controlled precipitation method has been pioneered by *Matijević* for fabrication of uniform size colloids as well as and hollow particles.[47] NiO hollow particles with a hierarchical structure have been fabricated via controlled precipitation of $Ni(OH)_2$ nanoflakelets on PS templates and subsequent calcination .[38] $Fe_2O_3$ hollow spheres with a novel cage-like structure have been also fabricated through a simple wet precipitation route.[81] $Fe_2O_3$ microcages, with uniform size and diameters of about 620 nm, have been successfully prepared by applying styrene acrylic acid (PSA) copolymer latex particles as the sacrificial template. The method involves the deposition of $Fe(OH)_3$ coatings on the surface of latex particles and subsequent removal of the latex particles by calcinations.

Metal oxide (NiO, ZnO, CuO and $Ga_2O_3$) hollow spheres have been Fabricated by using carbonaceous polysaccharide nanospheres as hard templates by controlled precipitation followed by calcination.[82] *Imhof* reported the fabrication of hollow spheres of $SiO_2$, $TiO_2$, and $ZrO_2$ by controlled hydrolysis of their metal alkoxide precursors in the presence of template particles, followed by removal of the templates. Control of the hydrolysis rate and heterocoagulation is crucial for the success of the process. This synthesis demands strict control of the reaction conditions to obtain smooth shell coatings.[83]

*Wu* and co workers reported the fabrication of ZnO hollow spheres through precipitation route. Sulfonated PS core-shell gel spheres were used as templates and $Zn(Ac)_2 \cdot 2H_2O$ as ZnO precursor. Zinc ions were first adsorbed onto the surfaces of template spheres *via* electrostatic interaction and then reacted with NaOH to form a ZnO crystal nucleus, which was followed by the growth step to form ZnO nanoshells. The sulfonated PS core-shell gel spheres were “dissolved” in the same media during the coating process or later on to form

ZnO hollow spheres directly. The wall thickness and the size of the ZnO hollow spheres could be easily tailored by altering the concentration of $Zn(Ac)_2 \cdot 2H_2O$ and the size of the template spheres, respectively.[84]

### 1.3.6 Soft templating method

Sacrificial templating methods applying hard (solid) templates could be considered the most effective, and certainly the most common method for synthesizing hollow micro-/nanostructures. However, another special class of sacrificial template synthesis method for obtaining hollow spheres, soft template synthesis has been widely employed for general fabrication of metal hollow structures and has attracted the greatest attention and significant progress has been made in the past decade. Some hollow inorganic spheres with nanometer to micrometer diameter have been successfully fabricated using these templates. The commonly used soft templates, including emulsion droplets, surfactant and other super-molecular micelles and gas bubbles.

Emulsion is formed when two immiscible liquids are mixed together through mechanical agitation (e.g., shaking, stirring), liquid droplets of one phase can be dispersed in the other continuous phase. In general, emulsions are thermodynamically unstable, thus surfactants or amphiphilic polymers, which self-assemble at the interface between the droplets and continuous phase, are required to increase kinetic stability.[85-86] Oil-in-water (O/W) or water-in-oil (W/O) emulsions are most commonly employed. The emulsion polymerization, where the droplets act as micro-reactors, has long been used to fabricate solid and hollow polymer spheres.[87] The basic idea here is to deposit the shell materials exclusively around the interface between the emulsion droplets and the continuous phase. The precursor of shell materials can initially exist in either the continuous phase or the droplets or both phases, depending on the chemistry chosen.

*L. Song et al.*[60] reported synthesis of pours hollow silica (PHS) in a water–oil (W/O) reverse emulsion system, at room temperature, that employs a water-soluble amine as catalyst and tetraethylorthosilicate (TEOS) as the silica source. Their findings showed that the pH value of the aqueous phase and the viscosity of external oil phase were found to be the key factors contributing to the formation of stable and regular spherical silica hollow particles. During the synthesis of the PHS in (W/O) reverse emulsion, there are three main steps as shown in Fig.1.4: (1) the association of TEOS with W/O emulsion; (2) TEOS hydrolysis and formation of monomers at the W/O interface; (3) condensation of monomeres and silica nucleation in-situ.

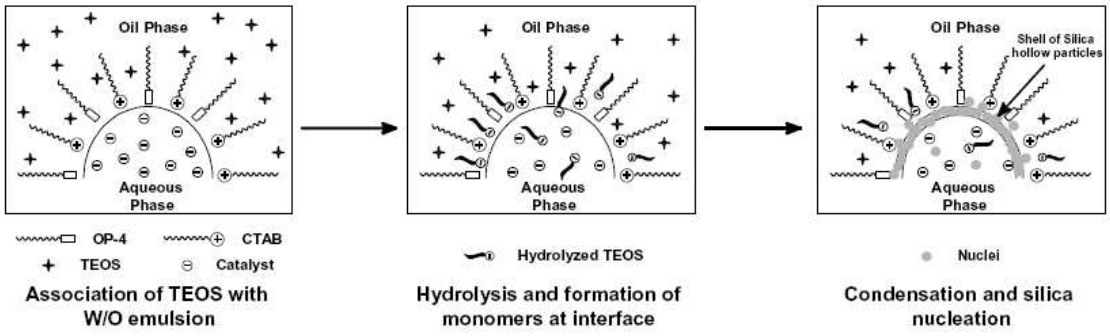


**Fig.1.4** *The schematic illustration of process of silica hollow particles' formation in W/O emulsion [from ref. 60]*

Gas bubbles are another soft template for the preparation of hollow capsules. *Xie et al.* have synthesized rutile-phase $TiO_2$ hierarchical hollow spheres using potassium titanium oxalate as the precursor, which could releases $O_2$ during the reaction. The spheres exhibited unique three-dimensional hierarchical architectures and demonstrated a significantly improved photocatalytic performance.[88]

### 1.3.7 Sonochemical route

Ultrasound is an important synthesis tool in liquid-solid chemical reactions. The chemical effect of the ultra sound is due to the acoustic cavitation, that is, formation, growth and implosive collapse of gas-filled micro-bubbles in a liquid subjected to ultrasonic irradiation.[89] During cavitation, bubble collapse produces intense local heating, high pressure, and very short lifetimes; these transient, localized hot spots drive high-energy chemical reactions. These hot spots have a temperature of ~ 5000 $^{o}$C., pressure of about 1000 atm and cooling rates above $10^{10}$ K/s.[90-91] Near a solid surface, bubble collapse becomes non-spherical, driving high-speed jets of liquid into the surface creating shockwave damage to the surface. During the sonication of liquid-powder slurries, cavitation and shockwaves it creates can accelerate solid particles to high velocities. The interpretable collisions that result are capable of inducing striking changes in surface morphology, composition, and reactivity.

Some authors reported the fabrication of hollow particles through ultrasonic synthesis which appears effective route for production of such class of material. Synthesis of PbS hollow nanospheres with diameters of 80–250nm were reported by a surfactant-assisted sonochemical route from Pb(Ac)2, thioacetamide, and sodium dodecylbenzenesulfonate (SDBS).[92] The ultrasound wave promotes assembly of SDBS molecules at the gas/liquid interface of the microbubble to form template structures, which directly determine the diameter of the final PbS spheres. CdSe hollow particles were fabricated by ultrasonically induced reactions between initial precursors at the gas/liquid interface of the cavitation microbubble.[93] Also CdSe hollow spheres with sizes of 100–200nm have previously been fabricated by a SDS-assisted sonochemical approach.[94] *Cai et al.* have presented an interesting CTAB-assisted sonochemical method for synthesis of biocompatible nearly amorphous calcium phosphate hollow nanospheres with average diameter of about 145 nm.[95] Importantly, the method also enables facile encapsulation of drug molecules.

### 1.3.8 Template free method

The fabrication of hollow structures is generally based on direct sacrificial templating methods, in which hard or soft sacrificial templates were used to create a hollow structure. As alternative to direct template methods, hollow inorganic particles have been developed by employing template free methods based on chemically induced transformations.[96]

Direct synthesis of silica coated α-$Fe_2O_3$ hollow spheres via aerosol pyrolysis method with sizes of 50–250 nm from a methanol solution containing iron ammonium citrate and TEOS has been reported.[97] As illustrated in Fig.1.5 the rapid evaporation of the methanol solvent, during the first stage, favors the surface precipitation (i.e., formation of hollow spheres) of the components. The low solubility of the iron ammonia citrate in methanol, compared to that of TEOS, promotes the initial precipitation of the iron salt solid shell. With the continuous shrinkage of the aerosol particles, iron salt and TEOS enrich at the surface, which eventually decompose to produce silica coated α -$Fe_2O_3$ hollow spheres.

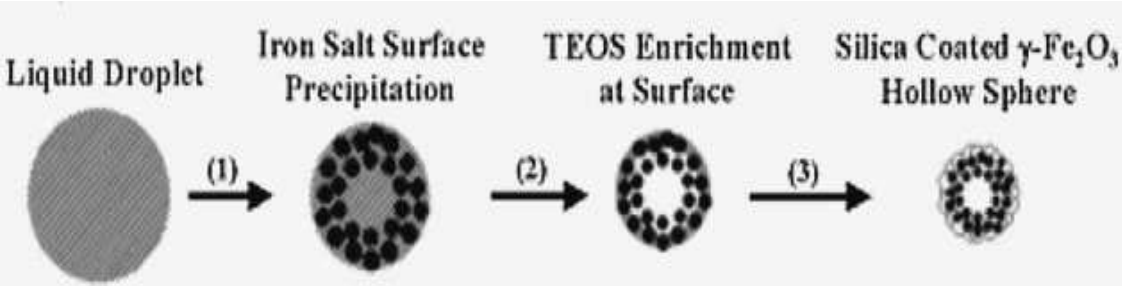


**Fig.1.5** *Schematic illustration of the direct formation of silica coated α -$Fe_2O_3$ hollow spheres. [from ref. 97]*

Another example for the free template method, *Mao et al.* have recently prepared high-quality $V_2O_3$ hollow spheres with controlled sizes of 0.2–1.1 µm by

simply heating vanadium(IV) acetylacetone dissolved in DMF at 210 $^{o}$C for 18h.[98] Moreover, these low-valent $V_2O_3$ hollow spheres can be thermally converted to $V_2O_5$ hollow spheres.

### 1.3.9 Some uncommon techniques

As another special method of sacrificial template synthesis, *galvanic replacement reactions* have been employed for general preparation of metal hollow nanostructures in a variety of shapes and sizes. In a typical reaction, the salt of a more noble metal (B) is reduced with preformed nanocrystals of a less noble metal (A), resulting in deposition of B on the surface of A. Upon complete consumption of metal A, hollow structures of metal B can be obtained under controlled conditions. The shape and cavity size of the derived hollow structure are then largely determined by the sacrificial nanocrystals of A.[99-101] Many reports have been published for the preparation *of* various metals (Au, Pt, Pd) hollow nanostructures in both aqueous and organic solutions through galvanic replacement reactions with Ag nanocrystals of sizes ranging from <10nm to several hundred nanometers.[99-101]

Recent progress has shown that hollow nanostructures can be readily synthesized by using the nanoscale *Kirkendall effect*.[102] This effect was initially proposed to describe the formation of voids at the interface of two bulk materials due to their different inter-diffusion rates.[103] In a nanoparticle system, the *Kirkendall* effect refers to preferred outward elemental diffusion leading to a net material flux across the spherical interface and the consequent formation of a single void at the center.[104] The first report rely on the exploitation of the *Kirkendall* effect was the preparation of hollow CoS nanoparticles by sulfidation (oxidation) of Co nanoparticles .[105] *Shouheng Sun et al.* reported a solution-phase synthesis of monodisperse hollow $Fe_3O_4$ nanoparticles by controlled oxidation of Fe–$Fe_3O_4$ nanoparticles. They nicely have demonstrated that hollow

nanoparticles with controllable size are formed due to the nanoscale Kirkendall effect, and the synthesis can be readily extended to produce various core–shell–void nanoparticles. The hollow $Fe_3O_4$ nanoparticles were prepared by controlled oxidation of amorphous core–shell Fe–$Fe_3O_4$ nanoparticles. The core–shell particles were obtained by high temperature solution-phase decomposition of [Fe(CO)5] and air oxidation of the amorphous Fe nanoparticles at room temperature as shown in Fig.1.6.[106]

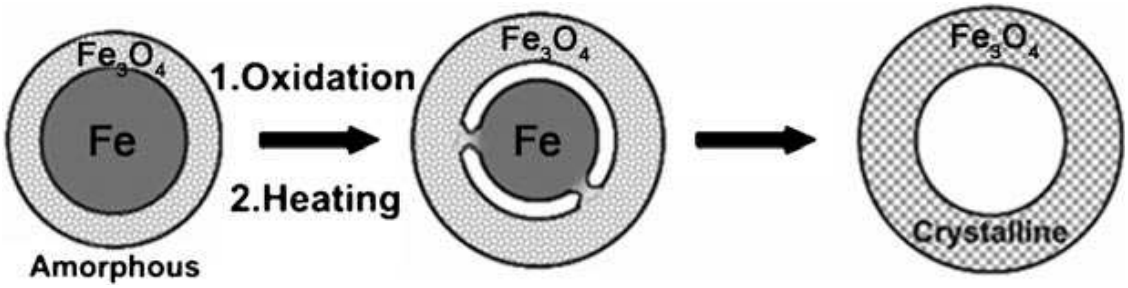


**Fig.1.6** *Synthesis of core–shell–void Fe–$Fe_3O_4$ and hollow $Fe_3O_4$ nanoparticles from Fe–$Fe_3O_4$ nanoparticle seeds based on kirkendall effect [from ref. 106]*

Another synthesis tool, spray pyrolysis has been applied for the fabrication of variety of materials such as metals, metal oxides, superconducting materials, fullerenes, and nanophase materials. *Messing et al.* have reported the formation of particles with different morphology using a variety of spray pyrolysis techniques.[107] They presented that the spray pyrolysis methods can be applied to produce dense (solid), hollow, porous or fibrous particles, and even to deposit thin film, as well as, the formation of hollow spherical particle.

## 1.4. Pitfalls and limitations of the synthesis methods

In accordance with the foregoing sections, it is obvious that, as a group templating methods have proven very effective and versatile for synthesizing a

wide array of hollow structures. Although the above mentioned works are very interesting, templating and free templating approaches have several intrinsic disadvantages. For example, hard templates have several intrinsic disadvantages, which are related to high cost, the inherent difficulty of controlling the homogeneity and the thickness of the coating process and high impurity levels which are related to the tedious multistep synthesis procedures, thus the preparation processes seem to be time-consuming. As a result, multi-step processes do not only significantly complicate the process, but also detrimentally affect the quality of the as-derived hollow particles.

Moreover, fabrication of non-spherical inorganic hollow structures through hard templating approaches exhibits more challenges. These stem from the difficulty in forming a uniform coating around surfaces with large variation in curvature to the paucity of non-spherical templates available for the synthesis. Because of these difficulties, reports on synthesis of non-spherical inorganic hollow structures are relatively few, and there is no established general method.[108-109]

Microemulsion templating approaches (soft templating approaches), involves the use of surfactant micelles/vesicles and the structure and stability of them are sensitive to many parameters, such as pH, temperature, concentration, solvent, additives, and ionic strength. Therefore, this required many handles to manipulate particle characteristics (e.g., size, shape, shell thickness, and morphology); as a result this sensitivity makes it difficult to control the synthesis. Also, gas bubbles as soft templates are a complex process, which is affected by many factors, such as particle surface properties, particle size, electrostatic interactions, and hydrodynamic conditions.[110]

In other syntheses, such as LbL approaches which are versatile and widely applied for the synthesis of hollow structures, it is not easy by applying LbL methods for fabrication of smaller inorganic hollow structures with particles

diameter less than 200 nm .[64] In addition, sonochemical approaches suffer from two key shortcomings. First, it involves applying of high intensity ultrasound that leads to high velocity collisions between particles in the reaction solution.[111] As a result, they make it hard to obtain the proper coating around the core particles and probably lead to the formation of incomplete hollow structure with broken shells. Second, hollow particles obtained through this method generally lack the mechanical robustness of particles prepared using other approaches. In nanocasting method, the obtained hollow materials are largely interconnected, since the method cannot ensure exclusive infiltration of the desired material precursors into the mesopores of the cores.[80]

In the light of these observations we can summarize some significant limitations in the next points:-

1. Previously mentioned methods are found to be slow process and time consuming.
2. Many efforts are required to separate the core/shell NPs from large amount of surfactant associated with micro-emulsion system.
3. The cost of the sacrificial templates.
4. Precipitation method is difficult to be controlled (Many factors pH, T, precipitation agent and solution concentration).
5. There is no systematic approach to control the hole size or maintaining the regular structure of the inorganic hollow materials without any collapse of the regularity of the morphology and inevitable shell collapse.

These limitations have prompt interest in simpler synthesis approaches for production of hollow inorganic materials. Therefore, developing a facile simple way to prepare hollow NPs with controlled void size and regular morphology remains a challenge to material scientists.

## 1.5. Carbonaceous spheres as sacrificial templates

Carbonaceous materials are derived from organic precursors with high carbon contents (e.g. carbohydrates). In recent years, the discovery of new forms of carbon [112] such as fullerenes [113] and carbyne-like one dimensional structure,[114] has greatly promoted the investigation of carbonaceous materials. X*uejie Huang et al.* were the first to use hydrothermal method to prepare the hard carbon spheres with smooth surface.[115]

Commonly, the carbonaceous materials synthesized through hydrothermal hydrolysis of carbohydrates inherit high functionalities on their surface layers due to the partial or incomplete hydrolysis of some sugar particles.[28,76,82] Despite many elegant reports are published presenting the hydrothermal hydrolysis of the carbohydrates, the mechanism of the formation of the carbonaceous spheres remains an open question for the material scientists.[116]

Hollow particles of metal oxides (e.g CuO, $Ga_2O_3$, CoO, $Al_2O_3$, $Y_2O_3$, $TiO_2$ $CeO_2$, MgO, NiO) can be synthesized using carbonaceous particles as sacrificial template.[28,76,82] The sacrificial templates then get removed thermally, generally above 500 $^oC$. The hollow spheres exhibit diameters from one to several micrometers and consist of nano-crystals of the respective metal oxide. The details of the synthesis vary a lot in literature. One attempt to create a general procedure for the synthesis of hollow metal oxide particles uses salts and µm-sized carbonaceous particles in aqueous solution. Since soluble salts are available for many metals, the procedure can be extended on other metal oxides of interest.[82,117]

The carbon particles can be synthesized prior to coating with the metal salt, but interestingly it can also be performed as a one-pot synthesis. The carbon template is produced by hydrothermal carbonization of saccharide like glucose at 170- 240 $^oC$.[118] If the metal salt is present during the synthesis, the

particle will be coated. The template is removed by calcination around 500 $^{o}$C, leaving a shrunk shell of metal oxide behind. This easy procedure uses cheap starting materials, making it appealing for industrial use.[76]

During the hydrothermal carbonization, the saccharide undergoes dehydration and fragmentation, which is followed by aromatization and polymerization of molecules. The latter can for example happen via aldol condensation. The products of the reaction are soluble organic compounds like acetic acid, but here more important also insoluble carbonaceous spheres. These spheres have a highly aromatic core and a saccharide like, hydrophilic surface. The carboxy-groups and derivates as well as the double bonds can be seen in infra red spectra as shown in Fig.1.7.[119] This automatic surface functionalization during synthesis is an advantage compared to e.g. polystyrene particles.

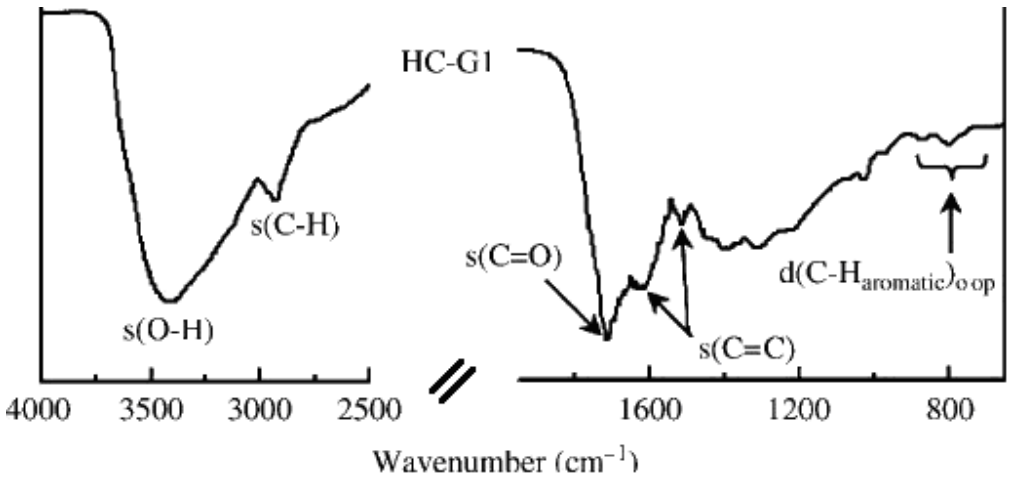


**Fig.1.7** *FTIR spectra of carbonaceous sample obtained by hydrothermal treatment of saccharides [From ref. 119]*

The carbon spheres are uniform in size (~1μ) and addition of metal salt yields higher particle as well. The metal ions adsorbed onto the hydrophilic surface and can undergo oxidation during the calcination. During thermal treatment, the forming metal oxide densifies and crystallizes.

## 1.6. Some common applications of inorganic hollow particles

Hollow micro-/nanostructures possess unique properties such as low density, large specific surface area, porous structure and hollow cores. Their capacity for encapsulating sensitive materials such as therapeutics and fluorescent markers, have been investigated by many groups for drug delivery and biomedical imaging as well as their ability as a catalyst support.

The applications of hollow nanoparticles in a variety of biomedical applications, such as drug delivery, cell imaging, and sensing of biomolecules, have been reported in several recent excellent articles.[119–121] Silica is widely used for drug/gene delivery, because of its non-toxicity, biocompatibility, biodegradability, thermal stability and chemical stability.[122,123] Porous hollow silica nanoparticles (PHSNPs) have been investigated as a carrier to study the controlled release behavior of a model drug.[122,123] The drug was loaded into the cavity and on the surface of the hollow nanoparticles, and it was observed that typical sustained release pattern without any burst effect.[123] Because of surface functionalization accessibility for both inner and outer walls of PHSNPs, additional functionalities could be added to the silica hollow particles to obtain products with special properties.

Hollow nanoparticles have also been used for delivering genetic material to cells. Synthesis of hollow calcium phosphate nanoparticles loaded with DNA was reported.[124] The transaction efficiency of these particles was shown to be significantly higher than that of the simple DNA-coated calcium phosphate

nanoparticles. In principle, different layers are able to deliver different agents sequentially, offering additional flexibility for the delivery system.

Hollow inorganic nanoparticles such as hollow gold or hollow magnetite nanoparticles could be used as imaging and diagnosis agents because of their unique optical/magnetic properties. *Chen et al.*[125] reported the use of gold nanocages (hollow nanostructures with porous walls) as optical imaging contrast agent for optical coherence tomography (OCT).

Progress in synthesis of hollow particles has provided opportunities for their wide use in catalysis. Some catalysts and co-catalysts are usually prepared with the utilization of support in order to get monodispersed active sites and to reduce the amount of consumed catalysts and co-catalysts. Therefore, it is extremely important to obtain a catalyst system where the active sites are distributed evenly and not just simply immobilized at the external surface of the support. As an elegant example of catalyst application, matallocene catalysts are considered as a major breakthrough in polyolefin technology.[126] *Li-Xiong Wen* and co workers have reported the use of porous hollow silica nanoparticles (PHSNPs) as a catalyst support for olefin polymerization catalyst (metallocene). They have presented that if PHSNPs are applied as the catalyst support, the active sites will be immobilized on the external surface, the pore channels as well as the internal surface of the support and as a result many more active sites can be supported on some amount of porous hollow supports as compared with their solid counterparts. In this way, a high yield of polyolefin can be achieved with an acceptable amount of support and catalyst.[127]

Moreover, hollow nanoparticle catalysts are playing an increasingly important role in electrocatalytic and photocatalytic reactions.[128,129] There are a number of reports on utilizing hollow metal/metal oxide nanoparticles in the electro-oxidation of methanol/ethanol/formic acid. For example, *Liang et al*.[130] have shown that Pt hollow nanospheres exhibit twice the catalytic activity for

methanol oxidation of solid Pt nanospheres with roughly the same size. Other groups [131,132] also reported that hollow particles (or noble metal catalysts supported on hollow structures) frequently showed enhanced electrocatalytic performance in these electroxidation reactions, which could be because of the larger electrochemical surface area and the ability of the empty core domain to accommodate larger number of guest molecules or guests with large size. Hollow $TiO_2$ nanospheres have been reported by several groups to exhibit high activities and as such have been targeted as the active electrode component in high-efficiency dye-sensitized solar cells.[133,134] α-$Fe_2O_3$ hollow nanospheres, for example, have been shown to yield improved photocatalytic performance over α -$Fe_2O_3$ nanocrystals in oxidation of salicylic acid.[135]

A considerable attention has been paid to environmental problems including organic pollutants and water treatment in recent years. As clean water, free from toxic chemicals and pathogens, is vital to the world health and critical feed stock in variety of industries. It is expected that hollow structures will have high removal capacity compared to bulk materials. Metal oxides hollow spheres (e.g., $TiO_2$, $Cr_2O_3$) have also been widely investigated for the removal of organic pollutants and water treatment.[88,136-138]

## 1.7. Aim of the work

The previous synthesis methods of the hollow inorganic materials mentioned before were found to be slow processes and mechanical stirring is necessary to obtain uniform oxide shell on the surface of the sacrificial templates. Many efforts are required in order to separate the core-shell nano-particles (NPs) from large amounts of surfactant associated with micro-emulsion system.

In addition, there is no systematic approach yet for controlling the void size or maintaining a regular structure of hollow oxide particles without any collapse of the regularity of the morphology. Therefore, developing a facile simple strategy to prepare hollow oxide nano-particles with controlled void size and regular morphology remains a challenge to materials scientists.

Due to unique properties of the hollow inorganic materials and their academic and technological importance, we intended to present a facile, environmental benign, economical sustainable and additive free synthesis protocol for the fabrication of hollow oxides which ultimately could enable the fine-tuning of the hollow material.

## References


1- A. Hett, *Nanotechnology. Small matter, many unknowns*, Zurich: Swiss Reinsurance Company (2004).

2- M. Ratner, D. Ratner, *Nanotechnology. A Gentle Introduction to the Next Big Idea*, Upper Saddle River, New Jersey, US: Prentice Hall (2003).

3- B. Bhushan. *Hand book of nanotechnology*, Springer-Verlag Berlin Heidelberg, Germany (2004)

4- K. M. Ryan, A. Mastroianni, K. A. Stancil, H.T. Liu, A. P. Alivisatos, *Nano Lett*. **6** (2006) 1479.

5- H. S. Nalwa , *Nanostructured Materials and Nanotechnology* , Academic, San Diego (2002).

6- J. Pacifico, J. Jasieniak, D. E. Gomez, P. Mulvaney, *Small* **2** (2006) 199.

7- I.V. Kityk, J. Ebothé, Q. Liu, Z. Sun, J. Fang, *Nanotechnology* **17** (2006) 1871.

8- R. J. Aitken, M. Q. Chaudhry, A. B. A. Boxall, M. Hull, *Occupational Medicine* **56** (2006) 300.

9- I.Fujimasa, *Micromachines: A New Era in Mechanical Engineering*, Oxford Univ. Press, Oxford (1996).

10- Y. Takahashi, T. Tatsuma, *Nanoscale* **2** (2010)1494.

11- M. M. Ardakani, Z. Taleat, H. Beitollahi, H. Naeimi, *Nanoscale* **3** (2011)1683.

12- C. Meili, M. Widmer, F. Husmann, P. Gehr, F. Blank, M. Riediker, K. Schmid, W. Stark, and L. Limbach, *Synthetische Nanomaterialien: Risikobeurteilung und Risikomanagement. Grundlagenbericht zum Aktionsplan*. (ed. BAFU and BAG), Berne (2007).

13- M. Faraday, *Phil. Trans. R. Soc. London* **147** (1857) 145.

14- R. P. Feynmann: *There's plenty of room at the bottom*, Eng. Sci. **23** (1960) 22, and www.zyvex.com/nanotech/feynman.html (1959).

15- E. Drexler, *Engines of creation*, Anchor Books, New York (1986).

16- A. Kowalski, M. Vogel, R.M. Blankenship, *US Patent 4427836* (1984).

17- N. Ren, B. Wang,, Y. Yang, Y. Zhang, W. Yang, Y. H. Yue, Z. Gao, Y. Tang, *Chem. Mater.* **17** (2005) 2582.

18- C. Chen, S. F. Abbas, A. Morey, S. Sithambaram, L. Xu, H. F. Garces, W. A. Hines, S. L. Suib, *Adv. Mater*. **20** (2008) 1205.

19- S. Ludtke, T. Adam, K. K. Unger, *J. Chromatogr. A* **786** (1997) 229.

20- J. Yu, H. Yu, H. Guo, M. Li, S. Mann*, Small* **4** (2008) 87*.*

21- J. Yuan, K. Laubernds, Q. Zhang, S. L. Suib, *J. Am. Chem. Soc*. **125** (2003) 4966.

22- Y. Zhu, J. Shi, W. Shen, X. Dong, J. Feng, M. Ruan, Y. Li, *Angew. Chem. Int. Ed.* **44** (2005) 5083.

23- J. Yu, S. Liu, H. Yu, *J. Catal.* **249** (2007) 59.

24- F. Caruso, *Chem. Eur. J.* **6** (2000) 413.

25- Y. Zhu, H. Chen, Y. Wang, Z. Li, Y. Cao, Y. Chi*, Chem. Lett.* **35** (2006) 756.

26- M. Li, Q. Lu, Y. Nuli, X. Qian, *Electrochem. Solid-State Lett.* **10** (2007) K33.

27- J.M. Gomez-Vega, M. Iyoshi, K. Y. Kim, A. Hozumi, H. Sugimura, O. Takai, *Thin Solid films* (2001) 398.

28- X. Sun, J. Liu, Y. Li, *Chem. Eur. J.* **12** (2006) 2039.

29- D. L. Wilcox, M. Berg, *Mater.Res. Soc. Symp. Proc.* **372** (2007) 3.

30- P. Jiang, J. F. Bertone, V. L. Colvin, *Science* **291** (2001) 453.

31- T. Nakashima, N. Kimizuka, *J. Am. Chem. Soc.* **125** (2003) 6386.

32- Q. Peng, Y. J. Dong, Y. D. Li, *Angew. Chem.* **115** (2003) 3135.

33- M. Yang, J. J. Zhu, *J. Cryst. Growth* **256** (2003) 134.

34- H. G. Yang, H. C. Zeng, *J. Phys. Chem. B* **108** (2004) 3492.

35- R. T. Tom, A. S. Nair, N. Singh, M. Aslam, C. L. Nagendra, R. Philip, K. Vijayamohanan, T. Pradeep, *Langmuir* **19** (2003) 3439.

36- K. P. Velikov, A. van Blaaderen, *Langmuir* **17** (2001) 4779.

37- L. Z. Wang, T. Sasaki, Y. Ebina, K. Kurashima, M. Watanabe, *Chem. Mater.* **14** (2002) 4827 .

38- D. B. Wang, C. X. Song, Z. S. Hu, X. Fu, *J. Phys. Chem. B* **109** (2005) 1125.

39- J. G. Yu, H. Guo, S. A. Davis, S. Mann, *Adv. Funct. Mater.* **16** (2006) 2035

40- H. Shiho, N. Kawahashi, *Colloid Polym. Sci.* **278** (2000) 270.

41- F.Caruso, M. Spasova, V. Saigueirino-Maceira, L. M. Liz-Marzan, *AdV. Mater.* **13** (2001) 1090.

42- V. Salgueirino-Maceira, M. Spasova, M. Farle, *AdV. Funct. Mater*. **15** (2005) 1036.

43- H. T. Schmidt, A. E. Ostafin, *Adv. Mater.* **14** (2002) 532.

44- M. M.Wu, G. G.Wang, H. F. Xu, J. B. Long, F. L. Y. Shek, S. M. F.Lo, I. D. Williams, S. H. Feng, R. R. Xu, *Langmuir* **19** (2003) 1362.

45- C. E.Fowler, D.Khushalani, S. J. Mann, *Mater. Chem.* **11** (2001) 1968.

46- D. L. Wilcox, M. Berg, T. Bernat, D. Kellerman, J. K. Cochran Jr, Hollow and Solid Spheres and Microspheres: Science and Technology Associated with Their Fabrication and Applications*, Mater. Res. Soc. Symp. Proc.* Vol. **372** (1995) MRS Pittsburgh, PA.

47- E. Matijevic, *Chem. Mater.* **5** (1993) 412.

48- T. Ung, L. M. Liz-Marzan, P. Mulvaney*, Langmuir* **14** (1998) 3740.

49- L. M. LizMarzan, M. Giersig, P.Mulvaney, *Langmuir* **12** (1996) 4329.

50- F. Caruso, R. A. Caruso, H. Mohwald, *Science* **282** (1998) 1111.

51- C. H. Zeng, *Mater. Chem.* **16** (2008) 649.

52- J. W. Tong, C. Y. Guo, *J. Mater. Chem.* **18** (2008) 3799.

53- R. Zhang, M. Hummelgard, H. Olin, *Carbon* **48** (2010) 424.

54- X. Yang, Y. Lu, *Polymer* **46** (2005) 5324.

55- S. Zhang, X. Li, *Powder Technology* **141**(2004) 75.

56- Y. G. Sun, Y. n. Xia, *Science* **298** (2002) 2176.

57- Y. S. Han, G. Y. Jeong, S. Y. Lee, H. K. kim, *J. Sol. state Chem.* **180** (2007) 2978.

58- D. Wang, Q. Luo, D. D. Jia, X. D. Li, X. Q. Wang, *Chinese Chemical Letters.* **14** (2003) 1306.

59- M. Tasi, M. J. Li, *J. Noncryst. Sol*. **352** (2006) 2829.

60- L. Song , X. Ge, M. Wang, Z. Zhang, *J. Non-Crystal. Sol.* **352** (2006) 2230.

61- G. Decher, *Science* **277** (1997) 1232

62- F. Caruso, H. Lichtenfeld, M. Giersig, H. Moehwald, *J. Am. Chem. Soc.* **120** (1998) 8523

63- D.G. Shchukin, G.B. Sukhorukov, H. Mohwald, *Angew. Chem. Int. Ed.* **42** (37) (2003) 4472.

64- F. Caruso, R. A. Caruso, H. Mohwald, *Science* **282** (1998) 1111.

65- F. Caruso, *AdV. Mater.* **13** (2001) 11.

66- F. Caruso, *Chem. Eur. J.* **6** (2000) 413.

67- S. Sadasivan, G.B. Sukhorukov, *J. Coll. Interf. Sci.* **304** (2006) 437.

68- N. Du, H. Zhang, J. E. Chen, J. Y. Sun, B. D. Chen, D. R. Yang, *J. Phys. Chem. B* **112** (2008) 14836.

69- F. Caruso, X. Shi, R. A. Caruso, A. Susha, *AdV. Mater.* **13** (2001) 740.

70- *D. H. Everett, Basic Principles of Colloid Science,* Royal Society of Chemistry, London (1988).

71- Z. Zhong, Y. Yin, B. Gates, Y. Xia, *Adv. Mater.* **12** (2000) 206.
72- G. C. Li, Z. K. Zhang, *Mater. Lett.* **58** (2004) 340.
73- I. Tissot, J. P. Reymond, F. Lefebvre, E. Bourgeat-Lami, *Chem. Mater*. **14** (2002) 1325.
74- Z. Z. Li, *J. Controll. Rel.* **98** (2004) 245.
75- Z. W. Deng, M. Chen, S. X. Zhou, B. You, L. M. Wu, *Langmuir* **22** (2006) 6403.
76- M. M. Titirici, M. Antonietti, A. Thomas, *Chem. Mater*. **18** (2006) 3808.
77- J. G. Yu, X. X. Yu, B. B. Huang, X.Y. Zhang, Y. Dai, *Crystal Growth Design* **9** (2009) 1474.
78- G. Buchel, K. K. Unger, A. Matsumoto, K. Tsutsumi, *Adv. Mater*. **10** (1998) 1036.
79- W. Stober, A. Fink, E. Bohn, *J. Colloid Interface Sci.* **26** (1968) 62.
80- F. J. Suarez, M. Sevilla, S. Alvarez, T. Valdes-Solis, A. B. Fuertes, *Chem. Mater.* **19** (2007) 3096.
81- D. B. Wang, C. X Song, , G. H. Gu, Z. S. Hu, *Mater. Lett.* **59** (2005) 782.
82- H. S. Qian, G. F. Lin, Y. X. Zhang, P. Gunawan, R. Xu, *Nanotechnology* **18** (2007) 355602.
83- A. Imhof, *Langmuir* **17** (2001) 3579.
84- Z. W. Deng, M. Chen, G. X. Gu, L. Wu, M. *J. Phys. Chem.* **112** (2008) 16.
85- C. Zimmermann, C. Feldmann,M. Wanner, D. Gerthsen, *Small* **3** (2007) 1347.
86- D. H. M. Buchold, C. Feldmann, *Nano Lett.* ***7*** (2007) 3489.
87- J. Han, G. P. Song, R. Guo, *Adv. Mater.* **18** (2006) 3140.
88- X. X. Li, Y. J. Xiong, Z. Q. Li, Y. Xie, *Inorg. Chem.* **45** (2006) 3493.
89- K. S. Suslick, G. J. Price, *Annu. Rev. Mater. Sci.* **29** (1999) 295.
90- K. S. Suslick, N. A. Dhas, *J. Am. Chem. Soc.* **127** (2005) 2368.
91- E. B. Flint, K. S. Suslick, *Science* **253** (1991) 1397.
92- S. F. Wang, F. Gu, M. K. Lu, *Langmuir* **22** (2006) 398.
93- J. J. Zhu, S. Xu, H. Wang, J. M. Zhu, H. Y. Chen, *Adv. Mater.* **15** (2003) 156.
94- X. W. Zheng, Y. Xie, L. Y. Zhu, X. C. Jiang, A. H. Yan, *Ultrason. Sonochem.* **9** (2002) 311.
95- Y. R. Cai, H. H. Pan, X. R. Xu, Q. H. Hu, L. Li, R. K. Tang, *Chem. Mater*. **19** (2007) 3081.
96- X. W. Lou, Y. Wang, C. Yuan, J. Y. Lee, L. A. Archer, *Adv. Mater.* **18** (2006) 2325.
97- P. Tartaj, T. Gonzalez-Carreno, C. J. Serna, *Adv. Mater.* **13** (2001) 1620.

98- L. J. Mao, C. Y. Liu, J. Li, *J. Mater. Chem.* **18** (2008) 1640.

99- J. N. Gao, X. L. Ren, D. Chen, F. Q. Tang, *J. Ren. Scr. Mater.* **57** (2007) 687.

100- Y. G. Sun, B. T. Mayers, Y. N. Xia, *Nano Lett.* **2** (2002) 481.

101- Y. D. Yin, C. Erdonmez, S. Aloni, A. P. Alivisatos*, J. Am. Chem. Soc*. **128** (2006) 12671.

102- J. H. Gao, B. Zhang,X.X. Zhang, B.Xu, *Angew. Chem. Int. Ed.* **45** (2006) 1220.

103- A. D. Smigelskas, E.O. Kirkendall, *Trans. Am. Inst. Min. Metall. Pet. Eng.* **171** (1947) 130.

104- K. N. Tu, U. GHsele, *Appl. Phys. Lett.* **86** (2005) 093111.

105- Y. D. Yin, R. M. Rioux, C. K. Erdonmez, S. Hughes, G. A. Somorjai, A. P. Alivisatos, *Science* **304** (2004) 711.

106- S. Peng and S. Sun, *Angew. Chem. Int. Ed.* **46** (2007) 4155.

107- G. L. Messing, S. C. Zhang, G. V. Jayanthi. *J. Am. Ceram. Soc.* **76** (1993) 2707.

108- K. M. Keville, E. I. Franses, J. M. Caruthers, *J. Colloid Interface Sci.* **144** (1991) 103.

109- Y. Lu, Y. D. Yin, Y. N. Xia, *Adv. Mater.* **13** (2001) 271.

110- X. Fan, Z. Zhang, G. Li, N. A. Rowson, *Chem. Eng. Sci.* **59** (2004) 2639.

111- K. S. Suslick, *Annu. Rev. Mater. Sci.* **29** (1999) 295.

112- P. Scatff, *Carbon* **36** (1998) 481.

113- S. Iijima, *Nature* **354** (1991) 56.

114- S. Tanuma, AV. Palinchenko, *J. Mater. Res.* **10** (1995) 1120.

115- Q. Wang, H. Li, L. Chen, X. Huang, *Carbon* **39** (2001) 2211.

116- M. M. Titirici, M. Antonietti, *J.Phys. Chem. C* **113** (2009) 9644.

117- X. Sun, Y. Li, *Angew. Chem. Int. Ed.* **43** (2004) 3827.

118- N, Baccile, G. Laurent, F. Babonneau, F. Fayon, M. Titirici, M. Antonietti, *J. Phys. Chem. C* **113** (2009) 9644.

119- C. R. Martin, P. Kohli, *Nat. Rev. Drug Discov*. **2** (2003) 29.

120- Z. P. Xu, Q. H. Zeng, G. Q. Lu, A. B. Yu, *Chem. Eng. Sci.* **61** (2006) 1027.

121- V. Sokolova, M. Epple, *Angew. Chem. Int. Ed.* **47** (2008) 1382.

122- Z. Z. Li, L. X. Wen, L. Shao, J. F. Chen, *J. Controlled Release* **98** (2004) 245.

123- J. F. Chen, H. M. Ding, J. X. Wang, L. Shao, *Biomaterials* **25** (2004) 723.

124- V. V. Sokolova, I. Radtke, R. Heumann, M. Epple, *Biomaterials* **27** (2006) 3147.

125- J. Chen, F. Saeki, B. J. Wiley, H. Cang, M. J. Cobb, Z. Y. Li, L. Au, H. Zhang, M. B. Kimmey, X. D. Li, Y. Xia, *Nano Lett.* **5** (2005) 473.

126- H. H. Brintzinger, D. Fischer. R. Muehlhaupt, B. Rieger, R. M. Waymouth, *Angew. Chem.* **34** (1995) 1143.

127- J. Chen, J. Song, L. Wen, H. Zou, L. Shao, *J. Non-Cryst. Sol.* **353** (2007) 1030.

128- S. B. Yoon, K. Sohn, J. Y. Kim, C. H. Shin, J. S. Yu, T. Hyeon, *Adv. Mater.* **14** (2002) 19.

129- G. S. Chai, S. B. Yoon, J. H. Kim, J. S. Yu, *Chem. Commun.* (2004) 2766.

130- H. P. Liang, H. M. Zhang, J. S. Hu, Y. G. Guo, L. J. Wan, C. L. Bai, *Angew. Chem. Int. Ed.* **43** (2004) 1540.

131- G. Chen, D. G. Xia, Z. R. Nie, Z. Y. Wang, L. Wang, L. Zhang, J. J. Zhang, *Chem. Mater.* **19** (2007) 1840.

132- J. Zhao, W. X. Chen, Y. F. Zheng, X. Li, *J. Power Sources* **162** (2006)168.

133- Y. Kondo, H. Yoshikawa, K. Awaga, M. Murayama, T. Mori, K. Sunada, S. Bandow, S. Iijima, *Langmuir* **24** (2008) 547.

134- H. J. Koo, Y. J. Kim, Y. H. Lee, W. I. Lee, K. Kim, N. G. Park, *Adv. Mater*. **20** (2008) 195.

135- W. S. Wang, L. Zhen, C. Y. Xu, B. Y. Zhang, W. Z. Shao, *J. Phys. Chem. B* **110** (2006) 23154.

136- Z. Y. Liu, D. D. Sun, P. Guo, J. O. Leckie, *Chem. Eur. J.* **13** (2007) 1851.

137- W. W. Wang, Y. J. Zhu, L. X. Yang, *Adv. Funct. Mater.* **17** (2007) 59.

138- L. Chen, Z. Song, X. Wang, S. Prikhodko, J. Hu, S. Kodambaka, R. Richards, *Appl. Mater.& Interf.* **1** (2009) 1931.

# Chapter 2

# Experimental Section

## 2.1 Introduction

Various synthesis routes have been proposed for the fabrication of hollow spheres. among them a heterophase polymerization combined with an emulsion/interfacial polymerization method as surface living polymerization processes or sol-gel process.[1] Furthermore, the lost-wax method, spray pyrolysis, the bubble-template method and template-free synthesis like self-assembly techniques or kinetically controlled methods are also known.[2] Generally, among the various synthesis procedures, templating approaches represent the most often used technique which is based on the synthesis of core-shell particles and subsequently removal of the core by dissolution in a solvent or calcination.[3] The sacrificial templating methods have been developed considerably in recent years and an interesting sacrificial core is represented by monodisperse carbon particles, which are generated by the hydrothermal treatment of aqueous solutions of glucose.[4] These sacrificial cores inherit functional groups and have reactive surfaces which facilitate the precipitation of metal precursors and nanoparticles as was shown by *Li et al.* for different materials [5], for example $TiO_2$ [6], $WO_3$ [7] and noble metal nanoparticles which could be fabricated as hollow spheres. *Thomas et al.* synthesized some hollow metal oxides by hydrothermal process using carbon as the sacrificial core; they reported that the hollow spheres exhibit diameters from one to several micrometers and consist of nanocrystals of the respective metal oxides.[8]

However, previous methods were found to be slow processes and mechanical stirring is necessary to obtain uniform oxide shell on the surface of the sacrificial templates. Many efforts are required in order to separate the core-shell nano-particles (NPs) from large amounts of surfactant associated with micro-emulsion system. In addition, there is no systematic approach yet for controlling the void size or maintaining a regular structure of hollow oxide particles without any collapse of the regularity of the morphology. Therefore, developing a facile simple strategy to prepare hollow oxide nano-particles with controlled void size and regular morphology remains a challenge to materials scientists.

In our work, we aimed at fabrication of the hollow oxide spheres through simple strategy in one-pot synthesis route. Therefore, we developed and modified the synthesis route described by *Li et al.*[5] and *Thomas et al.*[8] They presented sacrificial templating method using glucose as the sacrificial template via utilizing hydrothermal approach. In our synthesis recipe we applied glucose as well as fructose for the first time, to our knowledge, as sacrificed templates. We studied the impact of different synthesis parameters, such as the temperature, the concentration of the sugar, the concentration ratio between the sugar and the metal oxide precursor, time and the impact of acetic acid as a catalyst, on the as-obtained hollow oxides as well as the template which acting as shape and size directing agent. In addition, we studied the synthesis of hollow silica spheres via this approach for the first time to our knowledge.

This synthesis approach has many merits which make it attractive for the fabrication of many oxides hollow spheres among these merits are:

1- Commercial inexpensive fructose is suggested as a sacrificial template.
2- The carbonaceous spheres produced by the hydrothermal hydrolysis of sugar inherit surface functionalities like -C=O and -OH groups therefore, no need for surface modifications.

3- Saving time, by avoiding multistep synthesis approaches.
4- Only the template and the metal precursor are used for the synthesis of the hollow oxide spheres and no need for any chemical additives.
5- Simple strategy is easy to be understood and controlled than complex strategy with multistep and many chemical additives.
6- Fabrication of many different hollow metal and ceramic oxides can be studied by this approach.

## 2.2 Experimental setup

Fig.2.1 shows schematic illustration for the experimental set up and synthesis process of the hollow spheres. In a typical procedure reactants were dissolved in deionized water to form a clear solution. The solution was sealed in 100 mL Teflon-lined stainless steel autoclave. Heating the autoclave in an oven to temperature T($^{o}$C) for time t (h) resulted in in-situ formation of hybrid composite spheres. After thermal treatment, the desired hollow spheres were produced.

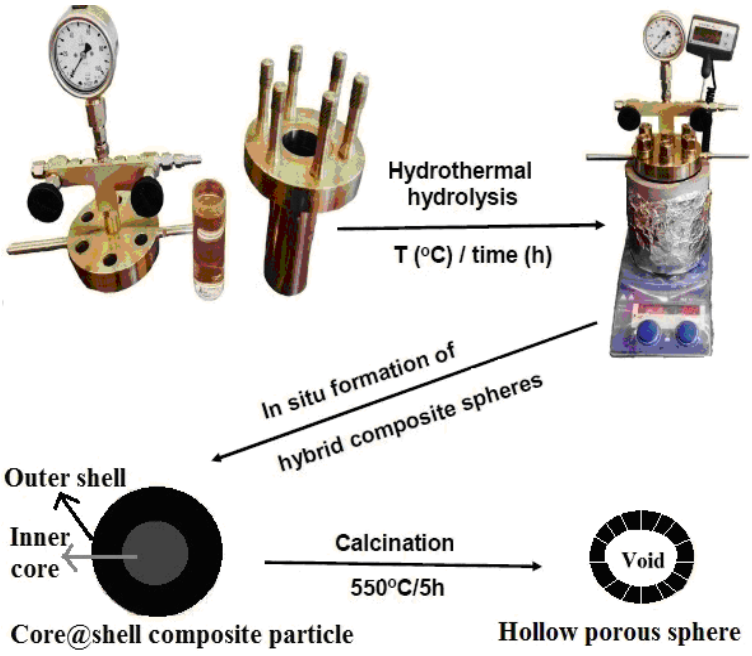


**Fig.2.1** *Schematic illustration of the synthesis process*

## 2.3 General recipe for the synthesis of the carbonaceous spheres

Carbonaceous spheres were fabricated by hydrothermal approach using glucose/fructose as a source of the carbonaceous material. In a typical synthesis, 1900 mg (9.5 mmol) of glucose in 100 mL deionized water / 2250 mg (12.5 mmol) of fructose in 20 mL deionized water was transferred into a 100 mL Teflon-lined stainless steel autoclave, followed by hydrothermal treatment of the solution at 180 $^{o}$C for 24 h in case of glucose and 135 $^{o}$C for 6 h in case of fructose. After hydrothermal hydrolysis reaction, the black or puce precipitate was centrifuged, and then was dried in a vacuum oven at 80 $^{o}$C for 5 h. Fig.2.2 shows a scheme for the synthesis process of the carbonaceous spheres with the different synthesis conditions.

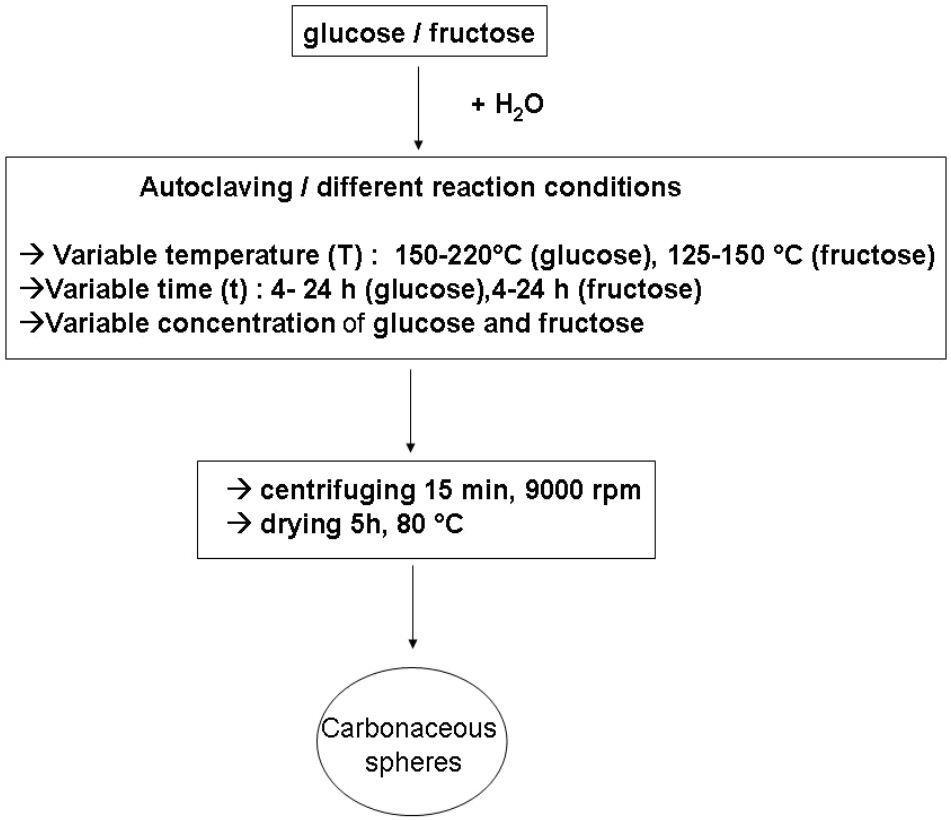


**Fig.2.2** *General scheme for the synthesis of carbonaceous spheres via hydrothermal hydrolysis of glucose and fructose*

## 2.4 General recipe for the fabrication of the hollow silica nanoparticles

In our recipes the carbohydrate used as a precursor for the sacrificed carbonaceous spherical cores is glucose. Variable concentrations of glucose were used. C1 stands for the initial glucose concentration of 0.96 mol/L, C2, C4, C10 and C15 for 1/2, 1/4, 1/10 and1/15 of C1, respectively as shown in Table2.1. Variable amounts of water glass were used as a silica precursor.

**Table 2.1** *Different concentration of glucose*

| Glucose sample | Molar mass / $H_2O$ mL |
|---|---|
| C1 | 19 mmol/ 20 mL |
| C2 | 19 mmol/ 40 mL |
| C4 | 19mmol / 80 mL |
| C10 | 9.5 mmol / 100 mL |
| C15 | 2.5 mmol / 40 mL |

The typical procedure can be described as follows: in a standard experiment glucose (1902mg, 9.5 mmol) was dissolved in 100 mL of distilled water and 0.2 mL of water glass was added to the solution. The mixture was placed in an autoclave which was heated up to 180 $^{o}$C for 24 h. The autoclave was cooled down in ice bath. The product was filtered by using a centrifuge at 9000 rpm and finally dried in a vacuum oven at 80 $^{o}$C over night. Subsequently, the carbonaceous spheres@silica precursor core-shell composite was calcined in air at 550 $^{o}$C (heating rate of 2 $^{o}$C/min) for 5 h to remove the carbon core, leading to nano-particles of fused hollow silica nano-spheres.

## 2.5 General recipe for the fabrication of the nano-oxides hollow spheres

In this recipe, metal oxide hollow spheres were fabricated by a hydrothermal route using metal chlorides as precursors for the desired metal oxide and glucose / or fructose as a precursor for the sacrificial carbonaceous core. In standard experiment, 1900 mg (9.5 mmol) of glucose / 2250 mg (12.5 mmol) of fructose and a certain amount of the metal chloride were dissolved together in 100 mL (in case of glucose) / or 20 mL (in case of fructose) deionized water under stirring. The molar ratios of sugar to the metal chloride varied from 5 to 30. Then the reaction solution was transferred into a 100 mL Teflon-lined stainless steel autoclave, followed by hydrothermal treatment of the solution at 180 $^{o}$C for 24 h in case of glucose and 135 $^{o}$C for 6 h in case of fructose as sacrificial templates. The black or puce precipitate were filtered by using a centrifuge at 9000 rpm, and then washed with deionized water five times. The washed precipitate were dried in air for 24 h then in a vacuum oven at 80 $^{o}$C for 5h and finally were calcined in air at 500 $^{o}$C (heating rate of 2 $^{o}$C/min) for 5 h to remove the carbon core, leading to the nano-oxide hollow spheres. Fig.2.3 shows a scheme for the synthesis process of the hollow oxide spheres with the different synthesis conditions.

## 2.6 Characterization

This section gives a short overview of the analytical methods which were used to characterize and identify the prepared samples. The hollow particles and their corresponding core@shell composites were characterized by means of scanning electron (SEM), transmission electron microscopy (TEM), X-ray diffraction (XRD), infrared spectroscopy (IR), thermo-gravimetric analysis (TGA) and sorption measurements.

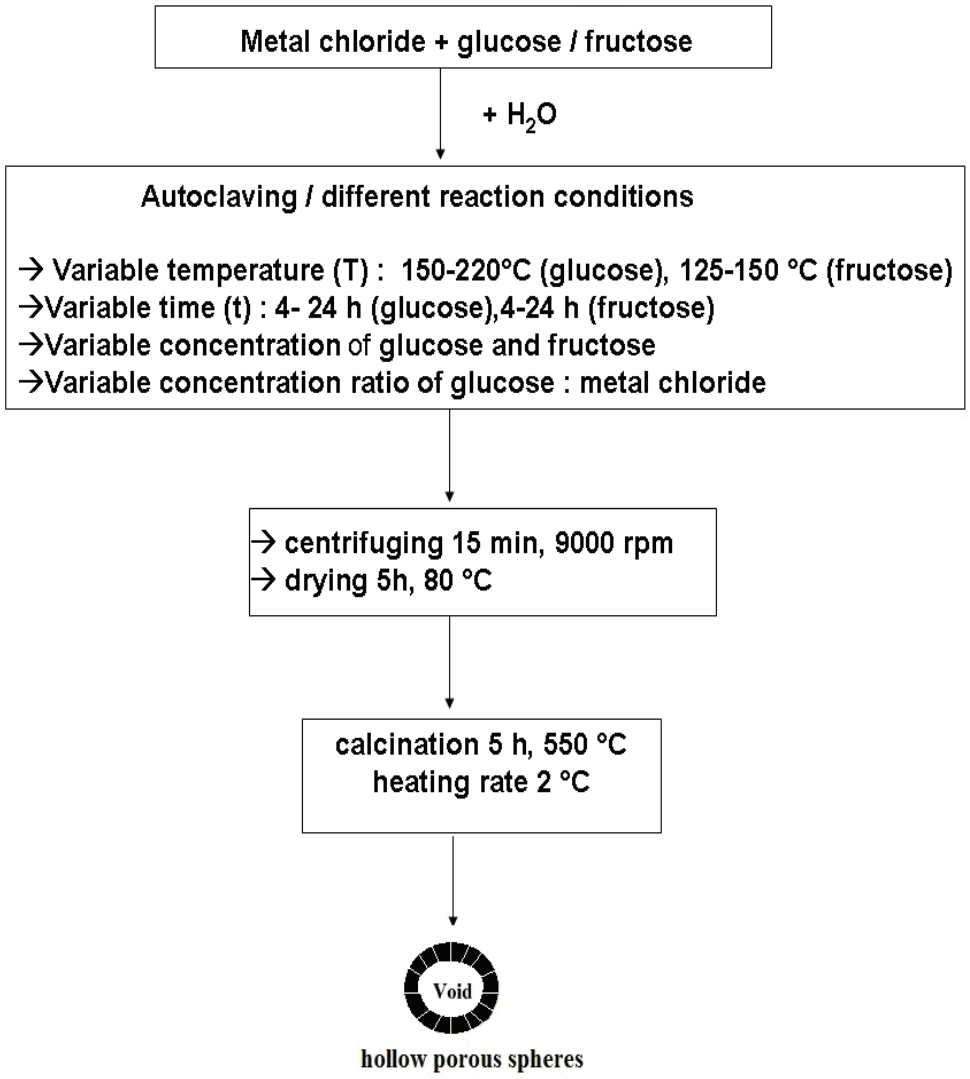


**Fig.2.3** *General scheme for the synthesis of the nano-oxides hollow spheres*

### 2.6.1 Scanning electron microscope (SEM) [9,10]

The SEM is an important technique that reveals the morphology and the surface of the particles. Consideration of the use of the interaction of an electron beam with a specimen to yield high resolution images of a specimen surface began in the late 1920's. In 1935, *M. Knoll* actually demonstrated the theory of scanning electron microscopy. The first scanning electron microscope was

constructed by *Von Ardenne* in 1938, however, it did not become commercially available until the early 1960's. Modern SEM machines make magnifications till about $10^6$ :1 possible with resolution capability in order of 1-4 nm at 1kV, therefore it is an important tool to identify the formation of the hollow structure .

The SEM utilizes a focused beam of high energy electrons that systematically scans across the surface of the specimen. The solid specimens interact with the electron beam and produce a large number signals at or near the specimen surface [Fig.2.4]. These interactions include lower energy electrons, termed secondary electrons that are generated by knocking-out of weakly bound electrons of the outer electron shells of atoms. Due to their low energy they are from the uppermost nanometers from the surface and thus form the surface characteristics of the sample. To analyze the specimen visually, the secondary electrons signal is collected and eventually converted to an electronic signal which is portrayed on cathode ray tube (essentially a television screen).

High vacuum is required for the operation of SEM. A vacuum is necessary for many reasons, (1) a hot tungsten filament (the source of the electron beam) will oxidize and burn out in the presence of air, (2) moisture in the air will cause corrosion and dust particles in the beam path can block the beam or may become charged and deflect the beam, (3) air molecule will scatter the electrons. For the electrons to be capable of passing through the specimen, the specimen should be conductive. In case of non-conductive specimens a thin layer of platinum is sputtered on the surface of the sample.

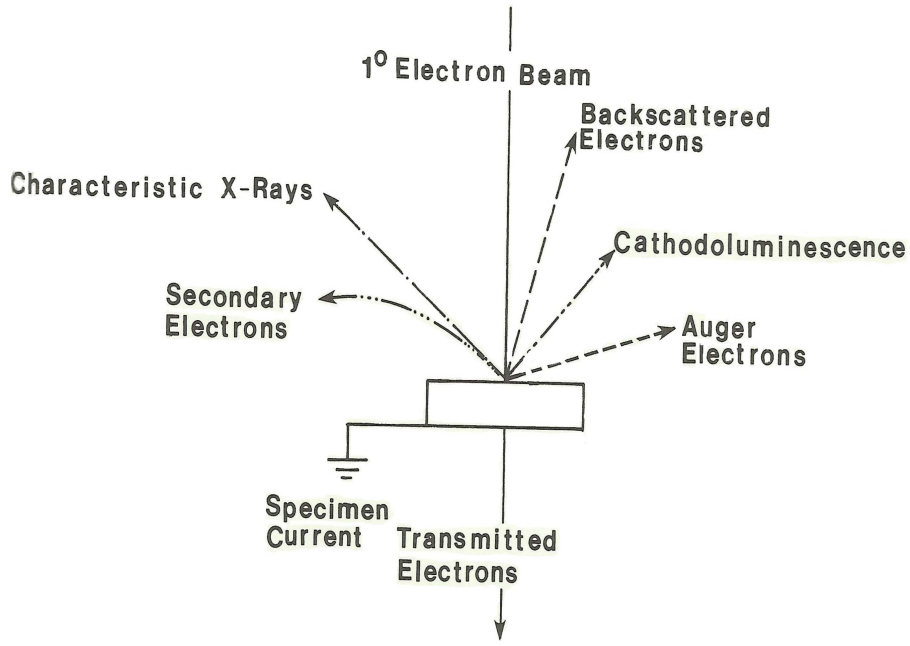


**Fig.2.4** *Illustration of seven of the possible signals generated by the primary electron beam-specimen interaction in the scanning electron microscope [from ref. 9]*

For the captured images, in our work, a *JEOL JSM-7500F* field emission scanning electron microscope at an accelerating voltage of 2-5 kV was used (Samples were ground to a powder and then mounted on an aluminum stub with conductive carbon tape and for electrically nonconductive samples a thin layer platinum coating was applied before SEM analysis). The examined samples were mounted on a self-adhesive graphite foil over an aluminum sample holder.

### 2.6.2 Transmission electron microscopy (TEM)

The TEM is one of the methods of electron microscopy which allows a resolution of up to approximately one nanometer. So the HR-TEM reaches a larger magnification than the SEM. In 1878, *Ernst Abbe* [11] proved that the resolution of the optical microscope is limited by the wavelength of light. No

means were conceived of resolving finer detail until two discoveries were made: (i) the wave properties of the moving electron, postulated by de Broglie, on theoretical grounds, in 1924 [12]; and (ii) the discovery by *Busch* [13] in 1926-1927 of the analogy between the effect of a magnetic coil - the focusing coil used since 1899 [14] - on an electron beam and the effect of a convex lens on a light beam.

Since the wavelength of the moving electron is smaller by many orders of magnitude than the shortest wavelength of light, these discoveries made it conceivable that extremely small objects might be imaged with an electron beam and electron lenses.[15] The first electron microscope was publicly demonstrated in 1931 by *Max Knoll* and *Ernst Ruska*, working at the High Tension Laboratory of the Technical University (Technische Hochschule), Berlin, under *A. Matthias* and the TEM instrument was first developed by *Ruska, M. Knoll* and *von Borries* in 1935.[10] It won *Ruska* a Nobel Prize in 1986 in physics.

Like other electron microscopic methods, it focuses an electron beam in high vacuum with magnetic fields onto the sample. Depending on the permeability of the sample for the electron beam electrons are detected on a charge-coupled device (CCD) sensor or not. This leads to brighter or darker points for each site, thus resulting in an overall picture. Therefore, materials with high electron densities are seen as dark spots in the TEM while for example carbon chains are bright and can not be seen.

In a typical TEM instrument setup, electron beam is generated by an electron gun with a tungsten or $LaB_6$ filament and then accelerated through a positive stabilized voltage V0(10 - 120 keV) under vacuum .

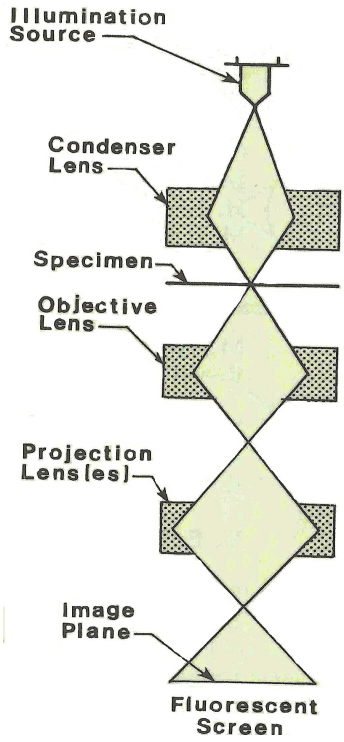


**Fig.2.5** *Basic component of a TEM instrument [from ref. 9]*

Electron microscopy is the most common method for the characterization of nanomaterials. For examination of nanostructures with dimensions smaller than 30 nm, transmission electron microscopy (TEM) is typically used.[16] Using this method, high-resolution imaging and elemental and crystal structure analysis can be simultaneously performed on single nanoparticles while irradiating with high-energy electrons. To confirm the preparation of a hollow or core/shell structure, it is typical to report observed variations in contrast between the inner core and outer shell. TEM images obtained as a function of time and electron beam accelerating voltage showed that the nanoparticles evolved from solid spheres to core/void/ shell structures and ultimately formed completely hollow nanoparticles over the course of minutes.[17]

In our work, the TEM measurements were conducted on a JEOL model JEM-3010 electron microscope operated at 300 kV. The samples were crushed

to a powder and mounted by drop-drying of a chloroform suspension onto TEM cupper grids before TEM analysis.

### 2.6.3 X-ray diffraction (XRD)

The discovery of X-rays was by *W. C. Roentgen* in 1895. The first X-rays diffractometer was developed in 1935 by *Le Galley.*[18] The first commercial equipment was introduced by North American Philips in 1947. The latest versions of the powder diffractometer differ in their construction and geometry, but considerable advances have been made in detection and counting systems, automation, and in the X-ray tubes themselves.[19]

The diffraction of X-rays by crystals is a phenomenon of great importance to chemists since diffraction studies provide much structural information on the arrangement of atoms, ions or molecules in crystals. *W. H. Bragg and W. L. Bragg* studied the diffraction of X-rays in detail. When monochromatic X-rays impinge upon the atoms in a crystal lattice within the examined sample, each atom acts as a source of scattering radiation of the same wavelength. The crystal acts as a series of parallel reflecting planes. A goniometer ensures that the detector is located exactly in the double angle (2θ) compared to the detector. Thus, the reflections in the diffraction pattern are plotted against the angle (2θ). In order to see a reflection at an angle, *Bragg's* law (2.1) must comply with the diffraction, so that there is constructive interference.

$$n\lambda = 2d \sin\theta \qquad (2.1)$$

Where $n$ Order of diffraction (natural numbers)

$\lambda$ Wavelength of the incident radiation

$d$ Lattice spacing

$\theta$ Diffraction angle

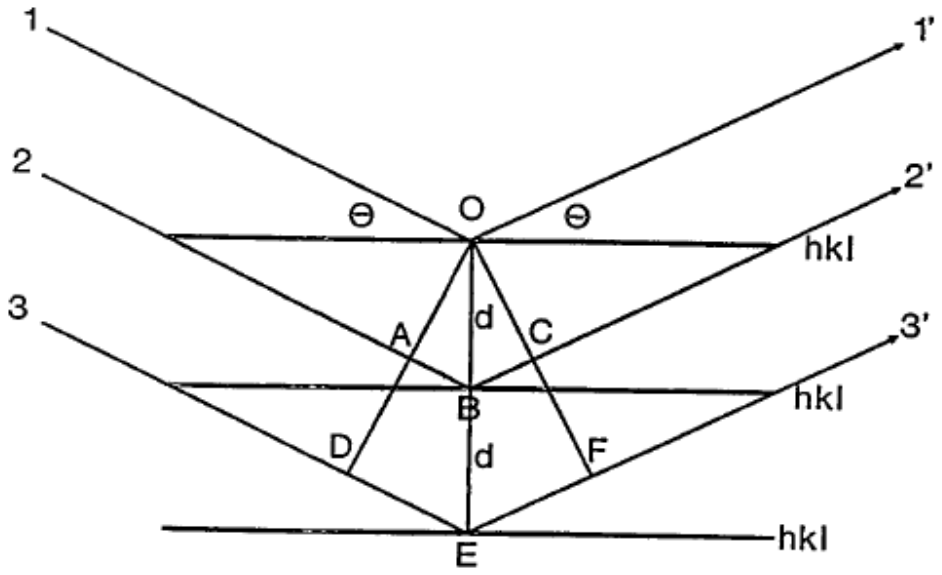


**Fig.2.6** *Bragg's law is easily seen to arise from an optical analogy to crystallographic plane reflecting X-rays [from ref. 19]*

It is evident from equation (2.1) that if the glancing angle $\theta$ is measured from the various order of maximum reflection, the distance $d$ between the successive lattice planes of a given type in the crystal can be calculated.[20] The position of the reflections depends on the lattice constants of the crystal system and thus on the structure of the crystal. By comparison of the diffractograms with literature, a statement about the purity of a crystal can be made based on the absence or presence of additional reflections. Moreover, the particle size of the crystals can be determined by the reflective broadening. Thus, the XRD can determine in addition to the lattice parameters, particle size and purity of a substance.

In the present work, the samples are ground finely and evenly on a sample holder made of pure, single-crystalline silicon and measured on a Philips powder diffractometer X'Pert MPD operating in Bragg-Brentano geometry using a secondary monochromator (graphite). For the measurements copper anode and its $K_\alpha$-radiation is used (CuKα = 1.5406 Å, 40 kV, 40 mA). The evaluation is performed with the program X'Pert High Score Plus. The calculation of the

theoretical diffraction patterns and the data collection and processing were performed with the X' Pert software package [21] supplied by the Pan Analytical company. The particle size is determined by the Scherrer equation (2.2). The Scherrer shape factor K is 0.9 and the wavelength from the Kα-radiation is 1.78901 Å.

$$\Delta (2\theta) = K \lambda / L \cos \theta^0 \qquad (2.2)$$

Where $\Delta (2\theta)$ Reflection broadening

$L$ Crystal size

$K$ Scherrer shape factor

$\theta^0$ Diffraction angle

### 2.6.4 Infrared spectroscopy (IR spectroscopy) [22, 23]

The IR spectroscopy is one of the molecular spectroscopy methods for the qualitative analysis that gives direct information about the existence of the different functional groups. The commercial IR instruments have been available since 1940s. Infrared spectroscopy is a technique based on the vibrations of the atoms of a molecule. An infrared spectrum is commonly obtained by passing infrared radiation through a sample and determining what fraction of the incident radiation is absorbed at a particular energy. The energy at which any peak in an absorption spectrum appears corresponds to the frequency of a vibration of a part of a sample molecule. It uses electromagnetic radiation in the wave number range of about 14300 $cm^{-1}$ to 10 $cm^{-1}$.

A distinction is made between near infrared (NIR wave number range of 12500 $cm^{-1}$ to 4000 $cm^{-1}$), middle infrared (MIR wave number range of 4000 $cm^{-1}$ to 200 $cm^{-1}$) and far infrared (FIR wave number range of 400 $cm^{-1}$ to 10 $cm^{-1}$). During irradiation, molecule specific wave numbers are absorbed which become

visible in the detected transmission spectrum. For a molecule to show infrared absorptions it must possess a specific feature, i.e. an electric dipole moment of the molecule must change during the vibration. This is the selection rule for infrared spectroscopy.

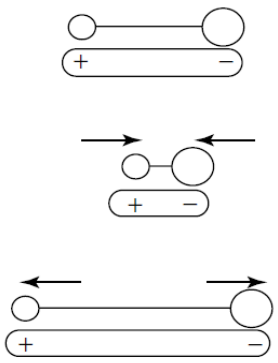


**Fig.2.7** *Change in the dipole moment of infra red-active molecule, heteronuclear diatomic molecule, the dipolemoment of such a molecule changes as the bond expands and contrast [from ref.22]*

The adsorption takes place by excitation of rotations and vibrations of the molecules around a common center of gravity. Vibrations can involve either a change in bond length (streching) or bond angle (bending).

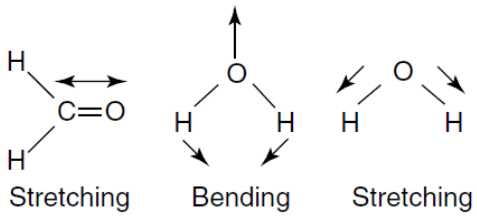


**Fig.2.8** *Illustration of stretching and bending vibrations [from ref.22]*

In the NIR overtone and combination vibrations, in the MIR fundamental vibrations and in the FIR pure rotational transitions are mainly observed. The transitions between the rotational and vibrational states are quantized, so that the

absorption is characteristic of a compound and thus structure determination is possible. In IR absorption, energy is transformed from the incident radiation to the molecule and a quantum mechanical transition occurs between two vibrational energy levels. The energy difference between the two vibrational energy levels is directly related to the frequency ($s^{-1}$) of the electromagnetic radiation by equation:

$$E2 - E1 = h\nu \qquad (2.3)$$

Where *h* is plank s constant ($6.63*10^{-34}$ Js) and $h\nu$ is known as a photon.

A frequency is unique to each molecule or each chemical bond; therefore, by observing the frequency absorbed, we are able to identify molecules and chemical bonds. When an IR spectrum is recorded, $\nu$ ($s^{-1}$) is a very large number and is inconvenient. Therefore, the radiation in the vibrational infrared region is been referred in terms of wavenumbers ($\tilde{\nu}$) which are expressed as $cm^{-1}$, and are easily computed by taking the reciprocal of the wave length (λ) expressed in centimeters.

$$\tilde{\nu}\ (cm^{-1}) = 1 / \lambda\ (cm) \qquad (2.4)$$

$$\nu\ (Hz) = \tilde{\nu}\, c = c/\lambda \qquad (2.5)$$

Where *c* is the speed of light; $\tilde{\nu}$ has the advantage that it is directly proportional to the energy.

The measurement of IR spectra is performed with a Fourier Transform Infrared (FT-IR) spectrometer. FTIR spectroscopy is based on the idea of the interference of radiation between two beams to yield an interferogram. The later is a signal produced as a function of the change of path length between the two beams. The two domains of distance and frequency are interconvertible by the mathematical method of Fourier- transformation.

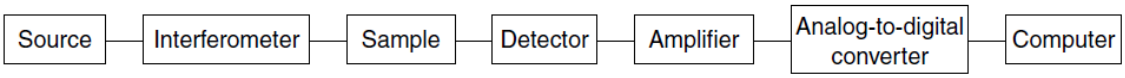


**Fig.2.9** *Basic components of FTIR spectrometer [from ref. 22]*

The products in our work were characterized by infrared spectroscopy using IFS 88 from Bruker.

### 2.6.5 Determination of the specific surface area and the porous structure [*Brunauer Emmett Teller* (BET) theory]

Surface area largely determines many physical and chemical properties of materials. The specific surface area of a solid material is measured by physical adsorption of a gas on the surface of the solid material and calculating the amount of adsorbate gas corresponding to a monomolecular layer on the surface. The physical gas adsorption results from relatively weak forces (Van der Waals forces) between the adsorbate gas molecules and the adsorbent surface of the solid material. Therefore, in contrast to chemical adsorption, also called chemisorption, during physical adsorption the sorbed molecules are not restrained to specific sites on the surface of the tested solid and are free to cover the whole surface. For this reason, determination of surface areas is possible. The measurement is usually carried out at the temperature of liquid nitrogen.[24]

Numerous techniques were developed for the determination of the surface area based on physical gas adsorption. The best known method for the measurment of surface areas of porous material is the so-called BET method. The BET theory is a rule for physical adsorption of gas molecules on a solid surface and it is the main base for the analysis techniques that are used for the measurement of specific surface areas of the material. In 1938, *S. Brunauer, P. H. Emmett and E. Teller* presented the BET theory for the first time [25]; BET consists of the first initials of their family names.

The concept of the theory is based upon the following assumptions: (a) gas molecules physically adsorb on a solid in layers infinitely; (b) there is no interaction between each adsorption layer. The resulting *BET equation* is expressed by (2.6):

$$P/V(P_0-P) = (1/V_mC) + [(C-1)\ P/V_mCP_0) \qquad (2.6)$$

Where $P$ and $P_0$ are the equilibrium and the saturation pressure of adsorbates at the temperature of adsorption, $V$ is the adsorbed gas quantity (for example, in volume units), and $V_m$ is the monolayer adsorbed gas quantity. $C$ is the BET constant, which is expressed by (2.7) :

$$C = exp\ [\ E_L - E_2]/RT \qquad (2.7)$$

Where $E_L$ is the heat of liquification of the gas, $E_2$ is the heat of adsorption of the first layer of adsorbate, $R$ is gas constant, and $T$ is the absolute temperature.

A plot of the amount of gas adsorbed at a certain temperature against the relative pressure is called a sorption isotherm. It is usually presented as the volume of adsorbed gas versus the relative pressure, $P/P^0$, see Fig.2.10.

From such a plot the amount of gas needed to form a monolayer can be determined and, assuming the cross-sectional area of the sorbate molecule, the surface area of the measured solid can be calculated. The relative humidity at which a monolayer completely covers the solid surface depends both on the nature of the used sorptive gas and the nature of the solid. Table 2.2 gives the approximate cross-sectional areas of some commonly used sorbates.[26]

**Table 2.2** *Most commonly used sorbates*

| Sorbate | Area in Å |
|---|---|
| Argon | 14.2 |
| Benzen | 40.0 |
| Nitrogen | 16.2 |
| Oxygen | 14.1 |
| Water vapor | 10.8 |
| Xenon | 2.5 |

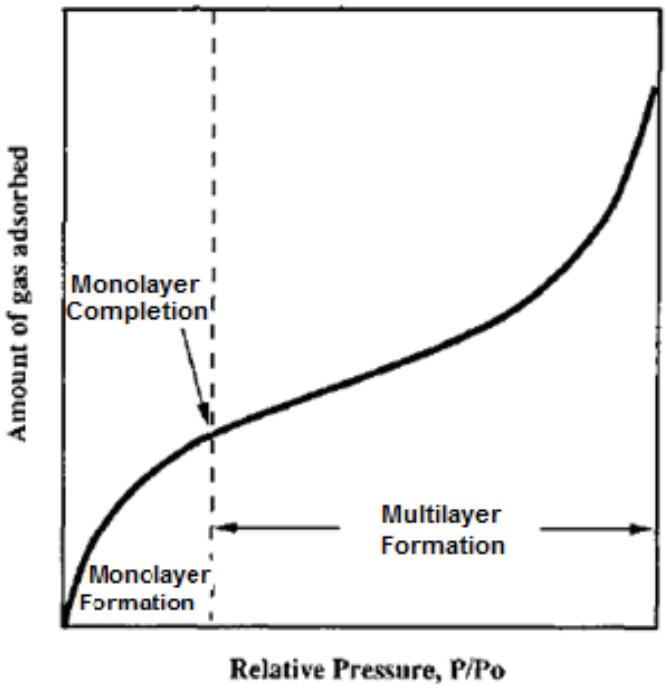


**Fig.2.10** *Sorption isotherm for a planar surface [from ref.* 27*)*

In addition to the outer surface, the surface area of a particle depends on the porosity of the particle. A substance is known as porous if a sizable part of its total volume is taken up by pores. As a consequence of different adsorption mechanisms, and for better distinction among the pore widths encountered, these have been subdivided into four categories by the International Union of Pure and Applied Chemistry (IUPAC).[28]

**Table 2.3** *Classification of pores according to IUPAC [28]*

| | | | | | |
|---|---|---|---|---|---|
| Submicropores | | | W | < | 0.8 nm |
| Micropores | 0.8 nm | < | W | < | 2.0 nm |
| Mesopores | 2.0 nm | < | W | < | 50.0 nm |
| Macropores | 50.0 nm | < | W | | |

Due to the capillary condensation in a set of pores of certain size, the adsorption cycle does not occur exactly at the same relative pressure as the desorption cycle in the combined adsorption-desorption isotherms, and usually show a hysteresis. A schematic example is shown in Fig.2.11 [29] several types of adsorption-desorption isotherms were identified (Fig.2.12).

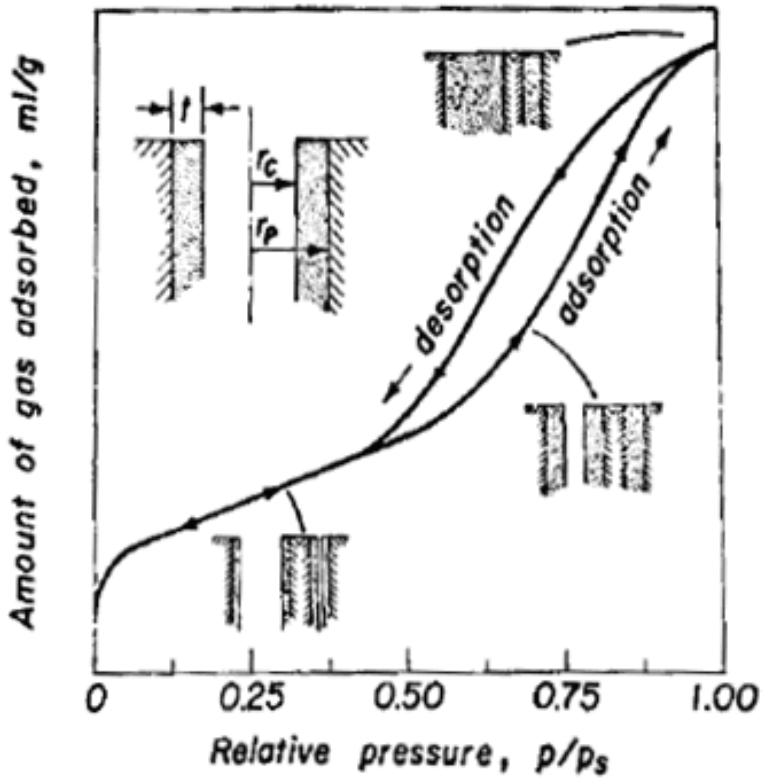


**Fig.2.11** *Adsorption isotherm showing capillary condensation [from ref. 29]*

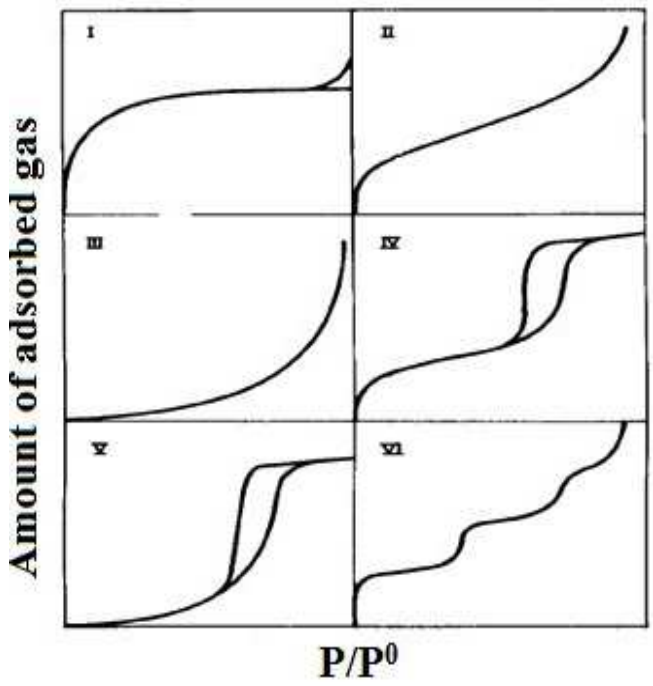


**Fig.2.12** *Classification of isotherms types according to the IUPAC s [from ref. 28]*

Figure 2.12 shows the isotherm categories according to IUPAC. The following types may be distinguished:

Type I: These isotherms are given by microporous solids having small external surface.

Type II: This type is normal for the isotherm obtained from non-porous or macroporous adsorbent.

Type III: This type is not common. In such isotherm, the adsorbate-adsorbent interactions are weak.

Type IV: The characteristic feature of those isotherms is its hysteresis loop, which is associated with capillary condensation taking place in mesopores.

Type V: Such isotherms are uncommon; they are related to the type III isotherm in that the adsorbate-adsorbate interaction is weak.

Type VI: This type is called step isotherm and represents stepwise multilayer adsorption on a uniform non-porous surface.

In this work the surface area and the pore size were studied by nitrogen-sorption measurements which were performed with use of a Micromeritics ASAP 2020 gas sorptometer. Samples were degassed in vacuum at a pressure of 0.4 Pa for at least 3 h at 350 ºC. The measurements were then carried out at 77 K over a wide range of relative pressures p/p* (p* = 970 hPa) from 0.01-1. Specific surface areas were calculated by assuming *Brunauer-Emmet-Teller* (BET) conditons method. The pore sizes and volumes were estimated from pore size distribution curves as derived from the adsorption branches of the isotherm. The classical pore size model develped by *Barret, Joyner* and *Halenda* (BJH) in 1951, is applied for the calculations of the mesoporous size distribution.[30]

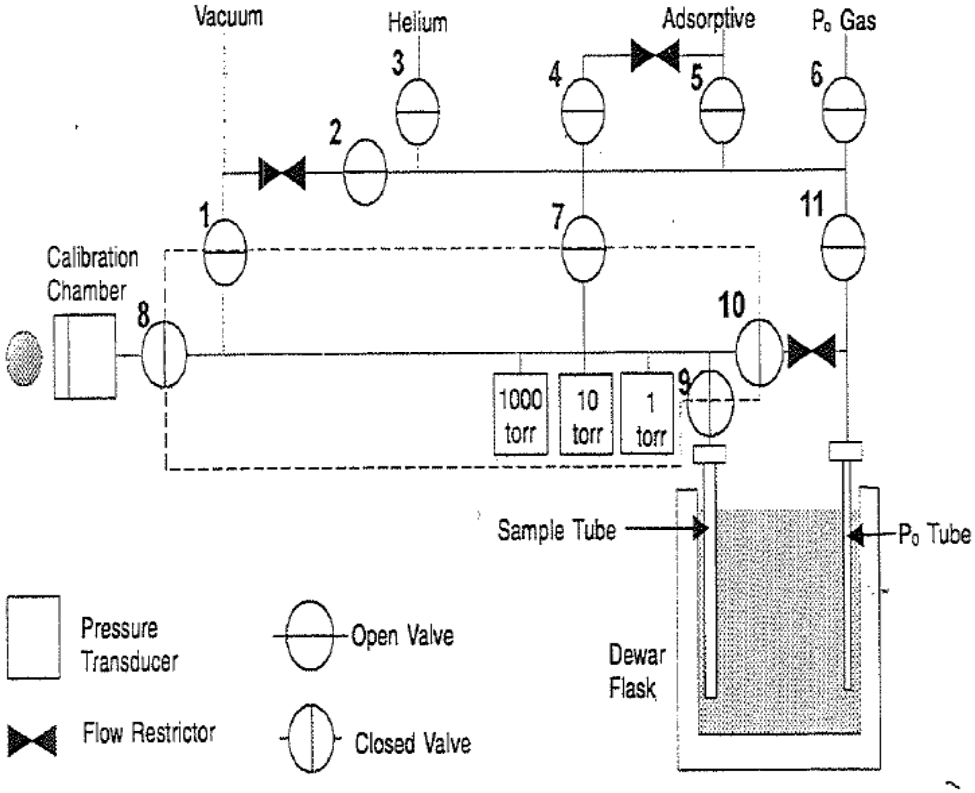


**Fig.2.13** *Functional diagram of ASAP 2020 series manifold. The dashed line indicates the separation of the upper (gas entry) and lower (analytical) manifold zones [from ref. 31]*

### 2.6.6 Thermogravimetric analysis (TGA)

Thermal analysis has been defined by the International Confederation of Thermal Analysis (ICTA) as a general term which covers a variety of techniques that record the physical and chemical changes occurring in a substance as a function of temperature.[32,33] Among the various techniques of the thermal analysis is thermogravimetry (TG).

Thermogravimetry (TG) measures the change in mass of a material as a function of time at a determined temperature (i.e., isothermal mode), or over a temperature range using a predetermined heating rate. Essentially, a TG consists of a microbalance surrounded by a furnace. A computer records any mass gains or losses. Weight is plotted against a function of time for isothermal studies and as a function of temperature for experiments at constant heating rate. Thus, this technique is very useful in monitoring heat stability and loss of components (e.g., oils, plasticizers, or polymers).[34] In our work, thermogravimeteric analysis (TGA) has been measured with use of a METTLER TOLEDO-TGA/ SDTA 851e device.

## 2.7 Materials

D (+)-Glucose monohydrate ($C_6H_{12}O_6.H_2O$), water glass, i.e., sodium silicate solution ($Na_2SiO_3$ solution containing about 25% $SiO_2$), chromium (III) chloride hexahydrate ($CrCl_3.\ 6H_2O$), cobalt (II) chloride hexahydrate ($CoCl_2.\ 6H_2O$), iron (III) chloride hexahydrate ($FeCl_3.\ 6H_2O$), zinc (II) chloride ($ZnCl_2$) and nickel (II) chloride ($NiCl_2$) were obtained from Merck (Darmstadt, Germany). Commercial fructose was bought from *dm* market in Germany. Acetic Acid ($CH_3COOH$) was obtained from J. T. Baker (Deventer, Holland). All mentioned chemicals were analytical grade and employed without further purification. Distilled water (conductivity ~ 1.7 µs/cm) was used.

## References


1- Y. Ma, L. Qi, *J. Coll. & Inter. Sci.* **335** (2009) 1.

2- J. Hu, M. Chen, X. Fang, L. Wu, *Chem. Soc. Rev.* **40** (2011) 5472

3- J. Yuan, T. Zhou, H. Pu, *J. phys. & Chem. Sol.* **71** (2010) 1013.

4- X. M. Sun, Y. D. Li, *Angew. Chem. Int. Ed.* **43** (2004) 597.

5- X. Sun, J. Liu, Y. Li, *Chem. Eur. J.* **12** (2006) 2039.

6- W. H. Shen, Y. F. Zhu, X. P. Dong, J. L. Gu, J. L Shi, *Chem. Lett.* **34** (2005) 840.

7- X. L. Li, T. J Lou, X. M. Sun, Y. D. Li*, Inorg. Chem*. **43** (2004) 5442.

8- M. M. Titirici, M. Antonietti, A. Thomas, *Chem. Mater.* **18** (2006) 3808.

9- M. T. Postek, K. S. Howard, A. H. Johnson K. L. McMichael, *Scanning electron microscopy: a student's handbook,* Ladd Research Industries, Inc. (1980).

10- J. P. Eberhart, *Structural and Chemical Analysis of Materials*, John Wiley & Sons Ltd: England (1991)**.**

11- E. Abbe, *Die optischen Hilfsmittel der Mikroskopie* [Vieweg, Brunswick, Germany] (1878) p. 411.

12- L. de Broglie, *thesis, University of Paris* (1924); *Ann. Phys*. (Paris) **3** (1925) 22.

13- H. Busch, *Ann. Physik* **81** (1926) 974; *Arch. Elektrotech*. **28** (1927) 583.

14- E. Wiechert, *Wied. Ann*. **69** (1899) 737.

15- Martin M. Freundlich, *Origin of the Electron Microscope*, Published by: American Association for the Advancement of Science (1963)

16- Z. L. Wang, *J. Phys. Chem*. *B* **104** (2000) 1153.

17- A. H. Latham, Mary Elizabeth Williams, *Langmuir* **24** (2008) 14195.

18- D. P. A. Le Galley, *Rev. Sci. Instrum*. **6** (1935).

19- R. Jenkins, R. L. Snyder, *Introduction to X-ray powder diffractometry*, John Wiley & Sons, New York (1996).

20- A. S. Negi, S. C. Anand, *A textbook of physical chemistry*, 2nd edt. , New Age International (P) Ltd. (2004).

21- Philips Analytical, X'Pert Plus (1.0) (Almelo) (1999).

22- B. Stuart, *Infrared Spectroscopy: Fundamentals and Applications*, John Wiley & Sons, Ltd (2004).

23- H. Günzler, H.-U.Gremlich, *IR spectroscopy: An introductionm*, Wiley-VCH, Weiheim, Germany (2002).

24- J. C. Groen, J. P. Ramirez, *Appl. Catalyst A: general* **268** (2004) 121.

25- P. Brunauer, H. Emmett, E. Teller, *J. Am. Chem. Soc*. **60** (1938) 309.

26- V. S. Ramachandran, J. J. Beaudoin, *Handbook of analytical techniques in concrete science and technology*, William Andrew publishing, LLC, New York (2001).

27- R.W. Cranston, A. F. Inkley, *Advances in Catalyst* **9** (1957) 143.

28- K. S. W. Sing, D. H. Everett, R. A. W. Haul, L. Moscou, R. A. Pierotti, J. Rouquerol, T. Siemieniewska, *Pure & Appl. Chem.* **57** (4) (1985) 603.

29- J. S. Gregg, W. S. K. Sing, *Adsorption, surface area and porosity*, Academic press, NY (1967).

30- E. P. Barrett, L. G. Joyner, P. P. Halenda, *J. Am. Chem. Soc.* **73** (1951) 373.

31- P. A. Webb, C. Orr, *Analytical methods in fine particles technology*, Micromeritics Instrument Corporation (1997).

32- R. C. Mackenzie, *Talanta* **16** (1969) 1227.

33- R. C. Mackenzie, C. J. Keattch, , D. Dollimore, J. A. Forrester, A. A. Hodgson, J. P. Redfern, *Talanta* **19** (1972) 1079.

34- V.S. Ramachandran, R. M. Paroli, J. J. Beaudoin, A. H. Delgado , *Thermal analysis of construction materials*, William Andrew publishing, New Yourk (2002).

# Chapter 3

## Hydrothermal synthesis of carbonaceous spheres from aqueous glucose and fructose solutions in closed system

We investigated the synthesis of carbonaceous spheres via the hydrothermal hydrolysis of aqueous solution of glucose as well as fructose in closed system (100 mL Teflon-lined stainless steel autoclave). Different synthesis parameters such as temperature, reaction time, sugar concentration and addition of acetic acid acting as catalyst, are important for tuning the diameter of the as-prepared carbonaceous spheres. Details on the composition and morphology of the carbonaceous materials were obtained from infra red spectroscopy (IR), carbon hydrogen analysis (CH) and scanning electron microscopy (SEM), showing that the carbonaceous materials posses' high functionalities and it has about 60 to 70 % carbon and have spherical morphology with smooth surface.

## 3.1 Introduction

Due to carbonaceous spheres (CSs) can be easily prepared from various kinds of low-cost sugar, colloidal carbonaceous micro- and nano-spheres synthesized from sugar have been a hot topic and a trend of researchers in many fields.[1-3] In the field of hollow materials, carbonaceous spheres (CSs) are optimal candidates to be used for the synthesis of many hollow oxides because of the richness of its surface with functionalities. Therefore, the surface of the sphere is hydrophilic and has a distribution of -OH and - C=O groups in which makes surface modifications unnecessary. When the carbonaceous spheres are dispersed in solutions of metal salts, the cations are readily adsorbed into the surface.

The thermal treatment of organic substances such as saccharides (glucose, sucrose, or starch) mixed with water in the range 150- 350 $^{o}$C under autogenous pressure, gives rise to water soluble organic compounds and a carbon rich solid product. This process termed hydrothermal carbonization, has generated widespread interest in recent years.[4] The hydrothermal carbonization is an aqueous phase based route to carbonaceous materials using water-soluble carbon precursors, typically carbohydrates or their derivatives as well as raw agricultural biomass.[5,6] The synthesis is involving the hydrothermal decomposition of various carbohydrates in aqueous solutions and carried out in an autoclave at moderate temperatures (< 200 $^{o}$C) and under self-generated pressures (< 10 bar) to typically yield a solid carbonaceous precipitate. The remarkable transformation of sugars molecules to form homogeneous carbonaceous spheres readily occurs by a dehydration mechanism and subsequent nano-scale sequestering in aqueous solutions when heated at temperatures (< 200 $^{o}$C).[2] Under such conditions, these molecules actually dehydrate even through they are dissolved in water.

The hydrothermal carbonization process has the advantage of being very cheap, mild, and absolutely ‘‘green’’ as the preparative process cause no contamination to the environment because it involves no organic solvents, catalysts, or surfactants.[7,8] One of the most widely used saccharides to produce carbonaceous materials is glucose. When an aqueous solution/dispersion of glucose is heat-treated at a moderate temperature in the 170–200 $^{o}$C range (under pressure), a carbon-rich black solid is obtained as insoluble product. This process gives rise to other substances besides the solid residue. These include aqueous soluble products (furfural, hydroxymethylfurfural, acids, and aldehydes) and gases ($CO_2$, $CH_4$, etc.).[9-12]

The hydrothermal treatment of saccharides is not a new process. The first research work on the hydrothermal carbonization of saccharides was carried out during the first decades of the 20$^{th}$ century with the aim of understanding the mechanism of coal formation. Thus, in 1913 *Bergius et al*. subjected cellulose to hydrothermal carbonization at temperatures in the 250–310 $^{o}$C range, as a result of which they obtained a black residue with a O/ C atomic ratio of 0.1–0.2 (O/C atomic ratio of cellulose: 0.84).[13] Later, in 1932, *Berl et al.* investigated the hydrothermal treatment of cellulose over a wider temperature range (200–350 $^{o}$C).[14] In 1960, *van Krevelen et al.*[15] noticed that the solid products derived from the hydrothermal treatment of the cellulose and glucose have the same composition, which suggests that the hydrolysis products for both substances are similar.

Renewed interest in the hydrothermal carbonization of saccharides has recently been established. However, the objectives of these new investigations are completely different to those previously mentioned. Now the main purpose is to use this process as a way to produce carbonaceous materials with specific properties (i.e., shape, size, chemical functionalities, etc.). In 2001, *Wang et al.* [1] reported the synthesis of carbonaceous microspheres of a tunable size (in the 0.25–5 μm range) through the hydrothermal carbonization of sucrose at 190$^{o}$C.

Much attention has also been focused on the hydrothermal carbonization of sugars in the presence of inorganic salts, which gives rise to the formation of hybrid carbon/metal materials (C/Ag, C/Cu, C/Au, C/Pd, and C/Te), with complex nanoarchitectures.[2,16-19] *Yao* and co workers [24] investigated the mechanism of formation of carbonaceous microspheres in the course of the hydrothermal treatment of glucose. They concluded that during hydrothermal treatment, glucose loses water first (T=160 $^{o}$C) through an intermolecular condensation reaction and that subsequently an aromatization (carbonization) process occurs. In addition, the microspheres resulting from the hydrothermal carbonization have been employed as sacrificial templates for fabricating hollow spheres of inorganic compounds.[20]

Recently, other groups have taken advantage of oxygen functionalities present on the outer surface of the carbonaceous spheres and employed them as sacrificial templates to fabricate hollow spheres of inorganic materials ($Ga_2O_3$, GaN, $SnO_2$, etc.).[20-23,25] The formation of metal oxides hollow spheres can be performed either in a two step process, by forming CSs in the first step followed by formation of hybrid particles (CSs@precursor of the desired oxide composites), or the formation of hybrid particles in one step hydrothermal process in closed vessel (autoclaves). In the following calcination process, the metal atoms in the shell become denser, the spheres contract and cross-link to form metal oxide hollow spheres which are a smaller replica of the CSs.

Among the potential saccharides that can be employed to produce carbonaceous materials through hydrothermal carbonization, *fructose* is one of the most promising material as it is by far one of the most widely available and inexpensive saccharides available. Although some authors have reported using of carbohydrates as sacrificial templates for the synthesis of hollow inorganic materials,[20-23] *to the best of our knowledge, no one has employed fructose as sacrificial templates for forming hollow spheres by means of hydrothermal carbonization*.

In this chapter we investigated the hydrothermal carbonization of glucose and fructose as promising candidates as sacrificial templates for the production of some hollow oxides spheres. The impact of the synthesis parameter such as temperature, reaction time, sugar concentration, and addition of acetic acid acting as catalyst on the formation of the carbonaceous spheres have been investigated as well.

## 3.2 Hydrothermal carbonization of glucose

The hydrothermal reaction of glucose in an autoclave at temperatures equal 180 $^{o}$C generates a solid residue, which we denote as carbonaceous spheres, a name that reflects both the nature of the product and the morphology. The carbonaceous materials were characterized by means of different experimental techniques: scanning electron microscopy (SEM), X-ray diffraction (XRD), infrared spectroscopy, nitrogen physisorption (BET), and elemental C/H/O chemical analysis.

The carbonaceous spheres is a carbon rich material made up of particles with a spherical morphology having diameters in the 50 nm– 950 nm range, as evidenced by the SEM images shown in Fig.3.1. These figures also include histograms of the diameter distribution of the carbonaceous spheres which clearly show a high degree of uniformity.

The mean diameter and standard deviations of the carbonaceous spheres microspheres synthesized under a variety of operational conditions are listed in Table 3.1 We observed that for temperatures in the range ≥200 $^{o}$C as well as long reaction times > 24 h, the carbonaceous spheres fuse, thereby giving rise to particles that have a shapeless morphology (Fig.3.2). The optimal temperature conditions to form regular spherical morphology of the carbonaceous spheres are 180 $^{o}$C for 24 h which are in accord with literatures.[9-12]

The $N_2$ adsorption measurements reveal that these of the carbonaceous spheres obtained have a poor porosity, the BET surface areas being less than 8 $m^2g^{-1}$ , as shown in Fig.3.4.

The diameter of the carbonaceous spheres can be modulated by modifying the concentration of glucose or adding catalyst. Variable concentrations of glucose were used. C1 stands for the initial glucose concentration of 960 mmol/L, C2, C4, C10 and C15 for 1/2, 1/4,, 1/10 and1/15 of C1, respectively, as shown in Table 3.1; the catalyst used was 0.5 mL of acetic acid. Actually, we observed that, increasing the concentration of the reaction mixture, leads to an increase in the mean diameter of the carbonaceous spheres. As well as, adding of 0.5 mL acetic acid increases the average particle size of the carbonaceous spheres due to the increase in the rate of hydrothermal hydrolysis of glucose (see Table 3.1 and Fig.3.3).

**Table 3.1** *Physical properties of carbonaceous spheres materials resulting from the hydrothermal treatment of glucose*

| Glucose sample code | c [$mmolL^{-1}$] | T [$^oC$] | t [h] | Sphere diameter [nm][a] |
|---|---|---|---|---|
| 1-C1 | 960 | 180 | 24 | 1000 (± 220) |
| 2-C2 | 480 | 180 | 24 | 485 (±140) |
| 3-C4 | 240 | 180 | 24 | 375 (±100) |
| 4-C10 | 96 | 180 | 24 | 325 (±120) |
| 5-C15 | 64 | 180 | 24 | 55 (±25) |
| 6-C10/AcOH | 96 | 180 | 24 | 970(±230) |
| 7-C2 | 480 | 180 | 36 | ---------- |
| 8-C10 | 96 | 180 | 36 | ---------- |
| 9-C2 | 480 | 200 | 24 | ---------- |
| 10-C10 | 96 | 200 | 24 | ---------- |

[a] Mean spherule diameter size. Standard deviation is indicated in parentheses.

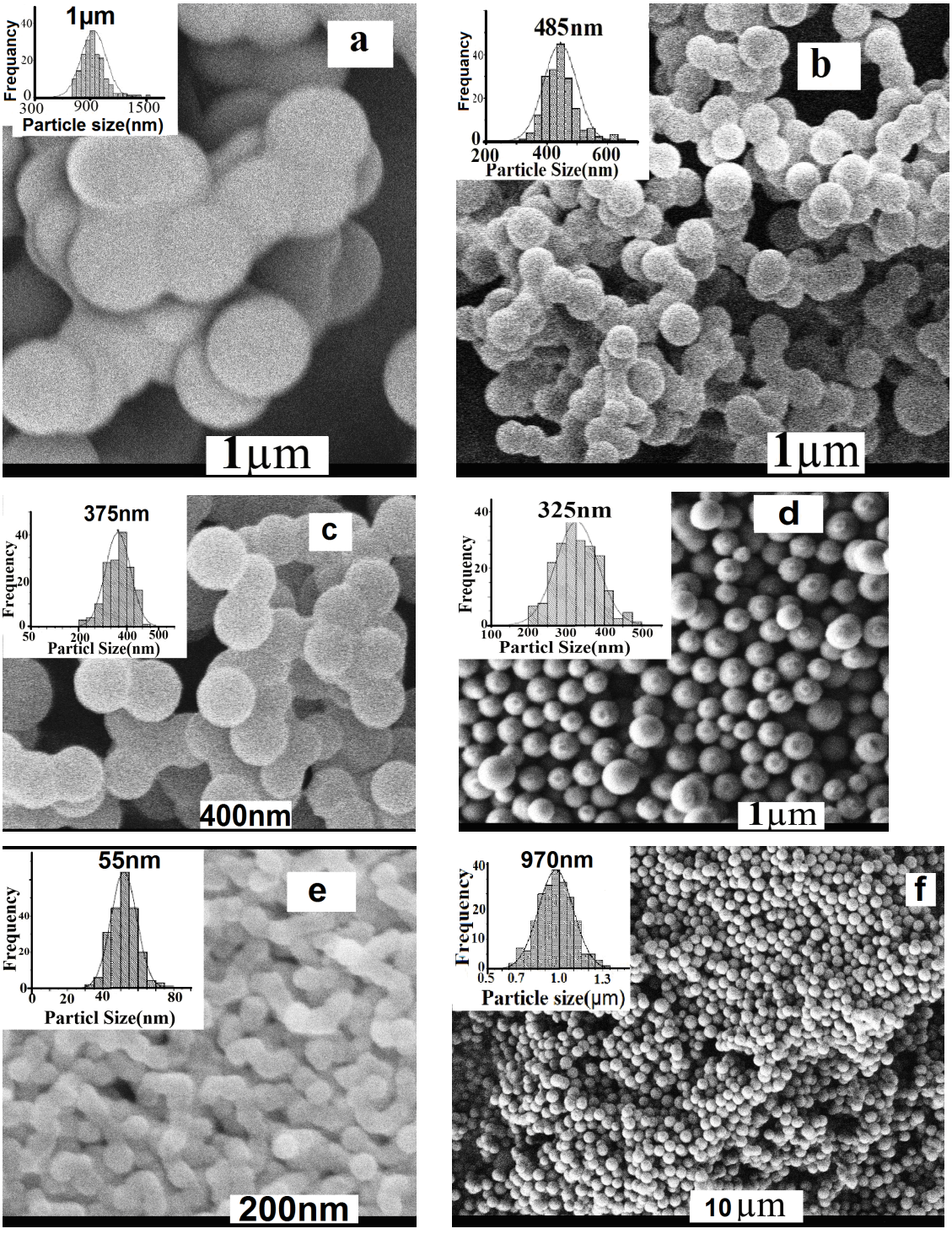


**Fig. 3.1** *SEM microphotographs and size histograms of the carbonaceous spheres obtained by hydrothermal carbonization of glucose samples a)1-C1, b) 2-C2, c) 3-C4, d) 4-C10, e) 5-C15, and f) 6-C10*

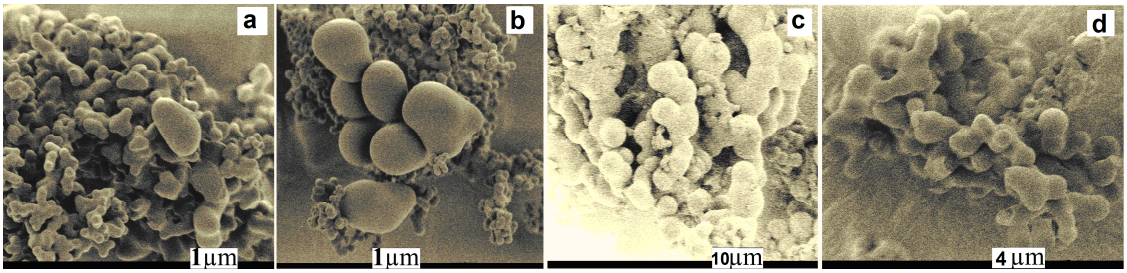


**Fig.3.2** [a] *SEM microphotographs of the fused carbonaceous materials obtained by hydrothermal carbonization of glucose samples a)7-C2, b) 8-C10, c) 9-C2, and d) 10-C10*

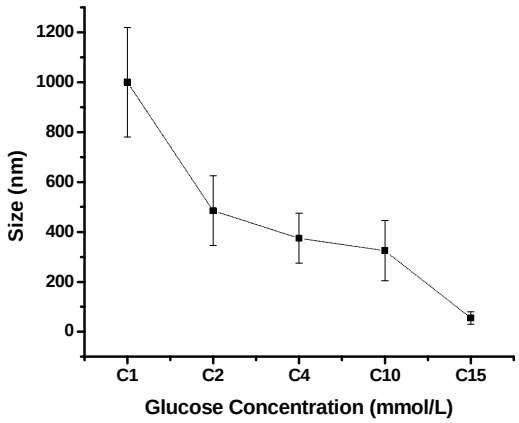


**Fig.3.3** *The relationship between the concentration of glucose and the size obtained of the carbonaceous spheres*

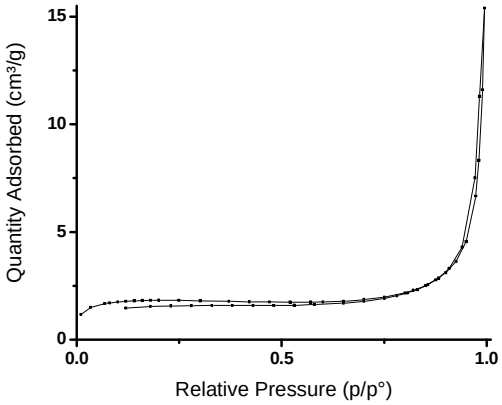


**Fig.3.4** *Nitrogen sorption isotherms of the as-obtained carbonaceous spheres sample 4-C10*

[a] The microphotographs are been colored for more resolution.

### 3.2.1 Chemical properties of the carbonaceous spheres samples

The elemental chemical composition (C, O, and H) of glucose and different carbonaceous spheres samples are listed in Table 3.2. It can be seen that the carbon content increases from approximately 36% to 64–66% in the carbonaceous spheres samples after the hydrothermal carbonization. At the same time there is a reduction in the oxygen and hydrogen contents. These variations become greater as the reaction temperature and the reaction time increase, as well as the presence of the catalyst which is consistent with a carbonization process. These observations reveal that the carbonaceous spheres are carbon-rich materials and posses high oxygen functionalities that make them attractive for the formation of hybrid particles without any further modification for their surface layers and, hence, they are suitable candidates to be applied as sacrificial templates in the formation of various hollow inorganic materials.

**Table 3.2** *Chemical elemental analysis of carbonaceous materials resulting from the hydrothermal treatment of glucose*

| Glucose sample code | C [Wt%] | H [Wt%] | O[Wt%] |
|---|---|---|---|
| glucose | 36.39 | 7.23 | 56.38 |
| 1-C1 | 63.64 | 4.55 | 31.81 |
| 2-C2 | 64.82 | 4.41 | 30.77 |
| 3-C4 | 64.28 | 4.24 | 31.48 |
| 4-C10 | 64.35 | 4.43 | 31.22 |
| 5-C15 | 61.6 | 3.95 | 34.45 |
| 6-C10/AcOH | 65.41 | 4.29 | 30.30 |
| 6-C2 | 65.17 | 4.15 | 30.68 |
| 7-C10 | 65.11 | 4.20 | 30.69 |
| 8-C2 | 65.92 | 4.12 | 29.96 |
| 9-C10 | 66.12 | 4.10 | 29.78 |

### 3.2.2 IR spectra

The IR spectra of all carbonaceous spheres samples contain the same IR bands which indicate that they have a similar chemical nature. As observed from Fig.3.5.a (IR of the chosen sample 4-C10), the bands at 1710 and 1620 $cm^{-1}$ (together with the band at 1513 $cm^{-1}$) can be attributed to C=O (carbonyl, quinone, ester, or carboxyl) and C=C vibrations, respectively, whereas the bands in the 1000–1450 $cm^{-1}$ region correspond to C-O (hydroxyl, ester, or ether) stretching and O-H bending vibrations.[2,27-28] The bands at 875–750 $cm^{-1}$ are assigned to aromatic C-H out-of-plane bending vibrations, whereas the bands at approximately 2900 and 3000–3700 $cm^{-1}$ correspond to stretching vibrations of aliphatic C-H and O-H (hydroxyl or carboxyl), respectively.[27-28]

Comparative analysis of the IR spectra of the carbonaceous spheres (Fig.3.5.a) and those of the glucose (Fig.3.5.b) suggests that dehydration and aromatization processes take place during the hydrothermal carbonization. Thus, the intensities of the bands corresponding to the hydroxyl or carboxyl groups (3000–3700 and 1000–1450 $cm^{-1}$) in the carbonaceous spheres are weaker than those of the corresponding glucose, thereby disclosing dehydration reactions. New vibration bands at 1710 $cm^{-1}$, corresponding to C=O groups, and 1620 and 1513 $cm^{-1}$, corresponding to C=C groups, appear in the carbonaceous material. The appearance of the bands at 1620 and 1513 $cm^{-1}$ indicates the aromatization of the samples. An increase in the temperature of the hydrothermal carbonization of glucose is accompanied by a diminution in the intensities of the band at 1710 $cm^{-1}$ (C=O) and the wide band at approximately 3000–3700 $cm^{-1}$ (O-H) (see Fig.3.5.a) due to oxygen removal. At the same time, both the aromatic hydrogen and aromatic carbon (C=C) content increase, as evidenced by the increase in the intensity of the bands at 875–750 $cm^{-1}$ and 1620 $cm^{-1}$, respectively. These data reveal an increase in the aromatization of the carbonaceous spheres as the reaction temperature rises which is the normal tendency for a carbonization process.[27]

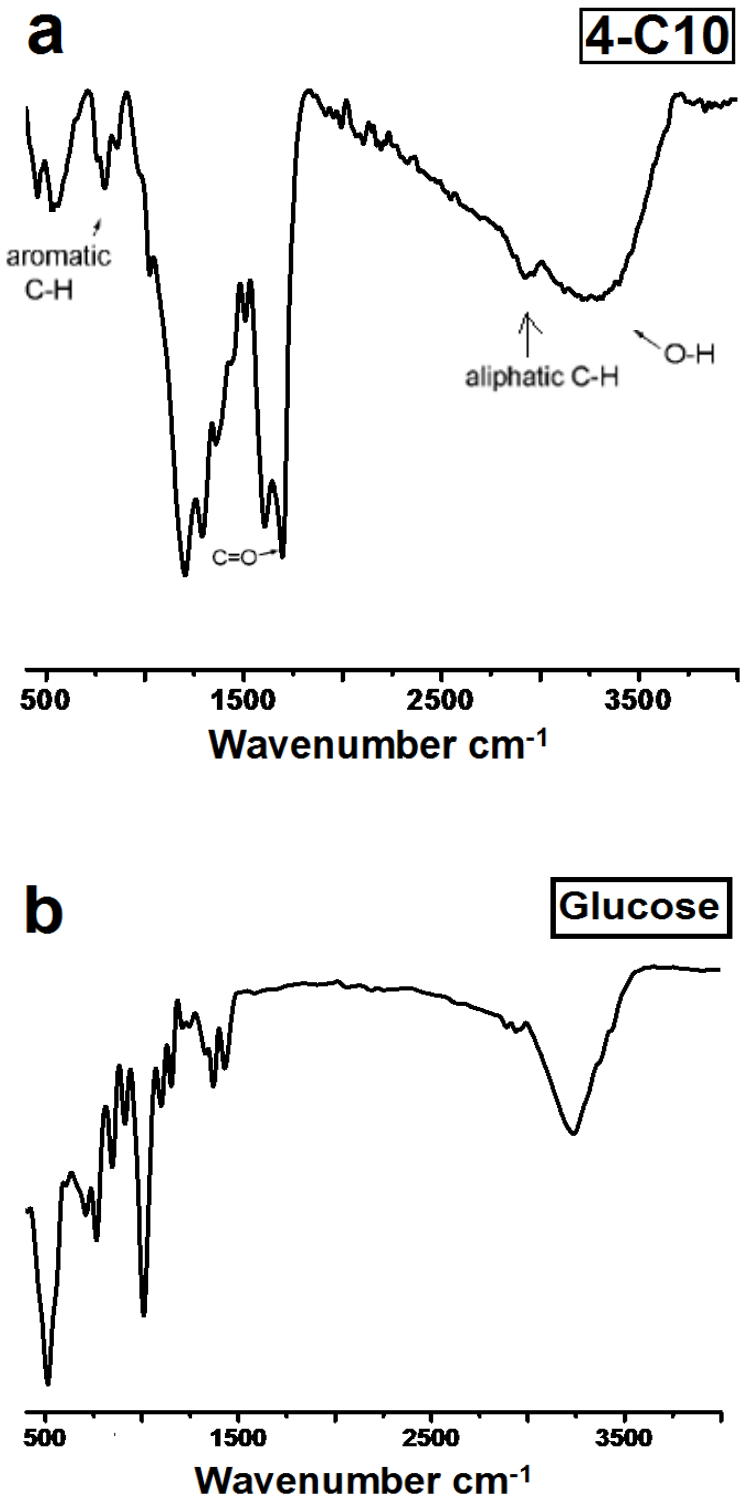


**Fig.3.5** *a) IR spectra of the carbonaceous spheres 4-C10 (sample obtained by hydrothermal treatment of glucose), b) IR spectra of glucose*

## .3.3 Hydrothermal carbonization of fructose

Colloidal carbon spheres are of great interest because the diffusion of guest species through the highly functionalized surface layers can be significantly manipulated by changing their particle sizes and shapes.[29] Surface modification is a key to realizing many of these applications as the prepared surface is often inert.[30] There have been only a few reports regarding colloidal carbon spheres.[31-32] The remarkable transformation of carbohydrate molecules including sugars to form homogeneous carbon spheres readily occurs by a dehydration mechanism and subsequent nanoscale sequestering in aqueous solutions when heated at moderate temperature in a pressurized vessel.[2,33] Under such conditions, these molecules actually dehydrate even though they are dissolved in water. The surface of colloidal sphere products is hydrophilic and a distribution of -OH and -C=O groups makes surface modification unnecessary. Size-tunable metal and metal oxides with uniform shell thickness have also been prepared by using the carbon spheres as templates.[16,20,22] However, the detailed dehydration mechanism during the colloidal carbon formation of glucose and fructose remains unknown.[8]

The goal in our work in this section is to study the hydrothermal dehydration and the impact of synthesis parameters on fructose to be used as sacrificial templates for some inorganic hollow oxides. *To the best of our knowledge, it is the first time that fructose as sacrificial templates for the synthesis of hollow materials is applied.*

When an aqueous fructose solution was heated in a closed vessel to 135-150 °C a solid black residue (carbonaceous spheres) is formed. The synthesis process is “green”, involves none of the toxic organic solvents, initiators, or surfactants that are commonly used for the preparation of polymer micro- or nanospheres. This highly regular form of carbon can be isolated with sphere

diameters in the range from a hundred nanometers to a few micrometers depending upon the processing conditions.

The mean diameter of the carbonaceous spheres micro- and nanospheres synthesized under a variety of operational conditions are listed in Table 3.3. We noticed that when the temperature is less than 135 $^{o}$C no precipitated material observed. For temperatures in the range ≥150 $^{o}$C as well as long reaction times > 6h, the carbonaceous spheres fuse, thereby giving rise to particles that have no detected morphology (Fig.3.8). In addition, the optimal temperature to produce regular spherical morphology of the carbonaceous spheres via the hydrothermal dehydration of fructose was in the range of 135- 150 $^{o}$C for 6 h. (Fig.3.6 and Fig.3.7).

Fig.3.6 shows the final products isolated from the fructose reaction mixtures prepared at different temperatures by centrifugation at 9000 rpm. They are homogeneous carbon spheres having a smooth nonporous surface in accord with BET measurements. The carbon spheres prepared at reaction temperatures (135 and 150 °C) show a regular morphology and homogeneous distribution while at lower temperatures than 135 °C no material is obtained. The diameters of the carbon spheres are influenced by reaction temperature, time, fructose concentration and catalyst.

As evidence from Figures 3.6, 3.7, 3.8, and 3.9 we observed that with decreasing concentration of fructose the size distributions show the average diameter (obtained as maximum of a Gaussian distribution) gets significantly smaller. Also the width of the size distribution shrinks with decreasing concentration. Variable concentrations of fructose were used. Fr1 stands for the initial fructose concentration of 2.5 mol/L, Fr2, Fr4, and Fr16 for 1/2, 1/4, and 1/16 of Fr1, respectively, as shown in Table 3.3. Thus, at the same processing conditions the mean diameter follows the tendency:

$$Fr16<Fr4<Fr2<Fr1$$

The optimal time observed at the same operational conditions was 6 h, above and below which no results of interest were obtained. Also, the addition of acetic acid as a catalyst has a conspicuous effect on the growth of carbonaceous spheres. The diameters of the carbonaceous spheres that form during the catalyzed reaction are much bigger than the ones that form during the uncatalyzed reaction. Acetic acid catalyzes the hydrothermal carbonization reaction and increases the rate of hydrothermal dehydration of fructose hence eventually leading to an increase in size. The optimal temperature range for the hydrothermal carbonization of fructose was 135-150 °C below which no measurable precipitates are recorded, above which no regular shape is formed. In addition, through this range the size is much smaller at lower temperature.

**Table 3.3** *Physical properties of carbonaceous spheres materials resulting from the hydrothermal treatment of fructose*

| Fructose sample code | c [mol $L^{-1}$] | T [$^{o}$C] | t [h] | Catalyst | Sphere average diameter[a] |
|---|---|---|---|---|---|
| 1-Fr1 | 2.5 | 150 | 6 | ----- | ----- |
| 2-Fr2 | 1.25 | 150 | 6 | ----- | 1150 nm |
| 3-Fr2 | 1.25 | 150 | 6 | 0.5 mL AcOH | 4.8 µm |
| 4-Fr4 | 0.625 | 150 | 6 | ----- | 250 nm |
| 5-Fr4 | 0.625 | 150 | 6 | 0.5mL AcOH | 2.2 µm |
| 6-Fr4 | 0.625 | 135 | 6 | ----- | 200 nm |
| 7-Fr4 | 0.625 | 135 | 24 | ----- | ----- |
| 8-Fr4 | 0.625 | 135 | 12 | ----- | ----- |
| 9-Fr16 | 0.313 | 150 | 6 | ----- | 150 nm |
| 10-Fr16 | 0.313 | 150 | 6 | 0.5 mL AcOH | 200 nm |

[a] Mean spherule diameter size. Standard deviation is indicated in parenthesis

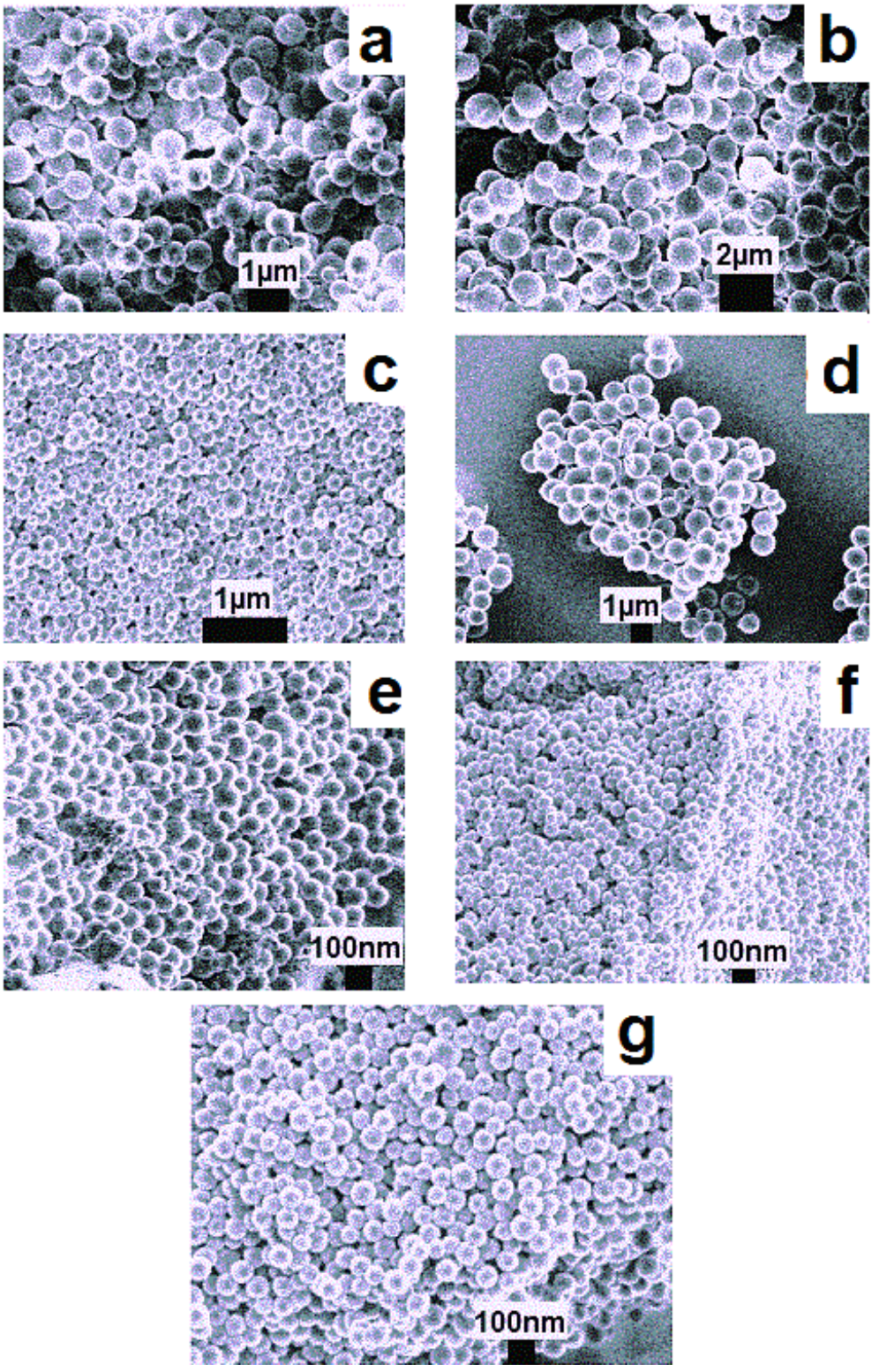


**Fig.3.6** *SEM microphotographs of the carbonaceous spheres obtained by hydrothermal carbonization of fructose samples a)2-Fr2, b) 3-Fr2, c) 4-Fr4, d) 5-Fr4, e) 6-Fr4, f) 9-Fr16, and g) 10-Fr16*

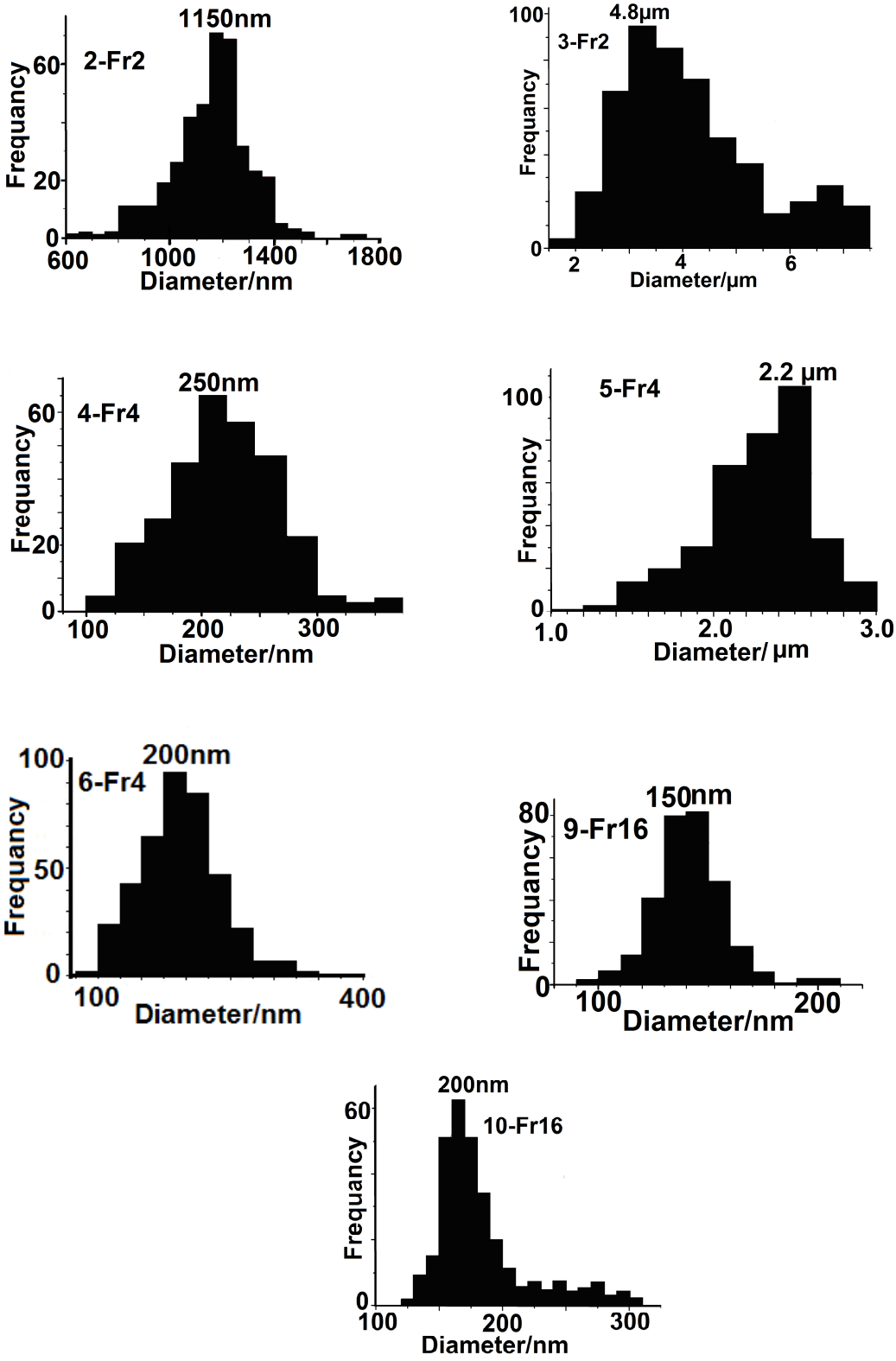


**Fig.3.7** *Particle size distributions (PSD) histograms of the different carbonaceous spheres samples formed by hydrothermal carbonization of fructose*

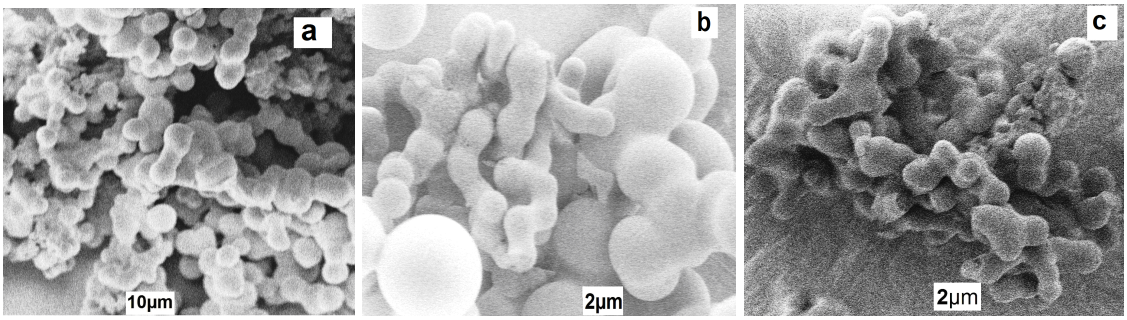


**Fig.3.8** *SEM microphotographs of fused carbonaceous materials obtained by hydrothermal carbonization of fructose samples a)1-Fr1, b) 7-Fr4 and c) 8-Fr4*

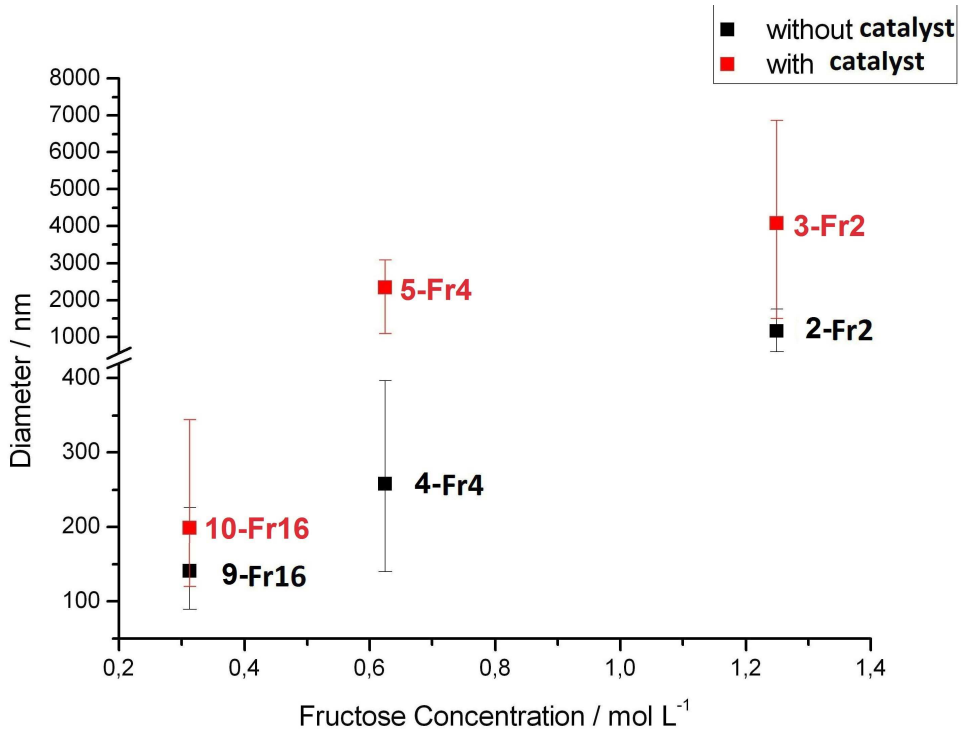


**Fig.3.9** *The relationship between concentration of fructose and the size of carbonaceous spheres with the presence and the absence of the catalyst*

The $N_2$ adsorption measurements (BET) show that the carbonaceous spheres obtained have a poor porosity also like glucose samples. However, the BET surface areas is 4 $m^2g^{-1}$ which is less than that of carbonaceous spheres obtained from the glucose samples. From that context, we can infer that the surface is less porous than that of glucose samples, as shown in Fig.3.10.

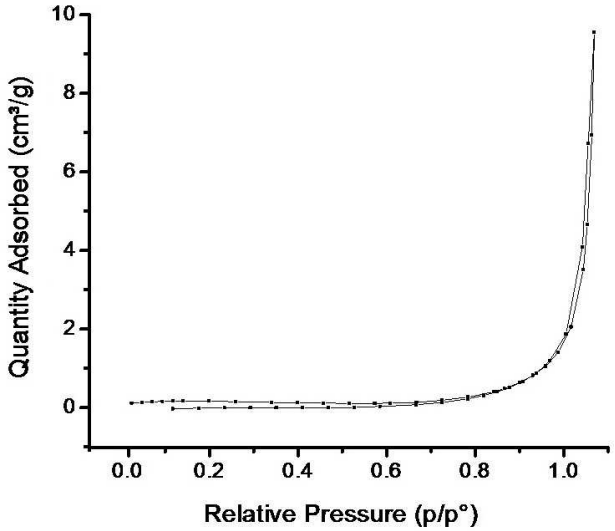


**Fig.3.10** *Nitrogen sorption isotherms of the as-obtained carbonaceous spheres sample 4-Fr4*

### 3.3.1 Chemical properties of the carbonaceous spheres samples

The elemental chemical composition (C, O, and H) of fructose and different carbonaceous spheres samples are listed in Table 3.4. It can be noticed that the carbon content is approximately 4-5 % less than that noticed in glucose samples. On the other hand, the oxygen content is nearly 4-5 % greater than oxygen content in glucose samples. This might be due to the reduction in the typical carbonization time from 24 h in case of carbonization of glucose to 6 h in case of fructose carbonization.

Like the trends of glucose samples, the carbon content in the carbonaceous spheres in fructose samples increases from approximately 40% to 58–62% after the hydrothermal carbonization reaction. At the same time there is a reduction in the oxygen and hydrogen contents. These variations become greater as the reaction temperature and the reaction time increase, as well as the presence of the catalyst which is consistent with a carbonization process.

**Table 3.4** *Chemical elemental analysis of carbonaceous materials resulting from the hydrothermal treatment of fructose*

| Fructose sample code | C [Wt%] | H [Wt%] | O[Wt%] |
|---|---|---|---|
| fructose | 40 | 6.9 | 53.1 |
| 1-Fr1 | 58.7 | 4.9 | 36.4 |
| 2-Fr2 | 58.8 | 4.8 | 36.4 |
| 3-Fr2 | 61.3 | 4.4 | 34.3 |
| 4-Fr4 | 58.9 | 4.7 | 36.4 |
| 5-Fr4 | 60.8 | 4.6 | 34.6 |
| 6-Fr4 | 56.9 | 4.9 | 38.2 |
| 7-Fr4 | 62.9 | 4.6 | 32.5 |
| 8-Fr4 | 60.7 | 4.4 | 34.9 |
| 9-Fr16 | 59.1 | 4.4 | 36.5 |
| 10-Fr16 | 62.2 | 4.3 | 33.5 |

For instant, sample 5-Fr4 has 2% carbon content more than sample 4-Fr4 due to the applying of 0.5 mL acetic acid as a catalyst. Another example, sample 6-Fr4 has approximately 2% carbon content less than that of 4-Fr4 due to the reduction in temperature from 150 to 135 $^{o}$C. A third example, sample 7-Fr4 has 4% carbon content greater than sample 4-Fr4 because of the increase in the carbonization reaction time.

These observations indicate that the carbonaceous spheres are carbon-rich materials and posses high oxygen functionalities that make them attractive for the formation of hybrid particles without any further modification for their surface layers and, hence, fructose will be suitable candidate to be applied as sacrificial template in the formation of various hollow inorganic materials.

### 3.3.2 IR spectra

The carbonaceous spheres samples obtained by the hydrothermal carbonization of fructose showed the same IR bands. This is an indication that all fructose samples prepared at different operational conditions have the same chemical nature. Fig.3.10 shows the IR spectra of a) sample 4Fr4 and, b) fructose which show the characteristic peaks related to O-functional groups. This proves that the spheres are not pure carbon but carbonaceous spheres that still got O functionalities. This is in accord with the chemical elemental analysis shown in Table 3.4.

IR spectra of isolated colloidal carbon show that they contain resident functionalities including carboxylate (1704 $cm^{-1}$), hydroxyl (3500 $cm^{-1}$), and C=C groups (1604 $cm^{-1}$). Table 3.5 presents the correlation between the characteristic peaks in Fig.3.10. a, and vibrations of functional groups.

**Table 3.5** *The correlation between the characteristic peaks of the IR spectrum of sample 4-Fr4 and vibrations of functional groups*

| $\tilde{\nu}$ / $cm^{-1}$ | $\tilde{\nu}_{literature}$/ $cm^{-1}$ [34] | Vibration |
|---|---|---|
| 779-809 | 800 | C-H out-of-plane bending vibrations |
| 1163, 1191 | 970-1250 | C-O bending (alcohols, phenols) |
| 1519 | 1500 | C=C bending vibration (aromatic compound) |
| 1618 | 1600 | C=C bending vibration |
| 1668-1707 | 1700 | C=O bending vibrations |
| 3413 | 3400 | O-H bending vibrations |

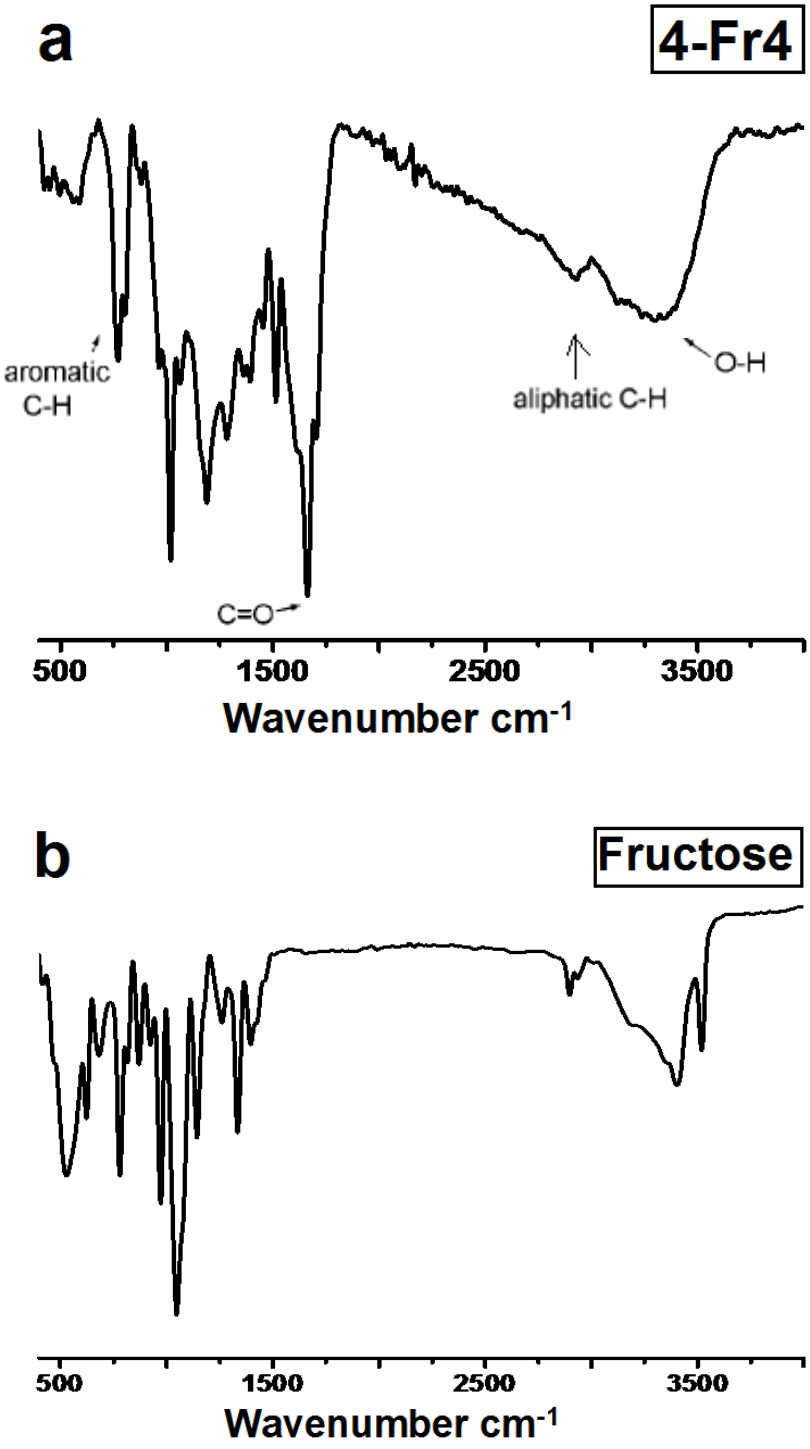


**Fig.3.11** *a) IR spectrum of the carbonaceous spheres of sample 4-Fr4 b) IR spectrum of fructose*

Comparative analysis of the IR spectra of the carbonaceous spheres (Fig.3.11.a) and those of the fructose (Fig.3.11.b) show that the carbonaceous spheres IR spectra (Fig.3.11.a) contain some prominent features assigned to the appearance of the bands at 1620 and 1513 $cm^{-1}$ which reveals the aromatization of the samples.[27,34] An increase in the temperature of the hydrothermal carbonization of fructose is accompanied by the broad absorption band at approximately 3000–3500 $cm^{-1}$ (O-H) due to oxygen removal. Concomitantly, both the aromatic hydrogen and aromatic carbon (C=C) content increase, as evidenced by the increase in the intensity of the bands at 875–750 $cm^{-1}$ and 1620 $cm^{-1}$, respectively. These data reveal an increase in the aromatization of the carbonaceous spheres as the reaction temperature rises which is the normal tendency for a carbonization process.[27-28,34]

### 3.4 XRD of glucose and fructose-derived carbonaceous spheres

From Fig.3.12 a) and b), we can notice the amorphous nature of the as-obtained carbonaceous spheres derived from the hydrothermal carbonization of glucose and fructose. It is noteworthy to mention that all glucose and fructose samples showed the same amorphous nature.

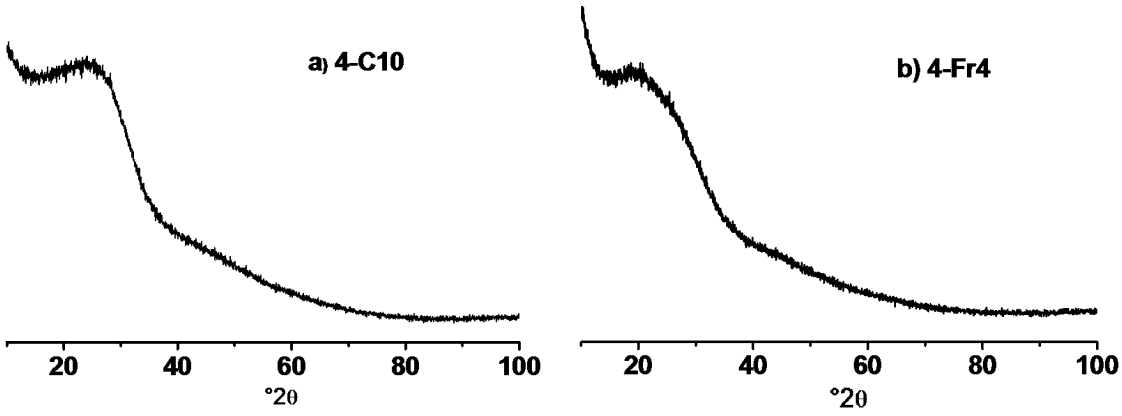


**Fig.3.12** *XRD of carbonaceous spheres derived from the hydrothermal carbonization of (a) glucose and (b) fructose*

## 3.5 The mechanism of the hydrothermal carbonization of monosaccharide

Highly functionalized carbonaceous materials were produced by means of the hydrothermal carbonization of glucose and fructose at temperatures in the180–200 $^{o}$C and 135-150 $^{o}$C range, respectively. The materials so formed are composed of carbonaceous spheres with size ranging between few hundred nanometers to several micrometers, as evidenced by SEM. The combination of the results of the elemental analysis with that obtained by infrared spectroscopy has allowed us to infer that, from a chemical point of view, the solid product surface layers possesses reactive/hydrophilic oxygen functionalities (i.e. hydroxyl, carbonyl, carboxylic, ester).

Although to our knowledge the mechanism of the hydrothermal carbonization of carbohydrates is an open question and remains a challenge to material scientists, there are few works on the chemical transformations that take place when carbohydrate is treated under pressure in water in the literature[4,6, 35-39].

Therefore, in order to gain some knowledge about the principals of the hydrothermal carbonization of glucose and fructose, we through some light on the mechanism of the formation of the carbonaceous products that demonstrated in the literatures.[4,6,35-39]

It was demonstrated that, under hydrothermal conditions, in a first step, when a monosaccharide aqueous dispersion is hydrothermally treated at temperatures typically equal 180 or 135 $^{o}$C in case of glucose or fructose, respectively, the monosaccharide hydrolyze. At this stage, the hydrolysis of the monosaccharide is giving rise to different organic acids (acetic, lactic, propenoic, levulinic and formic acids),[40] the hydronium ions formed from these acids being the catalysts of the degradation in subsequent reaction stages.[41] The subsequent dehydration and fragmentation reactions (i.e. ring opening and C-C bond breaking) leading to the formation of different soluble products, such as

furfural- like compounds (i.e. 5-hydroxymethylfurfural (HMF), furfural, 5-methylfurfural.[38-39,42]

The decomposition of the furfural-like compounds also generates acids/aldehydes and phenols.[36] The subsequent reaction stages consist of polymerization or condensation reactions which lead to the formation of soluble polymers. Concomitantly, the aromatization of polymers takes place. C=O groups appear due to the dehydration of water from the equatorial hydroxyl groups in the monomers.[43] Aromatic clusters may be produced by the condensation of the aromatized molecules generated in the decomposition/dehydration of monosaccharides. When the concentration of aromatic clusters in the aqueous solution reaches the critical supersaturation point, a burst nucleation takes place. The nuclei so formed grow outwards by diffusion towards the surface of the chemical species present in the solution. These species are linked to the surface of the microspheres via the reactive oxygen functionalities (hydroxyl, carbonyl, carboxylic, etc.) present in both the outer surface of the particles and in the reactive species.

Once the growth process stops, the outer surface of the carbonaceous particles will contain a high concentration of reactive oxygen groups. Whereas, the oxygen in the core forms less reactive groups than that in the shell or surface layers of the carbonaceous microspheres.

*A.B. Fuertes et al*.[4] speculated that the oxygen in the inner part of the microspheres probably consists of less reactive groups (i.e. ether, quinone, pyrone), whereas the shell mainly contains more reactive/ hydrophilic (i.e. hydroxyl, carbonyl, carboxylic, ester) oxygen functionalities.

Generally, from the mechanism information presented here, the formation of carbonaceous materials occurs through the following steps:

1. Hydrolysis of glucose or fructose,
2. Dehydration and fragmentation into soluble products of the monomers that come from the hydrolysis of glucose or fructose to HMF or furfural,
3. Polymerization or condensation of the soluble products,
4. Aromatization of the polymers thus formed,
5. Carbonization via further intermolecular dehydration.

The following figures present some schematic illustration for the hydrothermal carbonization of carbonaceous materials obtained from the hydrothermal carbonization of carbohydrate:-

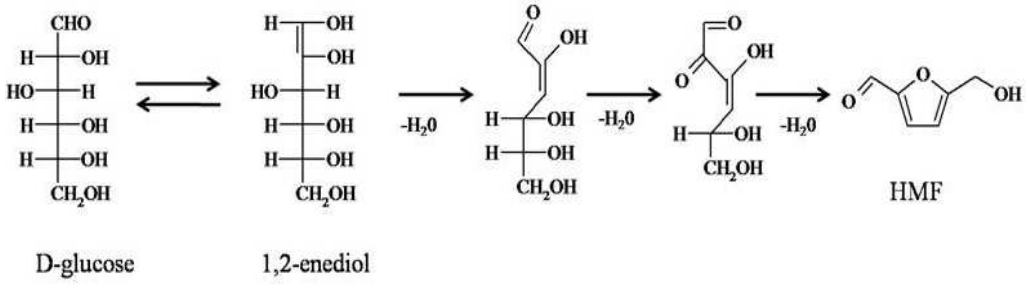


**Fig.3.13** *A generalized mechanism of dehydration of D-glucose into HMF [from ref. 39]*

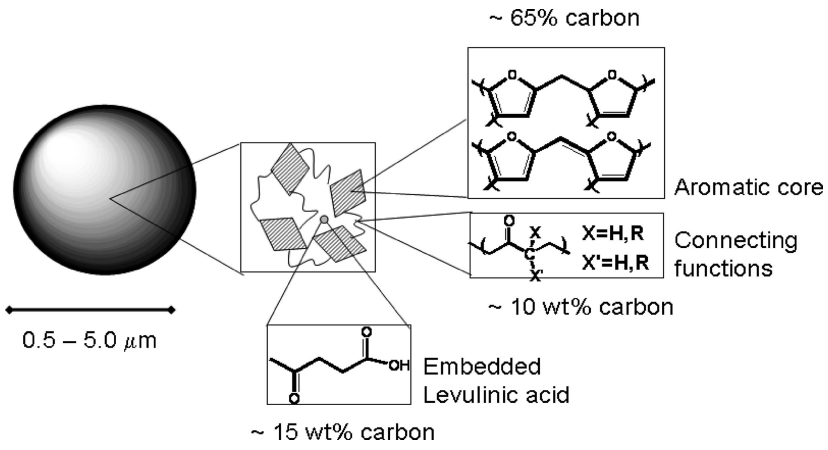


**Fig.3.14** *Structural model of carbon rich particle [from ref. 38]*

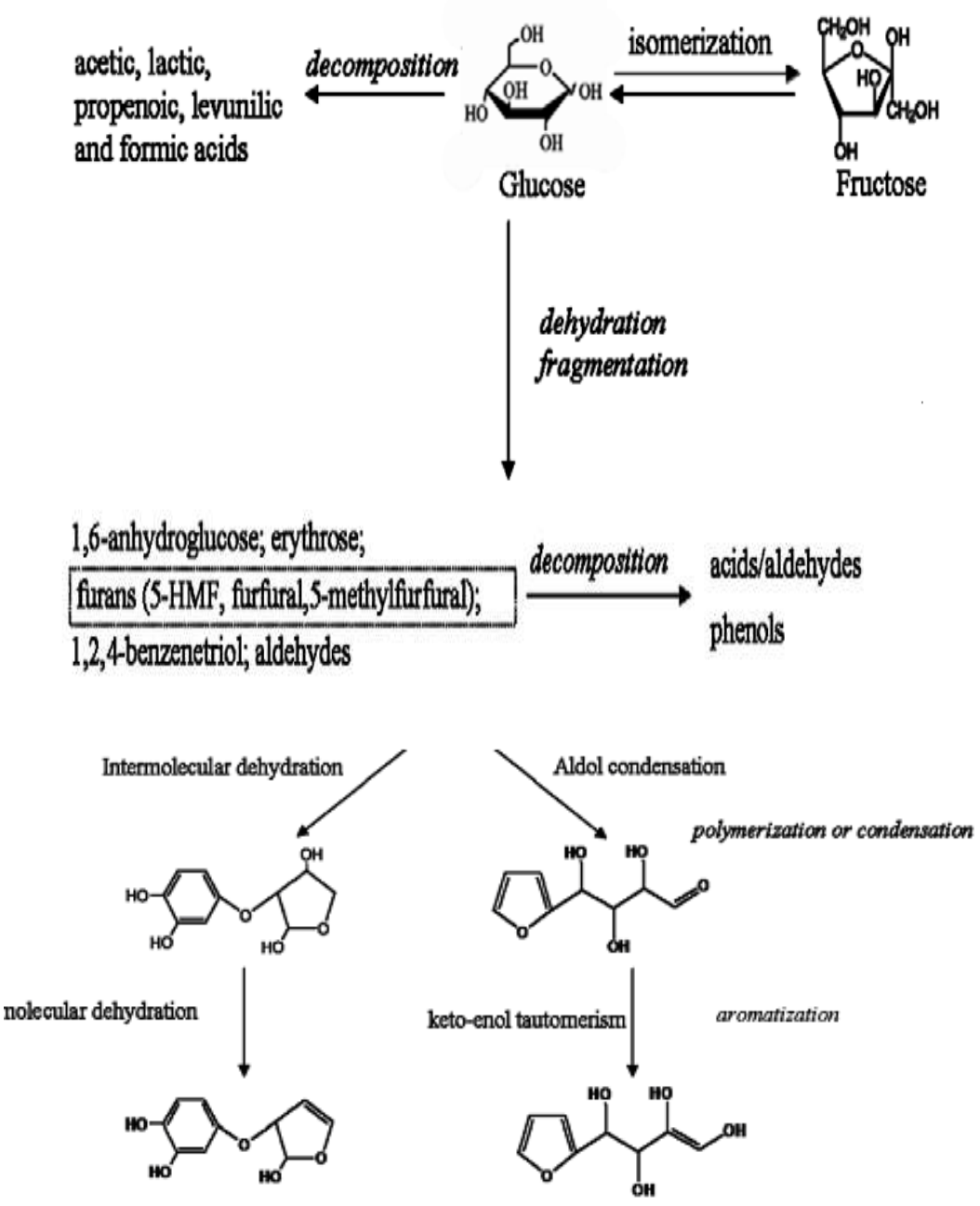


**Fig.3.15** *Dehydration and amortization of carbonaceous materials obtained from the hydrothermal carbonization of carbohydrate [from ref. 6]*

## 3.6 General conclusions from the trends of particle size and morphology

In the light of the present work the advantages of the hydrothermal carbonization reaction can be understood. With the applied simple and green procedure based on cheap sugar sources , in the most cases a good yield of the wanted spherical carbonaceous particles could be obtained. A comparison of the size distributions of the produced samples, carbonaceous spheres, showed some trends as following:

1. The size of the carbonaceous spheres is directly proportional to the sugar concentration.
2. The typical time for the formation of regular spherical morphology of the carbonaceous materials is 24 and 6 h when glucose and fructose, respectively, is carbonized.
3. The optimal temperature for the formation of uniform carbonaceous spheres is approximately 180 and 135 $^{o}$C through the hydrothermal carbonization of glucose and fructose, respectively.
4. Adding 0.5 mL of acetic acid catalyzes the hydrothermal reaction of the sugar and increases the rate of the sugar hydrolysis and hence increases the size of the carbonaceous spheres.
5. The typical operational procedure for the hydrothermal carbonization of glucose are 24 h, 180 $^{o}$C, and the concentration of glucose is 96 mmol$L^{-1}$ (C10), while the typical operational procedures for the hydrothermal carbonization of fructose are 6 h, 135 $^{o}$C and 0.625 mol$L^{-}$ (Fr4).
6. Shape abnormalities have been observed when the reaction time was >24 h and > 6 h for glucose and fructose samples, respectively. As well as, there was abrupt morphological change when the temperature is >180 and >135 $^{o}$C in case of glucose and fructose samples, respectively, while the other conditions are typical procedure.

7. Analysis of the textural properties of the glucose- and fructose -derived carbonaceous spheres shows that they have a poor porosity, as evidence from $N_2$ adsorption isotherm.
8. XRD analysis showed the amorphous nature of glucose and fructose-derived carbonaceous spheres.

Generally, all observed trends are summarized in Table 3.6.

**Table 3.6** *Conclusion of the found average particle size trends*

| Modified parameter | | Trend (average particle size) | |
|---|---|---|---|
| | | Glucose | Fructose |
| Temperature (T) | ↑ | ↑ | ↑ |
| | ↓ | ↓ | ↓ |
| Time (t) | ↑ | ↑ | ↑ |
| | ↓ | ↓ | ↓ |
| Carbohydrate concentration (c) | ↑ | ↑ | ↑ |
| | ↓ | ↓ | ↓ |
| Catalyst | Adding catalyst | ↑ | ↑ |
| | No catalyst | ↓ | ↓ |

## References


1. Q. Wang, H. Li, L. Chen, X. Huang, *Carbon* **39** (2001) 2211.
2. X. Sun, Y. Li, *Angew. Chem. Int. Ed.* **43** (2004) 597.
3. X. Z. Liang, J. G. Yang, *Catal. Lett.* **132** (2009) 460.
4. M. Sevilla, A. B. Fuertes, *Carbon* **47** (2009) 2281.
5. X. Cui, , M. Antonietti, S-H. Yu, *Small **2*** (2006) 756.
6. N. Baccile, M. Antonietti, M. Titirici, *Green Chem.* **10** (2008) 1204.
7. L. Kong, X. Lu, X. Bian, W. Zhang, C. Wang, *Langmuir* **26** (2010) 5985.
8. M. Titirici, A. Thomas, M. Antonietti, *Adv. Funct. Mater.* **17**(2007) 1010.
9. S. Karagçz, T. Bhaskar, A. Muto, Y. Sakata, *Fuel* **84** (2005) 875.
10. T. M. Aida, Y. Sato, M. Watanabe, K. Tarima, T. Nonaka, H. Hattori, K. Arai, *J. Supercrit. Fluids* **40** (2007) 381.
11. B. M. Kabyemela, T. Adschiri, R. M. Malaluan, K. Arai, *Ind. Eng. Chem. Res.* **38** (1999) 2888.
12. M. Sevilla , A. B. Fuertes, *Chem. Eur. J.* **15** (2009) 4195.
13. F. Bergius, H. Specht, *Die Anwendung hoher Drucke bei chemischen Vorgängen und eine Nachbildung des Entstehungsprozesses der Steinkohle*, Verlag Wilhelm Knapp, Halle an der Saale (1913) p. 58.
14. E. Berl, A. Schimdt, *Liebigs Ann. Chem.* **493** (1932) 97.
15. J. P. Schuhmacher, F. J. Huntjens, D. W. van Krevelen, *Fuel* **39** (1960) 223.
16. X. Sun, Y. Li, *Langmuir* **21** (2005) 6019.
17. S.-H. Yu, X. Cui, L. Li, K. Li, B. Yu, M. Antonietti, H. Cçlfen, *Adv. Mater.* **16** (2004) 1636.
18. W. Wang, S. Xiong, L. Chen, B. Xi, H. Zhou, Z. Zhang, *Cryst. Growth Des.* **6** (2006) 2422.
19. J. Y. Gong, S. H. Yu, H. S. Qian, L.-B. Luo, T. W. Li, *J. Phys. Chem. C* **111** (2007) 2490 .
20. X. Sun, Y. Li, *Angew. Chem.* **116** (2004) 3915; *Angew. Chem. Int. Ed.* **43** (2004) 3827.
21. X. Li, T. Lou, X. Sun, Y. Li, *Inorg. Chem.* **43** (2004) 5442.
22. M. Zheng, J. Cao, X. Chang, J. Wang, J. Liu, X. Ma, *Mater. Lett.* **60** (2006) 2991 .
23. X. Sun, J. Liu, Y. Li, *Chem. Eur. J.* **12** (2006) 2039 .

24. C. Yao, Y. Shin, L. Q. Wang, C. F. Windish, W. D. Samuels, B. W. Arey, C. Wang, W. M. Risen, G. J. Exarhos, *J. Phys. Chem. C* **111** (2007) 15141.
25. M. M.Titirici, M. Antonietti, A.Thomas, *Chem. Mater.* **18** (2006) 3808.
26. X. Sun, Y. Li, *Angew. Chem.* **116** (2004) 607.
27. T. Sakaki, M. Shibata, T. Miki, H. Hirosue, N. Hayashi, *Bioresour. Technol.* **58** (1996) 197.
28. C. Araujo-Andrade, F. Ruiz, J. R. Martinez-Mendoza, H. Terrones, *Theochem.* **733** (2005) 143.
29. H. T. Wang, B. A. Holmberg, Y. S. Yan, *J. Mater. Chem.* **12** (2002) 3640.
30. F. Caruso, R. A. Caruso, H. Moehwald, *Science* **282** (1998) 1111.
31. Q. Wang, H. Li, L. Q. Chen, X. J. Huang, *Solid State Ionics* **152** (2002) 43.
32. S. Lee, S. Yoon, C. Park, Y. Korai, I. Mochida, *Carbon* **41** (2003)1652.
33. M. S. Feather, J. F. Harris, *AdV. Carbohydr. Chem. Biochem.* **28** (1973) 161.
34. D. Ni, L. Wang, Y. Sun, Z. Guan, S. Yang, K. Zhou, *Angew. Chem. IE* **49** (2010) 4223.
35. M. Sasaki, B. Kabyemela, R. Malaluan, S. Hirose, N. Takeda, T. Adschiri, *J. Supercrit Fluids* **13** (1998) 26.
36. Y. Ogihara, Jr. Smith, H. Inomata, K. Arai, *Cellulose* **12** (2005) 595.
37. M. Sasaki, Z. Fang, Y. Fukushima, T. Adschiri, K.Arai, *Ind. Eng. Chem. Res.* **39** (2000) 2883.
38. N. Baccile, G. Laurent, F. Babonneau, F. Fayon, M. Titirici, M. Antonietti, *J. Phys. Chem. C* **113** (2009) 9644.
39. T.M. Aida, K. Tajima, M. Watanabe, Y. Saito, K. Kuroda, T. Nonaka, H. Hattori, Jr. Smith, K .Arai, *J. Supercrit. Fluids* **42** (2007) 110.
40. O. Bobleter, ,*Prog Polym Sci.* **19** (1994) 797.
41. A. Sinag, A. Kruse, V. Schwarzkopf *, Eng. Life Sci.* **3** (2003) 469.
*42.* G. Luijkx, F. van Rantwijk, H. van Bekkum, Jr. Antal, *Carbohydr. Res.* **272** (1995) 191.
43. M. Tang, R. Bacon, *Carbon* **2** (1964) 221.

Chapter 4

# Facile one-pot fabrication of hollow porous silica nano-particles

We describe a method for the fabrication of hollow silica nano-spheres via a facile one-pot hydrothermal route. Heating of an aqueous solution of water glass and D-glucose to 180 °C for 24 h affords - as indicated by transmission electron microscopy – a nanospherical composite consisting of a silica precursor shell sheathing a carbonaceous core. Subsequent removal of the carbonaceous interior through oxidation in air produces free standing hollow silica structures. Variation of the concentration of the two jointly dissolved chemicals enables a variation of the thickness and surface area of the silica shell. The hollow silica particles were characterized by means of scanning electron (SEM) and transition electron microscopy (TEM), by X-ray diffraction (XRD), infrared spectroscopy (IR), thermo-gravimetric analysis (TGA) and sorption mesurements.

## 4.1 Introduction

Silica, a major and natural component of sand and glass, has been employed in material sciences and engineering for many years. It is a versatile material due to the variety of chemical and physical modifications that can be realised. Silica is also a relatively benign material due to its biocompatibility and no toxicity.[1] Over the past few years, hollow silica nanoparticles (HSNPs) are of special interest because of their hydrophilic nature, easy formation of colloidal suspension, and surface functionalization accessibility for both inner and outer walls.[2] Moreover, HSNPs have high chemical and thermal stabilities, low density, large surface areas, permeability, penetrability, and good compatibilities with other materials.[3-4] Therefore, they have potential applications in many fields such as, selective separation,[5] catalysis,[6] dielectric materials,[7] drug carriers,[8] biosensors,[9] prosthetic materials,[10] gas adsorbents,[11] and heavy metal ions adsorbents.[12]

A variety of chemical and physicochemical methods have been explored for the fabrication of hollow spheres, including heterophase polymerization combined with a sol-gel process,[13] emulsion/ interfacial polymerization strategies,[14] spray-drying methods,[15] surface polymerization processes,[16] and colloidal templating.[17-19] In addition, layer-by-layer method developed by *Decher* in the early 1990s has been applied to three-dimensional templates and extensively used to obtain hollow shells of inorganic materials.[20-22]

*Chen et al.* presented a novel route for the synthesis of porous hollow silica nanoparticles (PHSNPs),[23] which adopted nanosized calcium carbonate as a structure directing template and they employed PHSNP as drug carrier to investigate its performance on the controlled release of cefradine. *Fujiwara et al.* reported the synthesis of silica hollow spheres by an interfacial reaction using a water–oil–water (W/O/W) emulsion;[24] silica hollow spheres were also synthesized at the air–water interface.[25] However, this method was rather

sensitive to the stirring conditions, induction time, and time delays between the dilution and neutralization steps of the synthesis procedure. Furthermore, in the preparation of hollow structured silica, organic compounds, such as polystyrene (PS)[26] and polymethylmethacrylate (PMMA),[27] were employed as templates. These organic templates had a size of several hundred nanometers, and hardly form nanosized hollow particles.

Generally, among the various synthesis procedures, templating approaches represent the most often used technique which is based on the synthesis of core-shell particles and subsequently removal of the core by dissolution in a solvent or calcination. The sacrificial templating methods have been developed considerably in recent years and an interesting sacrificial core is represented by monodisperse carbon particles which are generated by the hydrothermal treatment of aqueous solutions of glucose.[28-31] These sacrificial cores inherit functional groups and have reactive surfaces which facilitate the precipitation of metal precursors and nanoparticles as was shown by *Li et al.* for different materials, for example $TiO_2$,[29] $WO_3$ [30] and noble metal nanoparticles which could be fabricated as hollow spheres.[31] *Thomas et al.* synthesized some hollow metal oxides by hydrothermal process using carbon as the sacrificial core; they reported that the hollow spheres exhibit diameters from one to several micrometers and consist of nanocrystals of the respective metal oxides.[31] Recently, *Chen* and co workers reported the synthesis of poly(*N*-isopropylacrylamide)-coated Au@mesoporous-$SiO_2$ hollow spheres in a multistep synthesis procedures using carbon spheres derived from the hydrothermal treatment of glucose.[32]

This field of research is still relatively young and many reports are published every year, any overview of publications will be incomplete. Previous methods were found to be slow processes and mechanical stirring is necessary to obtain uniform silica shell on the surface of the sacrificial templates. Many efforts are required in order to separate the core-shell nano-particles (NPs) from large amounts of surfactant associated with micro-emulsion system. Therefore,

developing a facile simple way to prepare hollow silica nano-particles with controlled void size and regular morphology remains a challenge to materials scientists.

In the present contributions, we present a facile one-pot synthesis route for the synthesis of fused hollow porous silica spheres, with tunable mean size and shell thickness, by sacrificial templating method using carbonaceous spheres as the sacrificial template via utilizing hydrothermal approach.

To study the influence of each reagent on the morphology and the size of the final products, some crucial experimental conditions were systematically varied as shown in Table.4.1. In our recipes the carbohydrate used as a precursor for the sacrificed carbonaceous spherical-cores is glucose. Variable concentrations of glucose were used. C1 stands for the initial glucose concentration of 960 mmol/L, C2, C4, C10 and C15 for 1/2, 1/4,, 1/10 and1/15 of C1, respectively. Variable amounts of water glass were used as a silica precursor. The typical procedure for fabrication of HSNPs was described in chapter 2.

**Table 4.1** *Conditions of synthesizing nano-sized silica hollow spheres*

| Sample code | Glucose | Water glass | $H_2O$ (mL) | T ($^oC$) | Time (h) |
|---|---|---|---|---|---|
| 1 | C15 | 0.1 mL | 40 | 180 | 6 |
| 2 | C10 | 0.1 mL | 100 | 180 | 24 |
| 3 | C10 | 0.2 mL | 100 | 180 | 24 |
| 4 | C10 | 0.3 mL | 100 | 180 | 24 |
| 5 | C10 | 0.4 mL | 100 | 180 | 24 |
| 6 | C4 | 0.1 mL | 40 | 180 | 24 |
| 7 | C2 | 0.1 mL | 40 | 180 | 24 |
| 8 | C4 | 0.4 mL | 40 | 180 | 24 |
| 9 | C2 | 0.4 mL | 40 | 180 | 24 |
| 10 | C1 | 0.2 mL | 20 | 180 | 24 |

## 4.2 Results and discussion

To the best of our knowledge, in this work, fused hollow silica nanometer size spheres with tunable shell thickness and void volume have been obtained comfortably by a one-pot synthesis via *hydrothermal hydrolysis for the first time*. Glucose as sacrificial template and glass water were employed as starting materials. Herein, different concentrations of glucose were used in the synthesis process.

A sketch of a proposed mechanism of the fabrication of the PHSNPs is shown in Fig.4.1. The formation of the HSNPs involves the dehydration and carbonization of glucose into carbonaceous spheres (CCs) with high surface functionalities. Then, the adsorption of the silica precursor into the hydrophilic surface of the of the CCs and in-situ formation of core@shell (C@silica precursor) composite. Finally, the removal of CCs cores via thermal treatment.

Accordingly, the hydrolysis of glucose starts with its partial decomposition into organic acids like acetic, lactic, propenioc, levulinic and formic acids.[33] These acids release hydronium ions which in turn catalyze subsequent reaction stages eventually resulting in the formation of carbonaceous spheres. Furthermore, we assume that the carbonaceous spheres contain a multitude of functional groups like –OH and –C=O on the surface supporting the attachment of the silicic acid, which is formed as a result of the acidic hydrolysis of the water glass,[34] from the solution via hydrogen bonding in surface-near regions. Support for the assumption of a spatial separation of metal silicate-rich shells and carbonaceous cores is provided by an abrupt contrast variation in TEM images of the spherical hybrid particles, as can be seen from Fig.4.2 during the subsequent thermal treatment, the incorporated silicic acid is densified and cross-linked to form free standing structures of silica particles. The spherical shape is essentially maintained, yet hollow now and shrinked in diameter by some 65-80% relative to the size of the composite precursor.

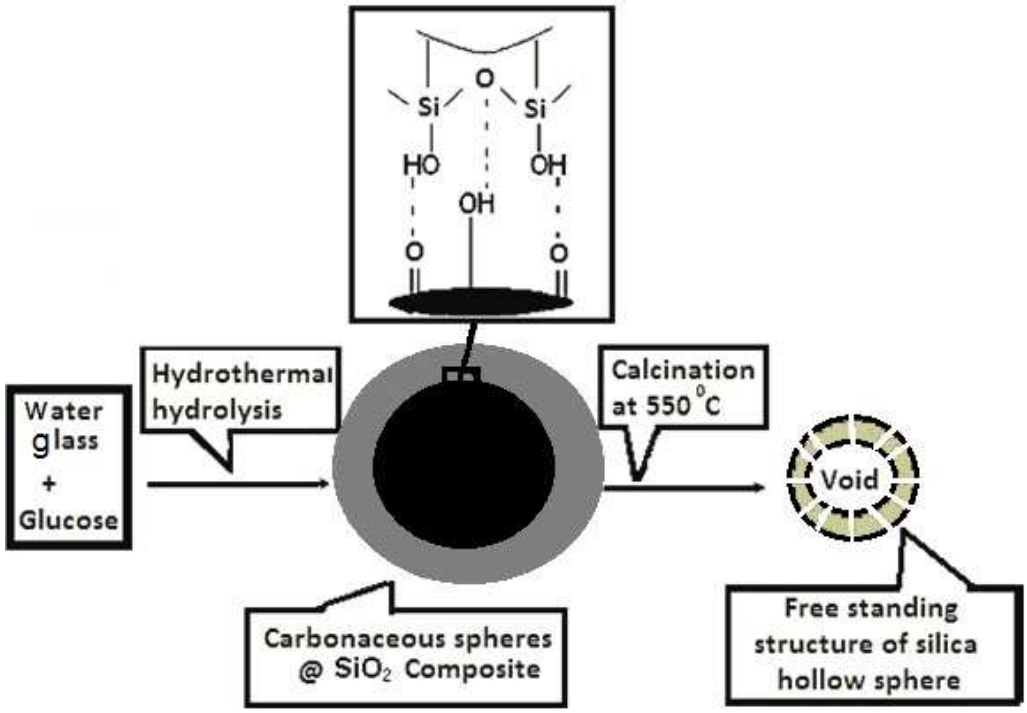


**Fig.4.1** *Proposed mechanism of the fabrication of porous $SiO_2$ hollow spherical nanoparticles starting from aqueous solution of glucose and water glass*

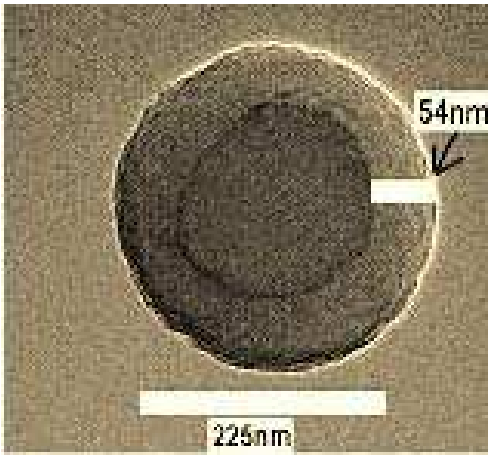


**Fig.4.2** *TEM images of a single core@shell composite particle of $C@SiO_2$ precursor (sample 5)*

Thermogravimetrical analysis (TGA) were performed in order to investigate the formation of the silica hollow nano-spheres from various hybrid precursors. As seen from Fig.4.3 (A) the composite (sample 3) looses weight in two steps. Below 100 ºC marginal weight loss of about 5 % occurs which is attributed to the evaporation of the physically adsorbed $H_2O$ from the surface of the composite. In a second step starting at about 280 °C the composite precursor undergoes pyrolysis as well as the condensation of the terminal silanol groups [35] ending at a total mass reduction of 95% at about 500 °C. TG analyses of sample 5 Fig.4.3 (B) which contained twice as much water glass as sample 3 results in an overall mass loss of 90%. Hence, TGA evidences that the silica uptake by the carbonaceous spheres is proportional to the concentration of the sodium water glass in the solution. This definite observation has two major implications: Firstly, it indicates that the residual silica content of the pyrolyzed hybrid precursors can – at least within the chosen concenration range - (c.f. Table 4.1)– be tuned by the concentration of the sodium water glass for the given concentration of glucose. Secondly, if control over the size of the carbonaceous hybrid precursor is gained, the thickness of the shell of the PHSNPs can be tuned by varying systematically the concentration of the water glass.

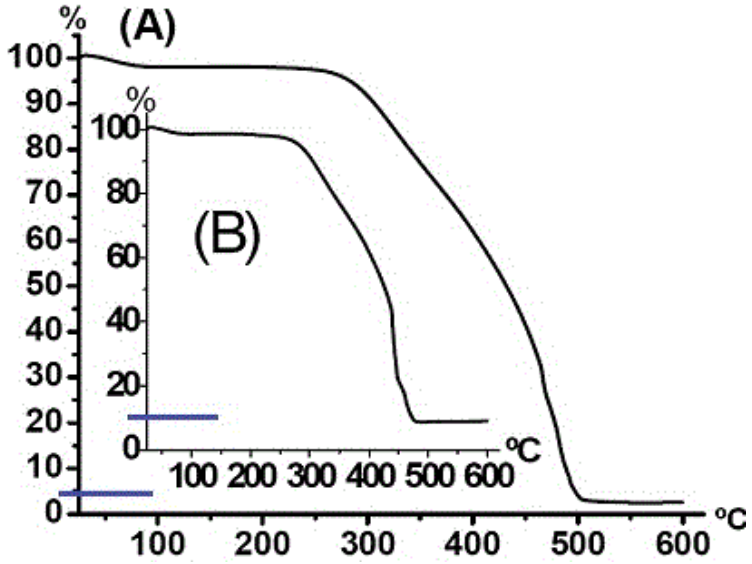


**Fig.4.3** *TGA curve of the decomposition of the core@shell composites, (A) sample 3, (B) sample 5*

From IR spectra Fig.4.4 sample number 5, the most noticeable difference between the two IR spectra of the hollow spheres and its related composite is the intensity of the broad peak between 3000 and 4000 $cm^{-1}$. This peak is characteristic to OH group that exists in water. This confirms the elimination of most water molecules after firing at 550 $^{o}C$ for 5 hours to form hollow silica particles. In addition, the absence of the peaks around 2932 $cm^{-1}$ and 1704 $cm^{-1}$ in the spectrum of the hollow spheres which are ascribed to C-H stretching and carbonyl group, respectively, after firing at 550 $^{o}C$ for 5 hours is an evidence for the removal of the carbon core.[36] The absorption bands present around 1634 $cm^{-1}$ in the two figures is assigned to the stretching and deformation vibration of adsorbed water molecules.[37] Peaks around 468 $cm^{-1}$ , 805 $cm^{-1}$ and 1102 $cm^{-1}$ correspond to the three vibration bands of the Si-O-Si bond. The peak at 1102 $cm^{-1}$ is due to the asymmetric stretching vibration band, at 805 $cm^{-1}$ is the bending vibration band, and at 468 $cm^{-1}$ is the rocking vibration band. The peak at about 3400 to 3450 $cm^{-1}$ in the hollow samples is ascribed to hydroxyl groups on the surface of silica.[38]

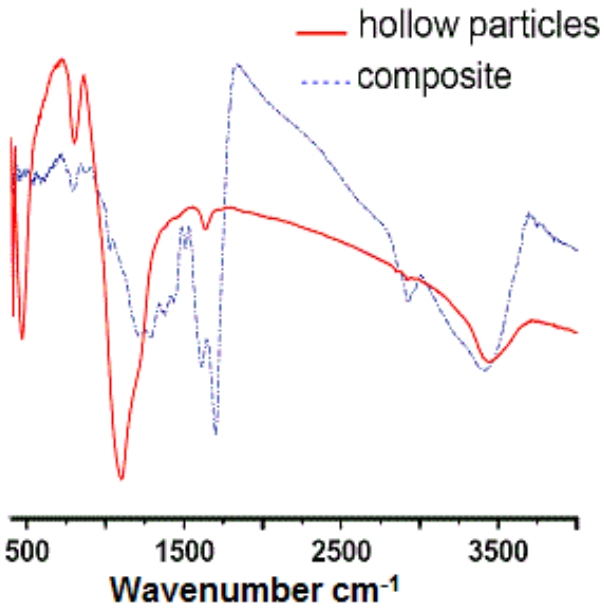


**Fig.4.4** *IR spectrum of (A) sample 5 ,the hollow particles and its related composite*

The morphology of the hollow nano-sized particles and their corresponding core-shell composites are shown in Fig.4.5. From TEM images, the strong contrast between the dark edge and bright centers reveal the hollow structure of the silica spheres. These TEM images also revealed that the utilization of glucose as a sacrificial template has resulted in the formation of spherical shells with relatively smooth surface and dense arrangement of nanoparticles $SiO_2$.

The effect of the concentration of water glass on the shell thickness and the particle size of the as-prepared hollow silica particles can be seen obviously from Fig.4.5. It can be noticed that the amount of water glass added has significant impact on the shell thickness and obvious impact on the size of the particles. By simply changing the amount of water glass, the thickness of the silica shell could be varied, and it was easy to anticipate that the silica shell would become thicker with increasing amount of water glass.

Moreover, particle size would be increased as well. As we can notice in Fig.5 (G, H, I, J) when the amount of water glass increased from 0.1 mL to 0.4 mL, the shell thickness increased from 6 nm to about 15 nm, and also the average diameter for the as-synthesized hollow spheres were increased under the influence of increasing the water glass, in samples from 1 to 5. (See Fig.4-S2 in the supporting material section).

The influence of the concentration of the glucose on the morphology and the size of the hollow silica particles was quit obvious. This is due to the template in this method acting as shape and size directing agent. Thus, it can be observed in Fig.4.5 (See Fig.4-S1 in the supporting material section) that the particle size of the core shell composites and therefore the hollow particles decrease as the glucose concentration decrease.

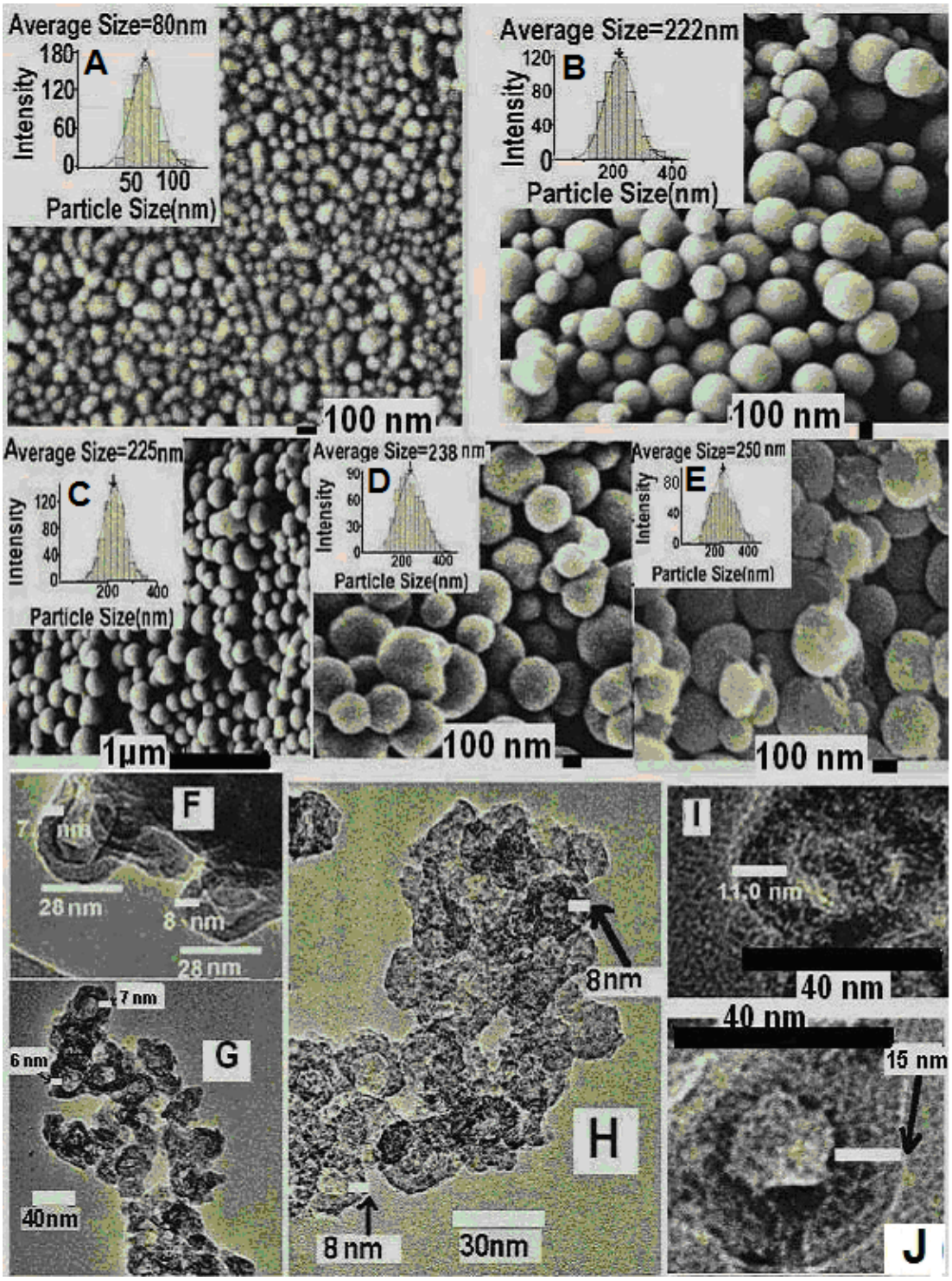


**Fig.4.5** *SEM images of the core@shell composites and their particle size distribution of samples: (A) 1, (B) 2, (C) 3, (D) 4, (E) 5, and TEM images of the hollow samples (F) 1, (G) 2, (H) 3, (I) 4, and (J) 5*

*Note: The term intensity refers to the number of counted particles*

In addition, it was noticed that the morphology is improving via decreasing the concentration of the glucose. It is obvious from Fig.4.5 that the hollow samples from 1 to 5 were in a size range ~ from 25 nm to 50 nm and possessed regular spherical shape. In these samples the template precursor concentrations were C10 and C15, the lowest concentration of the glucose used among the whole samples. Increasing the glucose concentration to C4, C2 and C1 increases the average size of the obtained composites which in turn lead to an increase in the size of hollow particles to more than 200 nm (Fig.4-S1). Concurrently, there is some loss in the regularity of the hollow particles.

From the particle size distribution for the core-shell composites of all samples and TEM images (Fig.4.5) of the corresponding hollow particles it can be predicted that, after the thermal treatment at 550 $^{o}$C for 5 hours, a shrinkage in size occurred and the size decreased from 65 to 80 %. This is due to the removal of the sacrificed core which is combined with the densification and the cross-linking of silicic acid polymer incorporated into the surface layers to form the oxide hollow spheres (See Fig. 4-S3 in the supporting material).

The powder X-ray diffraction patterns of the as-prepared HSNPs sample 5 after firing exhibit one broad peak centered at about $22^{0}$ (See Fig.4-S4 in the supporting material). This signature is characteristic for amorphous silica.[39]

Nitrogen sorption isotherms were measured to study the porosity and specific surface area of the as-synthesized hollow spheres. Fig.4.6 represents the sorption isotherm of hollow spheres.

It is typical type IV isotherm characteristic of mesoporous materials according to the International Union of Pure and Applied Chemistry (IUPAC).[40] Hysteresis loop can be observed in the curve which was evidence of the existence of mesoporous structure.

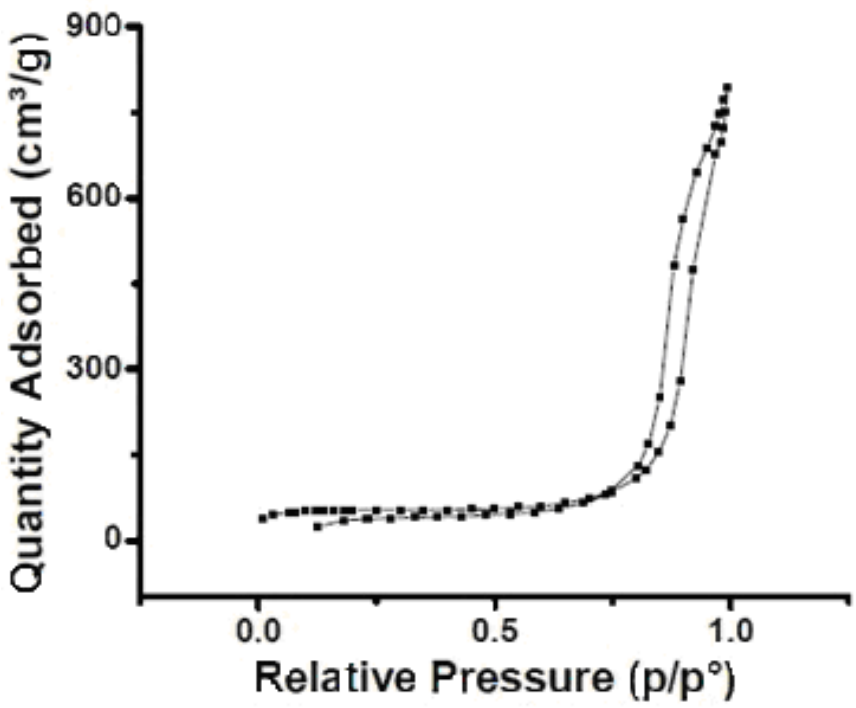


**Fig.4.6** *Nitrogen sorption isotherms of sample (5)*

The measured BET surface area was 180 $m^2$/g. The high surface area of the measured hollow sample may be assigned to the combination of the surface area of the outer surface, the inner surface and the mesopores, which form altogether the whole surface area of the particles. This large surface area showed that this kind of materials may have many potential applications in many fields.

## 4.3 Conclusions

It has been demonstrated that the meso-porous hollow silica spheres with a tunable shell thickness and particle size can be readily fabricated via hydrothermal hydrolysis by employing glucose as a sacrificial template and water glass as silica precursor through one pot synthesis route. Generally, the amount of water glass plays a vital role on the morphologies as well as the shell thickness of the hollow silica spheres (HSSs). The concentration of glucose has a significant influence on the size of the obtained HSSs as well. The obtained meso-porous hollow silica material with variable size and shell thickness may find potential application in different fields such as catalysts, selective separation, dielectric materials and as small vehicles in the controlled release application.

## 4.4 Supporting materials

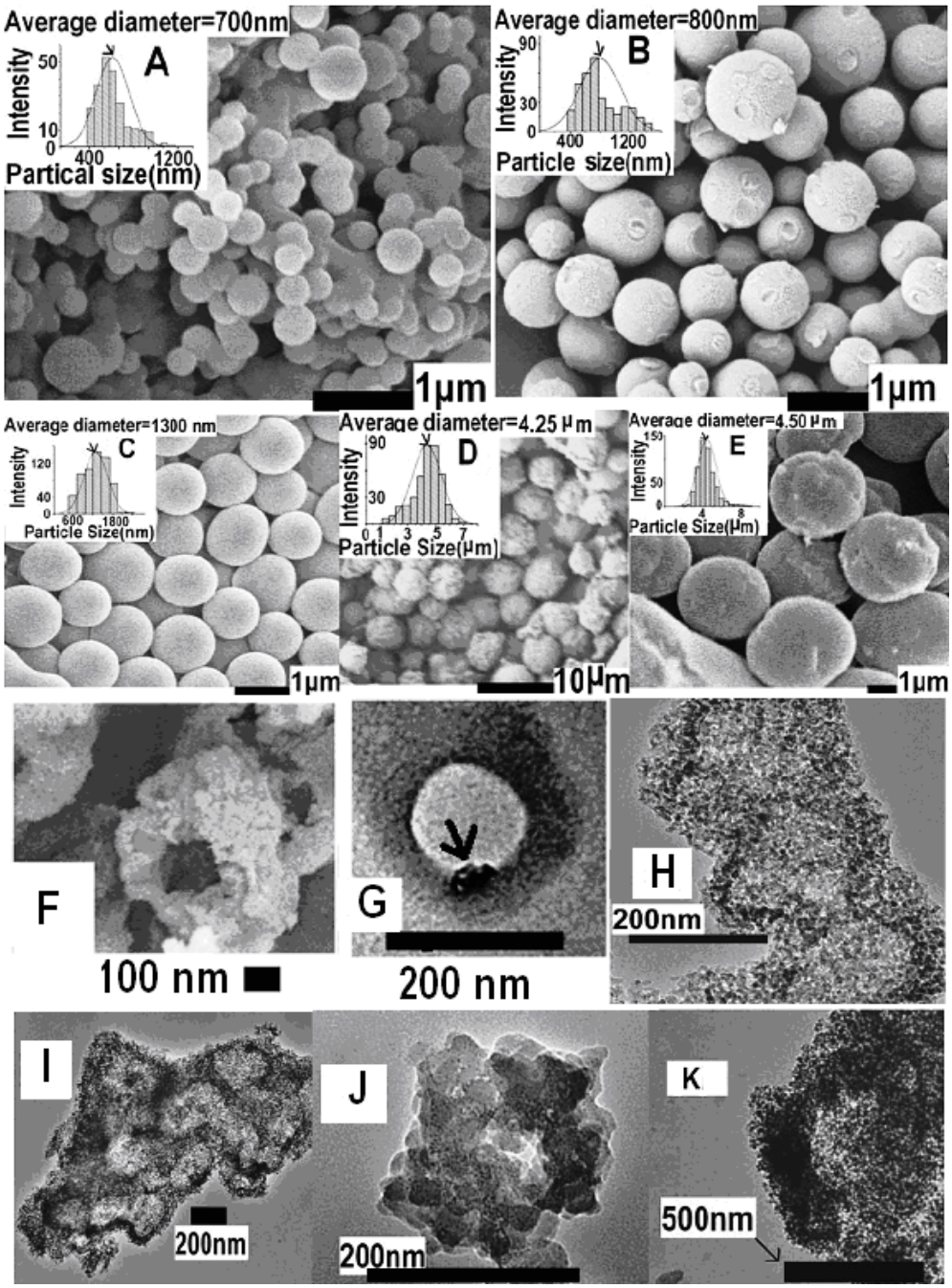


**Fig.4-S1** *SEM images of the core@shell composites (C@$SiO_2$ precursor) and their particle size distribution of samples (A) 6, (B) 7, (C) 8, (D) 9, (E) 10, (F) hollow particle of sample 10 and TEM images of samples (G) 6, the arrow refers to some carbon left after calcination (H) 7, (I) 8, (J) 9, and (k) 10*

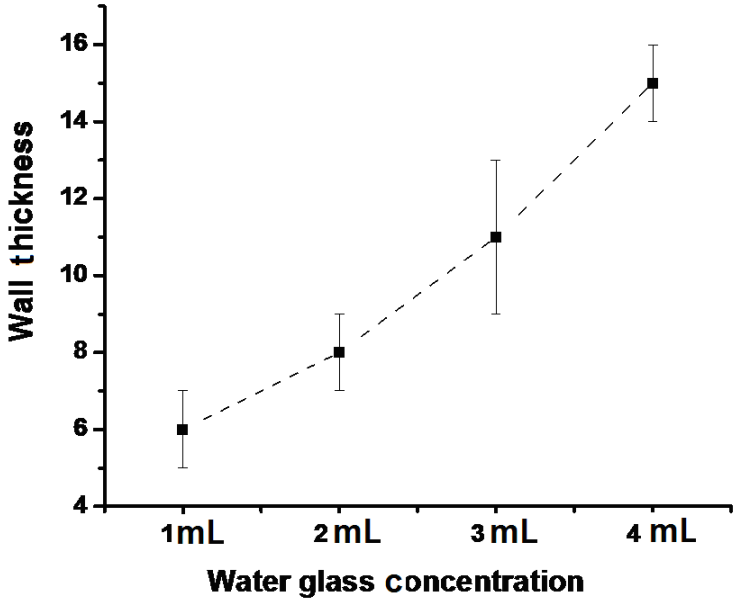


**Fig.4-S2** *The relationship between the concentration of glucose and the wall thickness of the hollow $SiO_2$ nanoparticles*

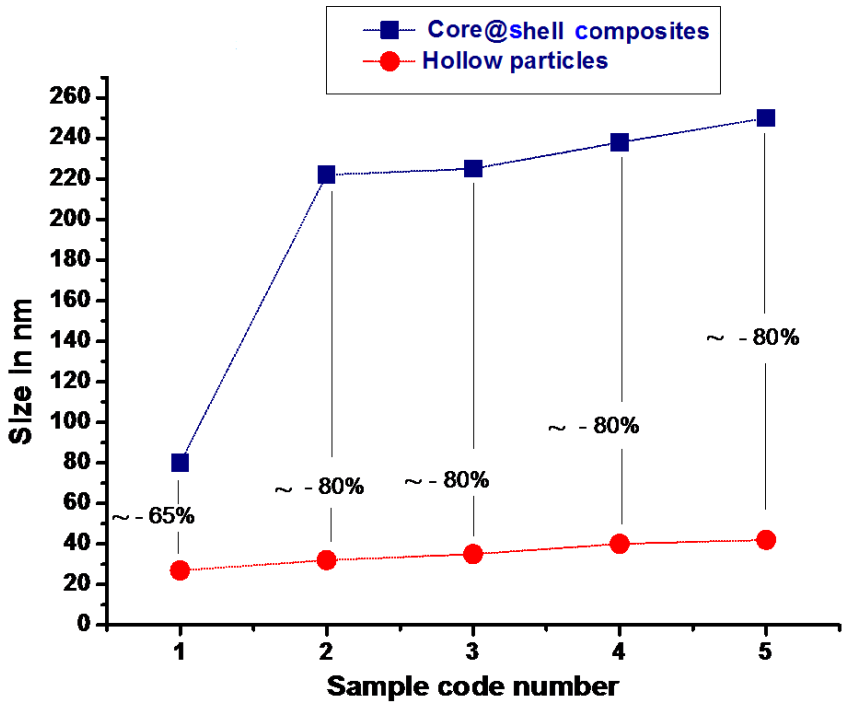


**Fig.4-S3** *The shrinkage in size after calcination at 550 $^{o}$C for 5 hours*

EDX Data in Table 1S reveals that the composite of C@$SiO_2$ precursor is only composed of C, O, Si as listed in the Table, the Si/O ratio were 0.22 based on wt%. This value is significantly different than the ratio of $SiO_2$( approx. 0.88) based on wt%. This different value may be due the oxygenated functional groups and some carbon fractions formed during the manufacturing process. Fig.4-S4 shows the EDX spectrum of the hollow silica spheres.

**Table 1S** *Element composition in Wt%*

| Sample | Si/O | Si | O | C |
|---|---|---|---|---|
| Core@shell composite | 0.22 | 14.2 | 62.6 | 23.2 |
| Hollow silica spheres | 0.95 | 48.8 | 51.2 | ------- |

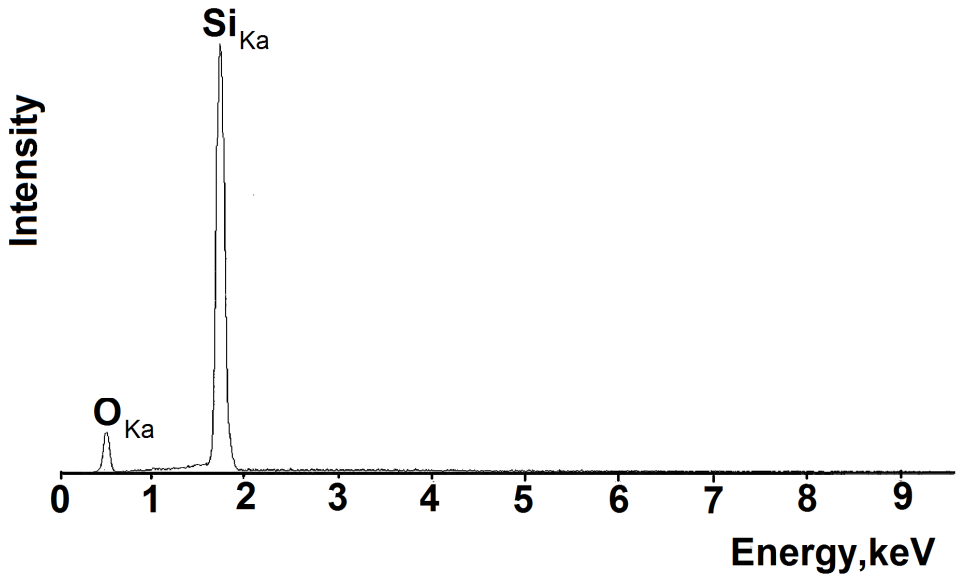


**Fig.4-S4** *EDX spectrum of hollow $SiO_2$ spheres of sample 5*

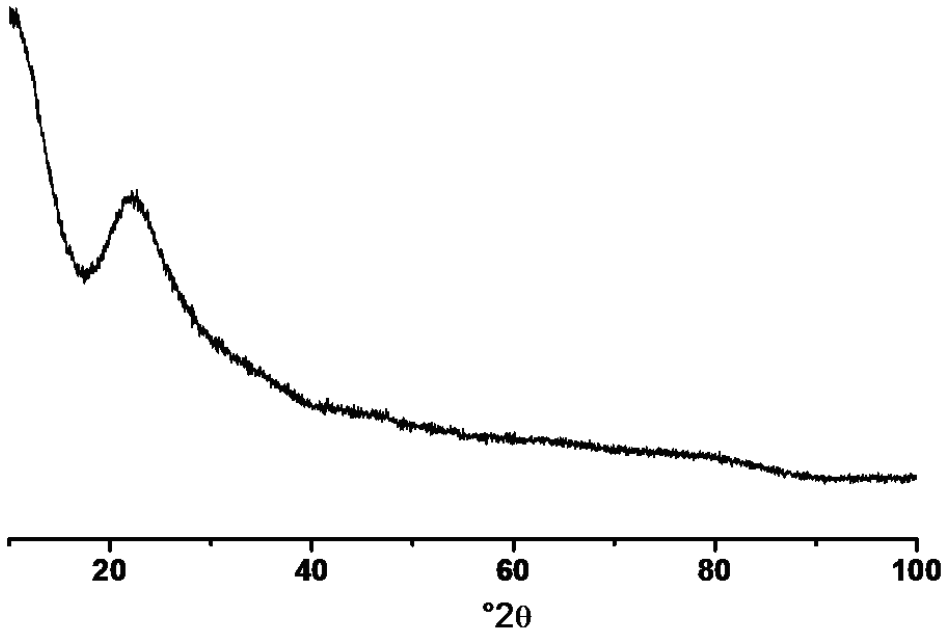


**Fig.4-S5** *XRD pattern of selected hollow silica spheres (sample 5)*

## References


1. Y. Liu, H. Miyoshi, M. Nakamura, *Colloids Surf. B: Biointerfaces* **58** (2007) 180.
2. K. Zhang, L. Zheng, X. Zhang, X. Chen, B. Yang, *Colloids Surf. A: Physicochem. Eng. Aspects* **277** (2006) 145.
3. Z. Feng, Y. Li, D. Niu, L. Li, W. Zhao, H. Chen, L.Li, J.Gao, M. Ruan, J. Shi, *Chem. Commun*. (2008) 2629.
4. J. Yuan, X. Zhang, H. Qian, *J. Mag. Mag. Mater.* **322** (2010) 2172.
5. N. H. Kim, H. Y. Lee, Y. Cho, W. S. Han, D. Kang, S. S. Leea, J. H.Jung, *J. Mat. Chem.* **20** (2010) 2139.
6. M. O. Coppens, J. H. Sun, T. Maschmeyer, *Catal Today* **69** (2001) 331.
7. A. Jain, S. Rogojevic, S. Ponoth, N. Agarwal, I. Matthew, W. N. Gill, P. Persans, M. Tomozawa, J. L. Plawsky, E. Simonyi, *Thin Solid Films* (2001) 513.
8. Z. Z. Li, L. Wen, L. Shao, J. F. Chen, *J. Control. Release* **98** (2004) 723.
9. S. W. Kim, M. Kim, W. Y Lee, T. Hyeon, *J. Am. Chem. Soc.* **124** (2002) 7642.
10. J. M. Gomez-Vega, M. Iyoshi, K.Y. Kim, A. Hozumi, H. Sugimura, O. Takai, *Thin Solid Films* (2001) 615.
11. K. Okada, A. Shimai, T. Takei, S. Hayashi, A. Yasumori, K. J. D. Mac-Kenzie, *Microporous Mesoporous Mater.* **21** (1998) 289.
12. B. Lee, Y. Kim, H. Lee, J. Yi, *Microporous Mesoporous Mater.* **50** (2001) 77.
13. I. Tissot, J. Reymond, F. Lefebvre, E. Bourgeat-Lami, *Chem. Mater*. **14** (2002) 1325.
14. J. Yuan, T. Zhou, H. Pu, *J. Phs. Chem. Solids* **71** (2010) 1013.
15. Y. Lu, H. Fan, A. Stump, T. Ward, T. Rieker, C. Brinker, *Nature* **398** (1999) 223.
16. O. Emmerich, N. Hugenberg, M. Schmidt, S. S. Sheiko, F. Baumann, B. Deubzer, J. Weis, J. Ebenhoch, *Adv. Mater*. **11** (1999) 1299.
17. C. Graf, A. van Blaaderen, *Langmuir* **18** (2002) 524.
18. W. Tong, C. Gao, *J. Mater. Chem*. **18** (2008) 3799.
19. J. Liu, F. Liu, K. Gao, J. Wu, D. Xue, *J. Mater. Chem*. **19** (2009) 6073.
20. G. Decher, *Science* **277 (**1997) 1232.
21. D. G. Shchukin, G. B. Sukhorukov, H. Mohwald, *Angew. Chem. Int. Ed.* **42** (2003) 4472
22. D. G. Shchukin, G. B. Sukhorukov, *Adv. Mater.* **16** (2004) 671.
23. J. F. Chen, H. M. Ding, J. X. Wang, L. Shao, *Biomaterials* **25** (2004) 723.

24. M. Fujiwara, K. Shiokawa, Y. Tanaka, Y. Nakahara, *Chem. Mater.* **16** (2004) 5420.
25. G. Fornasieri, W. Badaire, R. Backov, O. Mondain-Monval, U. Zakri, P. Poulin, Adv. Mater. **16** (2004) 1094.
26. F. Caruso, R. A. Caruso, *Science* **282** (1998) 1111.
27. A. Stein, *Microporous Mesoporous Mater.* **44 (**2001) 227.
28. X. M. Sun, Y. D. Li, *Angew. Chem. Int. Ed.* **43** (2004) 597.
29. W. H. Shen, Y. F. Zhu, X. P. Dong, J. L. Gu, J. L Shi, *Chem. Lett.* **34** (2005) 840.
30. X. L. Li, T. J Lou, X. M. Sun, Y. D. Li, *Inorg. Chem* **43** (2004) 5442.
31. M. M. Titirici, M. Antonietti, A. Thomas, *Chem. Mater.* **18** (2006) 3808.
32. Z. Chen, Z. Cui, C. Cao, W. He, L. Jiang, W. Song, *Langmuir* **28** (2012) 13452.
33. M. Sevilla, A. B. Fuertes, *Carbon* **47** (2009) 2281.
34. L. Sierra, B. Lopez, J. L. Guth, *Microporous Mesoporous Mater.* **39** (2000) 519.
35. C. E. Fowier, D. Khushalani, S. Mann, *Chem. Commun.* (2001) 2028.
36. G. Longhi, *G*. Paterlinil, S. Abbate, L. Ricard, G. Zerbi, *J. Molecular Structure* **142** (1986) 403.
37. L. H. Little, *Infrared Spectra of Adsorbed Species*, Academic Press, New York, (1966).
38. S. R. Ryu, M. Tomozawa, *J. Non-Cryst. Solids* **352** (2006) 3929.
39. J. Martinez, S. Sanchez, G. Zarzosa, F. Ruiz, Y. Chumakov, *Mater.Lett*. **60** (2006) 3526.
40. K. S. W. Sing, D. H. Everett, R. A. W. Haul, L. Moscou, R. A. Pierotti, J. Rouquerol, T. Siemieniewska, *Pure and Appl. Chem*. **5**7 (1985) 603.

# Chapter 5

## Use of fructose derived-carbonaceous spheres as templates for the fabrication of metal oxide hollow spheres

Hydrothermal route for the fabrication of hollow spheres of crystalline metal oxides has been developed using fructose derived-carbonaceous spheres as sacrificial template for the first time via a facile one-pot fabrication approach. Hollow spheres of a series of crystalline metal oxides ($Cr_2O_3$, $Co_3O_4$, α-$Fe_2O_3$, NiO and ZnO) have been fabricated this way. Heating of an aqueous solution of the metal chlorides and fructose to moderate temperature 135-150 $^oC$ in an autoclave affords - as indicated by transmission electron microscopy – a nanospherical composite consisting of a metal precursor shell coating a carbonaceous core. The removal of the interior carbonaceous cores via heat treatment through oxidation in air yields free standing hollow crystalline oxides spheres. Correlations between the particle size and the concentration of the fructose as well as the ratio of the amount of substance of metal precursor and fructose are uncovered; moreover, important factors critical to fine-tune the final particle size and shape are temperature, reaction time and the addition of catalyst.

## 5.1 Introduction

Hollow colloidal particles of metal oxides have proven to be promising in widespread applications, including nanoscale reactors, catalysis, drug delivery, controlled release, water treatment, photonic devices, chemical sensors and biotechnology.[1-5] In the last decade, hollow particles of metal oxides have been prepared by employing various novel mechanisms.[6-9] The most widely used approaches for the fabrication of hollow materials relies largely upon templating against monodisperse colloidal particles such as silica,[10] latex [11] and carbon.[12]

In previous chapter, we have demonstrated the synthesis of hollow silica nano-particles (HSNPs) *for the first time to the best of our knowledge* via facile one pot hydrothermal strategy utilizing glucose-derived carbonaceous spheres as sacrificial templates. We further demonstrated that the shell thickness of the as-obtained HSNPs can be varied by the variation of the silica precursor. Herein, we report a modified and developed hydrothermal approach for the fabrication of some crystalline metal oxides ($Cr_2O_3$, $Co_3O_4$, α-$Fe_2O_3$, NiO and ZnO) utilizing fructose-derived carbonaceous spheres as the sacrificial templates *for the first time*. Importantly, this strategy does not require prior surface modification of template and the as-obtained metal hollow oxides are polycrystalline as indicated by XRD measurements.

Fig.5.1 presents the schematic flowchart that illustrates the major process steps applied in the present work. Firstly, heating the metal chloride with fructose in closed system results in in-situ formation of hybrid particle, due to the incorporation of the metal ions on the surface layers of the fructose-derived carbonaceous spheres. Finally, calcination of the hybrid spheres lead to the formation of hollow metal oxide spheres in addition to ball in ball (bnb) particles as minor product.

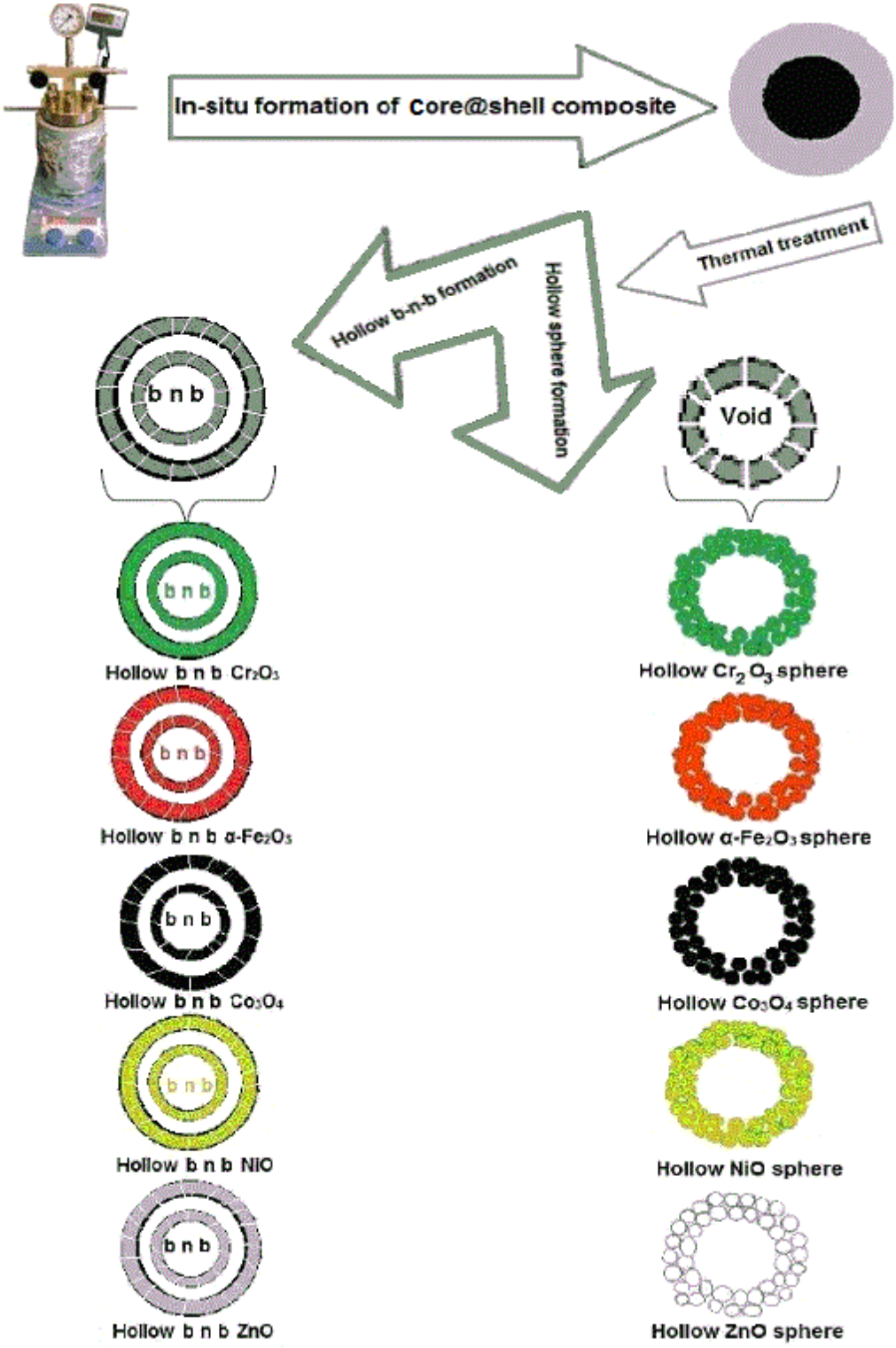


**Fig.5.1** *Schematic illustration (cross-sectional view) of the formation of the hollow metal oxide spheres. The thermal removal of carbonaceous cores results in the formation of hollow spheres plus the formation of ball in ball (bnb) hollow spheres as minor product*

For the formation of the hollow metal oxides spheres, fructose in our synthesis strategy is applied for *the first time as a sacrificial template* and it is the source of the carbonaceous spheres, while metal chlorides [chromium(III) chloride hexahydrate ($CrCl_3.6H_2O$), iron(III) chloride hexahydrate ($FeCl_3.6H_2O$), cobalt(II) chloride hexahydrate ($CoCl_2.6H_2O$), nickel(II) chloride ($NiCl_2$), and zinc(II) chloride ($ZnCl_2$), are the precursors for the desired $Cr_2O_3$, α-$Fe_2O_3$, $Co_3O_4$, NiO and ZnO, respectively. In a typical synthesis experiment, 2252mg (12.5 mmol) of fructose [a] was dissolved in 20 mL distilled water. The water soluble metal chloride during the hydrothermal carbonization was added to satisfy the fructose/metal chloride molar ratio 20:1. [b] The mixture was heated in a 100 mL Teflon-lined stainless steel autoclave at 135 $^oC$ for 6 h. After synthesis, the metal oxide-carbon composites were calcined in air at 500 $^oC$ ( heating rate 2 $^oC$/min, for 5 h) to remove the carbon core, leading to hollow metal oxide particles.

## 5.2 Characterization of the as-prepared hollow crystalline metal oxides spheres

The products and their corresponding composites were characterized by X-ray diffraction (XRD) to investigate the structure changes of the phase and crystallite size of the as-prepared hollow oxides before and after calcination and infrared spectroscopy (IR) to compare between the products before and after the thermal treatment. The morphology and the hollow nature of the products were characterized by scanning electron microscopy (SEM) as well as transmission electron microscopy (TEM). The surface area and the porous structure were characterizes by $N_2$ sorption measurements (BET). The elemental analysis has been performed by using energy dispersive X-ray spectroscopy (EDX).

[a]) Fr4 is $1/4_{th}$ of the initial fructose concentration applied in our study (see chapter 3)
[b]) See the general synthesis recipe in chapter 2

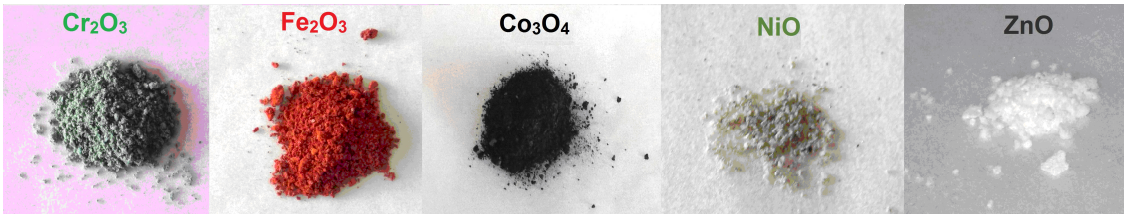


**Fig.5.2** *The as-obtained hollow oxides powders*

### 5.2.1 X-ray diffraction (XRD)

X-ray diffraction (XRD) technique can yield a great deal of structural information and phase identification about material under investigation. The as-obtained hollow metal oxides were analyzed by XRD technique following Rietveld refinement procedures using X'Pert software.[13] The Rietveld method refines a crystal structure by comparing the measured diffraction patterns with that calculated from a known crystal structure.

Fig.5.3 displays XRD patterns of the final products of the hollow metal oxides obtained through the standard experimental procedures after calcination at 500 $^{o}$C for 5h. It shows that, the hollow oxides obtained are well crystalline and single phase as no other diffraction peaks are found, indicating that the products are pure oxides.

From Fig.5.3 we can notice the XRD patterns of (a) pure $Cr_2O_3$ oxide (b) pure α-$Fe_2O_3$, (c) pure $Co_3O_4$ spinal oxide , (e) pure NiO, and (f) pure ZnO. The formation of hollow $Cr_2O_3$, α-$Fe_2O_3$, $Co_3O_4$, NiO and ZnO through applying $CrCl_3$. $6H_2O$, $CoCl_2$. $6H_2O$, $FeCl_3$. $6H_2O$, $NiCl_2$ and $ZnCl_2$, respectively, as metal oxide precursors, indicate that these metal ions undergo oxidation during calcination.

All peaks for sample (a) $Cr_2O_3$ (b) α-$Fe_2O_3$, (c) $Co_3O_4$, (e) NiO, and (f) ZnO are perfectly indexed to (a) rhombohedral $Cr_2O_3$ [ICSD-201102], (b) rhombohedral α-$Fe_2O_3$ [ICSD-81248], (c) cubic $Co_3O_4$ [ICSD-36256], (e) cubic NiO [ICSD-76669], and (f) hexagonal ZnO [ICSD-57478], respectively.

The average crystallite size were calculated from the Scherrer equation[c] (which assumes the small crystallite size to be the cause of line broadening) [14] using the full width at half maximum (FWHM) of the most intense peaks after correcting the instrument broadening. The calculated average crystallite size and comparison between the measured lattice parameters and literature values are shown in Table 5.1. The measured lattice parameters of the hollow oxide spheres are in very good agreement with the literature values.

No crystalline peaks were observed before calcination, as shown in Fig.5.3 which reveals that after hydrothermal treatment the metal ions are evenly dissolved in the hydrophilic shell of the carbonaceous spheres or dispersed in the shell as amorphous cluster.

**Table 5.1** *Crystallite size calculated by Scherrer equation for the as-obtained hollow oxides and comparison between the measured lattice parameters and literature values*

| Oxide sample | Crystallite size (nm) | Lattice parameters | | |
|---|---|---|---|---|
| | | measured [Å] | | reference values [Å] |
| $Cr_2O_3$ | 17 | a/ b:<br>c: | 4.9599(7)<br>13.601(2) | 4.9507(4) [15]<br>13.5656(7) |
| α-$Fe_2O_3$ | 19 | a/ b :<br>c: | 5.0358(3)<br>13.757(1) | 5.0355(5) [16]<br>13.7471(7) |
| $Co_3O_4$ | 21 | a: | 8.0844(6) | 8.072(3) [17] |
| NiO | 10 | a: | 4.168(1) | 4.1944 [18] |
| ZnO | 35 | a/ b:<br>c: | 3.2464(2)<br>5.2000(3) | 3.2533(5) [19]<br>5.2072(13) |

[c]) See chapter 2 (experimental section)

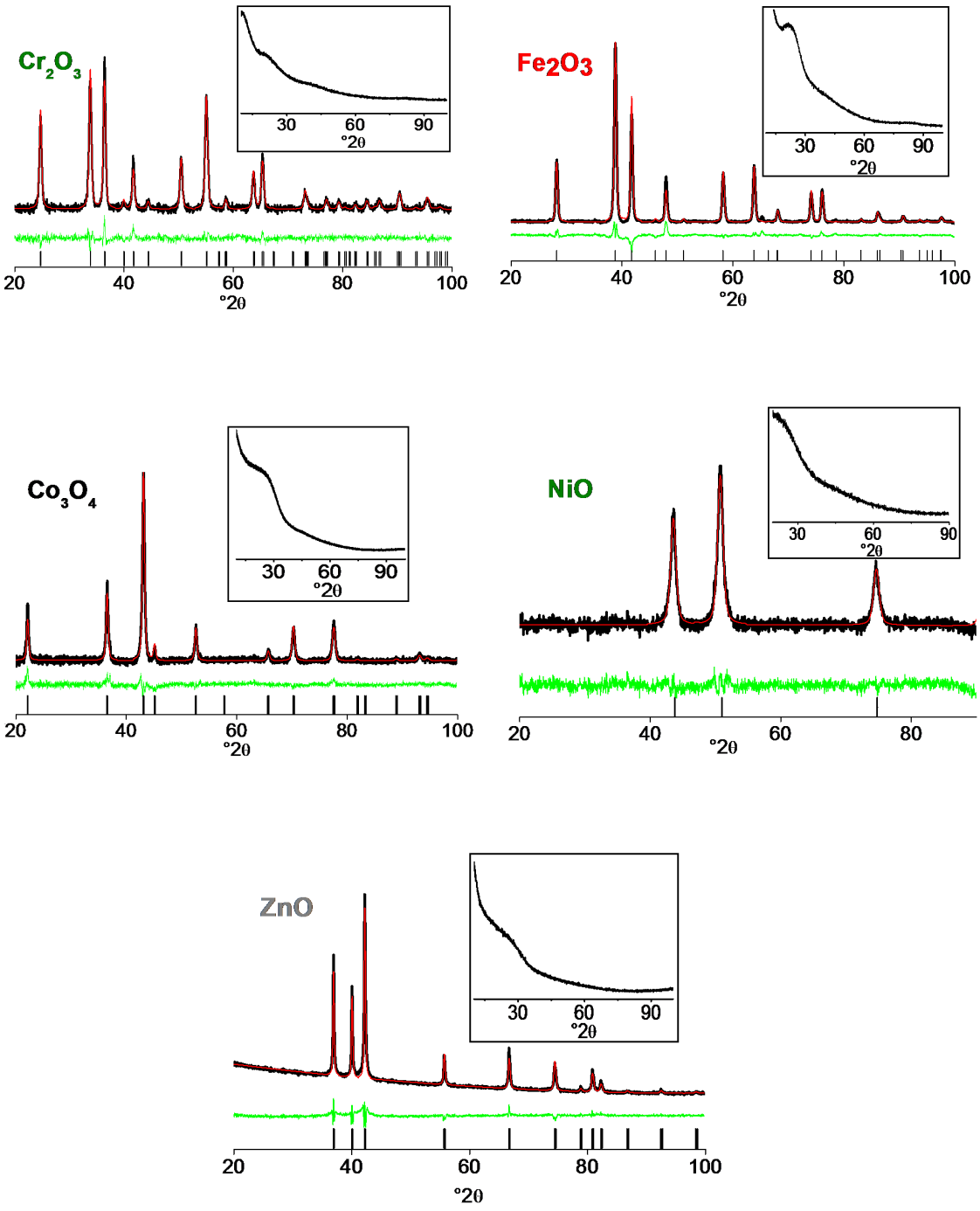


**Fig.5.3** *XRD patterns of the as-obtained oxides with Rietveld refinement (the black line is the observed pattern ,the red line is the calculated from the literatures and the green line represents the difference plot). The insets show the XRD patterns of the samples before calcination*

### 5.2.2 IR spectra

The comparison between IR spectrum before and after calcination, demonstrated the removal of the carbonaceous template materials and the formation of the hollow oxides under investigation as shown in Fig.5.4. In all samples, The IR spectrum before calcination shows a broad peak between 3000 $cm^{-1}$ and 3500 $cm^{-1}$ which likely to be the stretching vibration of O-H and the peak at 2900 is belonging to the stretching vibration of C-H bond. The vibrations at 1700 $cm^{-1}$ and 1611 $cm^{-1}$ can be assigned to C=O and C=C, respectively. The C=C double bonds indicate that dehydration has taken place during the hydrothermal carbonization of fructose.[20-21]

After calcination, the carbonaceous templates and most peaks related to the functionalities, like carboxylic or aromatic groups are gone. In Fig.5.4.a which represents hollow $Cr_2O_3$, a peak at 3400 $cm^{-1}$ is likely to be O-H stretching vibration of surface Cr-OH groups and the absorption at 1600 $cm^{-1}$ is due to the stretching and bending modes of surface-adsorbed/trapped (hydrogen-bonded) water molecules. The peaks at 560 and 621 $cm^{-1}$ are typical peaks for $Cr_2O_3$, which ascribed to stretching vibration of Cr-O bonds.[22] In Fig.5.4.b, the observed bands at 570 and 480 $cm^{-1}$ are due to Fe-O vibration mode of α-$Fe_2O_3$ which assures the hematite phase.[23] While in Fig.5.4.c the noticed signals at 560 and 660 $cm^{-1}$ can be attributed to the stretching vibrations of Co-O bond.[24]

The IR spectrum of hollow NiO in Fig.5.4.d shows the broad band at 3500 $cm^{-1}$ which is ascribed to the stretching mode of O-H group. The absorption at 1635 $cm^{-1}$ can also be ascribed to the stretching and bending modes of surface-adsorbed/trapped (hydrogen-bonded) water molecules.[25] The peaks at 519 and 459 $cm^{-1}$ is attributed to the stretching vibration of Ni-O.[25] The IR spectrum of hollow ZnO in Fig.5.4.e shows a strong band at 480 $cm^{-1}$ is attributed to the Zn-O stretching band which is consistent with that reported before.[26]

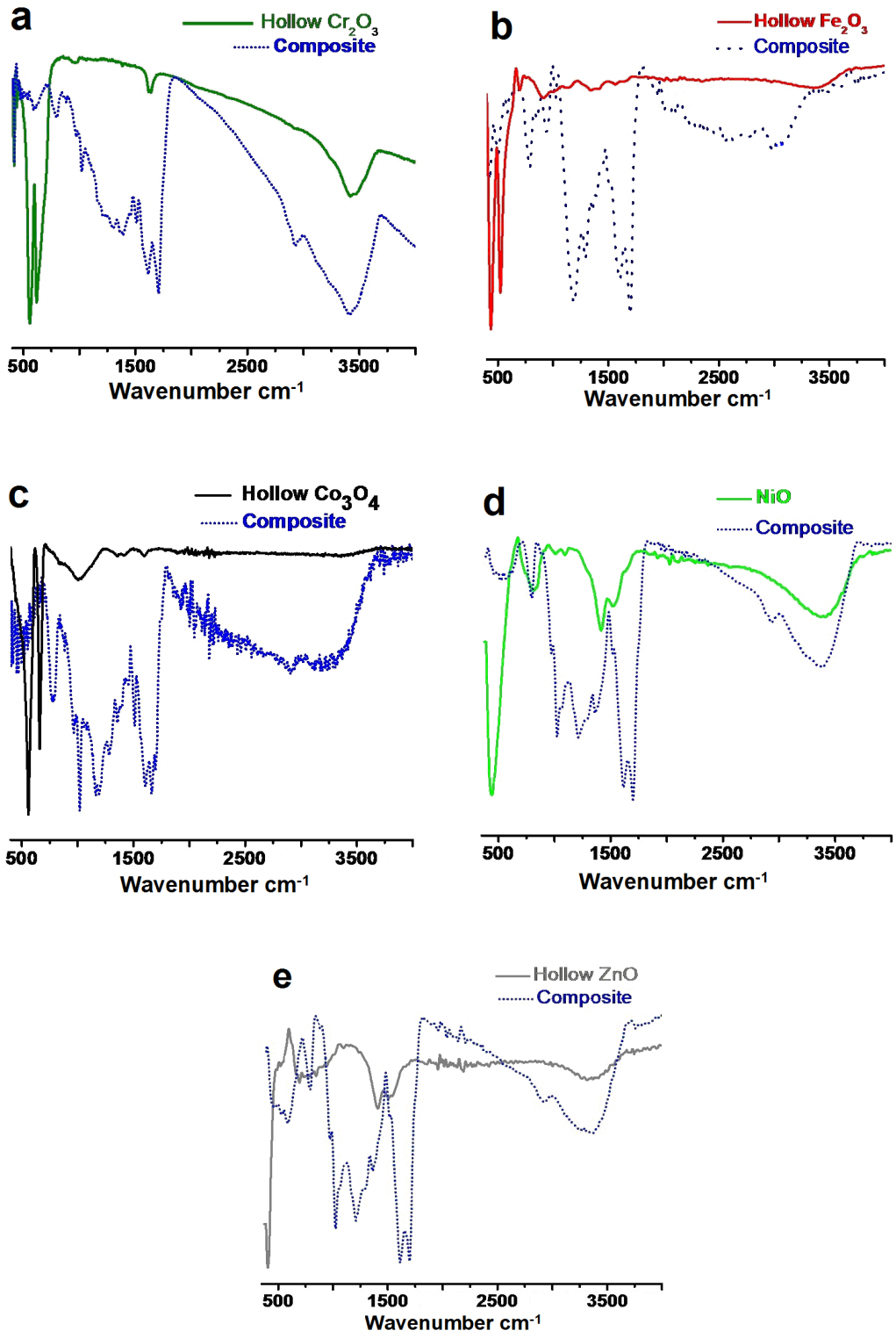


**Fig.5.4** *IR spectra of the hollow oxides, prepared according to the typical synthesis procedures, before and after calcination at 500 $^{o}C$*

### 5.2.3 Morphology and hollow structure

Electron microscopy (both scanning electron and the transmission electron microcopy) is considered definitely the most common method for the characterization of nanomaterials. For examination of nanostructures with dimensions smaller than 30 nm, transmission electron microscopy (TEM) is typically used.[27] Applying this method, high-resolution imaging and elemental and crystal structure analysis can be simultaneously performed on single nanoparticles, while irradiating with high-energy electrons. To confirm the preparation of a hollow or core/shell structure, it is typical to report observed variations in contrast between the inner core and outer shell. Scanning electron microscopy equipped (SEM) can further confirm particle morphology and surface properties. Recent reports of hollow particle formation via various methods,[28–30] present the formation of hollow structures through the observations of higher contrast between the wall layers and the empty cores. Furthermore, the formation of surface oxide layers on template particles,[31-33] new heterocomposite [34] and core/shell structures [35,36] are indicated via the contrast appeared between the different layers materials.

In this section we present the results of SEM and TEM analysis of the morphology of the hollow particles and their core@shell composite before calcinations, as well as their surface properties. It is noteworthy to mention, that all samples presented in this section have been fabricated via the typical experimental procedures.

Fig.5.5 shows the hybrid particles between the metal ions precursor and the carbonaceous template of a) $Cr_2O_3$ , b) α-$Fe_2O_3$ , and c) ZnO samples. We can notice that, a contrast appears in the images between the shell material and the core material. We assume that the shell is the metal oxide precursor sheathing the carbonaceous template core. In Fig.5.5.c we also can observe two fused hybrid particle of carbonaceous template@ZnO precursor before calcination.

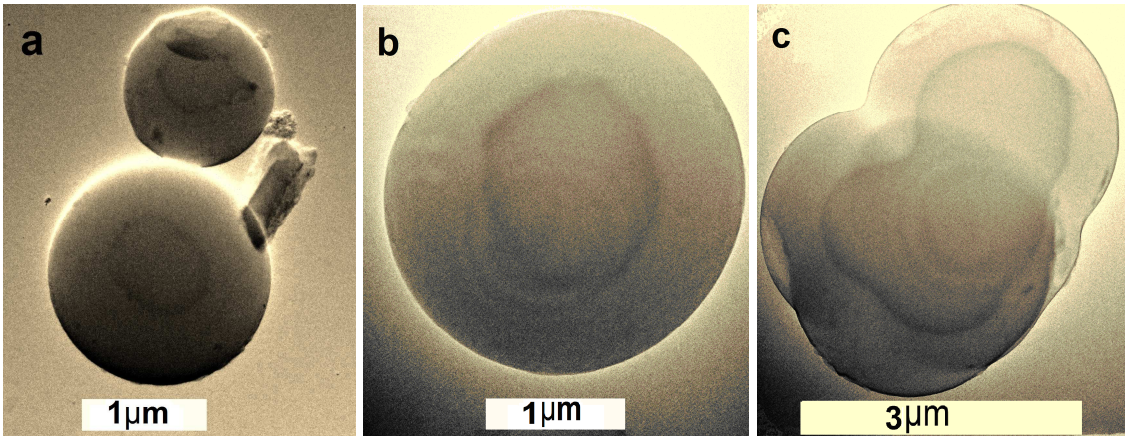


**Fig.5.5** *TEM images of the core@shell composite (carbonaceous sphere@metal ions) before calcination of a) $Cr_2O_3$, b) α-$Fe_2O_3$ and c) ZnO samples*

SEM micrographs shown in Fig.5.6 and in Fig.5.7 illustrate the hollow metal oxides before and after calcination, respectively. SEM micrographs of the products shown in Fig.5.7 give indication of the formation the hollow metal oxides; also reveal the spherical structures of the hollow particles. A careful observation of the surface of the hollow spheres shows that the walls of hollow metal oxides spheres are composed of many small nanoparticles of the corresponding metal oxide. From the broken shell, marked with a red arrow, we can notice the hollow porous nature of the hollow metal oxides spheres.

It is worth noting that after calcination the spheres remained intact and preserved the three dimensional spherical shape of particles after removing the carbonaceous core material. In addition, shrinkage in size by 40-60% occurred after calcination. This can be due to the thermal treatment during which the metal ions incorporated in the surface layer of the template are densified and cross-linked to form hollow oxide spheres replicas of the carbonaceous spheres template with reduced size (by 40-60% of the origin) as can be noticed in the particle size distribution of the hollow metal oxides and their corresponding composites Fig.5.10.

TEM images shown in Fig.5.8 are further confirming the hollow interior clearly. We can observe a contrast between the dark shell and the pale core. The wall thickness of the porous hollow metal spheres can be estimated according to the cross sectional view obtained by TEM images as approximately 60 nm, 30 nm, 45 nm, 60 nm, and 50 nm for $Cr_2O_3$, α-$Fe_2O_3$, $Co_3O_4$, NiO and ZnO hollow spheres, respectively.

SEM and TEM micrographs (Figures 5.6, 5.7 and 5.8) provide information about the formation of uniform hollow metal oxide spheres. However, as exceptions, a part of the product in all hollow oxides samples was ball in ball (bnb) hollow structure as shown in Fig.5.8. Further confirmation for the formation of bnb hollow spheres is shown in SEM micrographs Fig.5.9.

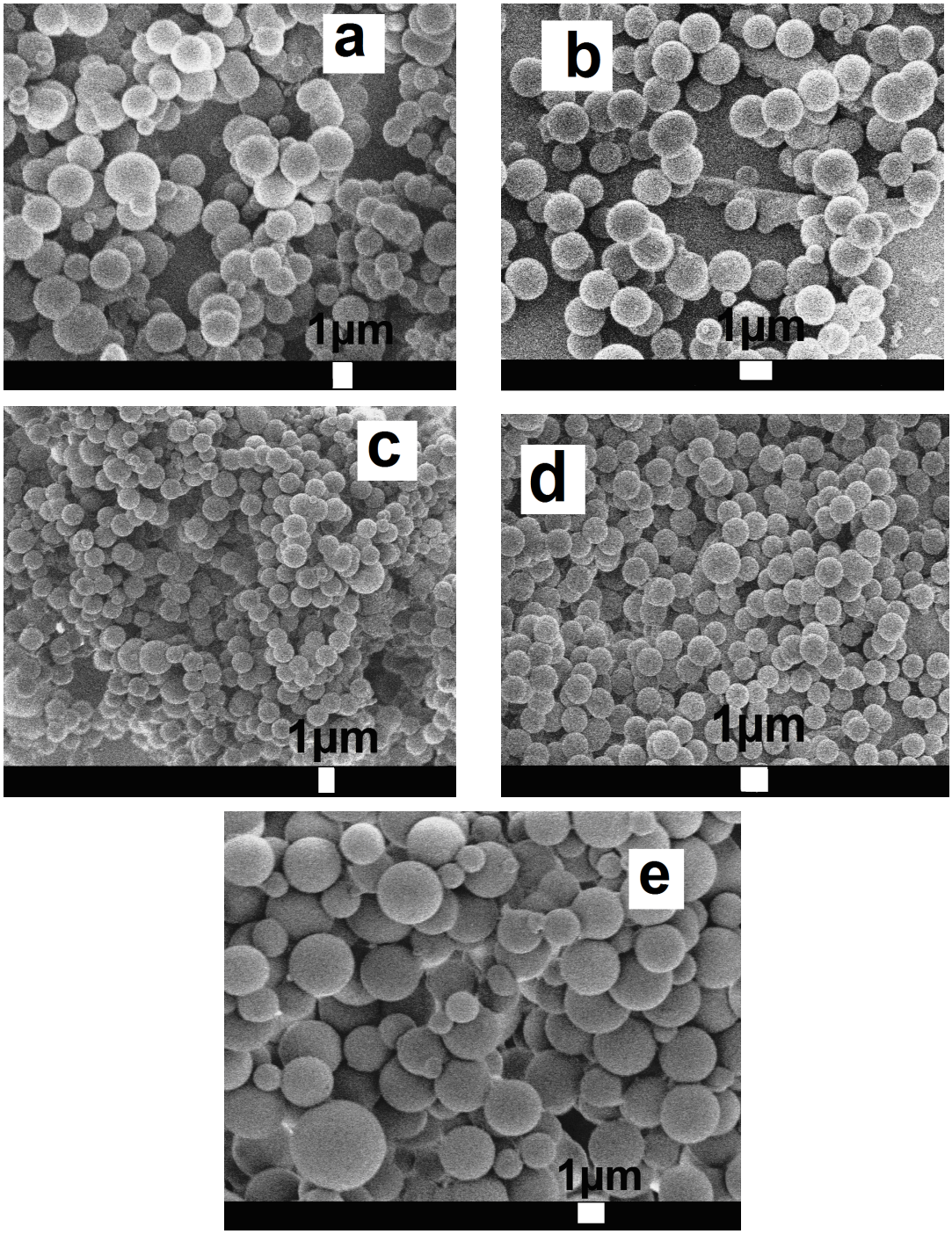


**Fig.5.6** *SEM micrographs of the composite materials, prepared according to the typical synthesis procedures, before calcination a) $Cr_2O_3$, b) α-$Fe_2O_3$, c) $Co_3O_4$, d) NiO, e) ZnO samples*

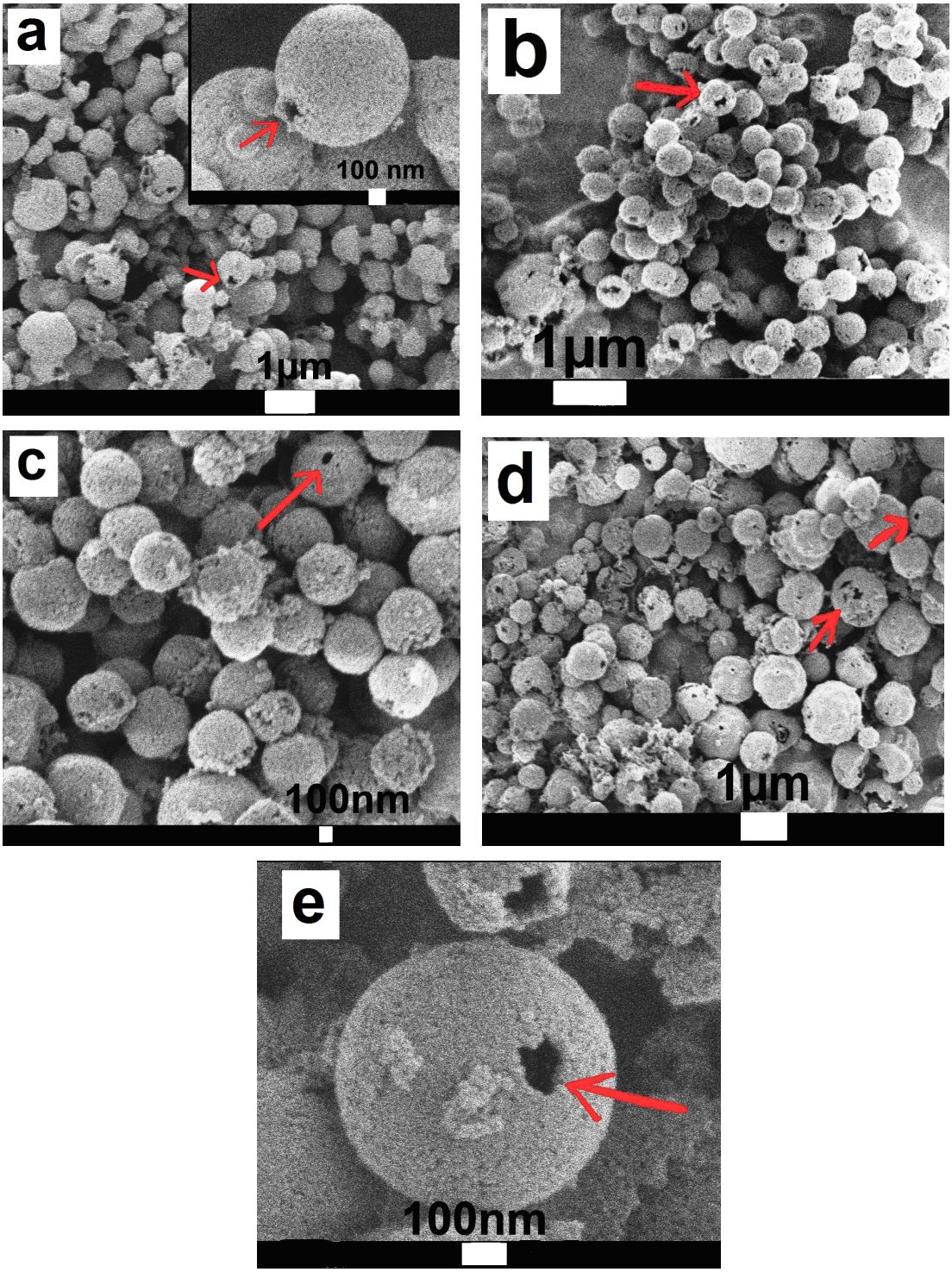


**Fig.5.7** *SEM micrographs of porous hollow metal oxide prepared according to the typical synthesis procedures, after calcination a) $Cr_2O_3$, b) α-$Fe_2O_3$, c) $Co_3O_4$, d) NiO, e) ZnO hollow samples. The red arrows refer to broken shells*

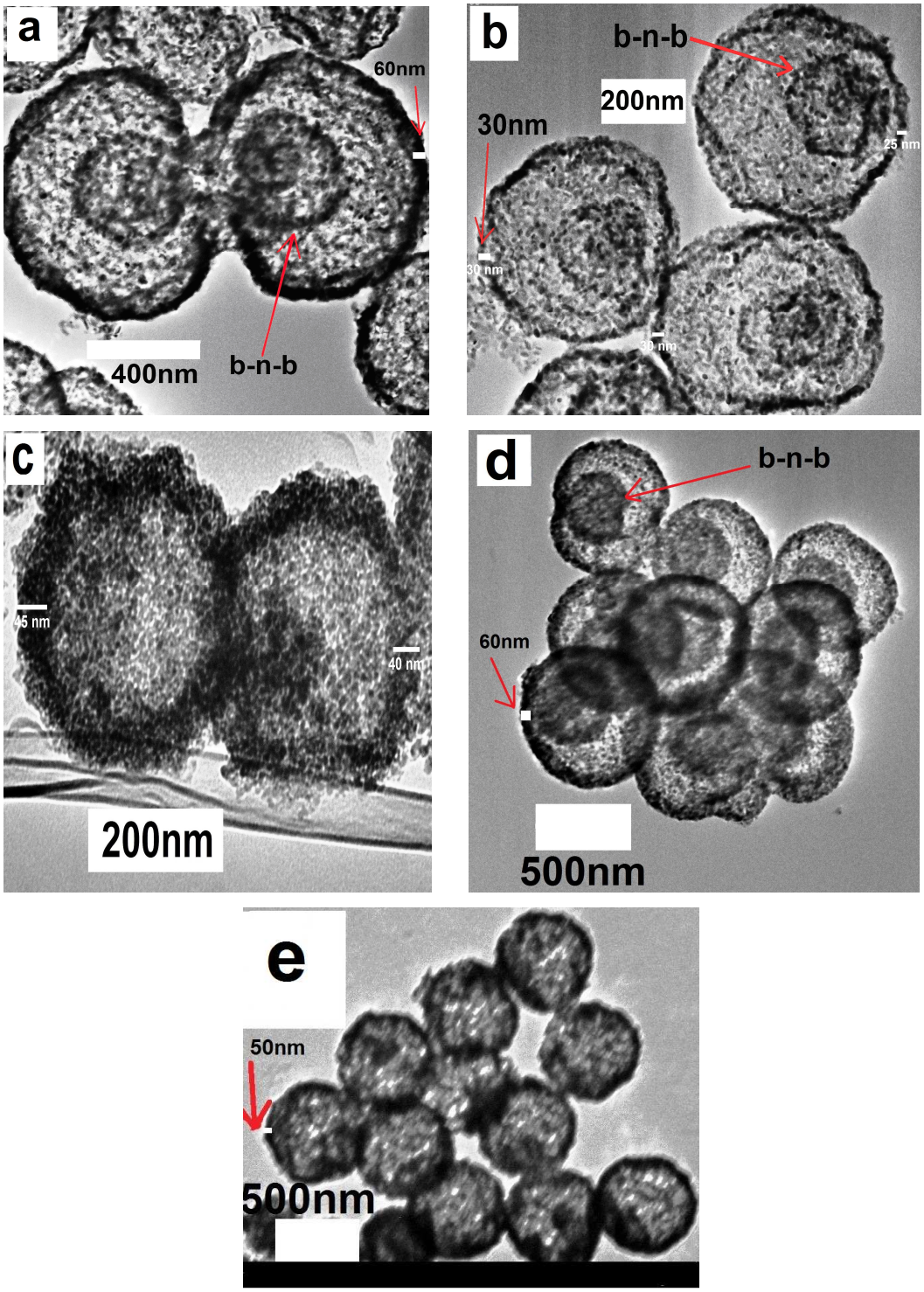


**Fig.5.8** *TEM micrographs of porous hollow metal oxide prepared according to the typical synthesis procedures, after calcination a) $Cr_2O_3$, b) α-$Fe_2O_3$, c) $Co_3O_4$, d) NiO, e) ZnO hollow samples*

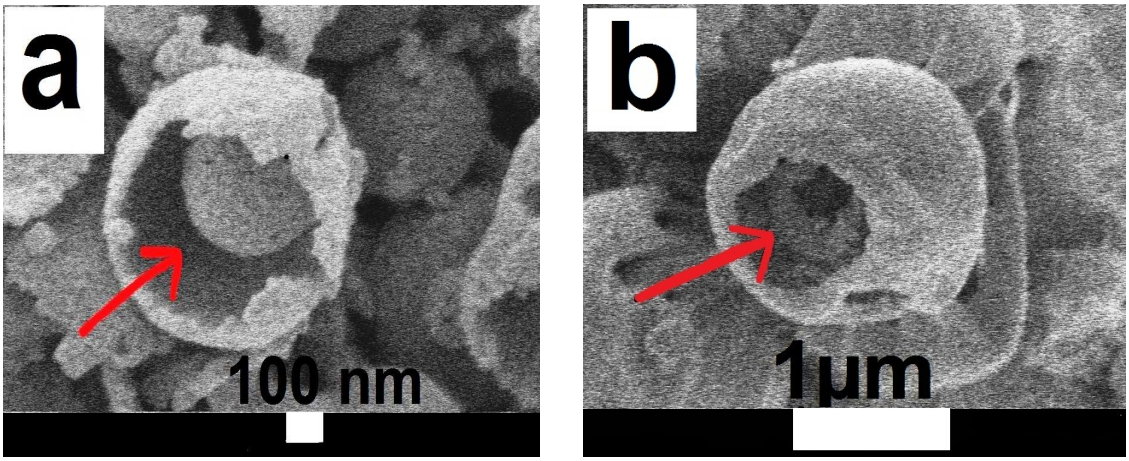


**Fig.5.9** *SEM micrographs of porous bnb hollow spheres of a) $Cr_2O_3$ and b) ZnO hollow samples as can be seen through the broken shell spheres*

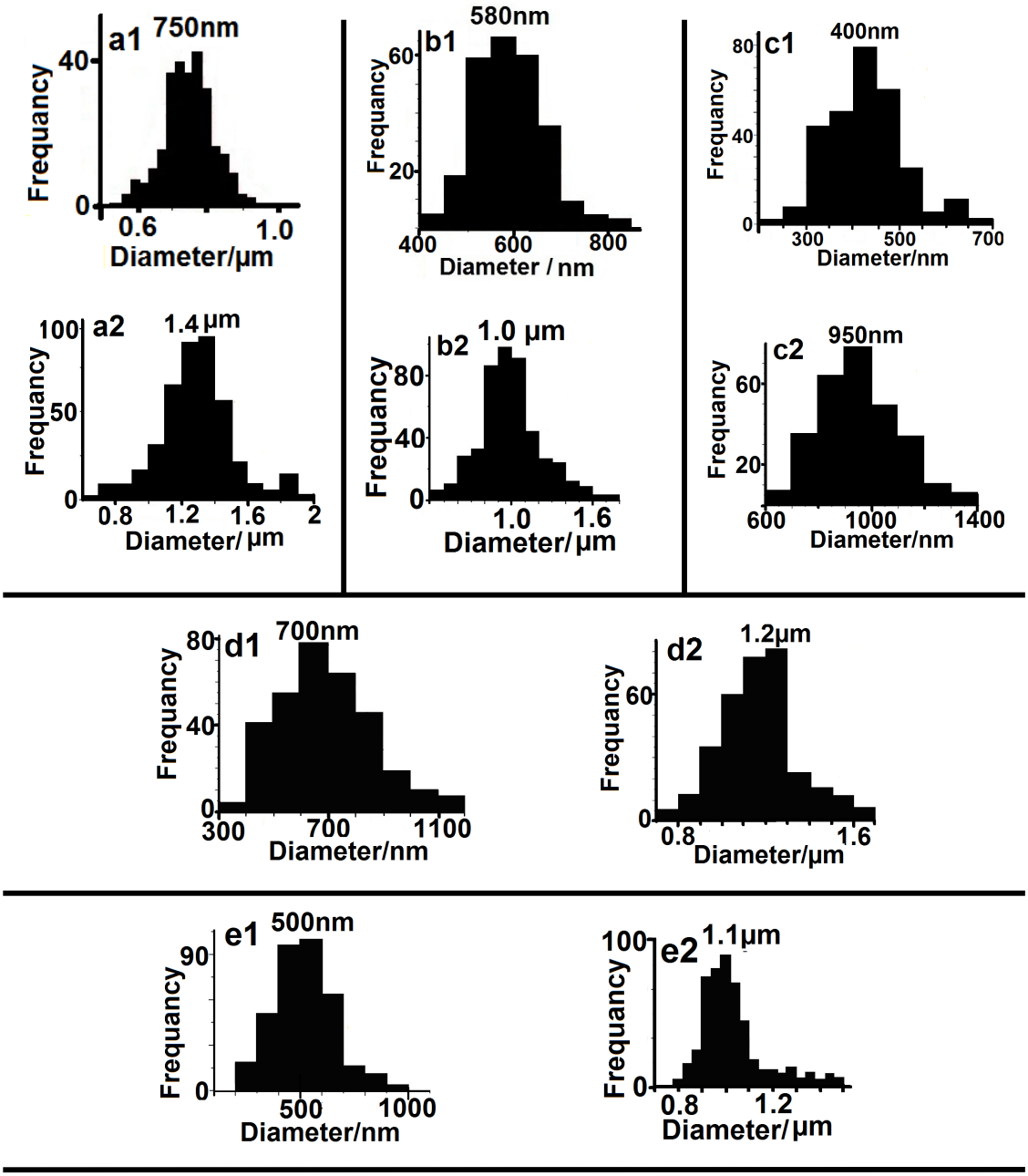


**Fig.5.10** *Particle size distribution (PSD) of:-*

*a1) hollow $Cr_2O_3$ , and a2) its corresponding composite,*

*b1) hollow α-$Fe_2O_3$ , and d2) its corresponding composite,*

*c1) hollow $Co_3O_4$ , and c2) its corresponding composite,*

*d1) hollow NiO , and d2) its corresponding composite, and*

*e1) hollow ZnO , and e2) its corresponding composite*

### 5.2.4 Surface area and porous structure (BET measurements)

The nitrogen adsorption/desorption isotherms were measured to study the porosity and specific surface area of the as-synthesized hollow metal oxides spheres as shown in Fig.5.11. These are typical type IV isotherms characteristic of mesoporous materials according to the International Union of Pure and Applied Chemistry (IUPAC).[37] Hysteresis loops can be observed in the curves of all samples evidencing of the existence of the mesoporous structure. The pore size distributions of the obtained metal oxide hollow spheres were measured by the nitrogen sorption method and calculated by Barrett−Joyner−Halenda (BJH) method from the desorption curves.[38] It can be seen that the pore size was mainly in the range of 5-50 nm for all samples, and they have a wide pore size distribution. This may be due to including the void volume of the hollow spheres in the pore volume distribution.

The surface areas of the hollow oxides samples are listed in Table 5.2. The specific surface areas of these hollow metal oxides is assigned to the combination of the surface area of the outer surface, the inner surface and the mesopores which form altogether the whole surface area of the particles. The large surface areas show that these kind of materials may have several potential applications in many fields.

**Table 5.2** *Surface area of the hollow metal oxide spheres*

| Oxide sample | $A_{BET}$ ($m^2g^{-1}$) |
|---|---|
| $Cr_2O_3$ | 55 |
| α-$Fe_2O_3$ | 51 |
| $Co_3O_4$ | 47 |
| NiO | 48 |
| ZnO | 60 |

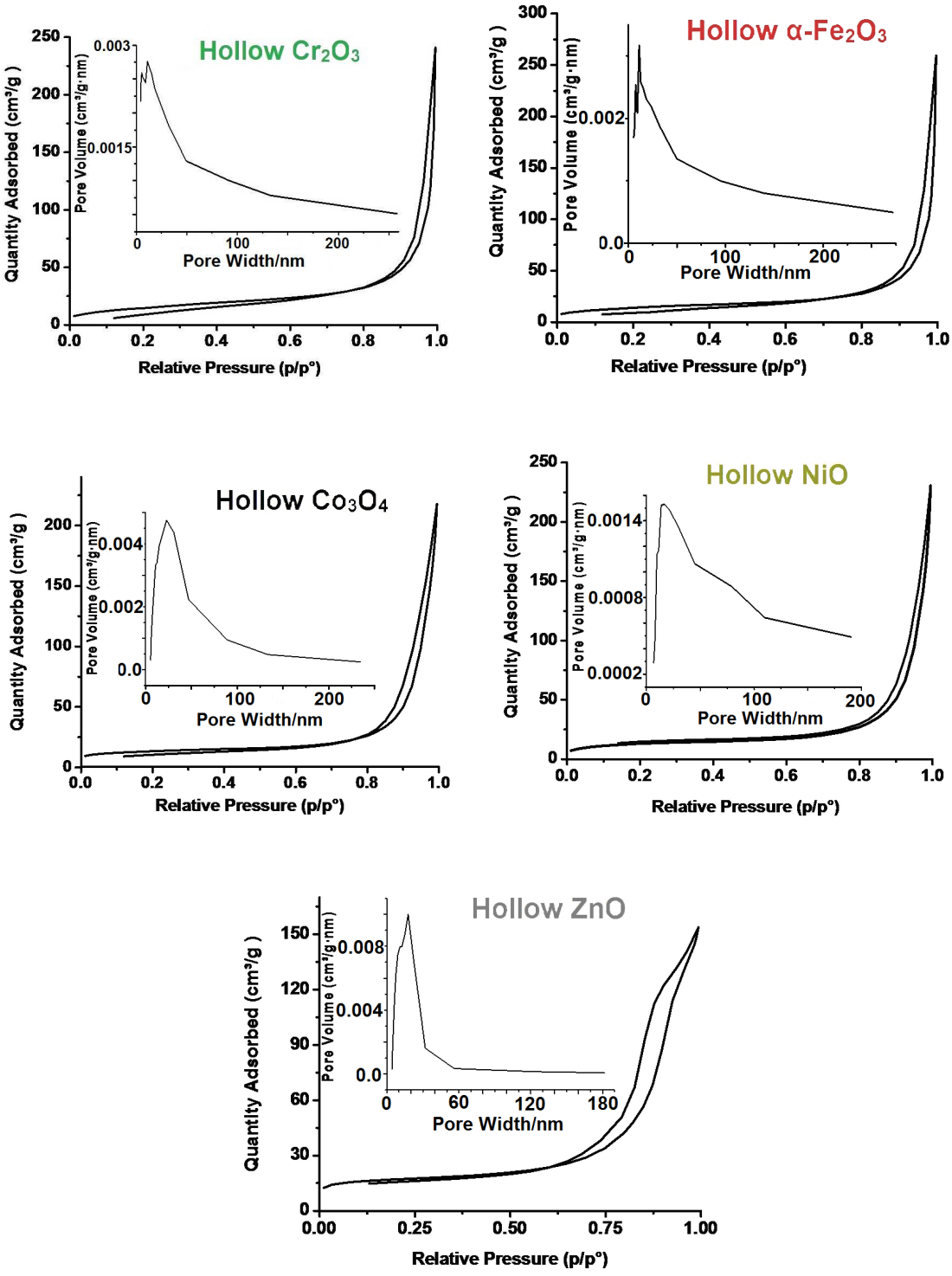


**Fig.5.11** *Nitrogen sorption isotherms of the hollow oxides. The insets show the pore size distribution of the corresponding sample from desorption branch*

### 5.2.5 EDX analysis

EDX data of $Cr_2O_3$ hollow spheres in Table 5.3 and Fig.5.12 reveals that it is composed only of Cr and O after calcination at 500 $^oC$ and Cr, O, C before calcination as listed in the Table.

**Table *5.3*** *Element composition in Wt%*

| | Cr | O | C |
|---|---|---|---|
| Before calcination | 22 | 44 | 34 |
| After calcination | 68 | 33 | ------- |

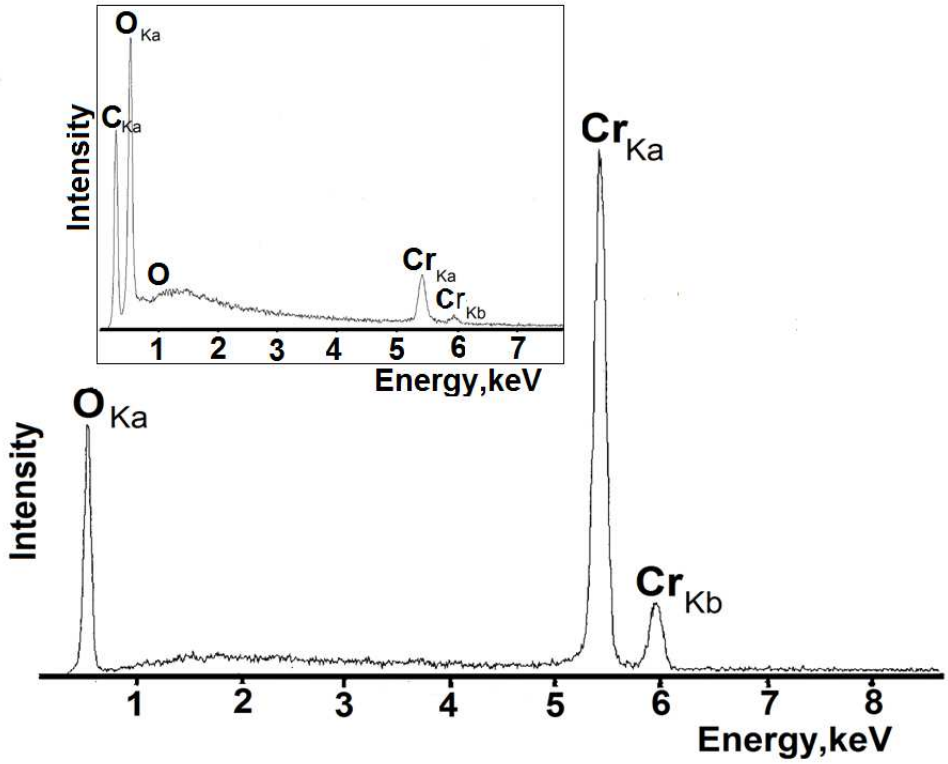


**Fig.5.12** *EDX spectrum of hollow $Cr_2O_3$ spheres .The inset show the sample before calcination at 500 $^oC$*

## 5.3 Proposal of a mechanism for the formation of hollow oxide spheres

The key to success in fabrication of the porous hollow metal oxides spheres via hydrothermal method using fructose as sacrificial template might be attributed to the fact that the surface layers of the fructose-derived carbonaceous spheres are rich of oxygen functional groups which facilitate the precipitation of the metal cations.

Fig.5.13 illustrates schematically the proposed mechanism of the formation of the porous metal oxide hollow spheres. According to the proposal the formation of hollow metal oxides spheres probably involves 4 stages as following:

1. Autoclaving of the reactants (fructose + metal chloride) at moderate temperature involves the dehydration and subsequent carbonization of fructose resulting in carbonaceous spheres (CSs). The surface layers of CSs are hydrophilic and rich in oxygen functionalities (e.g., -OH, C=O) due to non or partially dehydrated fructose.[39-40]
2. The metal ions dispersed in the solution mixture can anchor onto the surface of the CSs and bind with the functional groups in the surface layers by taking advantage of co-ordination or electrostatic interactions. This results in the in-situ formation of core@shell composite by deprotonation. This is consistent with EDX analysis which indicated that the composite before calcination contains no chlorine atoms.
3. Finally, the removal of the CSs cores via heat treatment in air and the surface layer incorporating the cationic metal ions are densified and cross-linked to form the free standing hollow spheres replicas of the fructose-derived CSs, but with about 40-60% less than the original corresponding composite size. The significant shrinkage in size during the thermal treatment indicates that the metal cations adsorbed loosely on the CSs cores have been oxidized and transformed into dense oxide networks that compose the shells of the hollow spheres.

4. It was surprising that this method resulted in ball in ball (bnb) hollow structure in all oxide samples without any extra step. It is noteworthy mentioning that the formation mechanism of the bnb structure is not fully comprehended at this stage. However, it is suggested that some nano-islands of metal oxide in the shell may migrate to or be stuck on the surface of the shrinking CSs cores during the calcination process. Further heating at elevated temperature, these nano-islands finally aggregate into a small ball in the interior when the CSs cores are completely burnt off. [41-42]

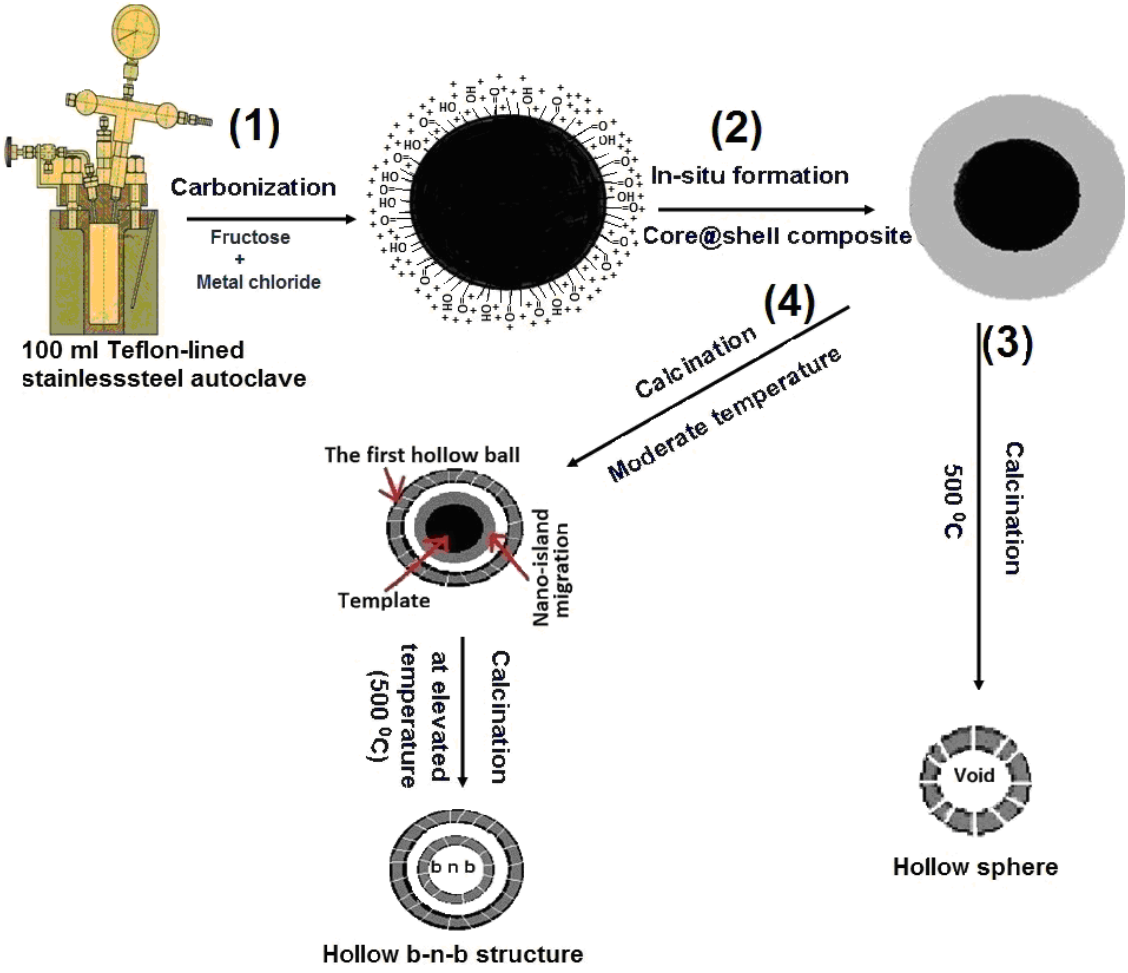


**Fig.5.13** *Schematic diagram of the fabrication of porous hollow metal oxides spheres via hydrothermal method*

## 5.4 The impact of the synthesis parameters

We demonstrated in the last sections of this chapter that fructose can be used as a powerful template for many kind of oxides hollow spheres. They are incorporated into composite core@shell structure and these are then converted into hollow spheres through calcination.

Temperature (T), reaction time (t), concentration of fructose, the concentration ratio c(fructose)/c(metal chloride), and adding acetic acid as catalyst are five significant parameters that are involved in the hydrothermal synthesis method of the hollow metal oxide spheres. To study the impact of each synthesis parameter many experimental conditions were systematically varied in which the parameter under investigation was varied while the other parameters remained unchanged according to the typical synthesis procedures.

The results show that each parameter of the previously mentioned parameters have similar impact on the different types of oxides. The similarity of the impact of each parameter on the formation of hollow oxides reported here might open the door for general understanding of the formation of the hollow metal oxides spheres with variable size.

The temperature has an obvious impact on the size and the shape of the hollow oxides. When the temperature was 125 $^{o}$C, no solid precipitate could be observed in all oxide types while at higher temperature (150 $^{o}$C) the hollow spherical shape was lost and the shape of the oxides was either fused spheres or foams or spongy like structure as seen in Table 5.4, and Figures 5.7 and 5.14. The only oxide that produced hollow spheres with regular shape at 150 $^{o}$C was hollow $Cr_2O_3$, and from PSD of the sample we can notice that the size is larger than that formed at 135 $^{o}$C.

**Table 5.4** *The impact of temperature on the shape and the size of the hollow oxides*

| Oxide sample | Shape and size at T($^{o}$C) | | |
|---|---|---|---|
| | 125 $^{o}$C | 135 $^{o}$C [Fig.5.7] | 150 $^{o}$C [Fig.5.14] |
| $Cr_2O_3$ | ----- | hollow spheres 750nm | hollow spheres 1050nm |
| α-$Fe_2O_3$ | ----- | hollow spheres 580nm | fused particles |
| $Co_3O_4$ | ----- | hollow spheres 400nm | foams |
| NiO | ----- | hollow spheres 700nm | fused particles |
| ZnO | ----- | hollow spheres 500nm | spongy like structure |

The optimal time observed for obtaining metal oxide hollow spheres is 6h. In case of increasing time from 6 to 12 h no hollow spheres was created for $Co_3O_4$ and NiO, while $Cr_2O_3$ and ZnO produced hollow fused particles. The only hollow spheres were observed with α-$Fe_2O_3$ sample with average particle size ~1.1µm which is larger than that observed for 6 h reaction as can be seen in Fig.5.15.

Increasing the fructose concentration from 0.625 molL$^{-1}$ (Fr4) to 1.250 molL$^{-1}$ (Fr2) resulted in increasing the average size of metal hollow oxides spheres about 40-46% in cases of $Cr_2O_3$, α-$Fe_2O_3$, and NiO. While in case of $Co_3O_4$ and ZnO fused hollow particles were observed. Fig.5.16 illustrates the SEM micrographs of the as-obtained metal oxides hollow particles when the fructose concentration was increased to 1.25 molL$^{-1}$ (Fr2).

Fig.5.17 illustrates the impact of adding 0.5 mL of acetic acid to the reaction mixture solution. It is obvious that acetic acid catalyzes the reaction and increase the rate of the hydrothermal reaction and as a result the average size of the metal hollow oxides spheres increased about 35-55%.

When the concentration ratio c(fructose)/c(metal chloride) increased from 20:1 to 40:1, we can anticipate that the amount of metal oxide forming the shell of hollow spheres will be decreased. One learns from the architecture that a multi wall should be much more robust than a single wall. Inspired from this concept we can expect that the wall thickness of the hollow spheres in case of concentration ratio 20:1 will be thicker and more robust than that in case 40:1. Fig.5.18 shows TEM micrographs for as-obtained hollow $Cr_2O_3$ samples through applying concentration ratio a) 20:1 b) 40:1. We can notice that the wall thickness of the hollow spheres is inversely proportional to the molar ratio between the reactants. The wall thickness decreased from 60 nm to 30 nm when the concentration ration increased from 20:1 to 40:1. If we know that the particle size of the $Cr_2O_3$ particles forming the wall of the hollow spheres calculated by Scherrer equation (Table 5.1) equal 17 nm, we can deduce that the wall thickness when the molar ration was 20:1 = 3-4 layers while in case of molar ration 40:1 = 2 layers. These findings show that the wall thickness is more robust in case of low molar ratio c(fructose)/c(metal chloride).

In general, the size of the hollow spheres is directly proportional to the fructose concentration, reaction time, temperature and adding of 0.5 mL of acetic acid acting as a catalyst. While the wall thickness of the hollow spheres is inversely proportional with the molar ratio c(fructose)/c(metal chloride). Table 5.5 summarizes the relationship between the synthesis parameters and the size and shape of the as-obtained hollow metal oxides spheres.

**Table 5.5** *Relationship between the synthesis parameters and size and shape of the as-obtained hollow metal oxides spheres*

| Oxide sample | Shape and size | | | | |
|---|---|---|---|---|---|
| | Typical experimental procedures[(d)] [Fig.5.7] | T= 150 °C[(e)] [Fig.5.14] | t=12 h[(e)] [Fig.5.15] | Fructose concentration[(e)] 1.25 molL$^{-1}$ (Fr2) [Fig.5.16] | Catalyst 0.5 mL acetic acid[(e)] [Fig.5.17] |
| $Cr_2O_3$ | 750nm hollow spheres | 1050nm hollow spheres | 1.1µm hollow spheres | 1.4µm hollow spheres | 1.2µm hollow spheres |
| α-$Fe_2O_3$ | 580nm hollow spheres | fused hollow particles | fused hollow particles | 800nm hollow spheres | 1µm hollow spheres |
| $Co_3O_4$ | 400nm hollow spheres | foams | ----- | fused hollow particles | 950nm hollow spheres |
| NiO | 700nm hollow spheres | fused hollow particles | ----- | 1.3µm hollow spheres | 1.07µm hollow spheres |
| ZnO | 500nm hollow spheres | spongy like structure | fused hollow particles | fused hollow particles | fused hollow particles |

d) In typical experimental procedures, t= 6 h, T= 135 °C, fructose concentration = Fr4 (0.625 molL$^{1-}$, molar ratio = 20, and no catalyst applied.
e) Only this parameter was changed while the other parameters remained constant

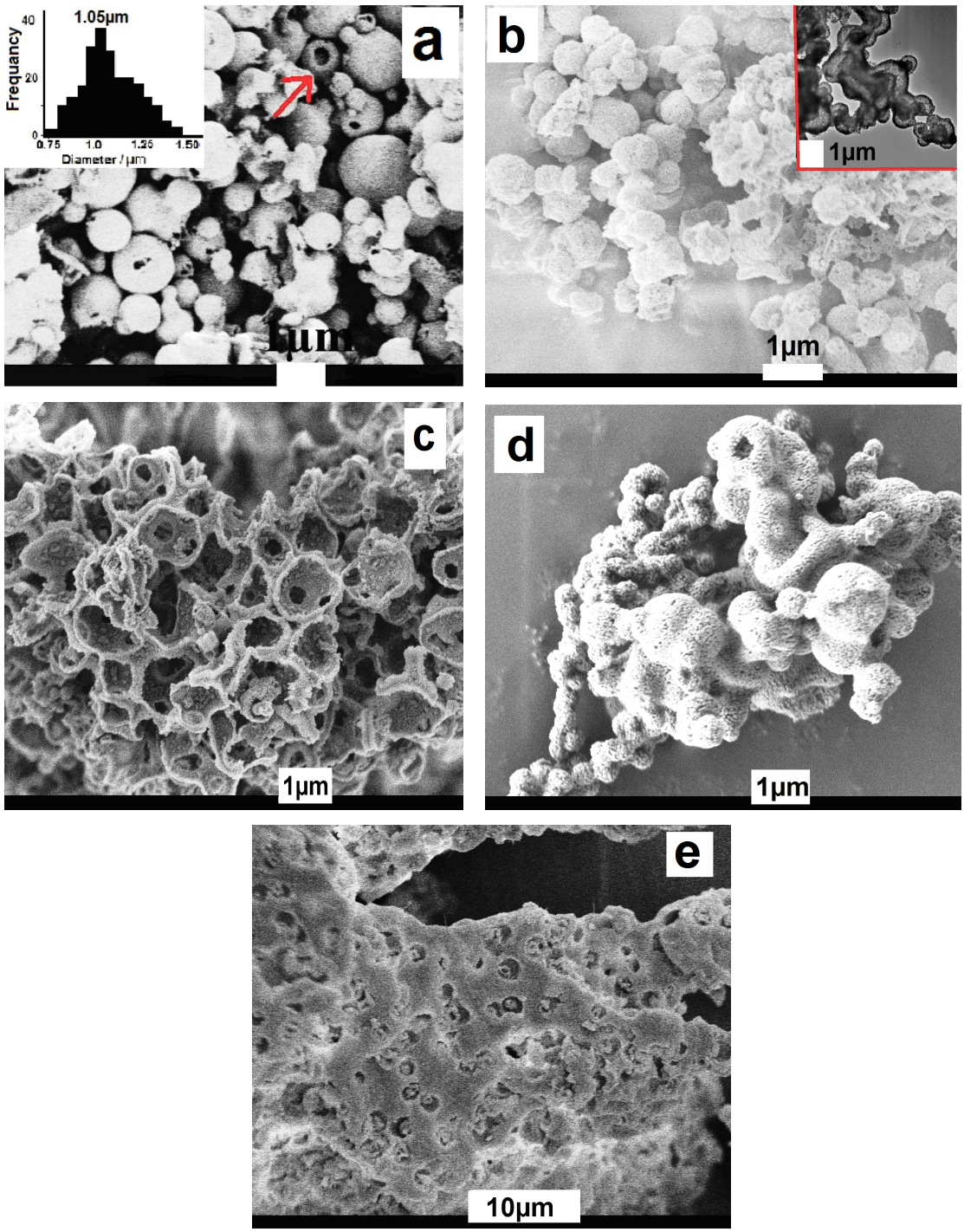


**Fig.5.14** *SEM micrographs of porous metal oxide prepared at 150 $^{o}$C after calcination, a) hollow $Cr_2O_3$ spheres (the inset is PSD of the sample and the red arrow refers to broken shells), b)fused hollow α-$Fe_2O_3$ particles ( the inset is TEM micrograph of the sample), c) $Co_3O_4$ foams, d) fused hollow NiO particles, e) spongy like ZnO*

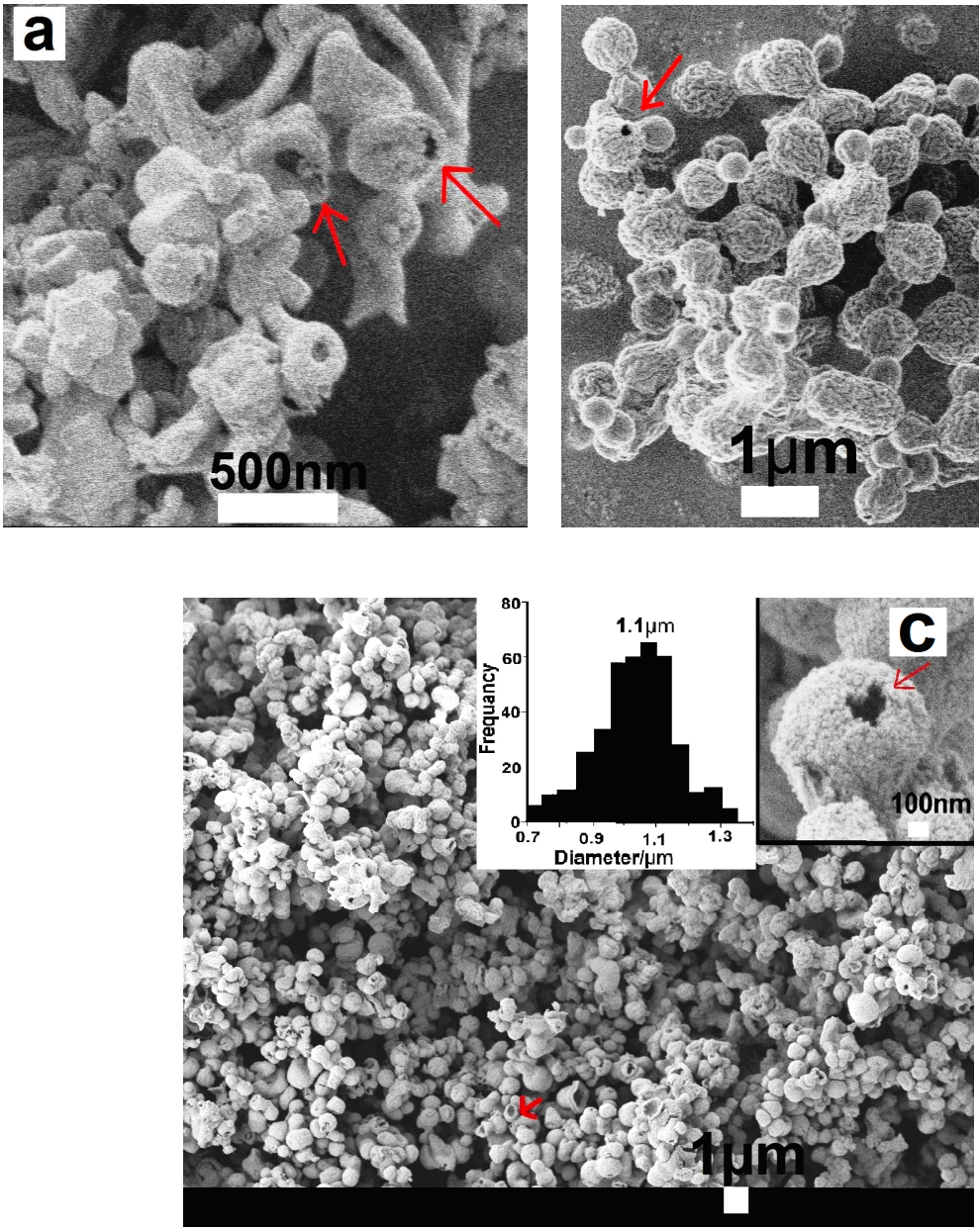


**Fig.5.15** *SEM micrographs of porous metal oxide prepared at 12 h after calcination, a) fused hollow ZnO particles, b) fused hollow $Cr_2O_3$ particles, and c) hollow α-$Fe_2O_3$ spheres, (the inset is PSD of the sample and the red arrow refers to broken shells)*

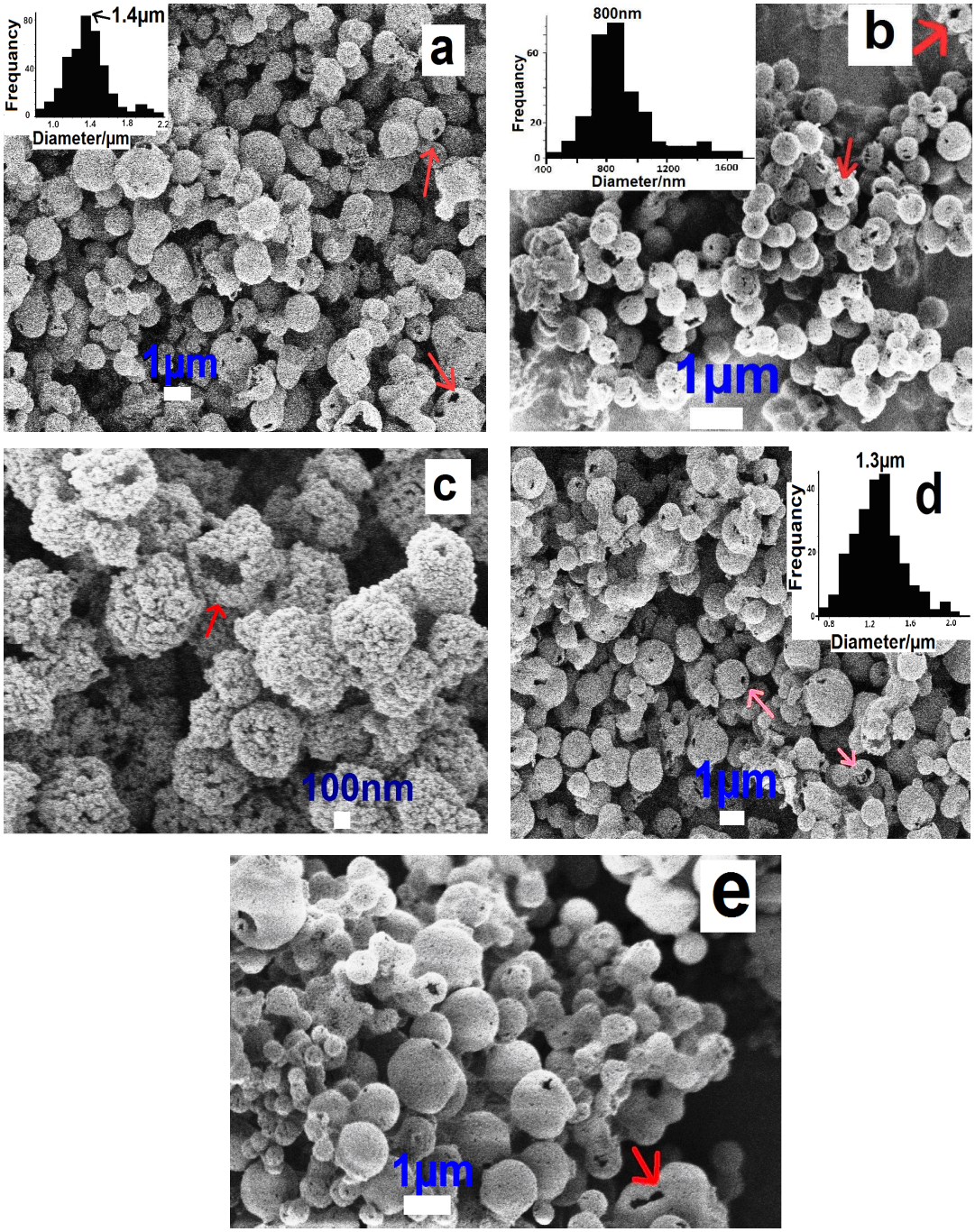


**Fig.5.16** *SEM micrographs of porous metal oxide prepared by using 1.25 molL$^{-1}$ (Fr2) as fructose concentration after calcination, a) hollow $Cr_2O_3$spheres b) hollow α-$Fe_2O_3$ spheres, c) fused $Co_3O_4$ hollow particles, d) hollow NiO spheres, and e) fused ZnO hollow particles (the inset is PSD of the sample and the red arrow refers to broken shells)*

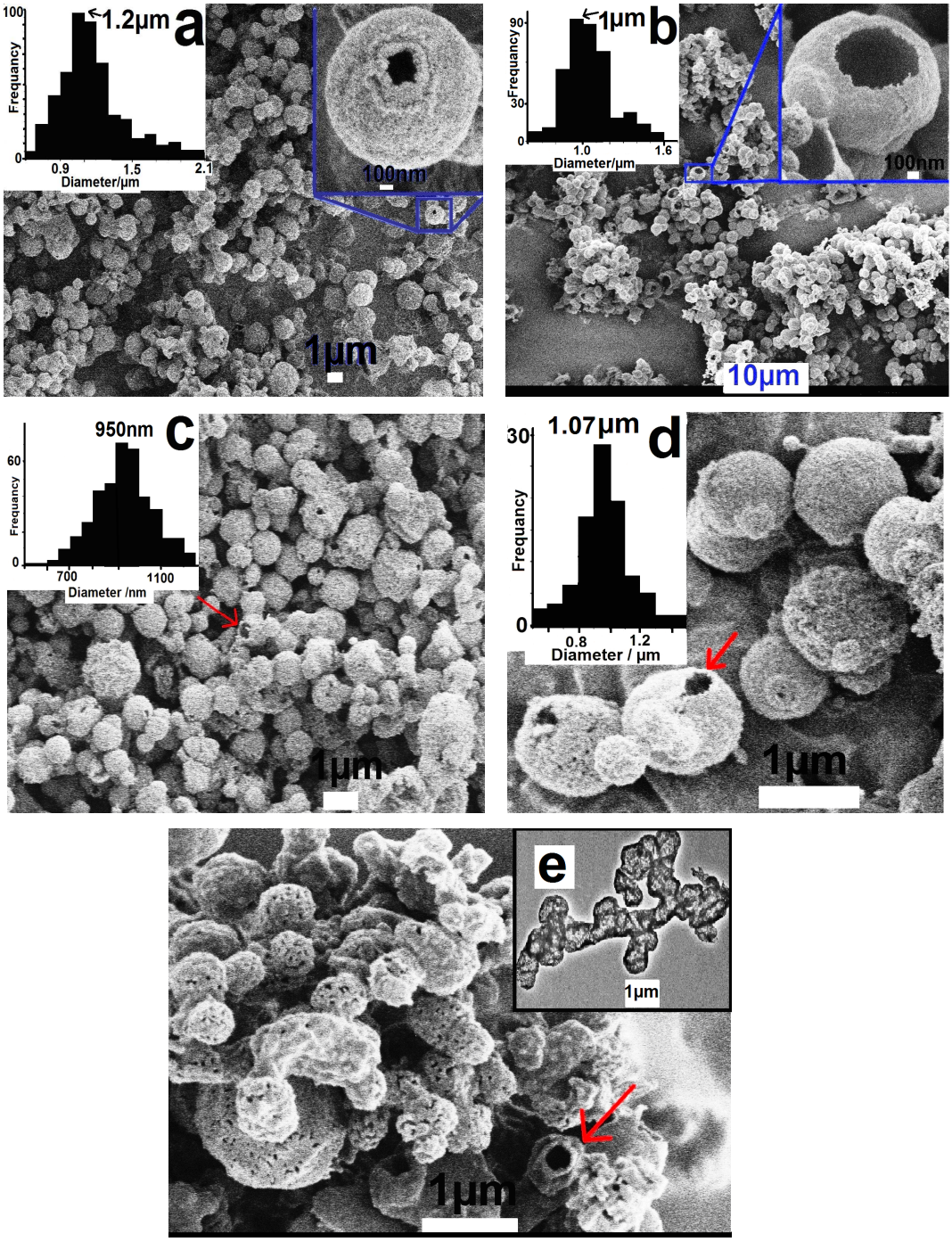


**Fig.5.17** *SEM micrographs of porous metal oxide prepared by applying 0.5 mL acetic acid as catalyst after calcination, a) hollow $Cr_2O_3$ spheres, b) hollow α-$Fe_2O_3$ spheres, c) hollow $Co_3O_4$ spheres, d) hollow NiO spheres (the insets are PSD of the samples and the red arrow refers to broken shells), and e) fused ZnO hollow particles (the inset is TEM micrograph of fused hollow ZnO particles)*

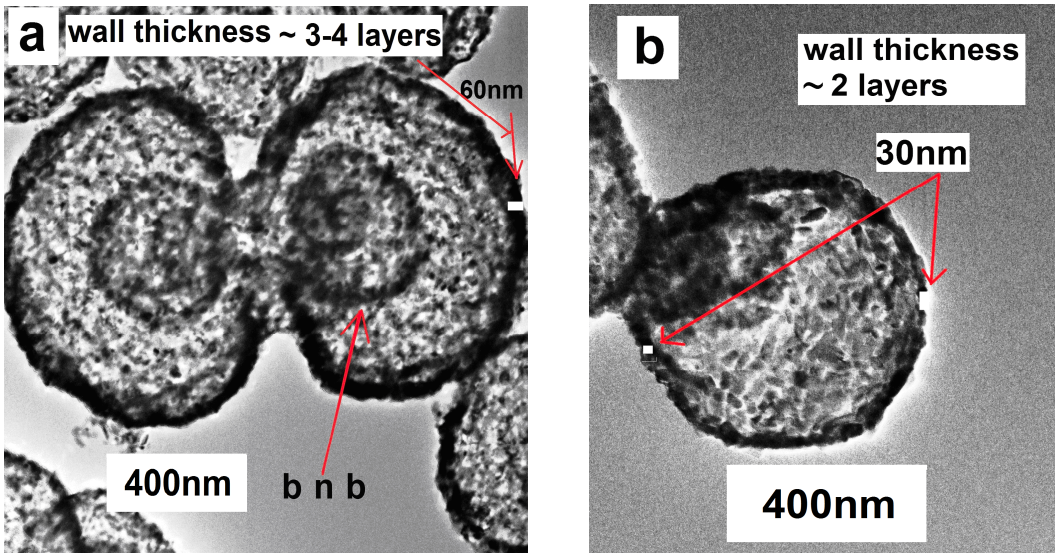


**Fig.5.18** *TEM micrographs for as-obtained hollow $Cr_2O_3$ samples [concentration ratio c(fructose)/c(metal chloride) a) 20:1 b) 40:1]*

## 5.5 Conclusion

Fructose has been successfully applied as a new sacrificed template for the synthesis of hollow oxides spheres through one-pot hydrothermal route. $Cr_2O_3$, $Co_3O_4$, NiO, $Fe_2O_3$ and ZnO hollow spheres have been obtained through this method. After thermal treatment of composites, a shrinkage in size occurred. The size decreased approximately by 40-60%.

Generally, correlations between the particle size and the concentration of fructose, as well as the ratio of metal precursor and the sugar concentrations are uncovered. Moreover, important factors critical to fine-tune the final particle size and the shape are temperature, reaction time and addition of acetic acid apparently acting as catalyst.

In general, the size of the hollow spheres is directly proportional to the fructose concentration, reaction time, temperature and adding of 0.5 mL of acetic acid. While the wall thickness of the hollow spheres is inversely proportional with the molar ratio c(fructose)/c(metal chloride).

In summary, using fructose as sacrificial template after application of a hydrothermal one-pot synthesis route is shown to be a general facile way for the synthesis of various hollow nano-oxides with variable size and shape. The results have shown that each of the previously mentioned parameters have similar impacts on the different types of oxides. The similarity of the impact of each parameter on the hollow oxides reported here might open the door for general understanding of the formation of the hollow metal oxides spheres with variable size.

## References


1. H. P. Liang, H. M. Zhang, J. S. Hu, Y. G. Guo, L. J. Wan, C. L. Bai, *Angew. Chem.* **116** (2004) 1566.
2. Y. Zhu, J. Shi, W. Shen, X. Dong, J. Feng, M. Ruan, Y. Li, *Angew. Chem.* **117** (2005) 5213; *Angew. Chem. Int. Ed*. **44** (2005) 5083.
3. J. Y. Chen, B. Wiley, Z. Y. Li, D. Campbell, F. Saeki, H. Cang, L. Au, J. Lee, X. D. Li, Y. N. Xia, *Adv. Mater*. **17** (2005) 2255.
4. U. Jeong, Y. Wang, M. Ibisate, Y. N. Xia, *Adv. Funct. Mater*. **15** (2005) 1907.
5. L. Chen, Z. Song, X. Wang, S. Prikhodko, J. Hu, S. Kodambaka, R. Richards, *Appl. Mater.& Interf.* **1** (2009) 1931.
6. C. Chen, S. Abbas, A. Morey, S. Sithambaram, L. Xu, H. Garces, W. Hines, S. Suib, *Adv. Mater*. **20** (2008) 1205.
7. N. Wang, Y. Yang, Y. Zhang, W. Yang, Y. Yue, Z. Gao, Y. Tang, *Chem. Mater.* **17** (2005) 2582.
8. K. An, S. Kwon, M. Park, H. Na, S. Baik, J. Yu, D. Kim, J. Son, Y. Kim, I. Song, W. Moon, H. Park, T. Hyeon, *Nano Lett.* **8** (2008) 4252.
9. N. Dhas, K. S. Suslick, *J. Am. Chem. Soc.* **127** (2005) 2368.
10. S.W. Kim, M. Kim, W. Y. Lee, T. Hyeon, *J. Am. Chem. Soc.* **124** (2002) 7642.
11. Z. Yang, Z. Niu, Y. Lu, Z. Hu, C. C. Han, *Angew.Chem.* **115** (2003) 1987.
12. X. Sun, Y. Li, *Angew. Chem.* **116 (**2004) 607.
13. Philips Analytical, X'Pert Plus (1.0) 1999 (Almelo).
14. H. P. Klug, L. E. Alexander, *X-ray Diffraction procedures*, Wiley: New York (1959).
15. L. W. Finger, R. M. Hazen , *J. Appl. Phys.* **51** (1980) 5362.
16. E. N. Maslen, V. A. Strel'tsov, N. R. Strel'tsova, N. Ishizawa, *Acta Crystallographica B* **50** (1994) 435.
17. J. P. Picard, G. Baud, J. P. Besse, R. Chevalier, *Journal of the Less-Common Metals* **75** (1980) 99.
18. D. Taylor, *Transactions and Journal of the British Ceramic Society* **83** (1984) 5.
19. K. Kihara, G. Donnay, *Canadian Mineralogist* **23** (1985) 647.
20. T. Sakaki, M. Shibata, T. Miki, H. Hirosue, N. Hayashi, *Bioresour. Technol.* **58** (1996) 197.

21. D. Ni, L. Wang, Y. Sun, Z. Guan, S. Yang, K. Zhou, *Angew. Chem. IE* **49** (2010) 4223.
22. I. Esparza, M. Paredes. R. Martinez, A. Couto, G. Sanchez, L. Velez, O. Dominguez, *Mater. Sci. & Appl.* **2** (2011) 1584.
23. G. Pradhan, K. Parida, *Appl. Mater. & Inter*. **3** (2011) 317.
24. J. Preudhomme, P. Tarte, *Spectrochimica Acta Part A: Molecular Spectroscopy* **27** (1971) 1817.
25. P. Oliva, J. Leonardi, J. F. Laurent, C. Delmas, J. Braconnier, M. Figlarz, F. Fievet, A. J. de Guibert, *Power Sources* **8** (1982) 229.
26. Y. He, B. Yang, G. Cheng, *Catal.Today* **98** (2004) 595.
27. Z. L. Wang, *J. Phys. Chem. B* **104** (2000) 1153.
28. J. Yang, J. U. Lind, W. C. Trogler, *Chem. Mater.* **20** (2008) 2875.
29. W. Leng, M. Chen, S. Zhou, L. Wu*, Langmuir* **26** (2010) 14271.
30. G. Jia, H. You, Y. Song, Y. Huang, M. Yang, H. Zhang, *Inorg. Chem.* **49 (**2010) 7721.
31. S.Peng, C. Wang, J. Xie, S. Sun, *J. Am. Chem. Soc.* **128** (2006) 10676.
32. S. Peng, S. Sun, *Angew. Chem., Int. Ed.* **46** (2007) 4155.
33. A. Cabot, V. F. Puntes, E. Shevchenko, Y. Yin, L. Balcells, M. A. Marcus, S. M. Hughes, A. P. Alivisatos, *J. Am. Chem. Soc.* **129**(2007) 10358.
34. R. K. Chiang, R. T. Chiang*, Inorg. Chem.* **46** (2007) 369.
35. I. S. Lee, N. Lee, J. Park, B. H. Kim, Y. W. Yi, T. Kim, T. K. Kim, I. H. Lee, S. R. Paik, T. Hyeon, *J. Am. Chem. Soc.* **128** (2006) 10658.
36. Y. Bao, A. B. Pakhomov, K. M. Krishnan, *J. Appl. Phys.* **97**(2005) 10J317.
37. K. S. W. Sing, D. H. Everett, R. A. W. Haul, L. Moscou, R. A. Pierotti, J. Rouquerol, T. Siemieniewska, *Pure & Appl. Chem*. **57** (1985) 603.
38. E. P. Barrett, L. G. Joyner, P. P. Halenda, *J. Am. Chem. Soc.* **73** (1951) 373.
39. M. Sevilla, A. B. Fuertes, *Carbon* **47** (2009) 2281.
40. N. Baccile, G. Laurent, F. Babonneau, F. Fayon, M. Titirici, M. Antonietti, *J. Phys. Chem. C* **113** (2009) 9644.
41. W. H. Suh, A. Jang, Y. Suh,K. S. Suslick, *Adv. Mater.* **18** (2006) 1832.
42. H. Qian, G. Lin, Y. Zhang, P. Gunawan, R. Xu, *Nanotechnology* **18** (2007) 355602.

# Chapter 6

## Use of glucose derived-carbonaceous spheres as templates for the fabrication of metal oxide hollow spheres

A series of hollow crystalline metal oxides spheres ($Cr_2O_3$, $Co_3O_4$, α-$Fe_2O_3$, NiO and ZnO) have been fabricated by hydrothermal route using glucose derived-carbonaceous spheres as sacrificial template and metal chlorides as metal oxide precursors. Heating of an aqueous solution of the metal chlorides and glucose at 180 $^{o}$C in an autoclave affords - as indicated by transmission electron microscopy (TEM) - a nanospherical composite consisting of a metal precursor shell sheathing a carbonaceous core. Hollow crystalline oxides spheres were obtained by removal of the carbonaceous cores through calcination in air. Correlations between the particle size and the various synthesis conditions such as glucose concentration, the concentration ratio [c(glucose)/c(metal chloride)], temperature, reaction time and the addition of acetic acid as a catalyst are uncovered. The as-obtained hollow metal oxides spheres were characterized by scanning electron microscopy (SEM), transmission electron microscopy (TEM), x-ray powder diffraction (XRD), infrared spectroscopy (IR), and nitrogen adsorption/desorption isotherms (BET).

## 6.1 Introduction

In both academic and technological studies, hollow materials are attracting great attention. Hollow micro- and nanocapsules with diverse shell compositions present a class of special materials that brings a series of new opportunities in the development of novel microreactors, catalysis, and optical or electrochemical architectures.[1-5]

In previous chapter, we have demonstrated the fabrication of some crystalline metal oxides hollow spheres *via* facile one pot hydrothermal strategy by applying fructose-derived carbonaceous spheres as sacrificial templates *for the first time to the best of our knowledge*. We further demonstrated that the size and the shape of the as-obtained hollow oxides can be varied by the variation of the synthesis conditions.

In this chapter, we report the use of a facile route, one pot hydrothermal hydrolysis, to fabricate porous hollow or ball in ball crystalline metal oxides (Fig.6.1). In addition, we have investigated the correlations between the particle size and the various synthesis conditions such as glucose concentration, the concentration ratio [c(glucose)/c(metal chloride)], temperature, reaction time and the addition of catalyst.

Our interest in this synthesis route and using monosaccharides as sacrificial templates for fabrication of the hollow crystalline metal oxides stems from the fact that the surface of the monosaccharide-derived carbonaceous material is rich of functionalities which facilitate the precipitation of the precursors of the desired oxide onto their surface layers without any further surface modifications. The former mentioned fact is definitely the key to success in fabrication the hollow particles.

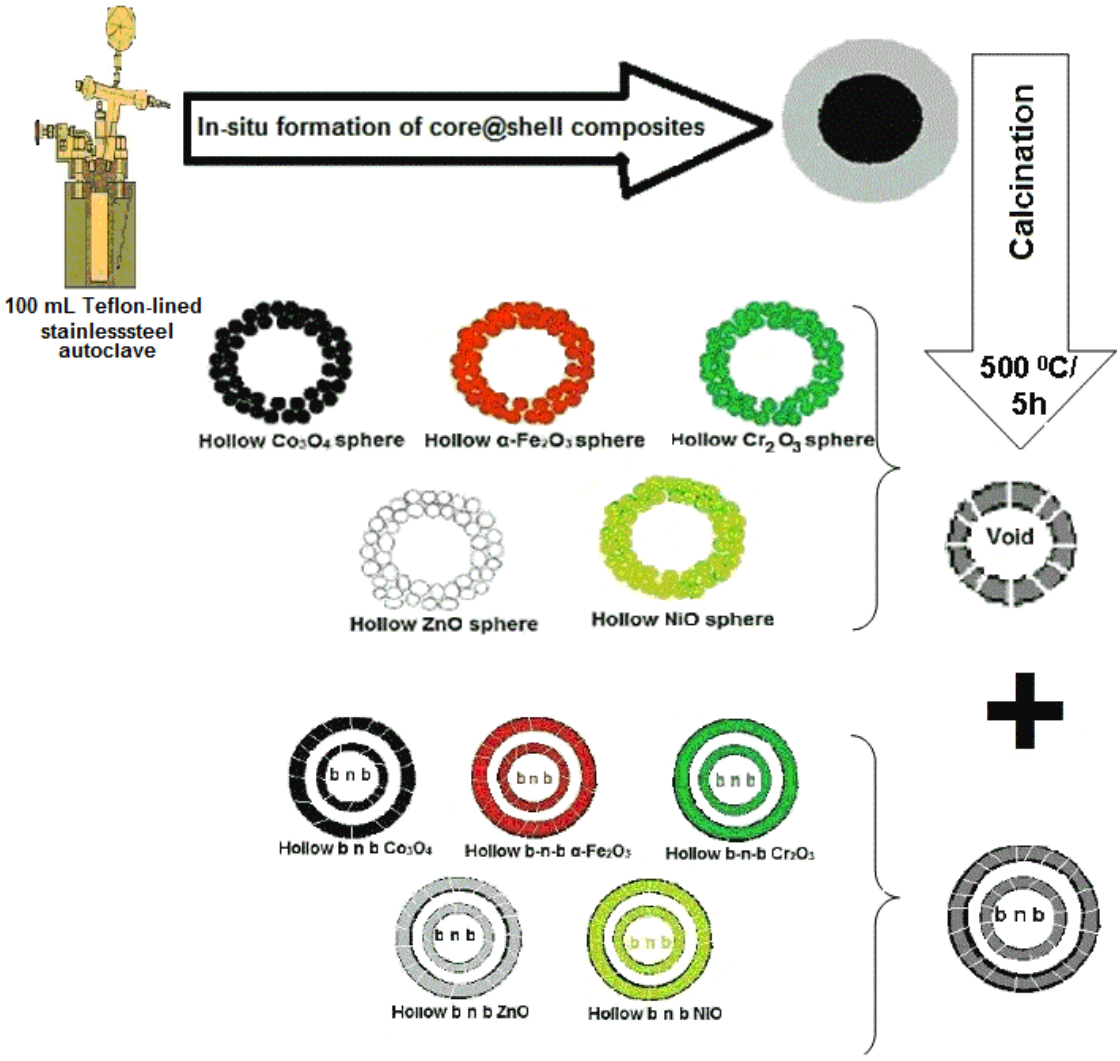


**Fig.6.1** *Schematic illustration (cross-sectional view) of the formation of the hollow metal oxide spheres. The thermal removal of carbonaceous cores results in the formation of hollow spheres plus the formation of ball in ball (bnb) hollow spheres as minor product*

Fig.6.1 presents the schematic flowchart that illustrates the major process steps applied in the present work. Firstly, heating the metal chloride with glucose in closed system results in in-situ formation of hybrid particle due to the adsorption of the metal ions on the surface layers of the glucose-derived carbonaceous spheres. Finally, calcination of the hybrid spheres lead to the formation of hollow metal oxide spheres in addition to ball in ball (bnb) particles as minor product.

For the formation of the hollow metal oxides spheres, glucose is applied as a sacrificial template, while metal chlorides [chromium(III) chloride hexahydrate ($CrCl_3.6H_2O$), iron(III) chloride hexahydrate ($FeCl_3.6H_2O$), cobalt(II) chloride hexahydrate ($CoCl_2.6H_2O$), nickel(II) chloride ($NiCl_2$), and zinc(II) chloride ($ZnCl_2$), are the precursors for the desired $Cr_2O_3$, α-$Fe_2O_3$, $Co_3O_4$, NiO and ZnO, respectively. In a typical synthesis experiment, 1902 mg of glucose was dissolved in 100 mL distilled water (C10) **[a]**. The water soluble metal chloride during the hydrothermal carbonization was added to satisfy the glucose: metal chloride molar ratio 10:1.**[b]** The mixture was heated in a 100 mL Teflon-lined stainless steel autoclave at 180 $^oC$ for 24 h. after synthesis, the metal oxide-carbon composites were calcined in air at 500 $^oC$( heating rate 2 $^oC$/min, for 5 h) to remove the carbon core, leading to hollow metal oxide particles.

## 6.2 Characterization of the as-prepared hollow crystalline metal oxides spheres

The as-obtained hollow metal oxides and their corresponding composites were characterized by X-ray diffraction (XRD) to investigate the changes of phase structure and crystallite size of the as-prepared hollow oxides before and after calcination and infrared spectroscopy (IR) to compare between the products before and after thermal treatment. The morphology and the hollow nature of the products were characterized by scanning electron microscopy (SEM) as well as

a) C10 (96 $mmolL^{-1}$) is $1/10_{th}$ of the initial glucose concentration applied in our study (see chapter 3)
b) See the general synthesis recipe in chapter 2

transmission electron microscopy (TEM). The surface area and the porous structure were characterizes by $N_2$ sorption measurements (BET).

### 6.2.1 X-ray diffraction (XRD)

The as-obtained hollow metal oxides were analyzed by XRD technique following Rietveld refinement procedures using X'Pert software.[6] Fig.6.2 shows the XRD patterns of the hollow metal oxides obtained through the typical experimental procedures after calcination at 500 $^{o}$C for 5h. It shows that, the hollow oxides obtained are well crystalline in a single phase and no other diffraction peaks are found, indicating that the products are pure oxides.

All peaks of sample (a) $Cr_2O_3$ (b) α-$Fe_2O_3$, (c) $Co_3O_4$, (e) NiO, and (f) ZnO are perfectly indexed to (a) rhombohedral $Cr_2O_3$ [ICSD-201102], (b) rhombohedral α-$Fe_2O_3$ [ICSD-81248], (c) cubic $Co_3O_4$ [ICSD-36256], (e) cubic NiO [ICSD-76669], and (f) hexagonal ZnO [ICSD-57478], respectively.

The average crystallite size were calculated from the Scherrer formula [c] (which assumes the small crystallite size to be the cause of line broadening) [7] using the full width at half maximum (FWHM) of the most intense peaks after correcting the instrument broadening. The calculated average crystallite size and comparison between the measured lattice parameters and literature values are shown in Table 6.1. The measured lattice parameters of the hollow oxide spheres are in accord with the literature values.

No crystalline peaks were observed before calcination, as shown in Fig.6.2 which reveals that after hydrothermal treatment the metal ions are evenly dissolved in the hydrophilic shell of the carbonaceous spheres or dispersed in the shell as amorphous cluster.

c) See chapter 2 (experimental section)

**Table6.1** *Crystallite size calculated by Scherrer equation for the as-obtained hollow oxides and comparison between the measured lattice parameters and literature values*

| Oxide sample | Crystallite size (nm) | Lattice parameters | |
|---|---|---|---|
| | | measured [Å] | reference values [Å] |
| $Cr_2O_3$ | 21 | a/ b: 5.0357(2)<br>c: 13.755(1) | 4.9507(4) [8]<br>13.5656(7) |
| α-$Fe_2O_3$ | 23 | a/ b : 5.0313(4)<br>c: 13.752(1) | 5.0355(5) [9]<br>13.7471(7) |
| $Co_3O_4$ | 12 | a: 8.080(1) | 8.072(3) [10] |
| NiO | 11 | a: 4.1693(2) | 4.1944 [11] |
| ZnO | 18 | a/ b: 3.2461(6)<br>c: 5.1994(9) | 3.2533(5) [12]<br>5.2072(13) |

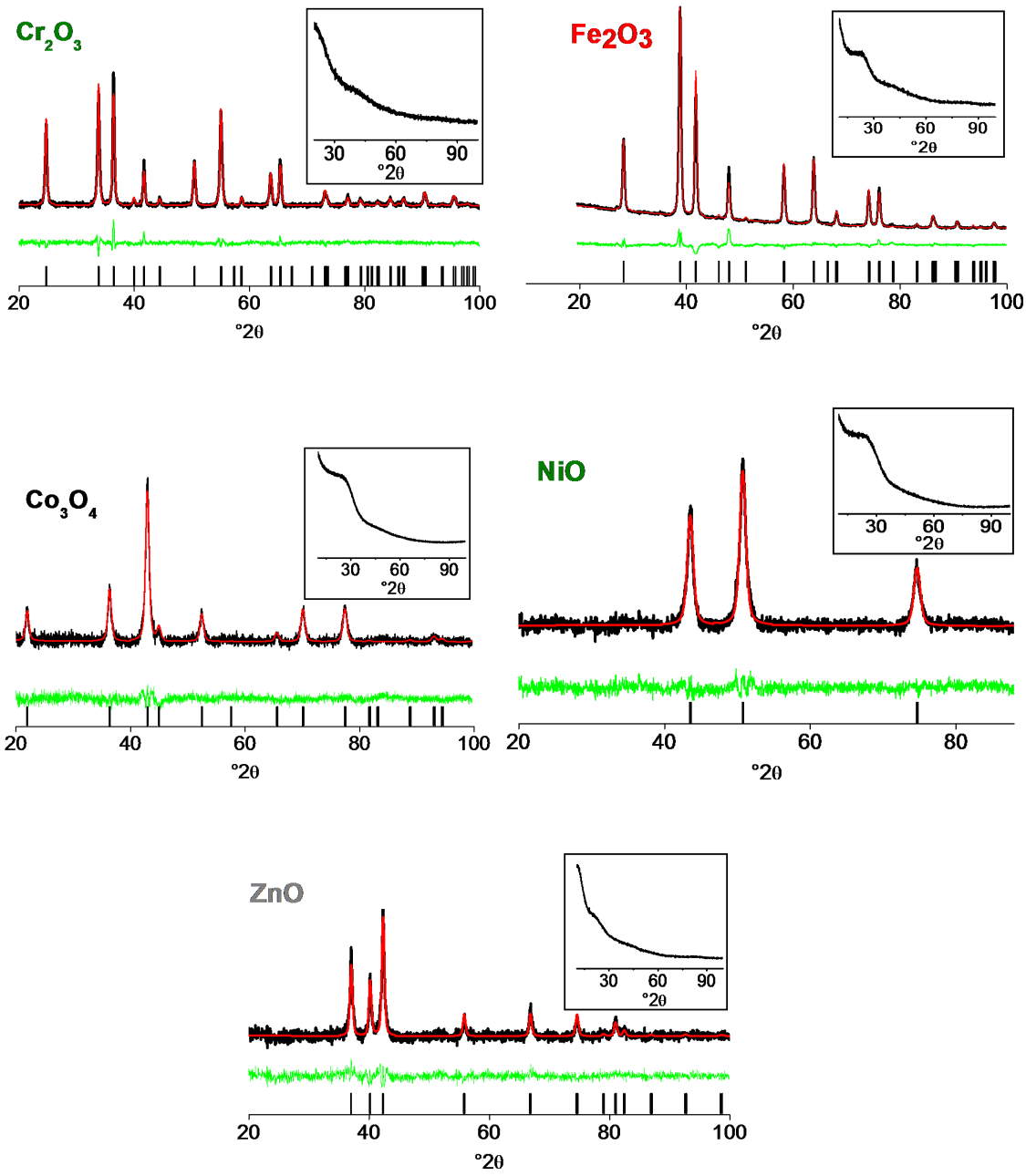


**Fig.6.2.** *XRD patterns of the as-obtained oxides with Rietveld refinement (the black line is the observed pattern ,the red line is the calculated from the literatures and the green line represents the difference plot). The insets show the XRD patterns of the samples before calcination.*

### 6.2.2 IR spectra

The comparison between IR spectrum before and after thermal treatment at 500 $^{o}$C for 5 h, demonstrated the removal of the carbonaceous template materials and the formation of the hollow oxides under investigation as shown in Fig.6.3. In all samples, The IR spectrum before calcination shows a broad peak at 3400 $cm^{-1}$, which likely to be the stretching vibration of O-H and the peak at ~ 2900 is belong to the stretching vibration of C-H bond. The vibrations at 1701 $cm^{-1}$ and 1630 $cm^{-1}$ can be assigned to C=O and C=C, respectively. The C=C double bonds indicate that dehydration has taken place during the hydrothermal carbonization of glucose.[13-14]

After calcination, the carbonaceous templates and most peaks related to the functionalities, like carboxylic or aromatic groups disappeared and the observed peaks are typically related to M-O bond stretching vibrations as shown in Table 6.2.

In Fig.6.3.a, d and c which illustrates the IR spectra of hollow $Cr_2O_3$, , NiO and ZnO, respectively, a peak at ~ 3400 $cm^{-1}$ is likely to be O-H stretching vibration of surface M-OH groups and the absorption at ~1630 $cm^{-1}$ is due to the stretching and bending modes of surface-adsorbed/trapped (hydrogen-bonded) water molecules.

**Table 6.2** *The correlation between the characteristic peaks of the IR spectrum of samples after calcination and vibrations of functional groups*

| Fig. | Oxide sample | $\tilde{\nu}$ / $cm^{-1}$ | Vibration |
|---|---|---|---|
| 6.4.a | $Cr_2O_3$ | 621 and 560 | stretching vibration of Cr-O bond [15] |
| 6.4.b | α-$Fe_2O_3$ | 570 and 480 | Fe-O vibration mode of α-$Fe_2O_3$ [16] |
| 6.4.c | $Co_3O_4$ | 660 and 560 | stretching vibrations of Co-O bond [17] |
| 6.4.d | NiO | 519 and 459 | stretching vibration of Ni-O [18] |
| 6.4.e | ZnO | 480 | Zn-O stretching band [19] |

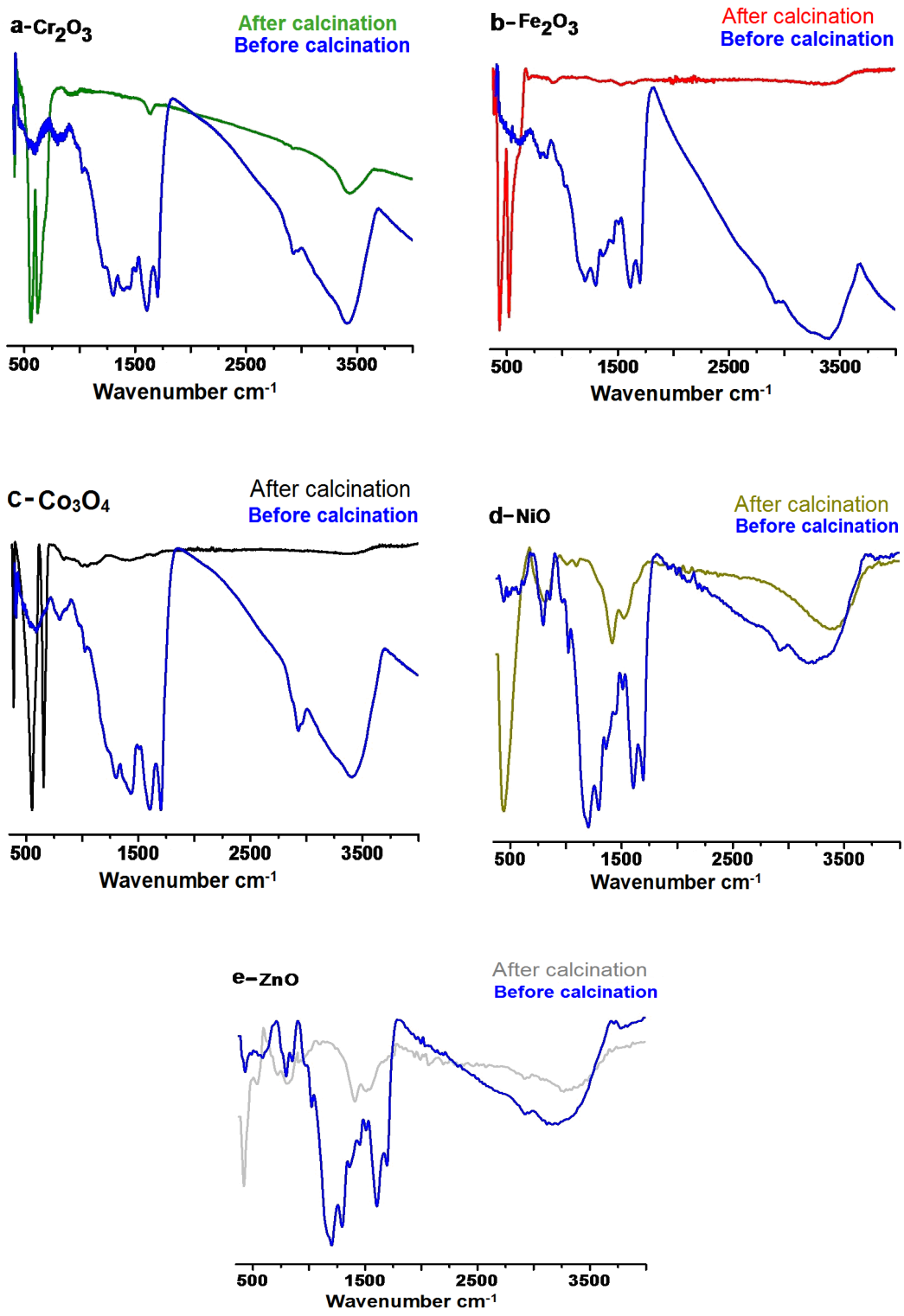


**Fig.6.3** *IR spectra of the hollow oxide, prepared according to the typical synthesis procedures, before and after calcination at 500 °C a) $Cr_2O_3$, b) α-$Fe_2O_3$, c) $Co_3O_4$, d) NiO, e) ZnO*

### 6.2.3 Morphology and hollow structure

In this section we show the results of scanning electron microscope (SEM) and transmission electro microscope (TEM) analysis of the morphology of the hollow particles and their core@shell composites before calcinations, as well as their surface properties. Its note worthy to mention, that all samples presented in this section have been fabricated via the typical experimental procedures.

Fig.6.4 shows TEM micrographs of the products before calcination. They depict the hybrid particles between the metal ions precursor and the carbonaceous template of a) $Cr_2O_3$, b) α-$Fe_2O_3$ and c) ZnO samples. We can see that a contrast appears in the images between the shell material and the core material. We assume that the shell is the metal oxide precursor sheathing the carbonaceous template core.

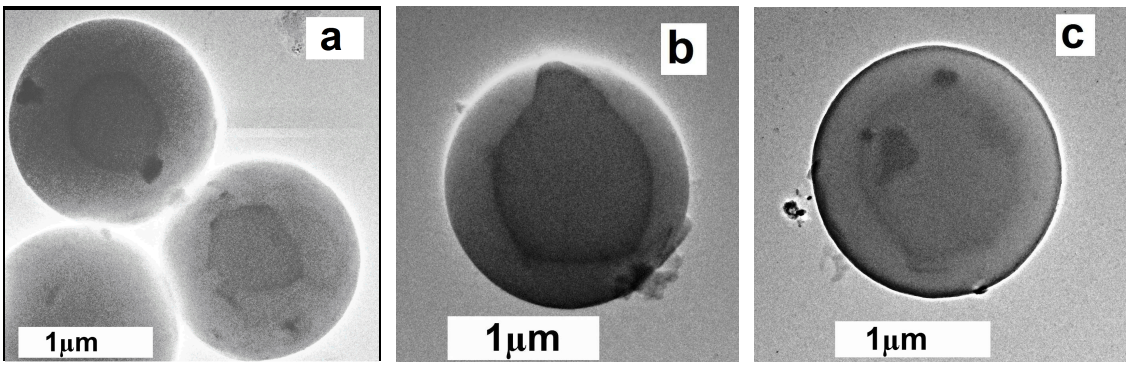


**Fig.6.4** *TEM images of the core@shell (carbonaceous spheres@metal ions) composites before calcination of a) $Cr_2O_3$, b) α-$Fe_2O_3$ and c) ZnO samples*

SEM micrographs in Fig.6.5 and in Fig.6.6 display the hollow metal oxides before and after calcination, respectively. SEM micrographs of the products shown in Fig.6.6 give indication of the formation the hollow metal oxides; also reveal the spherical structures of the hollow particles. A careful observation of the surface of the hollow spheres shows that the hollow metal oxides spheres walls are composed of many small nanoparticles of the corresponding metal oxide. From the broken shell, marked with a red arrow, we can notice the hollow porous nature of the hollow metal oxides spheres.

Another observation can be noticed from Fig.6.5 and in Fig.6.6 that after calcination the spheres remained intact and preserved the three dimensional spherical shape of particles after removing of the carbonaceous core material. In addition, about 60-80% shrinkage in size occurred after calcination as can be noticed from Fig.6.9 (the particle size distribution of the hollow metal oxides and their corresponding composites). This can be due to during the thermal treatment the metal ions incorporated in the surface layer of the template are densified and cross-linked to form oxide hollow spheres replicas of the carbonaceous spheres template with reduced size.

TEM images shown in Fig.6.7 are further confirming the hollow interior clearly. We can observe a variation in the contrast between the dark shell and the pale core. The wall thickness of the porous hollow metal spheres can be estimated according to the cross sectional view obtained by TEM images as approximately 80 nm, 40 nm, 20 nm, 30 nm, and 18 nm for $Cr_2O_3$, α-$Fe_2O_3$, $Co_3O_4$, NiO and ZnO hollow spheres, respectively.

SEM and TEM micrographs (Figures 6.5, 6.6 and 6.7) reveal the formation of uniform hollow metal oxide spheres. In addition, it is noticed that, part of the product in all hollow oxides samples was ball in ball (bnb) hollow structure as shown in Fig.6.7. Further confirmation for the formation of bnb hollow spheres is shown in SEM micrographs Fig.6.8.

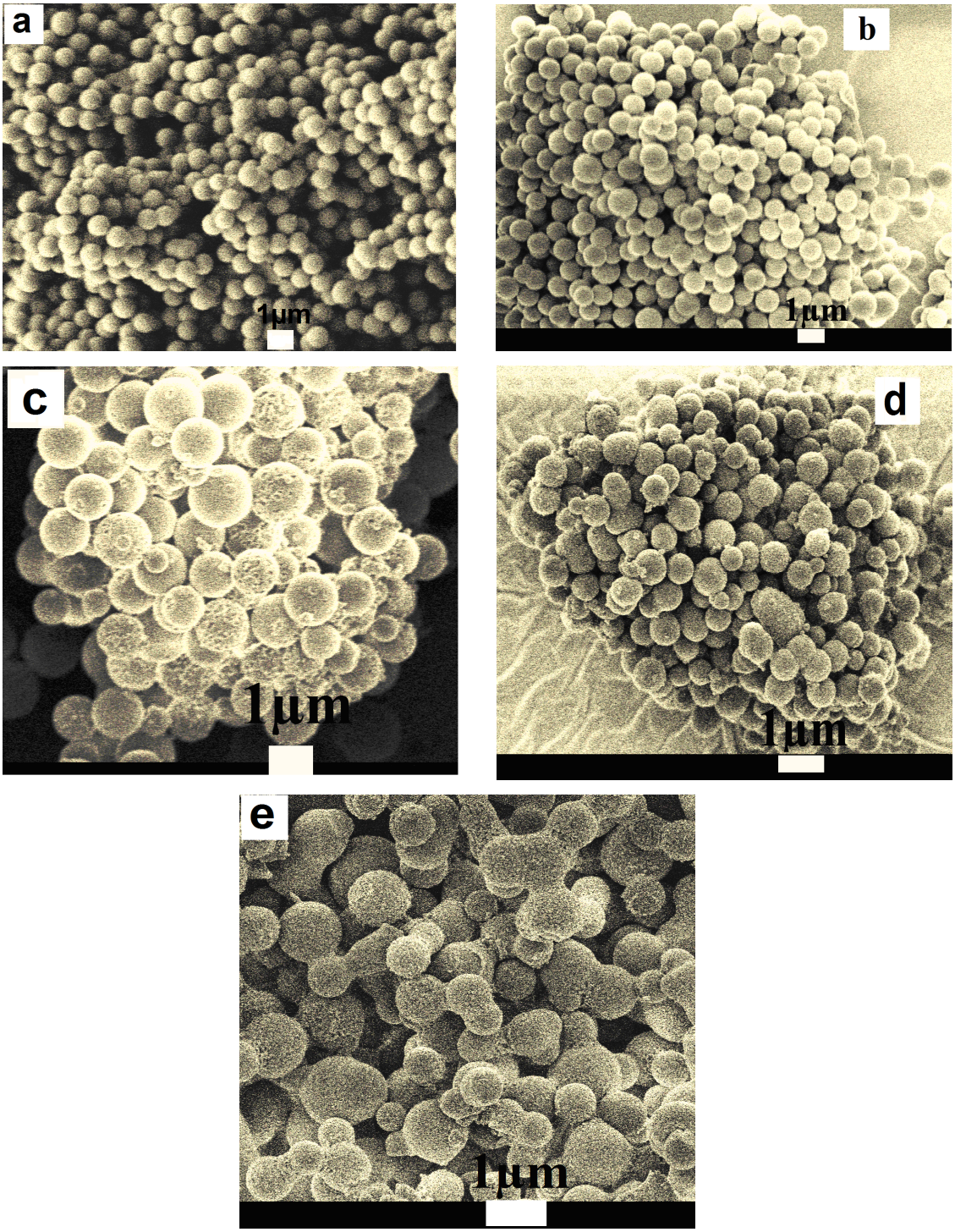


**Fig.6.5** *SEM micrographs of the composite materials, prepared according to the typical synthesis experiment procedures, before calcination at 500 $^{o}$C a) $Cr_2O_3$, b) α-$Fe_2O_3$, c) $Co_3O_4$, d) NiO, e) ZnO samples*

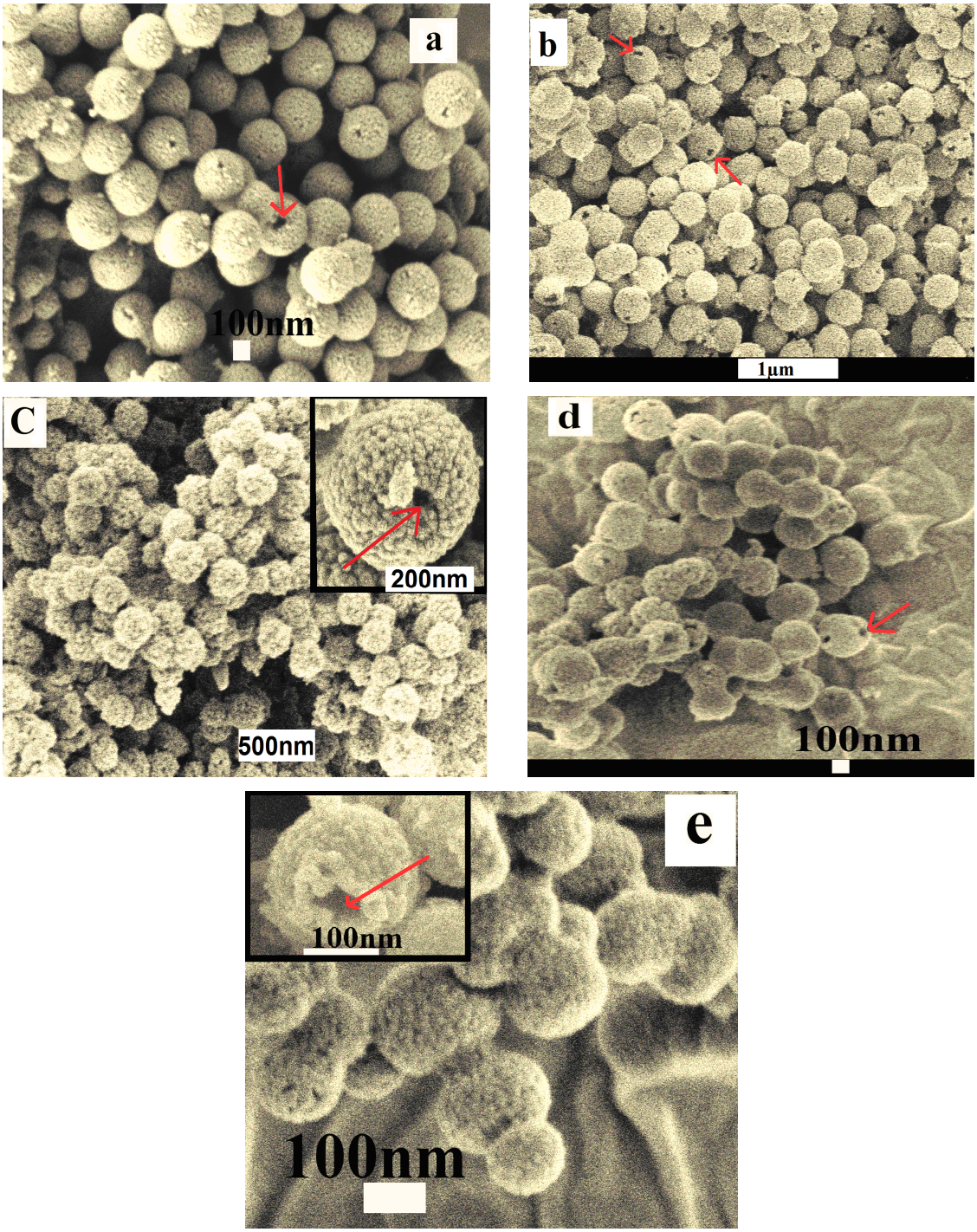


**Fig.6.6** *SEM micrographs of porous hollow metal oxide prepared according to the typical synthesis experiment procedures, after calcination at 500 °C a) $Cr_2O_3$, b) α-$Fe_2O_3$, c) $Co_3O_4$, d) NiO, e) ZnO hollow samples. The red arrows refer to broken shells*

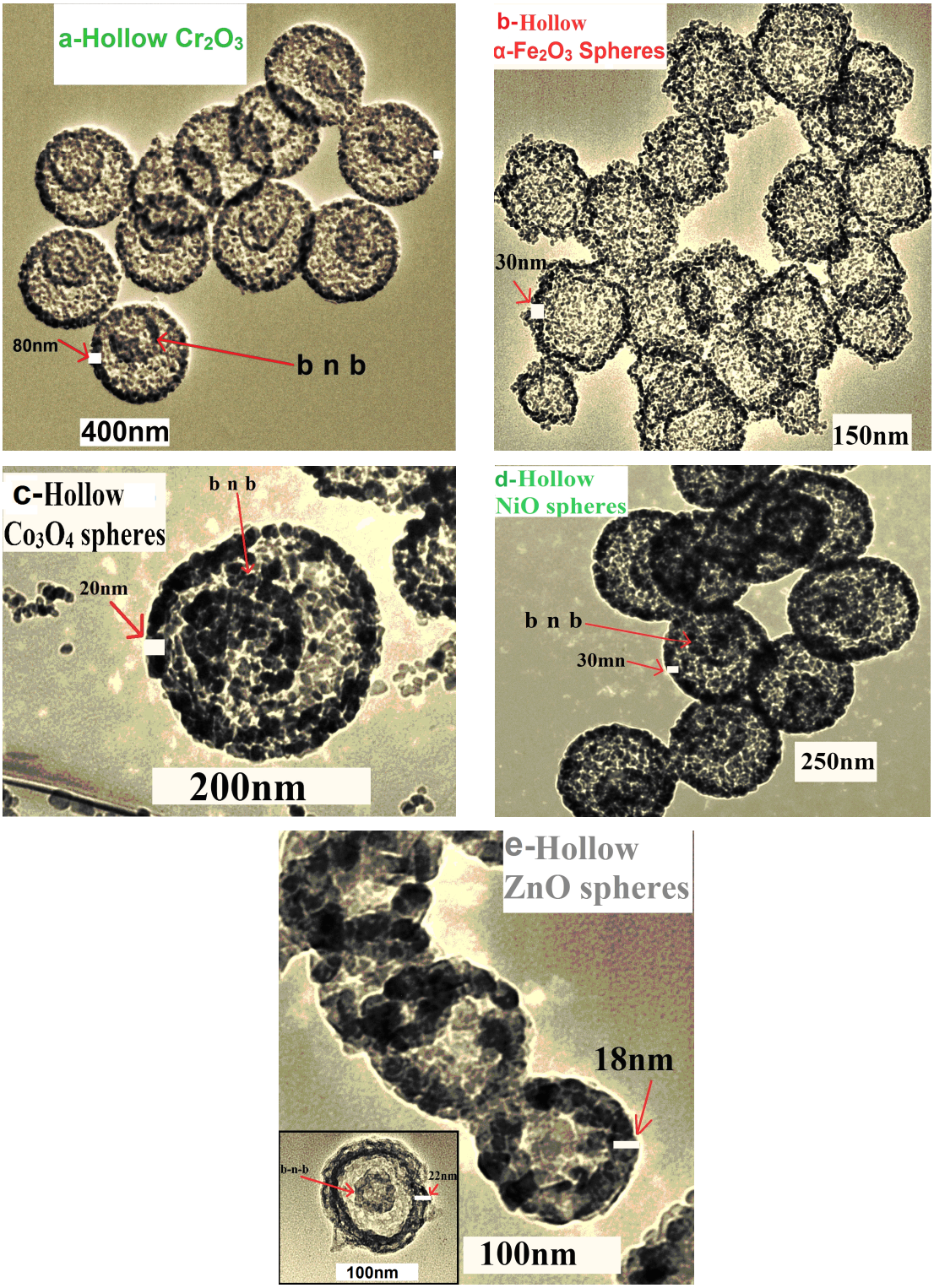


**Fig.6.7** *TEM micrographs of porous hollow metal oxide prepared according to the typical synthesis procedures, after calcination at 500 °C a) $Cr_2O_3$, b) α-$Fe_2O_3$, c) $Co_3O_4$, d) NiO, e) ZnO hollow samples*

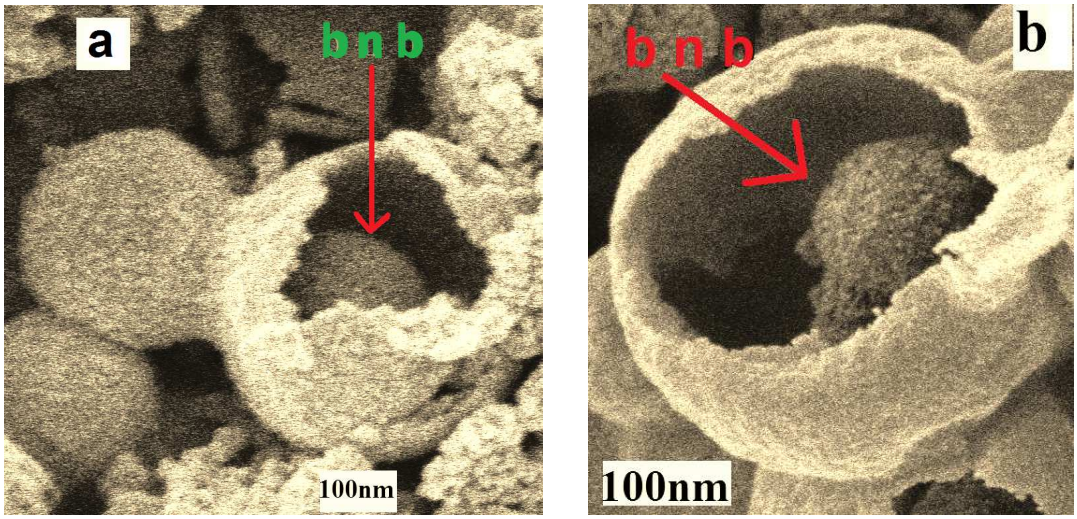


**Fig.6.8** *SEM micrographs of porous bnb hollow spheres of a) $Cr_2O_3$ and b) α-$Fe_2O_3$ hollow samples as can be seen through the broken shell spheres*

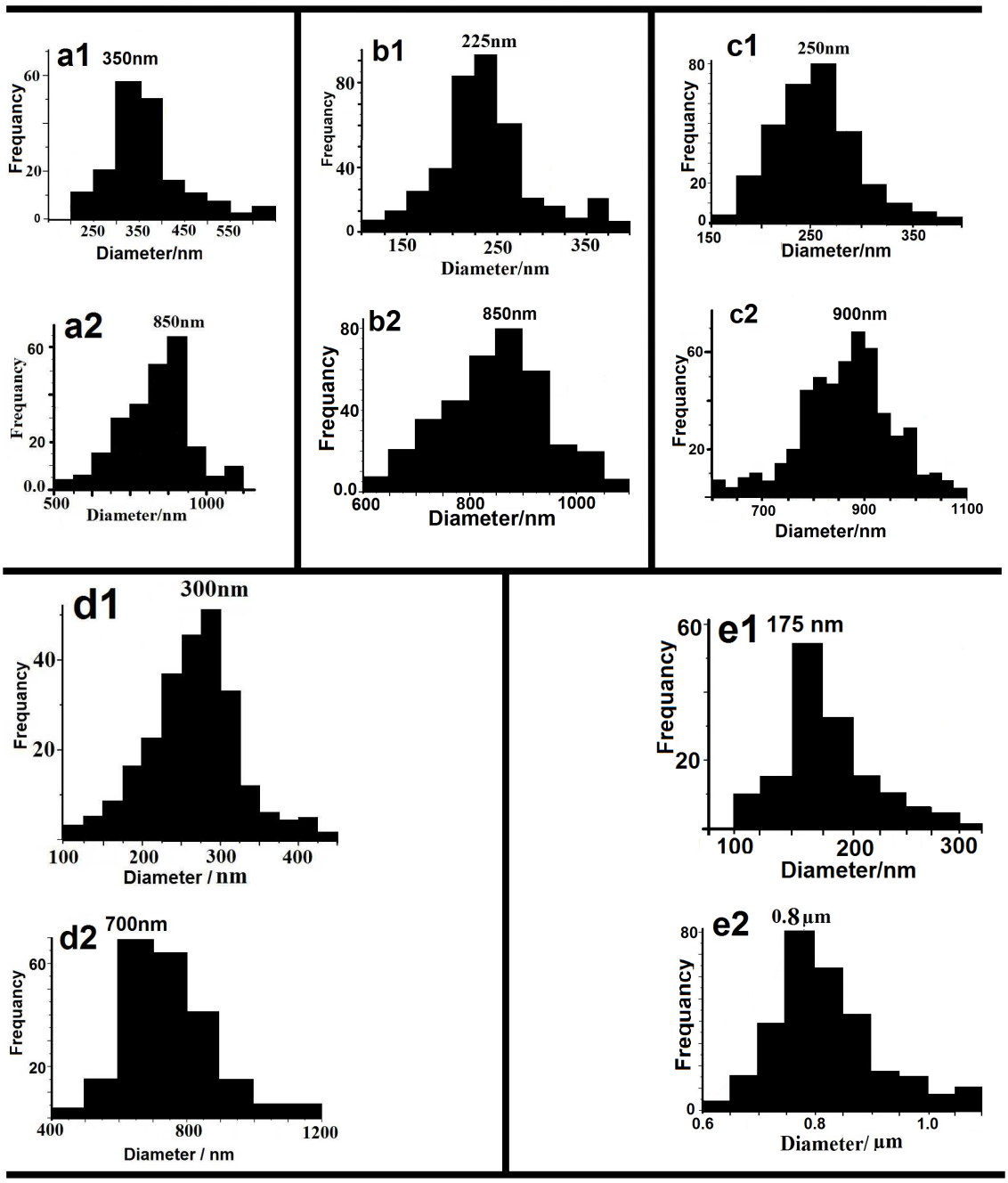


**Fig.6.9** *Particle size distribution (PSD) of :-*

*a1) hollow $Cr_2O_3$ , and a2) its corresponding composite,*

*b1) hollow α-$Fe_2O_3$ , and d2) its corresponding composite,*

*c1) hollow $Co_3O_4$ , and c2) its corresponding composite,*

*d1) hollow NiO , and d2) its corresponding composite, and*

*e1) hollow ZnO , and e2) its corresponding composite*

Fig.6.10 shows the high resolution TEM micrographs of $Cr_2O_3$, $Co_3O_4$, and ZnO porous hollow spheres. The size of small nano-particles (NPs) composing the wall of the hollow spheres are in good agreement with the size calculated by Sherrer equation for the as-obtained hollow $Cr_2O_3$, $Co_3O_4$, and ZnO, respectively.

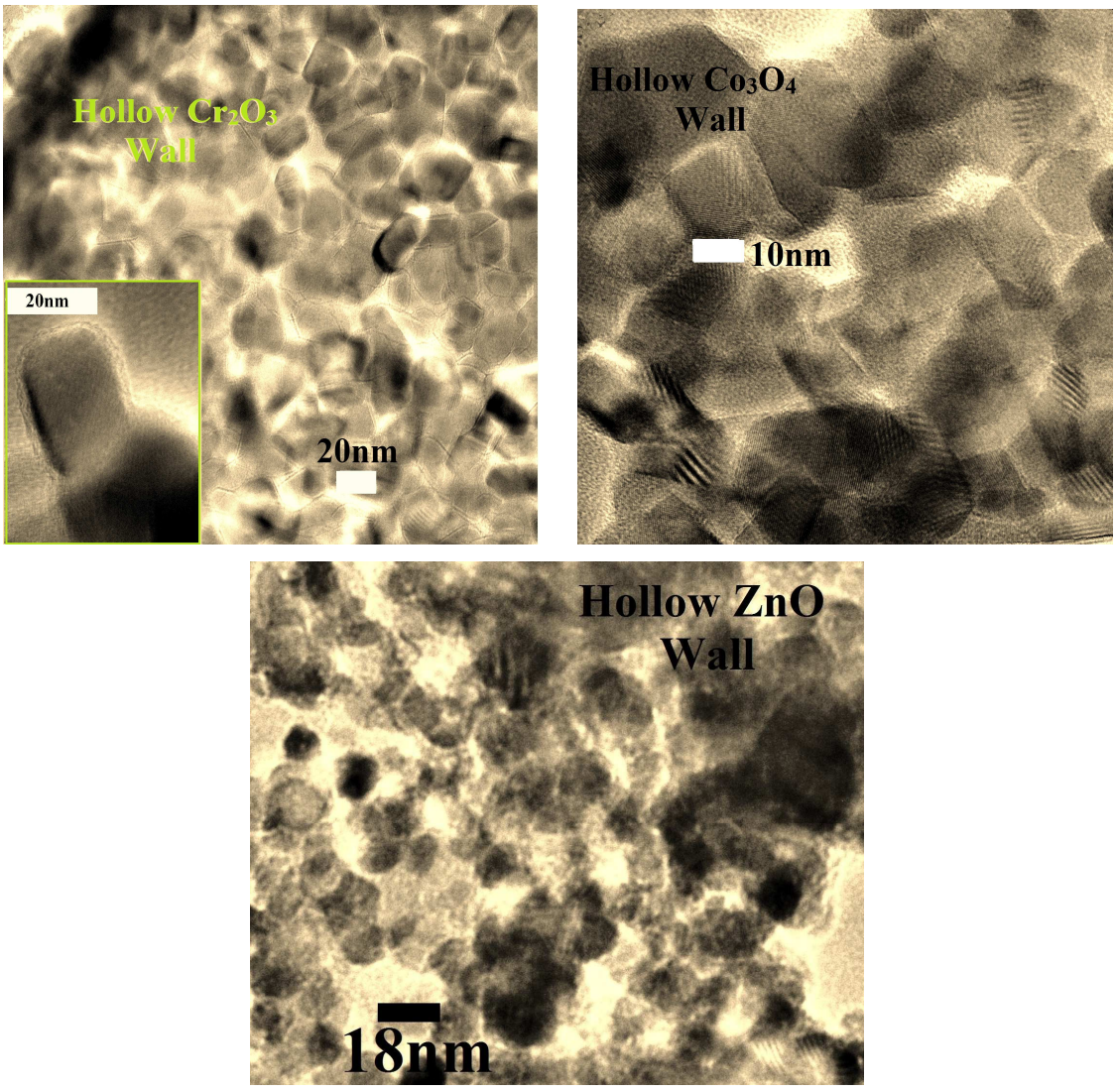


**Fig.6.10** *High resolution TEM micrographs of the wall of $Cr_2O_3$, $Co_3O_4$, and ZnO porous hollow spheres*

### 6.2.4 Surface area and porous structure (BET measurements)

The nitrogen adsorption/desorption isotherms were applied to study the porosity and specific surface area of the as-synthesized hollow metal oxides spheres as shown in Fig.6.11. These are typical type IV isotherms characteristic of mesoporous materials according to the International Union of Pure and Applied Chemistry (IUPAC).[20,21] Hysteresis loops can be observed in the curves of all samples, evidencing the existence of mesoporous structures.

The surface area of the hollow oxides samples are listed in Table 6.3. The specific surface areas of these hollow metal oxides is assigned to the combination of the surface area of the outer surface, the inner pores and the mesopores which form altogether the whole surface area of the particles. These large surface areas show that this kind of material has many potential applications in many fields.

**Table 6.3** *Surface area of the hollow metal oxide spheres*

| Oxide sample | $A_{BET}$ ($m^2g^{-1}$) |
|---|---|
| $Cr_2O_3$ | 77 |
| α-$Fe_2O_3$ | 54 |
| $Co_3O_4$ | 35 |
| NiO | 33 |
| ZnO | 65 |

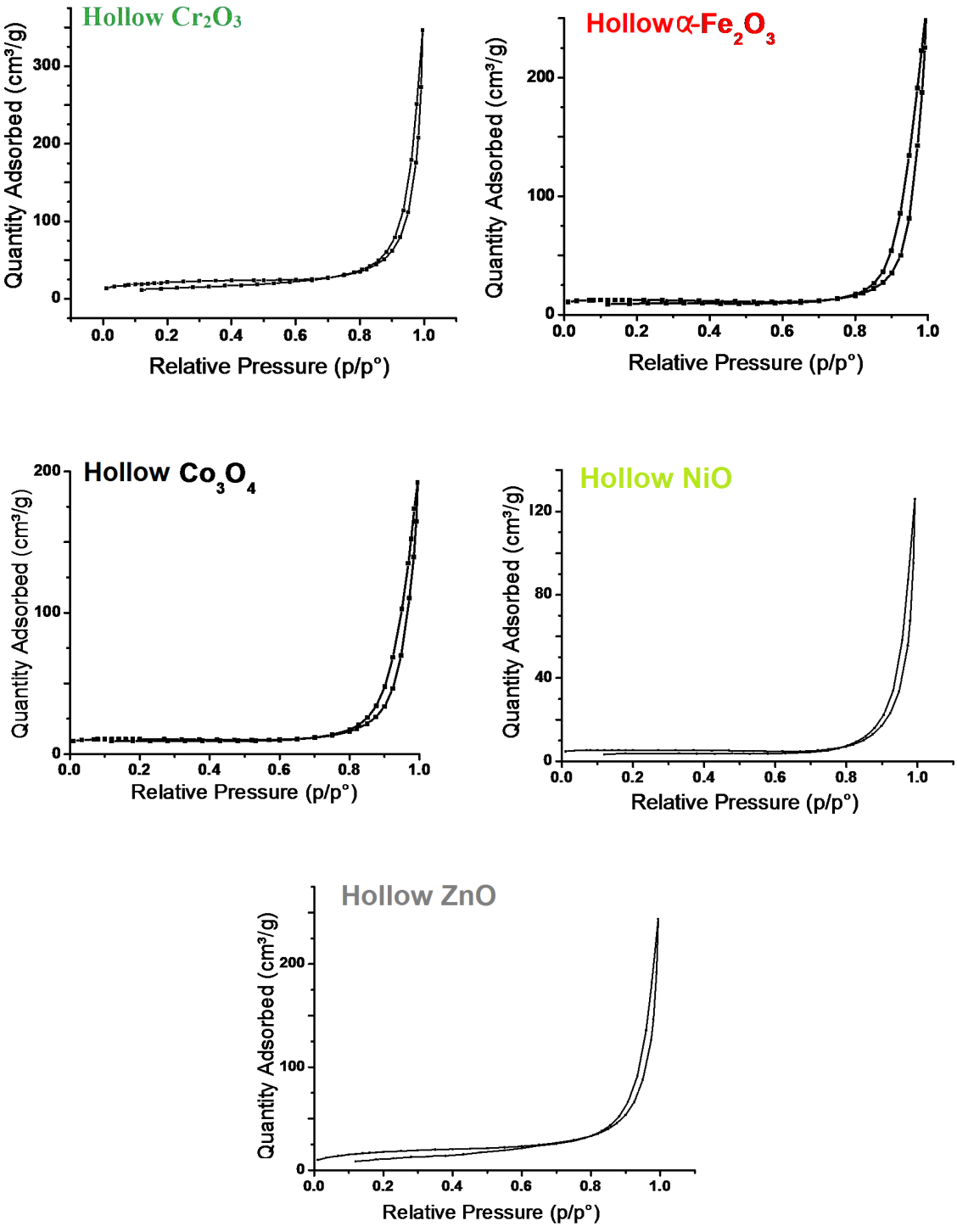


**Fig.6.11** *Nitrogen sorption isotherms of the hollow oxides*

## 6.3 Proposal of a mechanism for the formation of hollow oxide spheres

The proposal of the mechanism of the formation of hollow oxides spheres by using glucose-derived carbonaceous spheres as sacrificial templates is nearly similar to that been proposed when applying fructose-derived carbonaceous spheres as sacrificial templates (see chapter 5). The only differences are in the time and temperature in the synthesis procedures.

The formation of hollow oxides spheres through one-pot hydrothermal hydrolysis involves adsorption of the metal ions dispersed in the solution mixture into the hydrophilic surface layers of the glucose-derived carbonaceous spheres which are rich in oxygen functionalities such as -OH and C=O .[22-23] This results in the in-situ formation of core@shell composite (glucose-derived carbonaceous spheres@metal ions); these are finally densified and cross linked in a subsequent thermal treatment and oxidation step to form free standing porous hollow metal oxide spheres after the removal of the carbonaceous core materials. The as-obtained hollow metal oxide spheres replicas of the carbonaceous core spheres but with size about 60-80% less than the original corresponding composite size.

This significant shrinkage in size during the thermal treatment indicates that the metal cations adsorbed loosely on the carbonaceous spheres (CSs) have oxidised and transformed into dense oxides network that compose the shells of the hollow spheres. The final hollow spheres products include ball in ball (bnb) hollow structure in all oxide samples as minor product without any extra step.

The formation mechanism of the bnb structure is not fully comprehended at this stage. However, it was suggested that some nano-islands of metal oxide in the shell may migrate to or be stuck on the surface of the shrinking CSs cores during calcination process. Further heating at elevated temperature, these nano-

islands finally aggregate into a small ball in the interior when the CSs cores are completely burnt off.[24-25] Fig.6.12 presents schematic illustration for the proposed mechanism of the formation of the porous metal oxides hollow spheres.

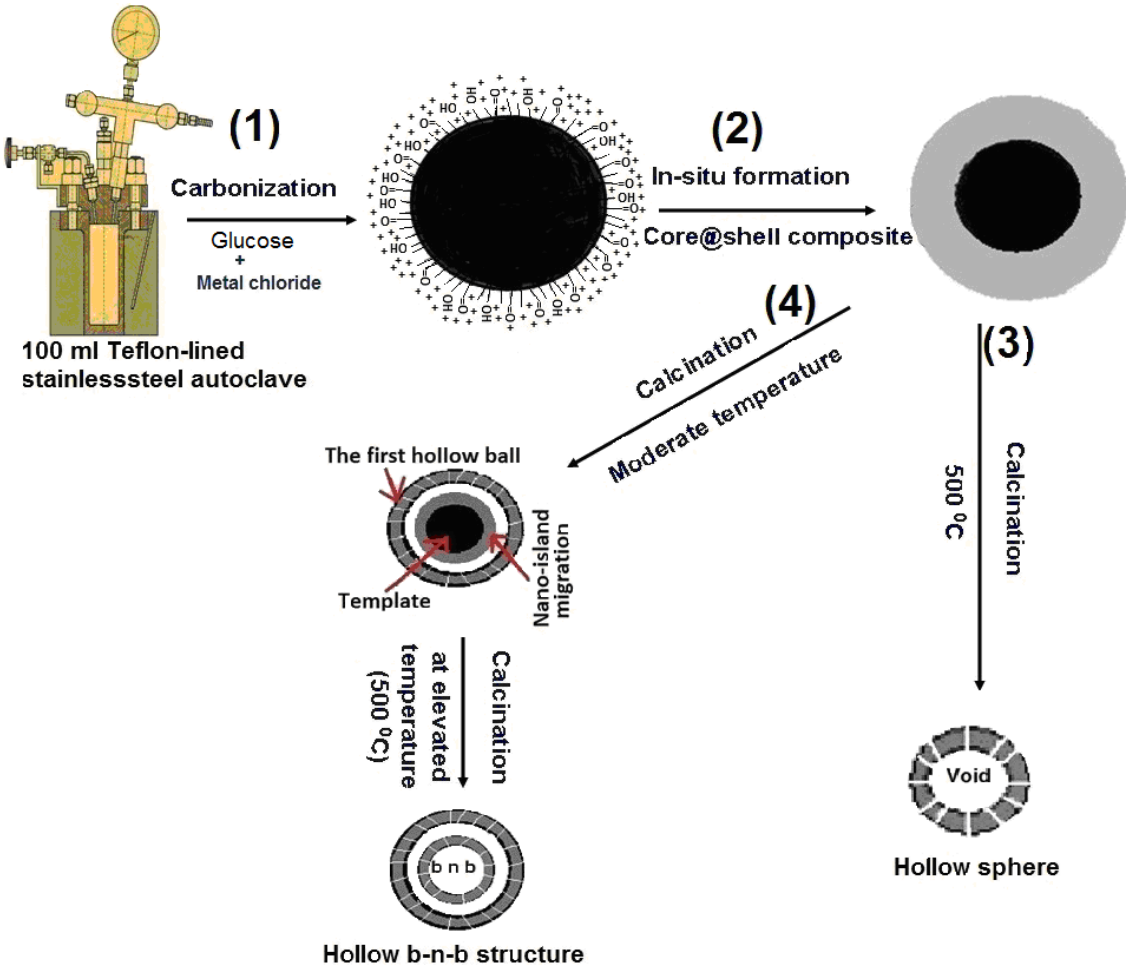


**Fig.6.12** *Schematic diagram of the fabrication of porous hollow metal oxides spheres via hydrothermal method*

## 6.4 The impact of the synthesis parameters

In last sections, glucose were used successfully as templates for many kind of oxides hollow spheres. The glucose-derived carbonaceous spheres used as templates have integral and uniform surface functional layer, which makes the modification of the surface unnecessary and ensures homogeneity of shell.

Temperature (T), reaction time (t), concentration of glucose, the concentration ratio c(glucose)/c(metal chloride), and adding acetic acid as catalyst are five significant conditions that involved in the hydrothermal synthesis method of the hollow metal oxide spheres. To study the impact of each synthesis parameter many experimental conditions were systematically varied in which the parameter under investigation was varied while the other parameters remained unchanged according to the typical synthesis procedures.

The results show that each parameter of the previously mentioned parameters have similar impact on the different types of oxides. The influence similarity of each parameter on the formation of the hollow oxide spheres reported here might open the door for general understanding of the formation of the hollow metal oxides spheres with variable size.

The typical temperature (T) for the formation of the hollow oxides using glucose as sacrificial templates was 180 $^{o}$C. When decreasing *T* to 170 $^{o}$C or raising it to 200 $^{o}$C, no significant precipitates were seen at the former and no hollow spheres were formed at the later temperature in all oxides under investigation.

The typical time (t) for the formation of metal oxide hollow spheres was 24 h. In case of increasing time to 36 h no hollow materials were observed except for $Cr_2O_3$ which formed fused hollow particles. While decreasing *t* to 12 h,

the only observed hollow spheres were those for $Cr_2O_3$ with average size ~210 nm (Fig.6.13).

Increasing glucose concentration from 96 $mmolL^{-1}$ (the typical glucose concentration) to 240 $mmolL^{-1}$ resulted in the formation of fused hollow particles for the oxides under investigation as seen in Fig.6.14. On the other hand, decreasing glucose concentration to 64 $mmolL^{-1}$, as illustrated in Fig.6.15, resulted in small hollow spheres dispersed in nanoparticles of the metal oxide in case of $Cr_2O_3$, α-$Fe_2O_3$, and $Co_3O_4$.

Fig.6.16 illustrates the impact of adding 0.5 mL of acetic acid to the reaction mixture solution. It is obvious that acetic acid catalyzes the reaction and increases the rate of the hydrothermal reaction and as a result the average size of the metal hollow oxides spheres increased about 40-50%.

When the concentration ratio c(glucose)/c(metal chloride) increased from 10:1 to 20:1, we can anticipate that the amount of metal oxide forming the shell of hollow spheres will be decreased. Fig.6.17 shows TEM micrographs for as-obtained hollow $Cr_2O_3$ samples through applying concentration ratio a) 10: 1 b) 20:1. We can notice that the wall thickness of the hollow spheres is inversely proportional to the molar ratio between the reactants. The wall thickness decreased from 80 nm to 33 nm when the concentration ration increased from 10:1 to 20:1. If we know that, the particle size of the $Cr_2O_3$ particles that form the wall of the hollow spheres calculated by Scherrer equation (Table 6.1) equal 21 nm, we can deduce that the wall thickness when the molar ration was 10:1 = 3-4 layers while in case of molar ration 20:1 = 1-2 layers. These findings likely show that the wall thickness is more robust in case of low molar ratio c(glucose)/c(metal chloride). This is due to lower metal concentration leads to light packing of metal oxide nanoparticles and a thin wall, while an increase in the metal ions concentration yields a much denser packing and the formation of a robust thicker shell.[26]

In summary, the size of the hollow spheres is directly proportional to the reaction time and adding of 0.5 mL of acetic acid (acting as a catalyst). While the wall thickness of the hollow spheres is inversely proportional with the increase of molar ratio c(glucose)/c(metal chloride). The shape of the hollow materials is affected by glucose concentration. The typical parameters given by the synthesis protocol procedures reported in this chapter are the optimized conditions for the fabrication of porous hollow metal oxides by using glucose as a sacrificial template. Table 6.4 summarizes the relationship between the synthesis parameters and the size and shape of the as-obtained hollow metal oxides spheres.

**Table 6.4** *Relationship between the synthesis parameters and size and shape of the as-obtained hollow metal oxides spheres*

| Oxide sample | Shape and size | | | | | | |
|---|---|---|---|---|---|---|---|
| | Typical experimental procedures[(d)] [Fig.6.6] | T °C | | t = h [(e)] [Fig.6.13] | | Glucose concentration 240 mmolL$^{-1}$ [(e)] [Fig.6.14] | Catalyst 0.5 mL acetic acid [(e)] [Fig.6.16] |
| | | 170 [(e)] | 200 [(e)] | 12 | 36 | | |
| $Cr_2O_3$ | 350nm hollow spheres | ----- | | 210nm hollow spheres | fused hollow particles | fused hollow particles | 650nm hollow spheres |
| α-$Fe_2O_3$ | 225nm hollow spheres | ----- | | ----- | | fused hollow particles | 550nm hollow spheres |
| $Co_3O_4$ | 250nm hollow spheres | ----- | | ----- | | fused hollow particles | 400nm hollow spheres |
| NiO | 300nm hollow spheres | ----- | | ----- | | fused hollow particles | 600nm hollow spheres |
| ZnO | 175nm hollow spheres | ----- | | ----- | | fused hollow particles | 300nm hollow spheres |

d) In typical experimental procedures, t= 24 h, T= 180 °C, glucose concentration = (96 mmolL$^{1-}$, molar ratio =10, and no catalyst applied.
e) Only this parameter was changed while the other parameters remained constant

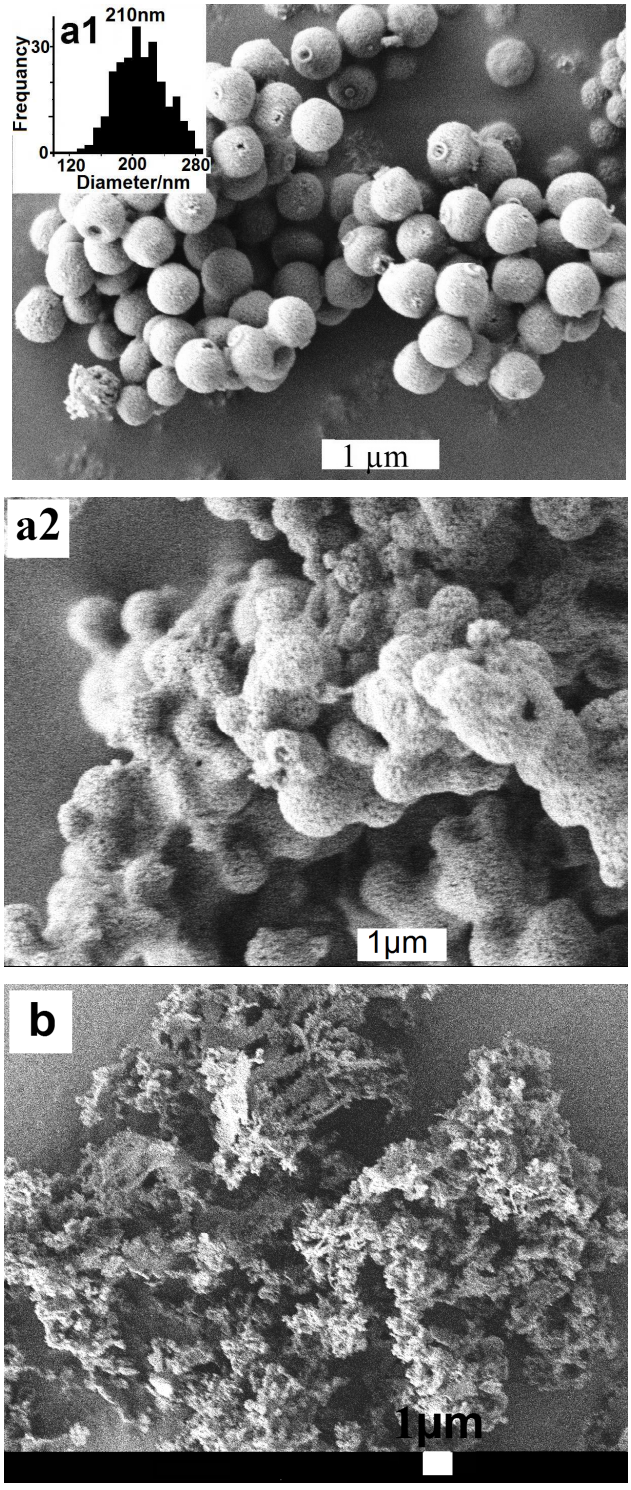


**Fig.6.13** *SEM micrographs of the metal oxide, after calcination, a1) hollow $Cr_2O_3$ spheres prepared at 12 h (the inset is PSD of the sample), a2) fused hollow $Cr_2O_3$ particles prepared at 36 h, and b) $Co_3O_4$ NPs prepared at 12 h*

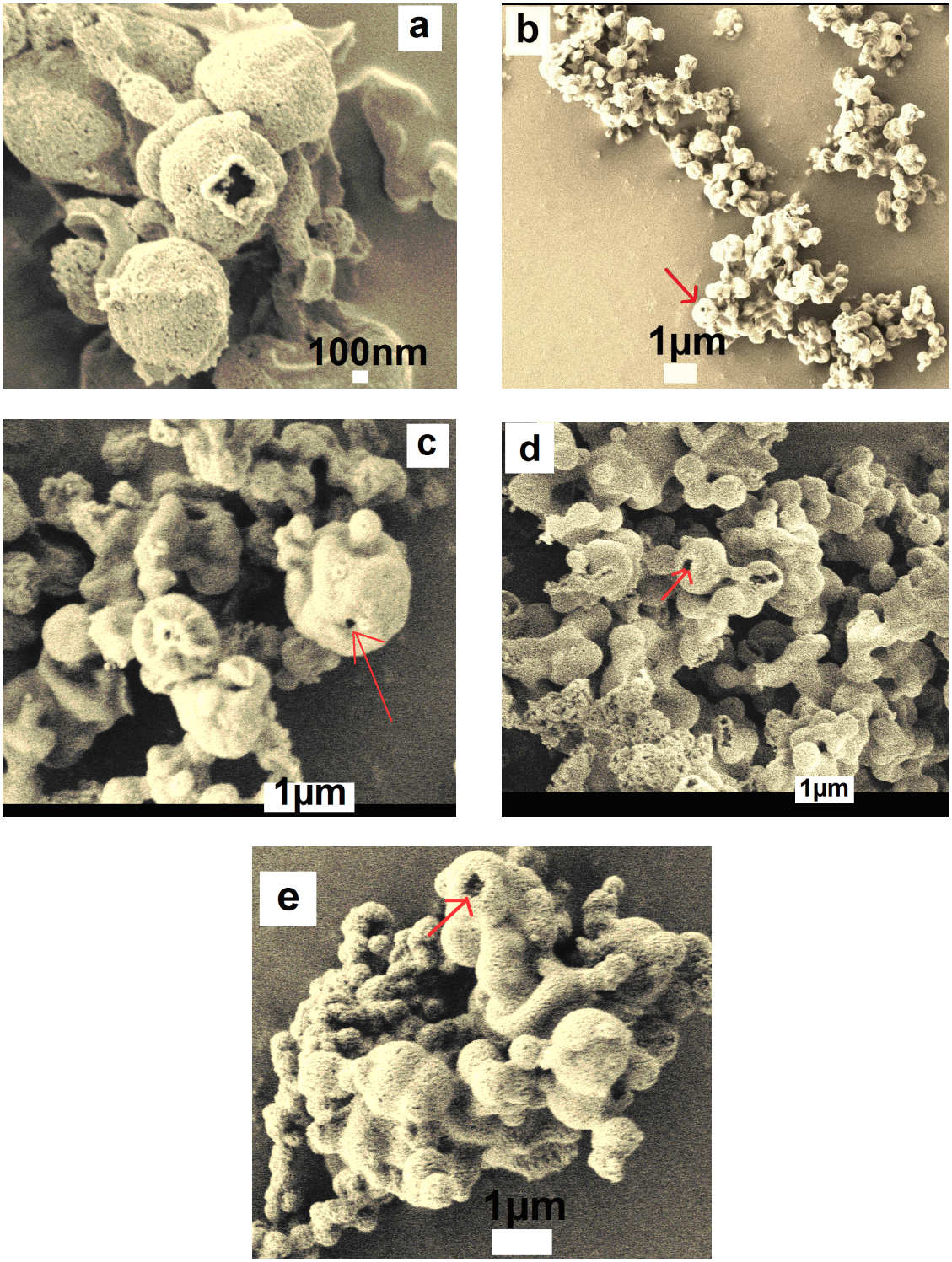


**Fig.6.14** *SEM micrographs of fused hollow porous metal oxide prepared by using 240 mmol*$^{-1}$*as glucose concentration, after calcination, a)* $Cr_2O_3$, *b) α-*$Fe_2O_3$, *c)* $Co_3O_4$, *d) NiO, and e) ZnO*

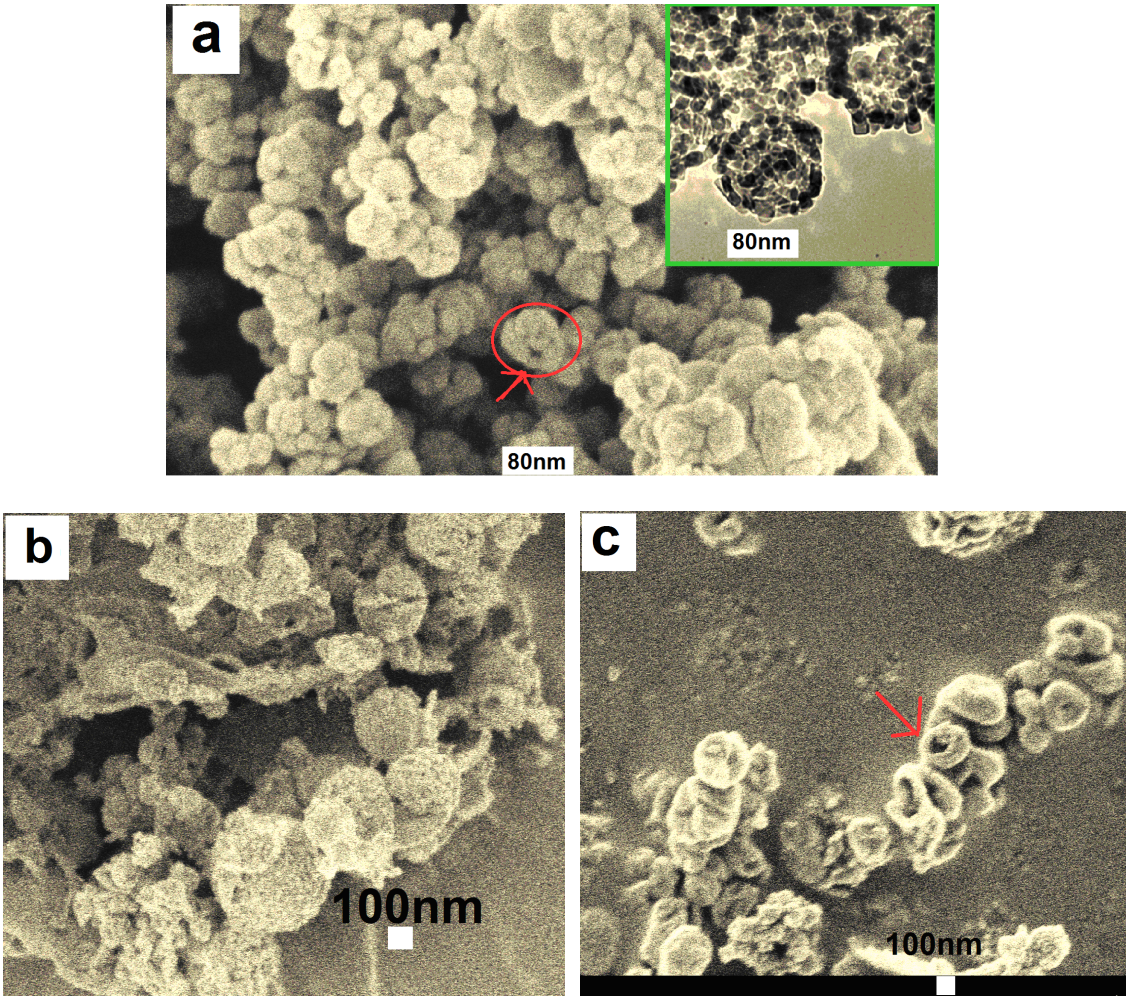


**Fig.6.15** *SEM micrographs of the porous metal oxide prepared by using 64 mmol$^{-1}$as glucose concentration, after calcination, a) hollow $Cr_2O_3$ spheres dispersed in $Cr_2O_3$ NPs (the inset is TEM micrograph of hollow $Cr_2O_3$ sphere) b) hollow α-$Fe_2O_3$ particles dispersed in α-$Fe_2O_3$ NPs, c) hollow $Co_3O_4$ spheres dispersed in $Co_3O_4$ NPs particles*

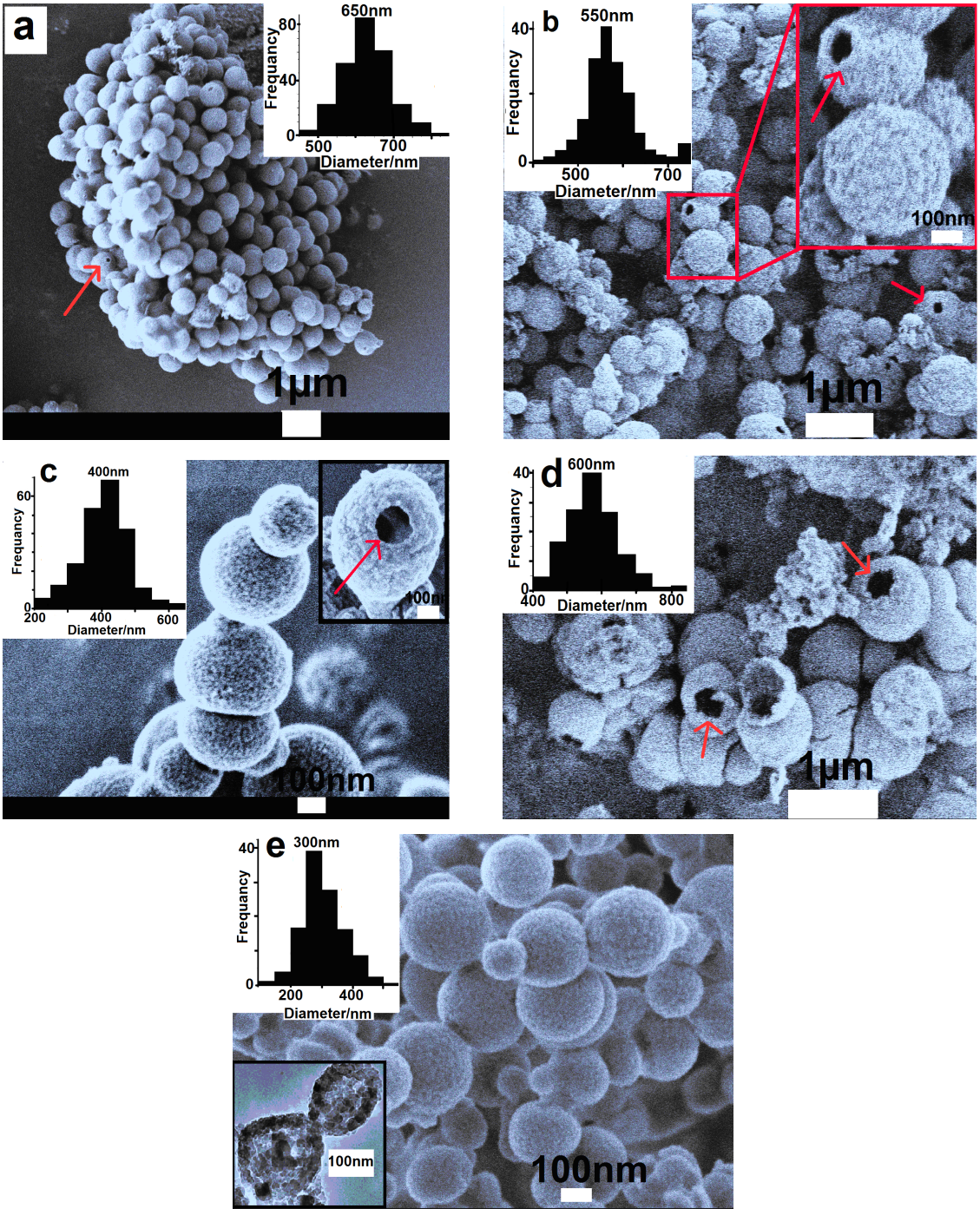


**Fig.6.16** *SEM micrographs of porous metal oxide hollow spheres prepared by applying 0.5 mL acetic acid as catalyst, after calcination, a) $Cr_2O_3$, b) α-$Fe_2O_3$, c) $Co_3O_4$, d) NiO, and e) ZnO, the inset is TEM micrograph of hollow ZnO spheres (the insets are PSD of the samples and the red arrow refers to broken shells)*

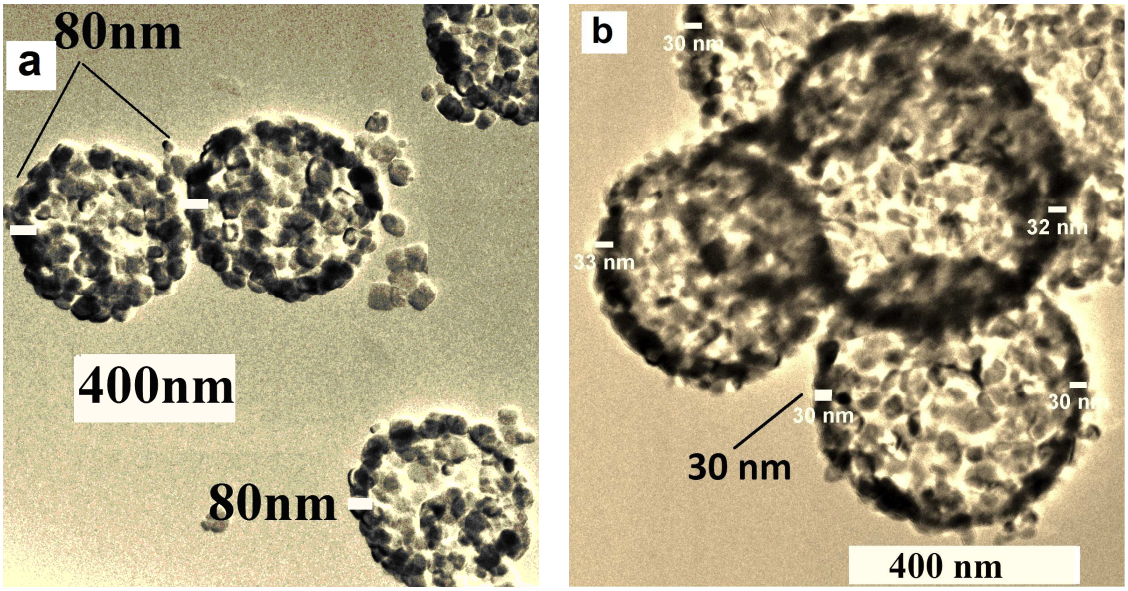


**Fig.6.17** *TEM micrographs of as-obtained hollow $Cr_2O_3$ samples [concentration ratio c(glucose)/c(metal chloride) a) 10: 1 b) 20:1]*

## 5.5 Conclusion

A series of porous metal oxides hollow spheres ($Cr_2O_3$, $Co_3O_4$, NiO, α-$Fe_2O_3$ and ZnO) have been obtained through one pot hydrothermal method by utilizing glucose as sacrificial templates. After thermal treatment of the composites a shrinkage in size occurred. The size decreased approximately 60-80%.

Important conditions critical to fine-tune the final particle size and the shape are temperature, reaction time, glucose concentration, concentration ratio c(glucose)/c(metal ions) and addition of acetic acid apparently acting as catalyst.

Generally, applying glucose as sacrificial template through hydrothermal one pot synthesis route is a general facile way for the fabrication of various hollow nano crystalline oxides. This is due to the fact that the surface of CSs core is rich of functionalities which facilitate the adsorption of the metal ions into their surface layers with out any surface modifications.

## References


1. Y. Hu, J. F. Chen, W. M. Chen, X. L. Li, *Adv. Funct. Mater.* **14** (2004) 383.
2. J. F. Chen, H. M. Ding, J. X. Wang, L. Shao, *Biomaterials* **25** (2004) 723.
3. N. Ren, B. Wang, Y. Yang, Y. Zhang, W. Yang, Y. Yue, Z. Gao, Y. Tang, *Chem. Mater.* **17** (2005) 2583.
4. S. Zeng, K. Tang, T. Li, Z. Liang, D. Wang, Y. Wang, W. Zhou , *J. Phys. Chem.* C **111** (2007) 10217.
5. Y. F. Zhu, D. H. Fan, W. Z. Shen, *J. Phys. Chem. C* **111** (2007)18629.
6. Philips Analytical, X'Pert Plus (1.0) 1999 (Almelo).
7. H. P. Klug, L. E. Alexander, *X-ray Diffraction procedures*, Wiley: New York (1959).
8. L. W. Finger, R. M. Hazen , *J. Appl. Phys.* **51** (1980) 5362.
9. E. N. Maslen, V. A. Strel'tsov, N. R. Strel'tsova, N. Ishizawa, *Acta Crystallographica B* **50** (1994) 435.
10. J. P. Picard, G. Baud, J. P. Besse, R. Chevalier, *Journal of the Less-Common Metals* **75** (1980) 99.
11. D. Taylor, *Transactions and Journal of the British Ceramic Society* **83** (1984) 5.
12. K. Kihara, G. Donnay, *Canadian Mineralogist* **23** (1985) 647.
13. T. Sakaki, M. Shibata, T. Miki, H. Hirosue, N. Hayashi, *Bioresour. Technol.* **58** (1996) 197.
14. D. Ni, L. Wang, Y. Sun, Z. Guan, S. Yang, K. Zhou, *Angew. Chem. IE* **49** (2010) 4223.
15. I. Esparza, M. Paredes. R. Martinez, A. Couto, G. Sanchez, L. Velez, O. Dominguez, *Mater. Sci. & Appl.* **2** (2011) 1584.
16. G. Pradhan, K. Parida, *Appl. Mater. & Inter*. **3** (2011) 317.
17. J. Preudhomme, P. Tarte, *Spectrochimica Acta Part A: Molecular Spectroscopy* **27** (1971) 1817.
18. P. Oliva, J. Leonardi, J. F. Laurent, C. Delmas, J. Braconnier, M. Figlarz, F. Fievet, A. J. de Guibert, *Power Sources* **8** (1982) 229.
19. Y. He, B. Yang, G. Cheng, *Catal.Today* **98** (2004) 595.
20. K. S. W. Sing, D. H. Everett, R. A. W. Haul, L. Moscou, R. A. Pierotti, J. Rouquerol and T. Siemieniewska, *Pure & Appl. Chem*. **57** (1985) 603.
21. E. P. Barrett, L. G. Joyner, P. P. Halenda, *J. Am. Chem. Soc.* **73** (1951) 373.

22. M. Sevilla, A. B. Fuertes, *Carbon* **47** (2009) 2281.
23. N. Baccile, G. Laurent, F. Babonneau, F. Fayon, M. Titirici, M. Antonietti, *J. Phys. Chem. C* **113** (2009) 9644.
24. W. H. Suh, A. Jang, Y. Suh,K. S. Suslick, *Adv. Mater.* **18** (2006) 1832.
25. H. Qian, G. Lin, Y. Zhang, P. Gunawan, R. Xu, *Nanotechnology* **18** (2007) 355602.
26. M. M. Titirici, M. Antonietti, A. Thomas, *Chem. Mater.* **18** (2006) 3808.

# Chapter 7

## Glucose and fructose as sacrificial templates: similarities and differences

A series of hollow oxides spheres have been prepared by applying either glucose or fructose as a sacrificial templates through one-pot hydrothermal method. The key to success in fabrication of hollow metal oxides spheres is due to the fact that the surface of their derived carbonaceous spheres (CSs) is rich of oxygen functionalities (e.g. -OH and -C=O) which facilitate the precipitation of the metal oxides precursors into their surface layers taking the advantage of co-ordination or electrostatic forces of attraction without any further surface modifications. Important differences have been observed between both monosaccharide templates. Applying fructose as a template enables reduction of the reaction temperature and time if compared with reaction with glucose. The particle size, however, is smaller if glucose is used as template.

## 7.1 Introduction [1, 2]

There are many similarities between glucose and fructose. They are both simple sugars, and are monosaccharides. Simple sugars contain only one type of carbohydrate as opposed to two like the disaccharide sucrose. The chemical formula of glucose and fructose is also the same [$C_6(H_2O)_6$]. While their chemical formula is the same, the molecules of glucose and fructose are set in different formations. Glucose is an aldohexose as it has six carbon atoms, five hydroxyl groups (one primary and the other four secondary) and an aldehyde function at one end. Fructose which is an isomer of glucose has a keto carbonyl function and is known as a ketohexose.

*Emil Fischer* and his students [3] were responsible for elucidating the structures and stereochemistry of the monosaccharides. The synthesis of glucose achieved by them in 1890 is considered as one of the important milestones in the development of organic chemistry. This was preceded by the discovery of phenyl hydrazine by *Fischer* in 1875. He used this reagent to explore the chemistry of glucose and related compounds.

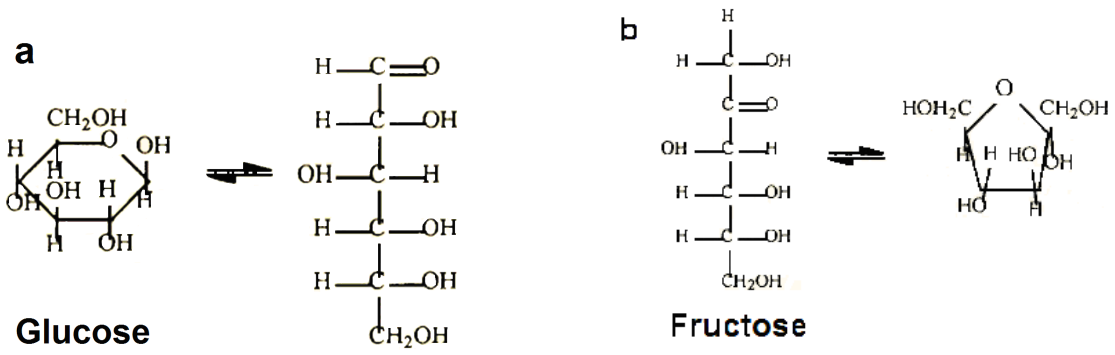


**Fig. 7.1** *a) glucose structure and its six member ring cyclic isomer glucopyranose b) fructose structure and its five member ring cyclic isomer fructofuranose [from ref.4]*

The transformation of carbohydrate molecules including glucose and fructose to form homogeneous carbonaceous spheres readily occurs by a dehydration mechanism and subsequent nanoscale sequestering in aqueous solutions when heated at 180 or 135 $^{o}$C in a pressurized vessel in case of glucose or fructose, respectively.[5, 6] Under such conditions, these molecules actually dehydrate even though they are dissolved in water. It was reported that for reactions involving glucose, it was difficult to detect 5-hydroxymethyl-2-furaldehyde (HMF) formation during initial hydrothermal treatment at <180 $^{o}$C [7], suggesting that carbon spheres were more likely formed via an intermolecular dehydration route followed by carbonization.[5] However, when an aqueous fructose solution was heated in a closed vessel to 125-140 $^{o}$C during the initial dehydration reaction, HMF was formed by intramolecular dehydration.[8]

Therefore, aqueous glucose solutions require relatively high temperature (≥180 $^{o}$C) and pressure 6-7 atm to transform into porous carbon sphere dispersions, while fructose dehydrates in water under 3-4 atm at somewhat lower temperature (>120 $^{o}$C) due to the presence of a more reactive furanose unit in contrast to glucose, where a stable pyranose group is present.

## 7.2 Comparison between glucose and fructose as sacrificial templates

Both glucose and fructose have been applied successfully as sacrificial templates for the fabrication of hollow metal oxide. The as-formed hollow oxides replicas of the glucose and fructose derived-carbonaceous spheres, but with reduced size. However, the findings that have been reported in the previous chapters demonstrated some significant differences between both templates.

The most significant noticed difference is that applying fructose as a template enables reduction of the reaction temperature and time if compared with

reaction with glucose. The particle size, however, are smaller if glucose is used as template.

A comparison between the typical synthetic procedures using glucose or fructose as sacrificial templates reported in this investigation (Table 7.1) summarizes the synthetic procedures differences between both templates.

**Table 7.1** *Comparison of optimized reaction conditions using glucose and fructose as sacrificial templates*

| Typical synthetic procedures | Glucose as sacrificial template | Fructose as sacrificial template |
|---|---|---|
| Temperature/ ($^{o}$C) | 180 | 135 |
| Time / h | 24 | 6 |
| Sugar concentration/ mmolL$^{-1}$ | 96 | 625 |
| Metal ions : sugar concentration | 1:10 | 1:20 |

In addition the comparison between the average sizes of the as-formed hollow porous metal oxides (Table 7.2) summarizes the product differences between both templates.

**Table 7.2** *Comparison between glucose and fructose as sacrificial templates*

| Metal hollow oxide | Size of the hollow products in case of:- | |
|---|---|---|
| | glucose as sacrificial template | fructose as sacrificial template |
| $Cr_2O_3$ | 350nm hollow spheres | 750nm hollow spheres |
| $\alpha$-$Fe_2O_3$ | 225nm hollow spheres | 580nm hollow spheres |
| $Co_3O_4$ | 250nm hollow spheres | 400nm hollow spheres |
| NiO | 300nm hollow spheres | 700nm hollow spheres |
| ZnO | 175nm hollow spheres | 500nm hollow spheres |

## References


1. T. K. Lindhorst, *Essentials of Carbohydrate Chemistry and Biochemistry*, 3rd Edition, Wiley-VCH, Weinjheim (2007).
2. A. P. Rauter, T. D. Lindhorst, Eds., *Carbohydrate Chemistry: Chemical and Biological Approaches*, Royal Society of Chemistry (2010).
3. (a) E. Fischer, J. Tafel, *Ber.* **23** (1890) 2114. (b) E. Fischer, J. Tafel, *Ber.* **20** (1887) 1088, 2566, 3384.
4. B. M. Kabyemela, T. Adschiri, R. M. Malaluan, K. Arai**,** *Ind. Eng. Chem. Res.* **38** (1999) 2888.
5. X. Sun, Y. Li, *Angew. Chem. Int. Ed.* **43** (2004) 597.
6. M. S. Feather, J. F. Harris, *Adv. Carbohydr. Chem. Biochem.* **28** (1973) 161.
7. (a) P. E. Shaw, J. H. Tatum, R. E. Berry, *Carbohydr. Res.* **5** (1967) 266. (b) B. F. M. Kuster, L. M. Tebbens, *Carbohydr. Res.* **54** (1977) 159. (c) K. Lourvanij, G. L. Rorrer, *Appl. Catal. A* **109** (1994)147. (d) K. Lourvanij, G. L. Rorrer, *Ind. Eng. Chem. Res.* **32** (1993) 11.
8. C. Yao, Y. Shin, L. Wang, C. F. Windisch, W. D. Samuels, B. W. Arey, C. Wang, W. M. Risen, G. J. Exarhos, *J. Phys. Chem. C* **111** (2007) 15141.

# Chapter 8

## Summary

My original goal in this dissertation to present a facile, environmental benign, economical sustainable and additive free synthesis protocol for the fabrication of hollow oxides which ultimately could enable the fine-tuning of the hollow inorganic materials has been achieved via facile one-pot hydrothermal strategy through using simple sugar (glucose and fructose) as sacrificial templates. This class of materials are of great importance from the scientific and the technological point of view due to their unique properties such as large specific surface area and low density, which make them attractive for many potential applications. A series of experiments was performed by which various of porous metal and ceramic oxides hollow spheres were obtained as a final products via hydrothermal approach. The as-obtained hollow oxides were characterized by SEM, TEM, XRD, IR and nitrogen adsorption isotherm (BET).

A brief introduction and broad applications of hollow inorganic materials have been described in chapter 1. Also I have thrown some light on the synthesis approaches of hollow inorganic materials and special attention has been paid to sacrificial templating synthesis methods due to their excellent results.

I have investigated the synthesis of glucose as well as fructose derived-carbonaceous spheres via the hydrothermal hydrolysis in closed system (100 ml Teflon-lined stainless steel autoclave). I found that different synthesis parameters such as temperature, reaction time, sugar concentration and addition of acetic acid acting as catalyst, are important for tuning the diameter of the as-prepared carbonaceous spheres. Details on the composition and morphology of the carbonaceous materials were obtained from infra red spectroscopy (IR), carbon

hydrogen analysis (CH). Scanning electron microscopy (SEM) has shown that the carbonaceous materials posses' high functionalities and it has about 60 to 70% carbon and have spherical morphology with smooth surface. These findings as described in chapter 3 demonstrated that monosaccharide are suitable candidates as sacrificial templates for the fabrication of metal oxides hollow materials in simple strategy without further surface modifications and this is due to the oxygen or hydroxy functionalities inherited in their surface layers.

In chapter 4, I have described a method for the fabrication of hollow silica nano-spheres via a facile one-pot hydrothermal route using glucose as sacrificial template and water glass as silica precursor for the first time. It has been demonstrated that meso-porous hollow silica nanoparticles (PHSNPs) with tuneable shell thickness and particle size can be readily fabricated through this approach. In my synthesis recipe, heating of an aqueous solution of water glass and D-glucose to 180 °C for 24 h affords - as indicated by transmission electron microscopy – a nanospherical composite consisting of a silica shell sheathing a carbonaceous core. Subsequent removal of the carbonaceous interior through oxidation in air produces free standing hollow silica structures. After thermal treatment of C@$SiO_2$ precursor composites at 550 $^{o}$C for 5 hours, a shrinkage in size occurred. The size decreased approximately 65 to 80 %. In addition, I found that PHSNPs varying between approx. 25 and 50 nm in diameter as shown in TEM images. Generally, the amount of water glass affects the morphology and the shell thickness of the hollow silica spheres (HSSs). The concentration of glucose has a significant influence on the size of the obtained HSSs as well. Increasing the glucose concentration, increases the average size of the obtained composites which in turn leads to an increase in the size of hollow particles .

I also succeeded in fabricating a series of oxides ($Cr_2O_3$, α-$Fe_2O_3$, $Co_3O_4$, NiO and ZnO) by using fructose as sacrificial template via facile one-pot hydrothermal approach for the first time. In my recipe, heating of an aqueous solution of the metal chlorides and fructose to moderate temperature 135-150 $^{o}$C

in an autoclave affords - as indicated by transmission electron microscopy - a nanospherical composite consisting of a metal precursor shell coating a carbonaceous core. The removal of the interior carbonaceous cores via heat treatment through oxidation in air yields free standing hollow crystalline oxides spheres. As minor product, ball in ball (bnb) hollow structures were found within the final products, without any further synthetic steps. I proposed a mechanism for the formation of the hollow products, however, the formation mechanism of bnb hollow spheres at this stage remains an open question and a challenge to material scientists. Correlations between the particle size and the concentration of fructose, as well as the ratio of metal precursor and the sugar concentrations are uncovered. Moreover, important factors critical to fine tune the final particle size and the shape are temperature, reaction time and addition of acetic acid apparently acting as catalyst. The results have shown that each parameter of the previous mentioned parameters have similar impacts on the different types of oxides. The similarity of the impact of each parameter on the formation of hollow oxides reported here might open the door for general understanding of the formation of the hollow metal oxides spheres with variable size.

Glucose also have been successfully applied as sacrificial template for preparing $Cr_2O_3$, α-$Fe_2O_3$, $Co_3O_4$, NiO and ZnO hollow spheres. I believed that the key to success, in fabrication of hollow metal oxides spheres using glucose or fructose as sacrificial templates is due to the fact that the surface of their derived carbonaceous spheres (CSs) is rich of oxygen functionalities (e.g. -OH and -C=O) which facilitate the bonding of metal cations into the surface layers of the carbonaceous spheres taking the advantage of co-ordination or electrostatic forces of attraction without any further surface modifications.

Finally and most importantly, significant differences have been observed between both monosaccharide templates (fructose and glucose). Applying fructose as a template enables reduction of the reaction temperature and time if it

is compared to reaction with glucose. The particle size, however, are smaller if glucose is used as template.

Overall, my work has suggested that using simple sugar as sacrificial template in one-pot hydrothermal method is efficient to fabricate nano-sized oxides with hollow structure. I succeeded in fabricating nanospheres of $SiO_2$ by applying glucose as sacrificial template by hydrothermal approach for the first time. In addition, I have applied fructose as a sacrificial template for fabricating $Cr_2O_3$, α-$Fe_2O_3$, $Co_3O_4$, NiO and ZnO with hollow structures for the first time to the best of our knowledge. Moreover, glucose have been successfully used for fabricating the previous oxides hollow spheres. Furthermore, correlations between the particle size and the concentration of the sugar as well as the ratio of the amount of substance of metal precursor and sugar are uncovered; moreover, important factors critical to fine-tune the final particle size and shape are temperature, reaction time and the addition of acetic acid as a catalyst.

Considering that metal salt are used as the metal precursor and that the precursor is available for many metallic elements, I anticipate that using monosaccharide as sacrificial templates through hydrothermal approach can widen the accessible field of metal oxide hollow spheres.

# Chapter 9

## Zusammenfassung

Mein Ziel in dieser Dissertation ist es eine einfache, umweltfreundliche, ökonomisch sinnvolle und additivfreie Syntheseroute für die Herstellung von oxidischen Hohlkörpern vorzustellen, welche letztendlich eine Optimierung der anorganischen Hohlmaterialien ermöglicht, die mittels einer einfachen hydrothermalen Eintopfsynthese unter Verwendung von Einfachzuckern (Glucose und Fructose) als Templat durchgeführt wird. Diese Klasse von Materialien ist vom wissenschaftlichen und technologischen Standpunkt aus gesehen von großem Interesse, da sie aufgrund ihrer einzigartigen Eigenschaften, wie zum Beispiel eine große spezifische Oberfläche und eine geringe Dichte, attraktiv sind für viele potentielle Anwendungen. Eine Serie von Experimenten wurde durchgeführt, welche verschiedene Hohlkugeln aus porösen Metall- bzw. keramischen Oxiden lieferte, welche als Produkt aus der hydrothermalen Synthese erhalten wurden. Die synthetisierten oxidischen Hohlkörper wurden mittels SEM, TEM, XRD, IR und isothermaler Stickstoffadsorption (BET) charakterisiert.

Eine kurze Einleitung zu den anorganischen Hohlmateralien, sowie der breite Anwendungsbereich wurden in Kapitel 1 aufgeführt. Ebenfalls wurde ein Licht auf die synthetischen Methoden zur Herstellung von anorganischen Hohlmateralien geworfen, wobei aufgrund der exzellenten Anwendungsmöglichkeiten das Hauptaugenmerk auf der Synthese über eine Templatroute lag.

Ich habe die aus Glucose sowie Fructose erhaltenen Kohlenstoffkugeln synthetisiert mittels hydrothermaler Hydrolyse in einem geschlossenem System

(100 mL mit Teflon ausgekleideter Edelstahl Autoklav) erforscht. Dabei habe ich herausgefunden, dass unterschiedliche Syntheseparameter wie Temperatur, Reaktionzeit, Zuckerkonzentration und Zugabe von Essigsäure als Katalysator wichtige Faktoren den sind, die Durchmesser der hergestellten Kohlenstoffkugeln sowie deren Wandstärke beeinflussen. Detailierte Informationen über die Zusammensetzung und Morphologie der kohlenstoffhaltigen Materialien wurden mittels Infrarotspektroskopie (IR), Elementaranalyse (CH), und Rasterelektronenmikroskopie (SEM) erhalten. Diese zeigten, dass die kohlenstoffhaltigen Materialien eine hohe Oberflächenfunktionalität aufweisen, 60-70 % Kohlenstoff enthalten und kugelförmig mit glatter Oberfläche sind. Diese Befunde, die in Kapitel 3 beschrieben sind, demonstrieren, das Einfachzucker geeignete Kanditaten sind zur Verwendung als Templat für die einfache Synthese von metalloxidischen Hohlmateralien, bei der aufgrund der vielen Saustofffunktionalitäten in der Oberflächenschicht keine weiteren Oberflächenbehandlungen nötig sind.

In Kapitel 4 habe ich erstmalig die Route zur Herstellung von Siliciumdioxid Nanohohlkugeln, mittels leichter hydrothermaler Eintopfsynthese unter Verwendung von Wasserglas als Silicaprecursor vorgestellt. Es wurde demonstriert, dass mesoporöse Siliciumdioxidpartikel (PHSNPs), welche Hohlkugeln mit definierter Wanddicke und Partikelgröße bilden, einfach mit dieser Methode hergestellt werden können. Meine Syntheseroute über Erhitzen einer wässrigen Lösung von Wasserglas und D-Glucose auf 180 °C für 24 h, liefert – wie mittels Transmissionelektroskopie gezeigt - ein nanosphärisches Komposit bestehend aus einem Siliciumdioxidmantel mit einem Kohlenstoffkern. Anschließendes Entfernen des kohlenstoffhaltigen Kerns über Oxidation an Luft mittels thermischer Behandlung erzeugt eine stabile Silicahohlstruktur. Nach thermischer Behandlung des C@$SiO_2$ Precursor Komposit bei 550 °C für 5 Stunden wird eine Volumenkontraktion beobachtet. Hierbei verringert sich die Größe um 65-80 %. Zusätzlich wurde über Transmissionselektronenmikroskopie herausgefunden, dass die PHSNPs zwischen einem Durchmesser von 25 und 50

nm variieren. Generell beeinflusst die verwendete Menge an Wasserglas die Morphologie und Wanddicke der Silica-Hohlkugeln (HSSs). Ebenfalls einen signifikanten Einfluss auf die Größe der erhaltenen HSSs hat die Glucosekonzentration. Eine Erhöhung der Glucosekonzentration bewirkt eine Vergößerung der mittleren Größe der erhaltenen Komposite, was wiederum zu größeren Hohlkörpern führt.

Ebenfalls zum ersten Mal erfolgreich war die Synthese einer Reihe von Oxiden ($Cr_2O_3$, α-$Fe_2O_3$, $Co_3O_4$, NiO und ZnO) unter Verwendung von einem Fructosetemplat bei der hydrothermalen Eintopfsynthese. Meine Syntheseroute, Erhitzen einer wässrigen Lösung von Metallchloriden und Fructose auf eine moderate Temperatur von 135-150 °C in einem Autoklaven, liefert – wie mittels Transmissionelektroskopie gezeigt - ein nanosphärisches Komposit bestehend aus einem metallprecursorhaltigen Mantel mit einem Kohlenstoffkern. Die Entfernung des kohlenstoffhaltigen Kerns mittels thermischer Behandlung und Oxidation an Luft liefert stabile, kristalline, oxidische Hohlkugeln. Überraschenderweise wurden als Nebenprodukt, ball in ball (bnb) Hohlstrukturen im erhaltenen Produkt gefunden, ohne dass weitere synthetische Schritte durchgeführt wurden. Es wurde ein Mechanismus für die Bildung der Hohlstrukturen vorgeschlagen, allerdings bleibt der Bildungsmechanismus der bnb Hohlkugeln gegenwärtig noch offen und bleibt ein noch zu lösendes problem für Materialwissenschaftler. Korrelationen zwischen der Partikelgröße und der Konzentration an Fructose, sowie auch des Verhältnisses von Metallprecursor zu Zuckerkonzentration wurden aufgedeckt. Weiterhin sind wichtige Faktoren zur partikelgrößen und -formselektiven Synthese die Temperatur, Reaktionszeit sowie die Zugabe von Essigsäure als Katalysator. Die Ergebnisse zeigen, dass jeder von den zuvor genannten Parametern eine ähnliche Auswirkung bei den unterschiedlichen Typen von Oxiden hat. Der vergleichbare Einfluss der Parameter auf die oxidischen Hohlmateralien der hier ermittelt wurde, könnte die

Tür zu einem generellem Verständnis von der Bildung der metalloxidischen Hohlkugeln mit unterschiedlicher Größe öffnen.

Glucose konnte auch erfolgreich als Templat zur Herstellung von $Cr_2O_3$, α-$Fe_2O_3$, $Co_3O_4$, NiO and ZnO Hohlkugeln angewandt werden. Vermutlich liegt der Schlüssel zum Erfolg bei der Synthese von metalloxidischen Hohlmateralien über Glucose- oder Fructosetemplate darin, dass die Oberfläche der erhaltenen kohlenstoffhaltigen Kugeln(CSs) reich an Sauerstofffunktionalitäten (z.B. -OH und -C=O) ist, welche, aufgrund von Koordination oder elektrostatischen Anziehungskräften, die Einlagerung der Metalloxidprecursor in die Oberflächenschichten ohne eine weitere Oberflächenmodifizerung fördern.

Letztich und als wesentlicher, signifikanter Unterschied bei der Verwendung von den beiden Einfachzuckertemplaten (Glucose und Fructose) wurde gefunden, dass bei der Verwendung von Fructose als Templat die Reaktionstemperatur sowie Zeit gegenüber der benötigten bei einem Glucosetemplat verringert werden kann. Jedoch sind die erhaltenen Partikel von einem Glucosetemplat kleiner.

Insgesamt ergibt sich aus meiner Arbeit, dass die Verwendung von Einfachzuckern als Templat in einer hydrothermalen Eintopfsynthese effizient ist um nanokristallone Oxide mit einer Hohlstruktur herzustellen. Es konnten zum ersten Mal erfolgreich $SiO_2$ Nanohohlkugeln mit Hilfe von einem Glucosetemplat über ein hydrothermales Verfahren herstellt werden. Zusätzlich konnte erstmalig Fructose als Templat für die Synthese von Hohlstrukturen aus $Cr_2O_3$, α-$Fe_2O_3$, $Co_3O_4$, NiO und ZnO anwendet werden. Was auch mit Hilfe eines Glucosetemplats für die zuvor genannten Oxide durchgeführt werden konnte. Weiterhin konnten Korrelationen zwischen der Partikelgröße und der Zuckerkonzentration sowie auch dem Verhältnis von Metallprecursor zu Zucker festgestellt werden. Weitere wichtige Faktoren zur Partikelgrößen und -

formselektiven Synthese sind Temperatur, Reaktionszeit und die Verwendung eines Katalysators.

Beachtet man, dass Metallsalze als Ausgangstoff verwendet wurden und diese für viele Metalle erhältlich sind, ist damit zu rechnen, dass die Verwendung von Einfachzuckern als Templat bei der hydrothermalen Synthese den zugängigen Bereich an Metalloxidhohlkugeln noch erweitern kann.

## Acknowledgement

It is with a great deal of pleasure that I thank those who have contributed in so many ways to the completion of this dissertation.

First, with my deep sense of affectionate and admiration, I want to thank my advisor Prof. Dr. *B. Harbrecht*, who continues to put up with his constant encouragement, kind support, invaluable guidance, and for his participation in the preparation of this thesis, and for many reasons.

I am deeply grateful to Prof. Dr. *M. F. Zawrah,* my supervisor at National Research Center, in Egypt, who suggested me to work on hollow silica nanoparticles, due to his constant support in every aspect.

Grateful acknowledgement is made to all my friends at the Harbrecht laboratory who made my research so intellectually stimulating and enjoyable. I would also thank *Alexendra Scmidt* for helping in translation of summary. I wish to convey my sincere thanks to undergraduate students, especially for partial experimental support for this project.

I particularly want to thank DAAD (*Deutscher Akademischer Austausch Dienst*) and MHESR (*the Ministry of Higher Education and Scientific Research, in Egypt*), for providing financial support .

National Research Centre administration in Egypt, in particularly Ceramics Department, for their encouragement to pursue my research in Germany.

Last but not least it is my pleasure to express gratitude towards my family in Egypt for their encouragement and moral support, and most importantly, I thank my wife, *Sherihan El-Oraki,* for things more than space allowed, but mostly for her love and support.

## Declaration

I declare that I myself wrote this study and carried out the experimental work described in it, without using any other sources and aids than those that are stated.

Marburg, January, 2013

# Curriculum Vitae

## ***Personal Data***

| | |
|---|---|
| Name | HAITHAM MOHAMMAD ABDELAAL |
| Martial Status | Married with son. |
| Nationality | Egyptian |

## ***Expertise***

**Academic Degrees**

1- MSc. in inorganic and physical chemistry - Sep. 2006 - Zagazig University - Egypt
2- Bsc. in chemistry - May 2002 – Zagazig University - Egypt

**Fellowships**

1. Master research studentship from Academy of Scientific Research, Egypt (April 2003- April 2006)
2. DAAD PhD scholarship in Marburg University (Germany) from the 1st of October 2009 to end of September 2011

**Past Experience**

1- Research assistant in Inorganic Chemistry Department, National Research Center, Egypt (7/04/2003– 10/6/2008)
2- Research assistant in Ceramics Department, National Research Center, Egypt (11/6/2008 – 30/09/2011)
3- Researcher assistant Marburg University, Germany (01/10/2011 – 31/03/2013)

**Professional Experience**

- Preparation and characterization of organometallic compounds
- Preparation and characterization of ceramic materials
- Synthesis of nanomaterials and hollow nano oxides
- Normal and sensitive condition such as IR, UV/VIS, XRD, EDX, TEM, SEM, BET, and thermal analysis

**Language Proficiency**

- Arabic (Native Language)
- English Language (Excellent)

- German Language :

1. A2 (Start Deutsch 2) [from Goethe Institute, Cairo]
2. Four months of intensive course at Speak &Write institute Marburg, Germany [fom 02-06-2009 to 25-09-2009], B2.1 level

Computer skills

- ICDL (*International Computer Driving License*)

Contributions

➢ Publications

1- M. F. R . Fouda and **Haitham M. Abdelaal** , Synthesis and spectroscopic characterization of some metal-EDTA complexes used as micronutrient fertilizers, *Egypt, J. of App. Sci*., **21** (7) 2006, 53

2- **Haitham Abdelaal** and B. Harbrecht, One-pot synthesis of hollow silica nanoparticles, (under publication in *J.Mat.Sci.)*

3- **Haitham Abdelaal** and B. Harbrecht, Hydrothemal synthesis of porous metal oxide hollow spheres by using fructose as sacrificial template , (under publication in *J.Mat.Sci.)*

➢ Presentations

4- "Facile synthesis of some metal and ceramic oxides hollow particles via hydrothermal route using monosaccharide as sacrificial templates", *Inorganic chemistry colloquium, 18/06/12,* ***Marburg University***, *Germany*

5- "One-pot fabrication of hollow nano metal oxides by use of sugars as sacrificial templates", *16th meeting - Materials Chemistry and Energy use of resources, 17th - 19 Sep. 2012,* ***Technische Universität Darmstadt****, Germany*

➢ Posters

*6-* "Synthesis and characterization of some complexes of micronutrient elements with DTPA", *1st International conference on materials science & nanotechnology(future*

*challenges), 2-4 Dec. 2007,* ***National Research Centre (NRC)****, Egypt*

*7-* "Facile one-pot fabrication of hollow porous silica particles"*. Materialforschungstag Mittelhessen. 30. June 2011,* ***Giessen University****, Germany*

*8-* "Facile hydrothermal one-pot fabrication of hollow porous $Cr_2O_3$ spheres" *Materialforschungstag Mittelhessen. 10. July 2012,* ***Marburg University****, Germany*

*9-* "Hydrothermal one-pot fabrication of hollow porous nano silica particles"*, 16th meeting - Materials Chemistry and Energy use of resources, 17th - 19 September 2012,* ***Technische Universität Darmstadt****, Germany*

- Thesis supervision

1. Silke Santner, *Herstellung kohleartiger Nanokugeln aus Zuckerlösung als Schablonen für Metalloxid-Hohlkugeln*, Bachelor thesis, **Marburg University** (2011)
2. Erik Pfeiffer, *Hollow $Ta_2O_5$ nanoparticles: synthesis, characterization and properties*, **Marburg University**, Bachelor thesis, Marburg University (winter semester 2012-2013)

Membership of Organizations

1. Membership of the Scientific Society for the Advanced Materials & the Nanotechnology (Egypt)
2. Member of the Association of Scientific Professions, (Egypt)
3. Member of the Marburg University Research Academy (MARA)
4. Member of the German Chemical Society (GDCh)

E-mail address: hmaa_77@yahoo.com
abdelaal@staff.uni-marburg.de
Telephone: +49 017-693-113-816